ALKYNYLATED ACENOTHIADIAZOLES AND N-HETEROACENES:

Synthesis, Functionalization, and Study of the Optical Properties for Optoelectronic and Sensory Materials

A Dissertation
Presented to
The Academic Faculty

By

Scott M. Brombosz

In Partial Fulfillment
Of the Requirements for the Degree
Doctor of Philosophy in Chemistry

Georgia Institute of Technology

December, 2010

ALKYNYLATED ACENOTHIADIAZOLES AND N-HETEROACENES:

Synthesis, Functionalization, and Study of the Optical Properties for Optoelectronic and Sensory Materials

Dr. Uwe Bunz, Advisor
School of Chemistry and Biochemistry
Georgia Institute of Technology

Dr. Christoph Fahrni
School of Chemistry and Biochemistry
Georgia Institute of Technology

Dr. Laren Tolbert
School of Chemistry and Biochemistry
Georgia Institute of Technology

Dr. Jake Soper
School of Chemistry and Biochemistry
Georgia Institute of Technology

Dr. Anselm Griffin
School of Polymer, Textile,
and Fiber Engineering
Georgia Institute of Technology

Date Approved: May 12th, 2010

ACKNOWLEDGEMENTS

To begin to think of everyone whom I would like to acknowledge is a terribly difficult thing to undertake when considering the countless lives that have touched me both professionally and personally. To begin with I would like to thank my advisor, Uwe Bunz, for his dedicated guidance and friendly, interesting chats. Uwe's tireless excitement for the understanding of our chemistry was a real driving force in my work.

I would also like to thank my thesis committee for their support throughout my graduate studies. I would also like to thank our collaborators, Dr. Seth Marder, Dr. Stephen Barlow, Dr. Jean-Luc Brédas, Dr. John Sears, Dr. Kenneth Hardcastle, and Dr. Paul von Ragué Schleyer.

To the Bunz group members past and present, I would like to express my appreciation for all of the help and assistance that everyone has provided over the past five years. Particularly I would like to thank Dr. Ik-Bum Kim, Dr. Yiquing Wang, Dr. Ronnie Phillips, Dr. Juan Tolosa, Dr. Selma Bakbak, Dr. Sandra Shotwell, Jake Leach, Jonny Bryant, Drew Zappas, Evan Davey, Chris Kub, Ewelina Kieley, Eric Gharakhanian, Imani Jones, and Steven Hayden.

I would also like to thank all those who worked on the heteroacenes project who contributed significantly to the body of this work: Dr. Carlito Bangcuyo, Dr. Shaobin Miao, Anthony Appleton, Nancy Berger, and Allen Zhang. Without their dedication and fostering of wonderful intragroup collaborations, this work would not have been possible.

I would like to especially thank Psaras McGrier who joined the group at the same time as me and has been extremely helpful and a great labmate.

Additionally, I would like to extend a special thanks to Dr. A.J. Zucchero who, along with Dr. Ronnie Phillips, took me under his wing when I first joined the group and helped show me the ropes of the lab. He has been a great friend and collaborator; I'm sure that when you weigh out all the time AJ has saved me by helping me in lab, it was slightly more than the time we wasted together at lunch and in long conversations.

On a more personal note, I would like to thank my parents, Michael and Sheila Brombosz. My whole life they have been so very supportive in all of my endeavors even when it meant I would be moving across the country to attend Georgia Tech. I believe they were able to instill in me a foundation of values and beliefs that have carried me this far.

To Elizabeth Whitehill, I am so glad you came into my life. Our time together has been wonderful. I only hope to be able to reciprocate the support you gave me as you pursue you graduate career as well.

I would also like to thank my brother Dan and sister-in-law Melissa. It was always exciting to see them when they came to visit, not only because they brought me furniture when my apartment had none, but because it made home seem a little bit closer when they were here. I especially enjoyed playing uncle for once when their beautiful children, Katelyn and Michael, would visit. I look forward to seeing them grow up.

Of course I can't forget about my little sisters Kim and Kelly who will always remain my little sisters no matter how much they seem to grow and mature. They still have their

academics to finish, but I'm sure they will be very successful and happy wherever they find themselves.

In a more general sense, I would like to thank my extended family. With so many uncles, aunts, and cousins it is hard to thank them all. I would especially like to thank Nick and Ryan Higens, who grew up so close that it felt like I had three brothers, which is even truer when you realize that we have the same set of grandparents.

Finally, I would like to thank all of my friends both home and away: Justin Stec, Ian Cunniff, Sean Wiggins, Jon Ulfig, Bob Clyde, Matt Briddick, Jeremy Higgins, Brandon Bromberek, Trevor Sierra, T.J. Wessel, Tyler Bennett, Rosie Mulcahey, Kaelen Westlake, Laura Clapp, Adam Offenbacker, Chip and Jess Humpheries, Carley Shulman, John Bustamante, Nick Haase, and Anthony Baldridge.

TABLE OF CONTENTS

LIST OF TABLES

LIST OF FIGURES

LIST OF SCHEMES

LIST OF SYMBOLS AND ABBREVIATIONS

Å	angstrom
Abs	absorbance
AcOH	acetic acid
Ar	aryl
°C	degrees Celsius
cm^{-1}	wavenumber
d	days
DCM	dichloromethane
DI	deionized
DMF	dimethylformamide
DMSO	dimethylsulfoxide
ε	molar absorptivity
Et_2O	diethyl ether
EtOAc	ethyl acetate
EtOH	ethanol
Eq	equivalents
Ex	excitation
FMO	frontier molecular orbital
g	gram
HOMO	highest occupied molecular orbital
h	hour
ITC	isothermal titration calorimetry
IR	infrared

K_a	association constant
L	liter
LED	light emitting device
LUMO	lowest unoccupied molecular orbital
MP	melting point
MeOH	methanol
mg	milligram
MHz	megaHertz
min	minute
mL	milliliter
mmol	millimole
μL	microliter
μm	micrometer
M	molarity
nm	nanometer
NMR	nuclear magnetic resonance
NaOH	sodium hydroxide
OTf	trifluoromethanesulfonate
%	percent
Φ_F	fluorescence quantum yield
Ppb	parts per billion
Ppm	parts per million
PV	photovoltaic
rt	room temperature
TBAF	tetrabutylammonium fluoride

TEA	triethylamine
TFA	trifluoroacetic acid
TFT	thin film transistor
THF	tetrahydrofuran
THP	tetrahydropyranyl
TIPS	triisopropylsilyl
TMS	trimethylsilyl
Triflate	trifluoromethanesulfonate
UV	ultra-violet
XF	cruciform

Summary

For organic electronic device applications materials are needed which display good charge carrier mobility, good processability, and stability towards oxygen and moisture. Alkynylated N-Heteroacenes fulfill many of these requirements. Substitution with alkyne groups as well as the introduction of the pyrazine subunit both inhibits oxidative degradation at sensitive position in the molecules. Additionally the trialkylsilylethynyl group aides in directing the packing motif as well as vastly increases the solubility over unsubstituted analogues.

A requisite precursor in the synthesis of alkynylated N-heteroacenes is alkynylated acenothiadiazoles. These thiadiazoles display interesting photophysical properties and can be functionalized to produce a wide range of properties in closely related materials. The acenothiadiazoles themselves have potential applications as an N-type semiconductor. Optical gaps and calculated HOMO-LUMO gaps show that these molecules, when compared to known N-type materials, should be easily injected with electrons. Additionally the crystal packing of these compounds shows favorable π-orbital overlap which should provide excellent charge carrier mobilities.

We have also substituted benzothiadiazoles with dialkylaniline groups as well as phenol group to yield benzothiadiazole trimers. These molecules are acid/base sensitive and exhibit similar properties in their isoelectronic states. Utilizing their solvatochromic behaviors, we are able to tease out the interplay of dipole, hydrogen bond accepting, and hydrogen bond donating interactions of the chromophore with the solvent.

Additionally, we have reacted the alkyne groups on the acenothiadiazoles with triethylene glycol monomethyl ether azide to produce bis(1,2,3-triazole)benzothiadiazole and bis(1,2,3-triazole)naphthothiadiazole. These molecules are both water-soluble and exhibit strong selective binding of nickel and copper in aqueous solutions.

Chapters 3 and 4 are related and explore the photophysical interactions of hydroxy- and dibutylamino-substituted fluorophores with the solvent environment. These compounds were expected to be acid/base sensitive and display similar properties among their isoelectronic pairs. Kamlet-Taft analysis was utilized to separate the dipole, proton-accepting, and proton-donating characteristics of the solvent-fluorophore interactions. These results showed that the in the case of the protonated dibutylamino and phenol compounds hydrogen-bond interactions play a small role. In the case of the phenolate, there are strong hydrogen-bond interactions. The dibutyl compounds unexpectedly showed little hydrogen-bond interactions which is a result of the decreased basicity of the amine compared to the phenolate.

Chapter five demonstrated that dihydrodiazatetracenes are stable, antiaromatic species. These compounds were characterized utilizing x-ray crystallography as well as NICS Calculations which show that the antiaromatic destabilization of the dihydropyrazine subunit was offset by the aromatic stabilization of the adjoining rings resulting in a net aromatically stabilized material.

Finally we explored the concept of functionalizing N-heteroacenes for the purpose of reducing the bandgap of these molecules. Tetrahalogenated species were able to take advantage of an unsymmetrically distributed HOMO to furnish materials which possess significantly and somewhat unexpectedly redshifted absorption and emission profiles.

Chapter 1: Introduction

1.1 Electronic Devices: Applications and Design Requirements

Electronic architectures such as photovoltaics (PVs), light emitting diodes (LEDs) and thin film transistors (TFTs) play an important role in modern electronic devices. PV solar cells are able to harness sunlight to provide clean, renewable electricity. LEDs are able to efficiently produce light and have become a popular alternative to incandescent lighting due to their lower operating cost and increased product lifetime. Recently TFTs have found use in flat panel displays, particularly for use in televisions and computer displays.

These devices are not without problems, however. These devices have historically been manufactured utilizing inorganic substrates as the semiconducting material. Depending upon the type of device being constructed, inorganic semiconductors have several manufacturing drawbacks. Oftentimes the inorganic material needs to be crystalline and requires time and energy intensive processes to be produced. Another option is vapor deposition which again requires energy to sublime the material. In addition, the semiconductor must be stable to the high temperatures required to deposit the material under vacuum. A final consideration when producing semiconductors from inorganic material is the reliance on limited mineral resources. These materials must be mined from the earth and could be inaccessible in the future either due to low abundance once need surpasses supply or due to unpredictable geopolitical conflicts.

Semiconductors which are rationally designed based on conjugated organic materials have the ability to overcome many of the limitations of inorganic based materials. Generally, the carbon building blocks are widely available and very low cost. These materials have a range of properties, but can easily be functionalized to imbue solubility. Solubilization of these materials allows for solution phase processing including drop casting and spin casting in addition to the tradition vapor deposition. Vapor deposition still requires thermally stable molecules, but generally this requirement can be met with many of the materials discussed below. The main limitation that organic materials need to overcome is the low charge carrier mobility which is a measure of how easily charge carriers (holes or electrons) move within a given material.

1.2 Acene Materials for Device Applications

For applications in organic devices, particularly thin film transistors, pentacene has shown great promise due to its processability and relatively high charge carrier mobility reaching upwards of 5.5 $cm^2V^{-1}s^{-1}$.[1,2] While pentacene has become the standard among organic semiconductors due to it intrinsic properties and synthetic simplicity, it is not without its inherent problems. The compound is prone towards oxidation and degradation upon exposure to air and light, particularly UV light.[3] Additionally, the low solubility of the unsubstituted acene precludes solution phase processing, although vapor deposition has been successfully utilized in numerous examples.[4]

A viable option that has been explored by Anthony *et al.* is substituting pentacene

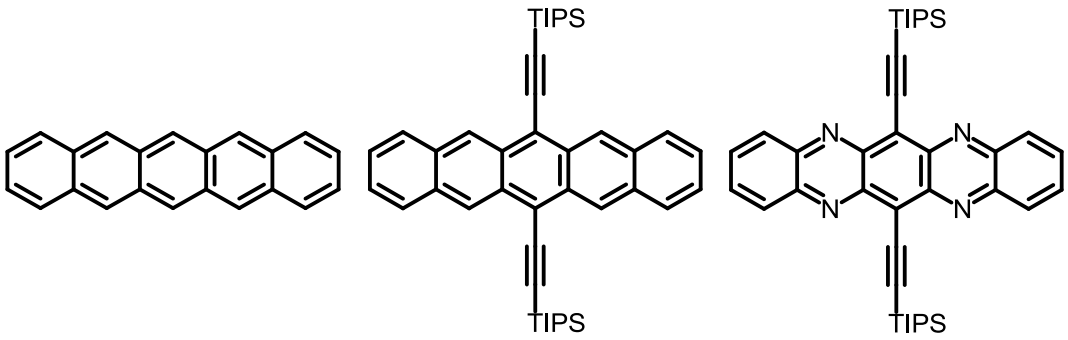

Pentacene John Anthony's TIPS Pentacene TIPS Tetraazapentacene

Figure 1.1. Stepwise development of nitrogen substituted TIPS azapentacenes.

with TIPS-alkynyl groups in oxidation prone positions. These bulky substituents increase the pentacene's stability while maintaining relatively high charge carrier mobility.[5] At the same time, the alkylsilyl groups contribute to the physical properties which show improved solubility in organic solvents and the ability to be solution processed.

Peralkynylated pentacene derivatives would be very attractive targets. However, these compounds remain unknown due to the steric crowding caused by the bulky substituents.[6] It would, however, be possible to substitute the pentacene with oxidation stable pyrazine units which would alleviate the steric crowding of the peralkynylated pentacene while maintaining the stability of the compound (Figure 1.1). These compounds would be electron rich arenes with favorable properties for use in electronic device applications such as thin-film transistors and organic light emitting diodes.

1.3 N-Heteroacenes and Acenothiadiazoles

The synthesis of N-heteroacenes can be achieved by the simple acid catalyzed condensation of an *ortho*-arylenediamine and a suitable *ortho*-dione. While in the majority of the dione species that we utilize are commercially available, alkynylated aryldiamines need to be efficiently synthesized in order to produce a wide range of potential products. Generally, unsubstituted aryldiamines can be purchased (e.g.; phenylene diamine) or can be synthesized by the Gabriel amine synthesis from the corresponding dibromoaceno-*p*-quinones.

Coupling of the alkyne to the aryldiamine utilizes either Sonogashira coupling to arylhalides or a more aggressive technique utilizing the coupling of a lithium acetylide to a quinone followed by a reduction step utilizing potassium hypophosphite and potassium iodide (Scheme 1.1). Both of these conditions require that the amino functional groups first be protected. This is easily accomplished utilizing refluxing thionyl chloride to produce a thiadiazole. Thiadiazoles are stable towards acid/base and oxidizing conditions but can be easily removed with a suitably strong reducing agent.

These acenothiadiazoles are interesting in their own right since they are an aromatic

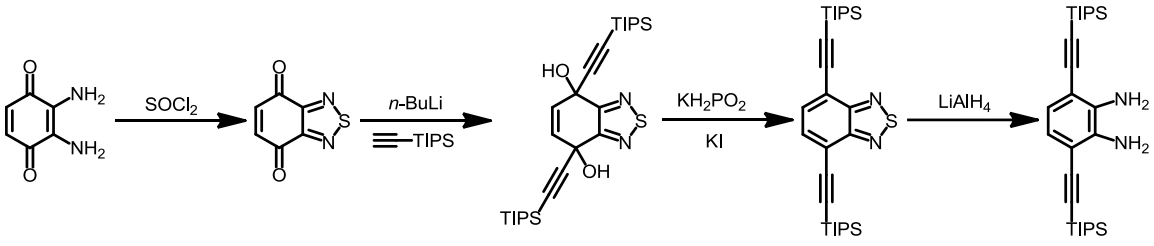

Scheme 1.1. Synthesis of diethynyl-substituted aryldiamines utilizing the benzothiadiazole group and the Bunz-Miao alkynylation procedure.

system which has exceedingly strong electron-withdrawing character. This gives rise to a unique set of photophysical behaviors that could be applicable in electronic materials, photophysical studies and sensory applications. Benzothiadiazoles have been utilized in conjugated polymers[7] as well as small molecules in order to take advantage of its electron accepting abilities, its ability to form intramolecular charge transfer (ITC) species, and it ability to produce molecules with large two photon cross-sections[8].

We envisioned that diethynylacenothiadiazoles could be utilized as a jumping off point for the synthesis of a wide array of molecules not limited to N-heteroacenes (Figure 1.2). While the larger linearly annulated acenes should provide materials with interesting

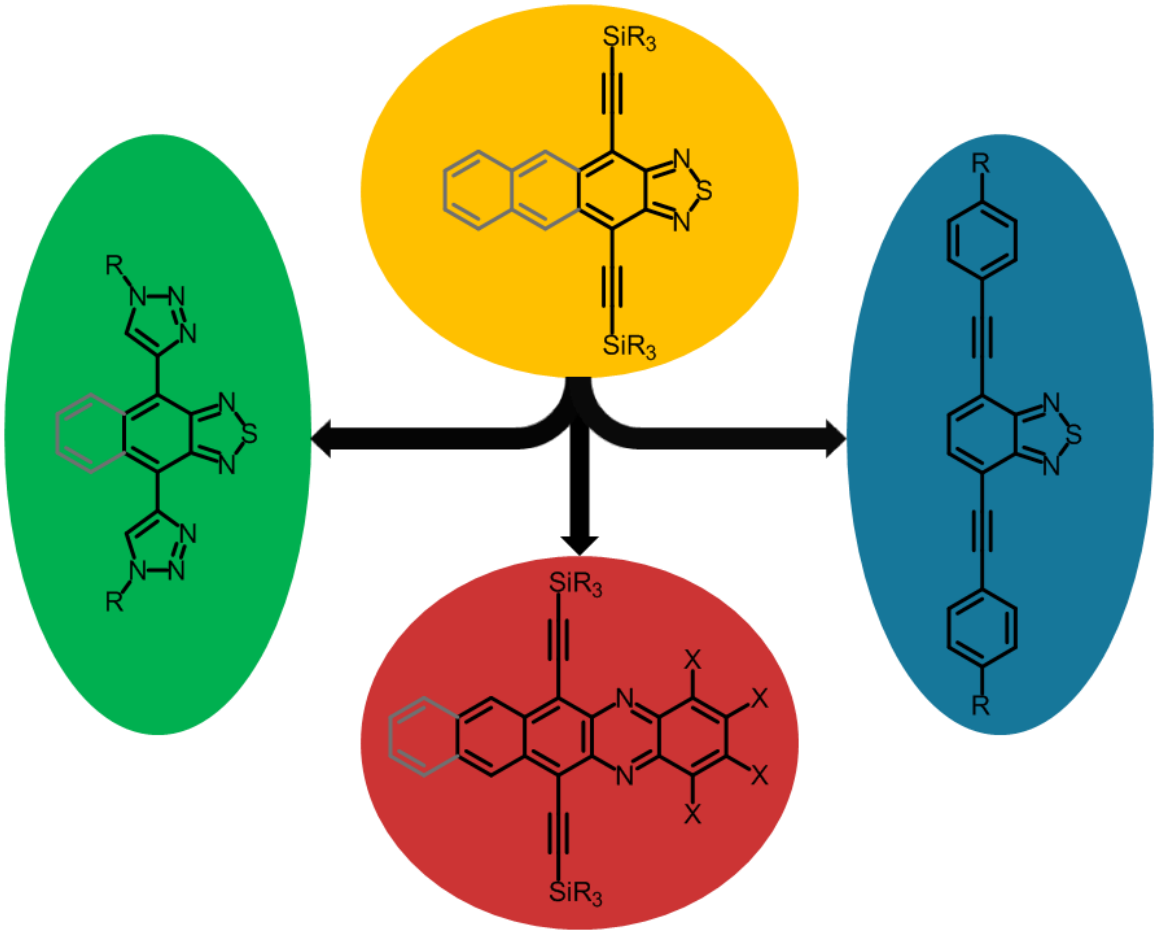

Figure 1.2. Synthetic Divergence of Acenothiadiazoles.

photophysical properties and excellent characteristics for device applications, the thiadiazoles will be able to be functionalized providing molecules which can be useful as either ratiometric sensors or model compound to probe the photophysical interactions of chromophores with their environment.

This ability to be utilized for so many varying applications is due to the many different functional handles present on the molecules. In particular the molecule can be coupled with any number of aryl halides to extend the conjugated framework utilizing Sonogashira coupling.[9] With the appropriate substitution of donor and acceptor substituents, these molecules should absorb and emit light redshifted relative to similar molecules which don't contain the thiadiazole group.

The alkynes, once deprotected, could also be substituted with any azide utilizing the copper catalyzed Huisgen-Szeimies cycloadditions.[10] These molecules should photophysically behave differently than the parent thiadiazole due to the extended conjugation. Sensory responses are expected as the triazole functional group will provide a binding site.

Lastly, the diethynylacenothiadiazoles can be used as originally envisioned by deprotecting the *ortho*-diamine and coupling with a variety of *ortho*-diones to furnish a large library of N-heteroacenes. These diazaacenes have very interesting properties including antiaromatic character as well as the ability for their absorption and emission profiles to be easily tuned.

1.4 References

[1] Horowitz, G, *J. Mater. Res.***2004**, *19,* 1946-1962.

[2] Keegstra, M.A.; DeFeyter, S.; DeSchryver, F.C.; Mullen, K. *Angew. Chem.* **1996**, *35*, 774-776.

[3] Keegstra, M.A.; DeFeyter, S.; DeSchryver, F.C.; Mullen, K. *Angew. Chem.* **1996**, *35*, 774-776.

[4] Kitamura, M.; Arakawa, Y. *J. Phys.: Condens. Matter* **2008**, *20,* 184011.

[5] (a) Odom, S.A.; Parkin, S.R.; Anthony, J.E. *Org. Lett.* **2002**, *4,* 15-18. (b) Anthony, J.E.; Brooks, J.S.; Eaton, D.L.; Parkin, S.R. *J. Am. Chem. Soc.* **2001**, *123,* 9482-9483. (c) Brooks, J.S.; Vasic, R.; Tokumoto, T.; Graf, D.; Chung, O.H.; Anthony, J.E.; Odom, S.A. *Curr. Appl.Phys.* **2004**, *4,* 479-483. (d) Sheraw, C.D.; Jackson, T.N.; Eaton, D.L.; Anthony, J.E. *Adv. Mater.* **2003**, *15,* 2009-2011.

[6] (a) Zhang, J.J.; Ho, D.M.; Pascal, R.A. *J. Am. Chem. Soc.* **1987**, *123,* 10919-10926. (b) Wenk, H.H.; Winkler, M.; Sander, W. *Angew Chem.* **2003**, *42,* 502-528.

[7] Zhou, H; Yang, L; Xiao, S; Liu, S; You, W. *Macromolecules* **2010**, *43,* 811-820.

[8] Ishi-I, T; Nakamura, N; Mine, T; Imamura, S; Shigeiwa, M; Gorohmaru, H; Maeda, S *Chemistry Letters* **2009**, *38,* 1042-1043.

[9] Sonogashira, K. J. *Organomet. Chem.* **2002**, *653*, 46-49.

[10] (a) Huisgen, R.; Szeimies, G.; Moebius, L. *Chem. Ber.* **1967**, *100*, 2494. (b) Huisgen, R.; Knorr, R.; Moebius, L.; Szeimeis, G. *Chem. Ber.* **1965**, *98*, 4014.

Chapter 2: Alkynylated Aceno[2,1,3]thiadiazoles

2.1 Introduction

As an initial step in the process of constructing N-heteroacenes, a series of acenothiadiazoles needed to be synthesized. These materials are interesting in their own right as they display attractive absorption and emission modulation, crystal packing which can be tuned for various electronic applications and could potentially have the ability to easily inject electron for use in electronic devices. Organic electronics[1] often utilize sophisticated organic synthesis, combined with processing technology, thin-film and surface science, and electrical engineering to deliver cheap, effective, and easily processable, flexible devices. While many significant advances have been made in the development of materials for organic electronics there is still a need for stable processable organic materials with high charge-carrier mobilities, in particular for electron transport materials.

For organic electronic-based devices, such as organic light-emitting diodes, thin-film

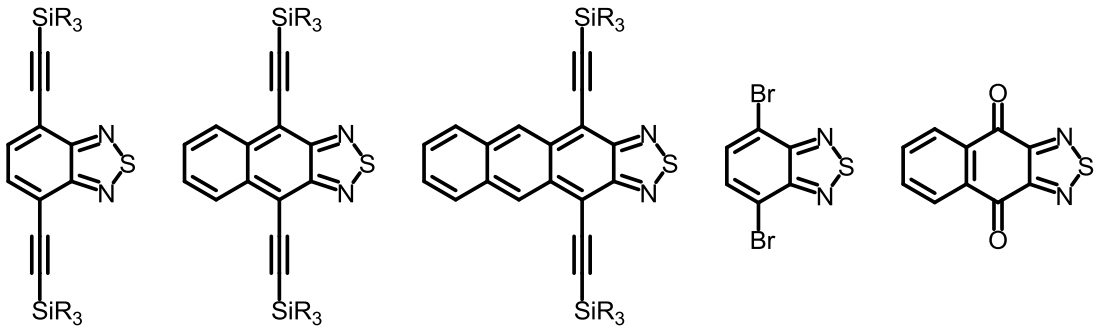

2.1 **2.2** **2.3** **2.4** **2.5**

a R = Me; **b** R = Et; **c** R = *iso*-Pr

Scheme 2.1. Structures of compounds **2.1-2.5**.

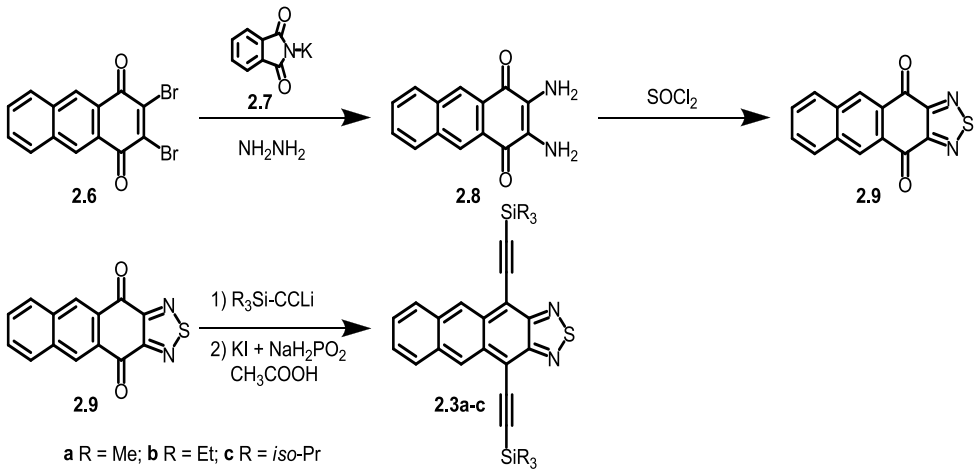

Scheme 2.2. Synthesis of **2.3a-c**.

transistors or photovoltaic cells, materials must have both the correct molecular and solid-state properties to be effective.[2,3,4] The larger acenes have had and have a significant impact in organic electronics with the hole-transporting pentacenes and rubrene (tetraphenyltetracene) being most popular. Anthony *et al.* have exploited alkynylated pentacene and thiophene-fused pentacene derivatives as easily processable materials with utility in p-channel field-effect transistors.[5]

2.2 Results and Discussion

Here, we introduce thiadiazole-based acene[6] materials[7,8,9,10] with size-dependant optical properties and with electrochemical and solid-state packing properties suggesting the potential for facile electron injection and transport. The synthesis of **2.1a-c** is achieved by Sonogashira alkynylation of **2.4**,[11] while **2.2a-c** are obtained from **2.5** in yields ranging from 11-87% in a procedure adapted from ref.[12] As derivatives of **2.3** are unknown, we started from **2.6**, which was synthesized according to a modification of the

Table 2.1. Comparison of Calculated and Measured HOMO-LUMO Gaps

Compound	HOMO[a] (eV)	LUMO (eV)	Gap (10^3 cm^{-1}) calculated	Gap (10^3 cm^{-1}) experimental[b]
2.1a	-5.90	-2.67	26.1	24.4[c]
2.2a	-5.38	-2.98	19.4	18.7
2.3a	-5.03	-3.16	15.1	15.2

[a] Obtained by SPARTAN 08/windows using the B3LYP method with the 6-31G**// 6-31G** basis set. [b] Gap obtained from the λ_{max} of absorption [c] Gap obtained from the average of λ_{max} absorption and λ_{max} emission.

procedure of Bedworth *et al.*[13] Reaction of **2.6** with potassium phthalimide (**2.7**), followed by treatment with hydrazine, afforded the diaminoquinone **2.8** in 40% yield

(Scheme 2.1). Dissolution of **2.8** in refluxing thionyl chloride forms the thiadiazole ring to give **2.9** (91%), that is then treated with suitable alkynyllithiums. After hydrolysis, the corresponding diols are directly reduced by sodium hypophosphite and potassium iodide in acetic acid to afford **2.3a-c** as blue-black crystalline materials, displaying a metallic luster in 9-92% yield after column chromatography over silica gel (hexane/dichloromethane 10:1 – 3:1). The UV-vis and emission spectra (Figure 2.1) of **2.1b-2.3b** in hexane solution provide insight into the electronic structure of the molecules.

Compound **2.1b** has a broad absorption with a maximum at 382 nm with a comparably broad emission peaking at 439 nm. In the case of **2.2b** an absorption spectrum with significant vibronic structure (λ_{max} = 530 nm) and an emission peaking at 538 nm is observed.[14] In the case of **2.3b**, the absorption is also structured with the peak absorbance at 655 nm, while the emission is centered at 659 nm and strongly 0-0 peaked. As expected, the Stokes shifts for **2.2** and **2.3** are small, due to the rigidity of the molecules; however, the small spectral band width and the occurrence of some vibronic

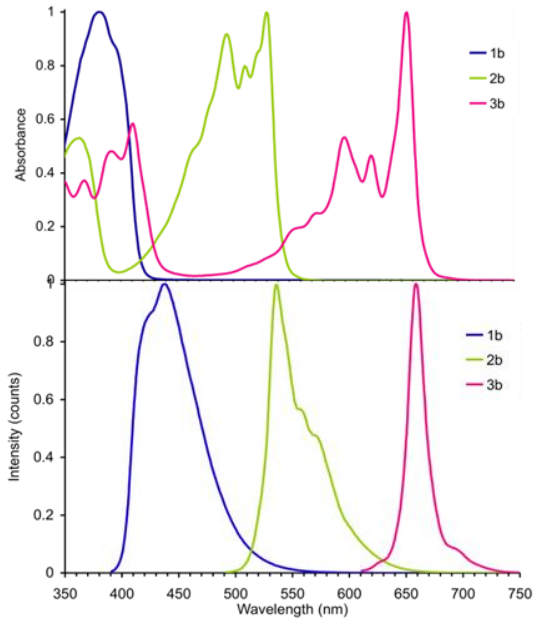

Figure 2.1. Normalized absorption (top) and emission spectra (bottom) of **2.1b**-**2.3b** in hexanes.

structure in the emission spectra are unusual when compared to the spectra of diethynylacenes of analogous structure. The experimental transition energies closely follow the trends observed in the values of the HOMO-LUMO gap obtained from quantum-chemical DFT calculations (Table 2.1); the calculations also show via the convergence of the frontier molecular orbital (FMO) positions that both the HOMO and the LUMO energy levels are shifted upon increasing the size of the acenothiadiazoles. Figure 2.2 shows the dependence of the absorption maxima, λ_{max}, of **2.1-2.3** on the number of rings in comparison to the dependences seen for Anthony's dialkynylacenes[5,7] and dialkynylacenodithiophenes.[14] Naphthothiadiazole **2.2**, which contains a total of three rings, displays similar optical properties to the four-ring tetracenes and the five-ring acenodithiophenes, while **2.3** has a similar absorption maximum as a dialkynylated pentacene and the 6-ring based acenodithiophenes.

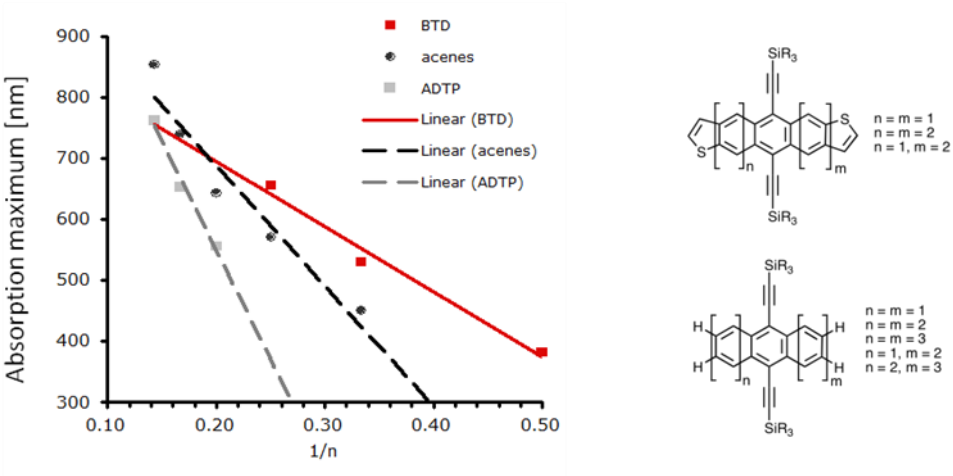

Figure 2.2. Plot of the absorption maxima versus 1/n, with n being the number of rings in a specific class of compounds. BTD: acenothiadiazoles **2.1**-**2.3**. Acenes: 9,10-bis(trimethylsilylethynyl)-anthracene, bis(trialkylsilylethynyl)tetracene, -pentacene, -hexacene, and -heptacene.[5,7] ADTP: bis(trialkylsilylethynyl)acenodithiophenes.[13]

The reason for the increased auxochromic effect of the annulated thiadiazole ring in comparison to a benzene or thiophene is the enforced quinoidal character of **2.3**, resulting in an absence of resonance structures that one can draw for **2.3** that contains an aromatic sextet. A similar observation has been made by Wudl *et al.* in the case of the isoquinolones.[15]

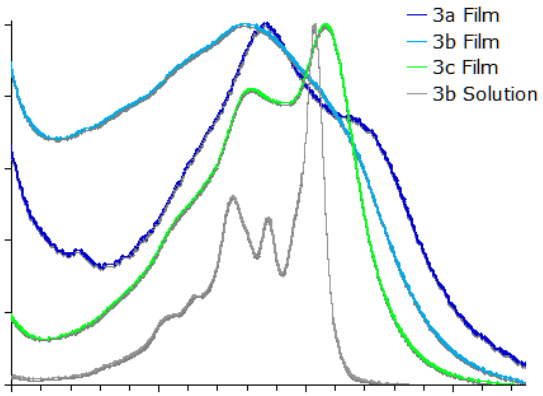

Figure 2.3. Normalized absorption spectra of **2.3b** in hexanes and of **2.3a-c** in thin films.

The ease of oxidation and reduction of **2.3** was investigated using cyclic voltammetry of **2.3c** in dichloromethane / 0.1 M $^{n}Bu_4NPF_6$; one reversible oxidation (+0.74 V vs. ferrocene) and two reversible reductions (-1.18 V, -1.78 V) were observed. The electrochemical "band gap" of 1.92 eV (≡ 646 nm) is in surprisingly good agreement with the UV-vis data absorption maximum and with the HOMO-LUMO gap obtained from quantum chemical calculations. The reduction potential of **2.3c** is similar to that for a four-ring dialkynyldiazatetracenes (-1.2 V)[12] and close to those for perylene diimides (ca. -1.0 V), which are a well-established class of materials for n-channel field-effect transistors, indicating the possibility of facile electron injection into **2.3**. On the other hand, a large barrier to hole injection from typical electrode materials is anticipated. The thin-film UV-vis spectra of **2.3a-c** are shown in Figure 2.3. Films of **2.3c** are amorphous and show spectra somewhat broadened and with the absorption maximum shifting ca. 10 nm relative to its solution spectrum, but retaining a similar vibronic envelope, suggesting relatively minor intermolecular interactions in the solid state. On the other hand, films of **2.3a** and **2.3b**, which are microcrystalline, exhibit very different spectra from those seen in solution, being much broader with the strongest feature blue-shifted relative to the solution maximum and with a weaker low-energy feature. In both cases the spectra suggest significant intramolecular interaction of the π-systems in the solid state. Single crystal X-ray analyses of **2.3a** and **2.3b** (Figures 2.4, 2.5) reveal π-stacking columns with intrastack intermolecular distances of 3.4 Å; this type of intermolecular interaction is similar to that of H aggregates and is consistent with blue-shifts of the most intense features in the UV-vis spectra. In the case of **2.3a** the π-systems of adjacent columns are

isolated, while in **2.3b** adjacent columns interact via S···N interactions. Noticeable is the absence of intercolumn π–π, a hallmark of the diethynylacenes[14] and heteroacenes.[12]

The π-stacking seen in the structures of **2.3a** and **2.3b** may also be promising for high intrastack electron and/or hole mobility; if films of the materials can be grown with appropriately aligned stacks, these materials may, therefore, be useful in thin-film transistors or photovoltaic cells.

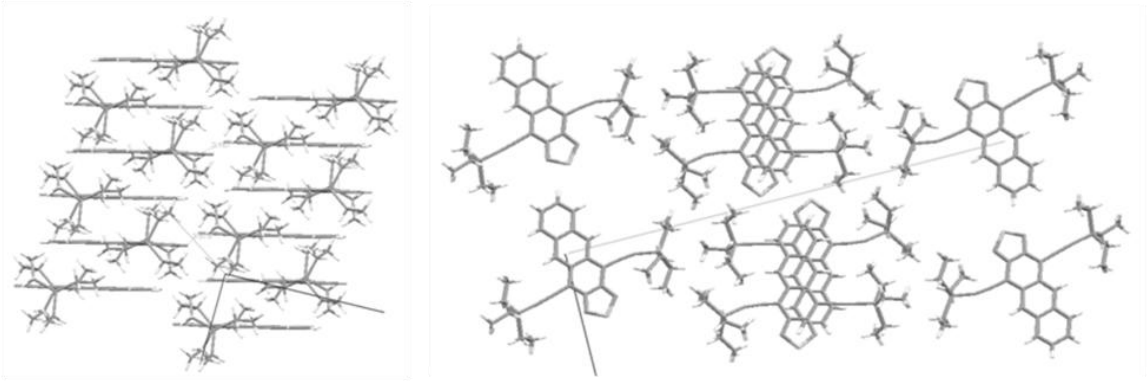

Figure 2.4. Packing of **2.3b.** The molecules pack in stacks that are connected by supramolecular S-N interactions, and in which the intrastack π-stacking distance in a single column is 3.4 Å.

2.3 Conclusion

In conclusion, we have prepared a series of acenothiadiazoles, of which the three largest members **2.3a-c** were hitherto unknown. In relation to their size, **2.1-2.3** display small band gaps. Films of **2.3** have absorptions that could be interesting for use in photovoltaic systems. The solid-state packing of **2.3** can be manipulated by different alkyne-substituents; the π-stacking seen in the structures of **2.3b-c** combined with

electrochemical data suggest that these materials may serve as electron-transport counterparts of alkynylated pentacene derivatives.

This work has been published in *Organic Letters*:

Appleton, Anthony Lucas; Miao, Shaobin; Brombosz, Scott M.; Berger, Nancy J.; Barlow, Stephen; Marder, Seth R.; Hardcastle, Kenneth I.; Bunz, Uwe H. F. *Organic Letters*, 2009, **11**, 5222-5225.

2.4 Experimental and Supplementary Information

2.4.1 4,7-Bis((trimethylsilyl)ethynyl)benzo[*c*][1,2,5]thiadiazole, **2.1a**.

To an oven-dried Schlenk flask was added dry THF (20 mL) and triethylamine (20 mL), which was then vacuum degassed three times. 4,7-dibromobenzo[*c*][1,2,5]thiadiazole **2.4** (1.43 g, 4.86 mmol), trimethylsilylacetylene (2.13 mL, 15.0 mmol), copper(I) iodide (9.26 mg, 0.05 mmol), and bis(triphenylphosphine)palladium(II) chloride (35.10 mg, 0.05 mmol) were all added at room temperature. The Schlenk flask was sealed and heated to 80°C, whereupon the solution was stirred for 12 h. After the reaction was cooled to room temperature, water (200 mL) was added to the mixture and the aqueous solution was extracted with dichloromethane (2 x 100mL). The combined organic layers were washed with water (3 x 200mL), dried with magnesium sulfate, filtered, and dried *in vacuo*. The residue was purified by column chromatography on silica gel using pure hexane. Compound **2.1a** (0.70 g, 45% yield) was isolated as yellow crystals. m.p. = 104°C. **2.1a**: IR (ATR, cm^{-1}) 3050, 2955, 2898, 2370, 2331, 2151, 1876, 1487, 1356, 1337, 1252, 1165. ^{1}H-NMR (δ in $CDCl_3$): 7.692 (s, 2H), 0.323 (s, 18H). ^{13}C-NMR (δ in $CDCl_3$): 154.201, 133.124, 117.245, 103.618, 99.974, -0.136. Accurate mass for $C_{16}H_{20}N_2SSi_2$: m/e = 328.09065 [M^+], calc. m/e = 328.09008.

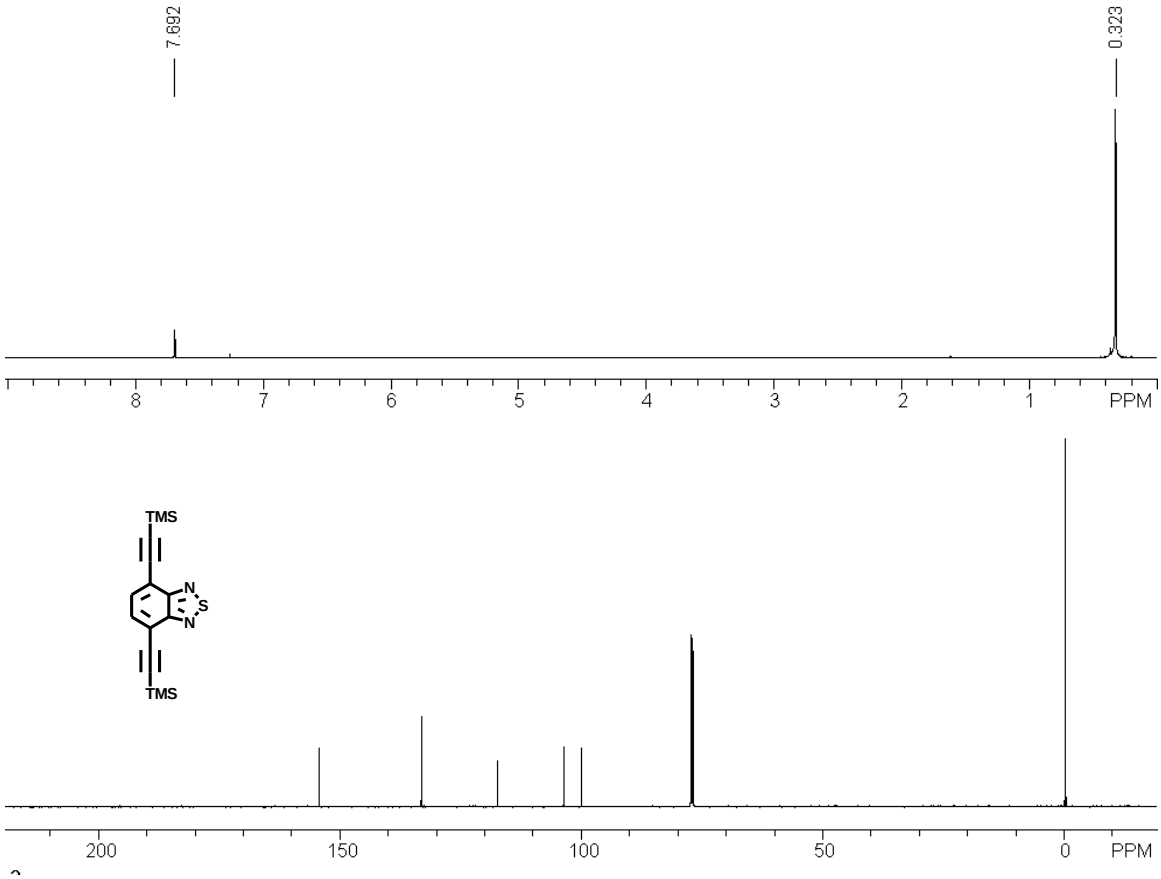

Figure 2.5. ^{1}H (top) and ^{13}C (bottom) NMR of **2.1a** with structure inset

2.4.2 4,7-Bis((triethylsilyl)ethynyl)benzo[*c*][1,2,5]thiadiazole, **2.1b**.

In a procedure identical to that of **2.1a**, **2.1b** was synthesized in 33% yield and isolated as yellow crystals. m.p. = 35-37 ^{o}C. **2.1b**: IR (ATR, cm^{-1}) 3054, 2972, 2954, 2922, 2899, 2796, 2730, 2681, 2635, 2586, 2197, 2147, 1866, 1231, 1169. ^{1}H-NMR (δ in $CDCl_3$): 7.693 (s, 2H), 1.100 (t, 18H), 0.754 (q, 12H). ^{13}C-NMR (δ in $CDCl_3$): 154.403, 132.942, 117.339, 101.354, 101.269, 7.471, 4.331. Accurate mass for $C_{22}H_{32}N_2SSi_2$: m/e = 412.18351 [M^+], calc. m/e = 412.18398.

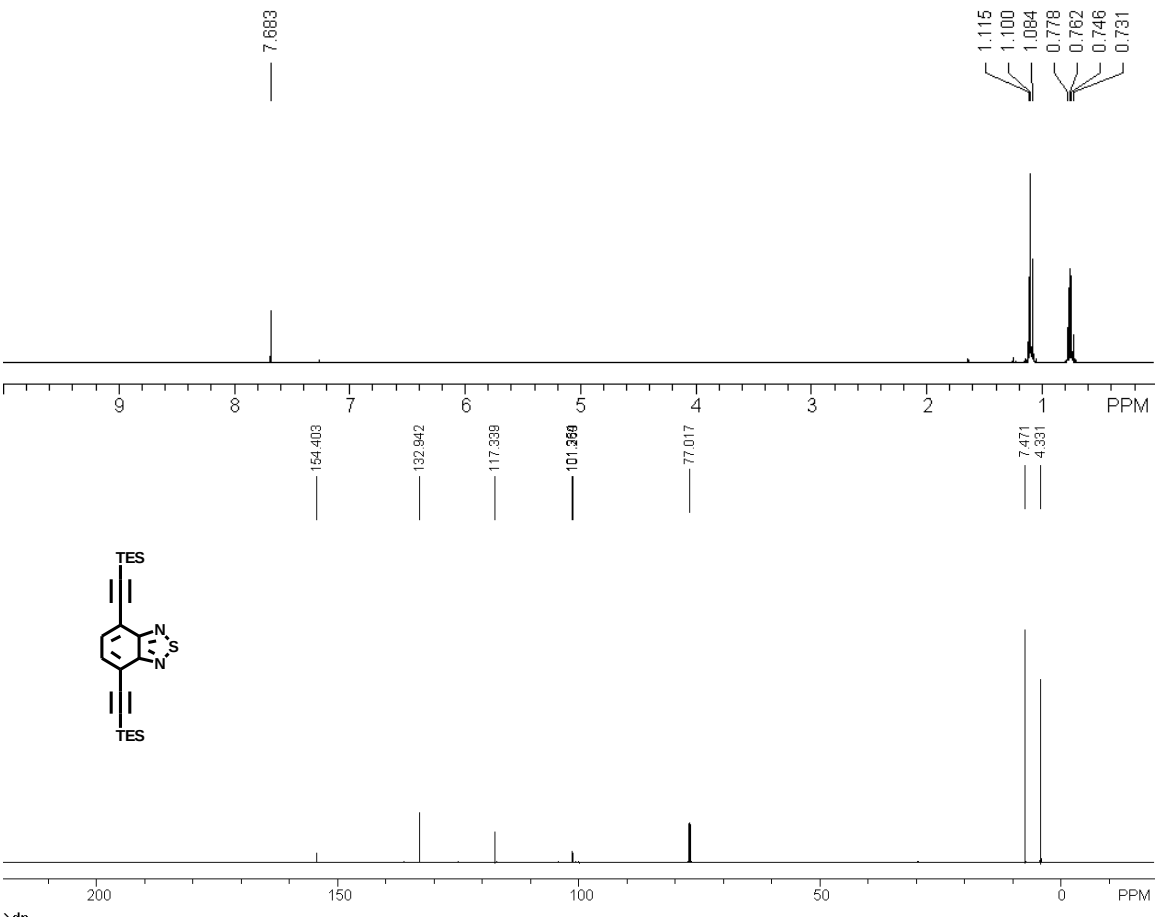

Figure 2.6. ^{1}H (top) and ^{13}C (bottom) NMR of **2.1b** with structure inset

2.4.3 4,7-Bis((triisopropylsilyl)ethynyl)benzo[*c*][1,2,5]thiadiazole, **2.1c**.

In a procedure identical to **2.1a**, **2.1c** was synthesized in 47% yield and isolated as yellow crystals. m.p. = 135°C. **2.1c**: IR (ATR, cm^{-1}) 3048, 2971, 2950, 2890, 2759, 2718, 2619, 2149, 1880, 1694, 1261, 1168. ^{1}H-NMR (δ in $CDCl_3$) 7.677 (s, 2H), 1.196 (m, 42H). ^{13}C-NMR (δ in $CDCl_3$) 154.621, 132.647, 117.446, 102.252, 100.205, 18.692, 11.325. Accurate mass for $C_{28}H_{44}N_2SSi_2$: m/e = 496.27511 [M^+], calc. m/e = 496.27554.

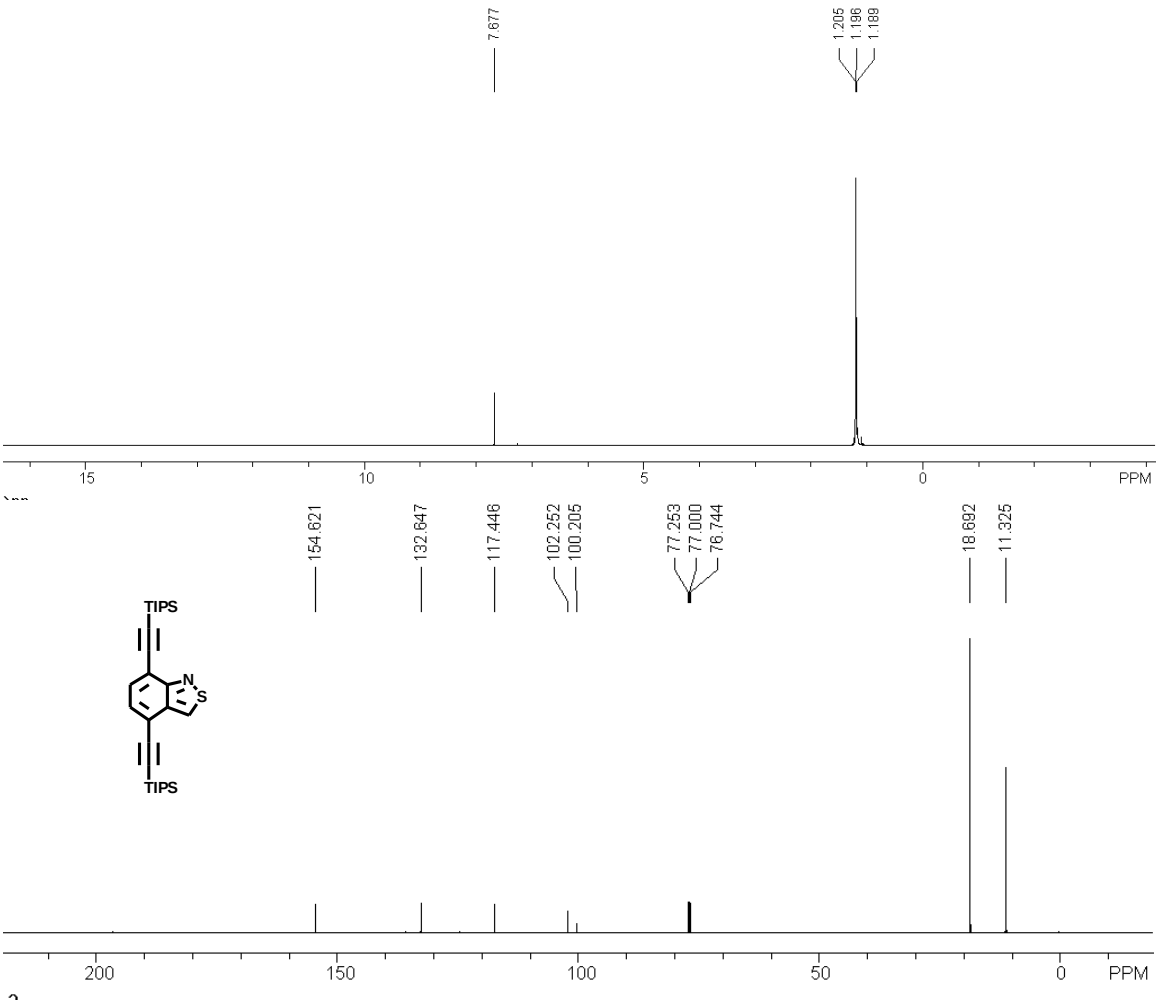

Figure 2.7. ^{1}H (top) and ^{13}C (bottom) NMR of **2.1c** with structure inset

2.4.4 4,9-Bis(trimethylsilylethynyl)naphtho[2,3-c][1,2,5]thiadiazole, **2.2a**.

To an oven-dried Schlenk flask was added trimethylsilylacetylene (1.65 mL, 11.6 mmol) and dry THF (10 mL), followed by 1.6 M n-butyllithium in hexane (5.70 mL, 9.12 mmol) at 0 °C. The solution was stirred at room temperature for 1 h, and then compound naphtho[2,3-*c*][1,2,5]thiadiazole-4,9-dione (0.500 g, 2.31 mmol) was added to the solution. The mixture was stirred at ambient temperature for 12 h and then quenched with wet diethyl ether. After evaporation of the solvent, the residue was filtered over silica gel

using hexane/ethyl acetate (v/v, 5:1) to yield the corresponding diol. After the solvent was evaporated, the crude diol was, without further characterization, suspended in acetic acid (20 mL) and potassium iodide (3.80 g, 22.9 mmol) and NaH_2PO_2 (2.00 g, 22.8 mmol) were added. The mixture was heated to reflux for 1 h. After cooling to room temperature, water (100 mL) was added to the mixture and the aqueous solution was extracted with hexanes (3 x 100 mL). The combined organic layers were dried *in vacuo*. The solids were further purified by chromatography on silica gel using a hexane/CH_2Cl_2 (v/v, 6:1) solvent mixture. Compound **2.2a** (0.10 g, 11% yield, two steps) was isolated as a red crystalline solid. m.p. = 214-223 °C (Decompose). **2.2a**: IR (ATR, cm^{-1}) 3073, 3037, 2956, 2917, 2914, 2898, 2846, 2785, 2652, 2536, 2475, 2186, 2136, 2009, 1937, 1816, 1538, 1385, 13281279, 1251, 1163, 1142. ^{1}H-NMR (δ in $CDCl_3$) 8.498 (dd, 2H), 7.577 (dd, 2H), 0.420 (s, 18H). ^{13}C-NMR (δ in $CDCl_3$) 152.626, 135.244, 128.101, 127.556, 112.668 110.662, 99.558, 0.073. Accurate mass for $C_{20}H_{22}N_2SSi_2$: *m*/*e* = 378.10601 [M^+], calc. *m*/*e* = 378.10573.

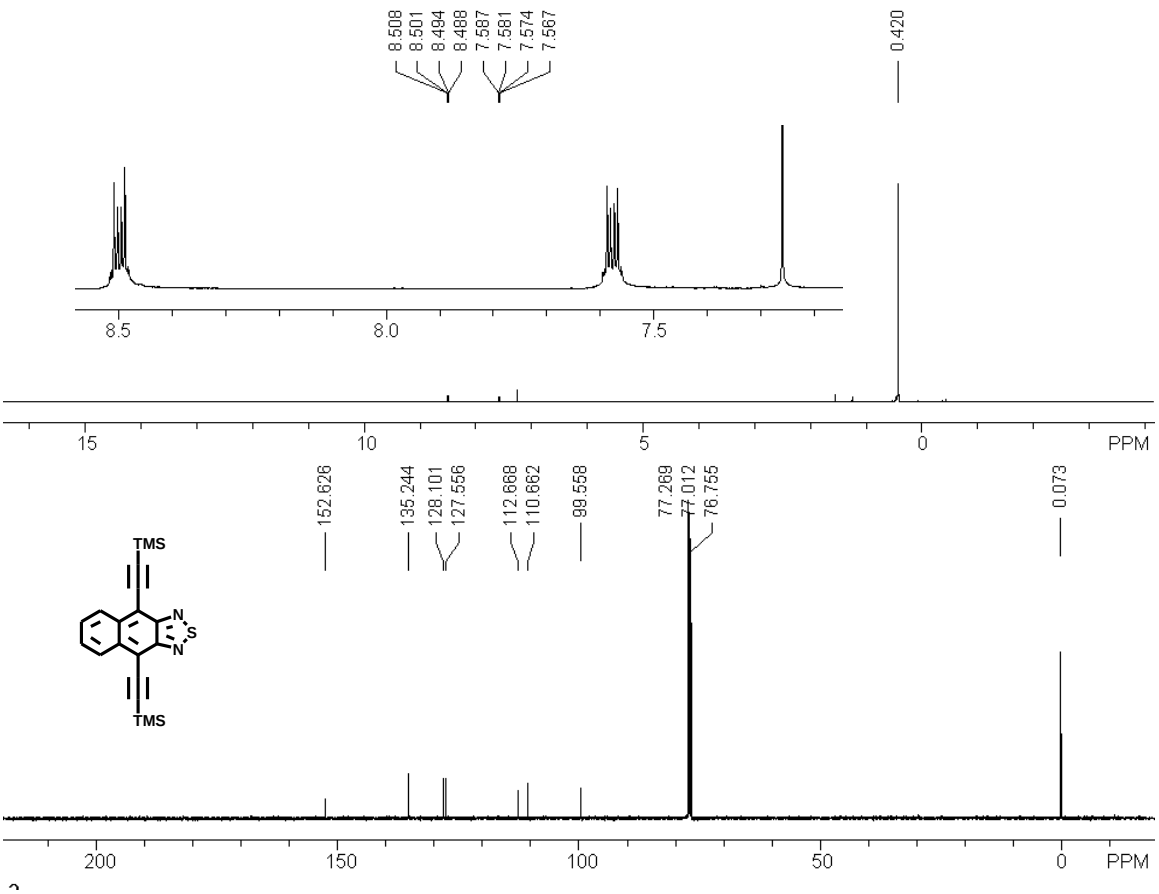

Figure 2.8. ^{1}H (top) and ^{13}C (bottom) NMR of **2.2a** with structure inset

2.4.5 4,9-Bis(triethylsilylethynyl)naphtho[2,3-c][1,2,5]thiadiazole, **2.2b**.

In a procedure identical to **2.2a**, **2.2b** was synthesized in 61 % yield and isolated as a red crystalline solid. m.p. = 113 °C (decompose). **2.2b**: IR (KBr, cm^{-1}) 2954, 2873, 2132, 1534, 1457, 1383, 1237, 1041, 973, 924, 742, 726. ^{1}H-NMR (δ in $CDCl_3$) 8.55-8.52 (q, 2H), 7.58-7.55(q, 2H), 1.20-1.16 (t, 18H), 0.88-0.82 (q, 12H). ^{13}C-NMR (δ in $CDCl_3$) 152.86, 135.12, 127.93, 127.54, 112.76, 108.35, 100.78, 7.67, 4.48. Accurate mass for $C_{26}H_{34}N_2SSi_2$: *m/e* = 462.19902 [M^+], calc. *m/e* = 462.19813.

2.4.6 4,9-bis(triisopropylsilylethynyl)naphtho[2,3-c][1,2,5]thiadiazole, **2.2c**.

In a procedure identical to **2.2a**, **2.2c** was synthesized in 87% yield and isolated as red crystals. m.p. = 181 °C. **2.2c**: IR (KBr, cm^{-1}) 2943, 2863, 2136, 1533, 1458, 1387, 1241, 1041, 925, 882, 767, 734. ^{1}H-NMR (δ in $CDCl_3$) 8.58-8.56 (q, 2H), 7.57-7.55(q, 2H), 1.28-1.27 (m, 42H). ^{13}C-NMR (δ in $CDCl_3$) 153.20, 135.05, 127.81, 127.56, 112.89, 107.36, 101.64, 18.82, 11.44. Accurate mass for $C_{32}H_{46}N_2SSi_2$: *m*/*e* = 546.28598 [M^+], calc. *m*/*e* = 546.29203.

2.4.7 2,3-Diaminoanthracene-1,4-dione, **2.8**.

A mixture of 2,3-dibromo-1,4-anthraquinone **2.6** (14.0 g, 0.0382 mol) and potassium phthalimide **2.7** (14.9 g, 0.0804 mol) in DMF (50 mL) was heated at 120 ºC for 18 h. Upon completion of the reaction water (500 mL) was added to the reaction vessel. The mixture was filtered. The precipitates were washed with water until no color was apparent in the filtrate. The yellowish solid was collected and dried *in vacuo*. The yellowish solid and NH_2NH_2 (15.0 mL) were suspended in water (50 mL) and stirred at 80 ºC for 24 h. The mixture was filtered and the precipitates were washed with water (3 x 100 mL), and dried *in vacuo*. 2,3-Diaminoanthracene-1,4-dione **2.8** was obtained as a dark-brown solid (2.80 g, 31% yield, two steps). ^{1}H-NMR (δ in DMSO-d_6): 8.317 (s, 2H), 8.104 (dd, 2H), 7.630 (dd, 2H), 5.700 (s, 4H). Due to a lack of solubility, only the proton NMR was attainable.

2.4.8 Anthra[2,3-*c*][1,2,5]thiadiazole-4,11-dione, **2.9**.

A mixture of 2,3-diamino-anthracene-1,4-dione **2.8** (2.40 g, 0.0101 mol) in $SOCl_2$ (15 mL) was refluxed for 12 h. The solvent was removed *in vacuo*. The residue was separated by a column on silica gel using CH_2Cl_2 as the solvent. The anthra[2,3-

c][1,2,5]thiadiazole-4,11-dione **2.9** was yielded as the yellow solid (2.10 g, 78%). m.p. = 296–298 ^{o}C. IR (KBr, cm^{-1}) 3633.64, 3355.91, 3062.75, 3020.32, 2688.58, 2538.15, 2410.85, 2183.27, 1974.97, 1874.68, 1685.67, 1616.24, 1585.38, 1411.80, 1234.36, 975.91, 833.19, 775.33, 524.6. ^{1}H-NMR (δ in $CDCl_3$): 9.178 (s, 2H), 8.339 (dd, 2H), 7.979 (dd, 2H). ^{13}C-NMR (δ in $CDCl_3$): 176.35, 157.27, 135.39, 131.77, 130.69, 130.49, 129.66. Accurate mass for $C_{14}H_6N_2O_2S$: *m*/*e* = 266.01434 [M^+], calc. *m*/*e* = 266.01500.

2.4.9 4,11-Bis(trimethylsilylethynyl)anthra[2,3-*c*][1,2,5]thiadiazole, **2.3a**.

To an oven-dried Schlenk flask was added trimethylsilylacetylene (1.33 mL, 9.39 mmol) and dry THF (10 mL), followed by 1.6 M n-butyllithium in hexane (4.69 mL, 7.49 mmol) at 0 °C. The solution was stirred at room temperature for 1 h, and then compound **2.9** (0.500 g, 1.89 mmol) was added to the solution. The mixture was stirred at ambient temperature for 12 h and then quenched with wet diethyl ether. After evaporation of the solvent, the residue was filtered over silica gel using hexane/ethyl acetate (v/v, 5:1) to yield the corresponding diol. After the solvent was evaporated, the crude diol **2.9a** was, without further characterization, suspended in acetic acid (20 mL) with KI (1.30 g, 7.83 mmol) and NaH_2PO_2 (0.690 g, 7.84 mmol). The mixture was heated to reflux for 30 min. After cooling to room temperature, H_2O (100 mL) was added to the mixture and the aqueous solution was extracted with hexanes (3 x 100 mL). The combined organic layers were dried *in vacuo*. The solids were further purified by chromatography on silica gel using a hexane/CH_2Cl_2 (v/v, 10:1) solvent mixture. Compound **2.3a** (0.066 g, 9% yield, two steps) was isolated as dark-blue crystals. **2.3a**: m.p. = 175-180 ^{o}C. IR (KBr Plate, cm^{-1}) 3440, 2959, 2924, 2854, 2357, 2125, 1678, 1647, 1454, 1369, 1246, 1092, 1014, 841, 802, 760, 741, 698. ^{1}H-NMR (δ in $CDCl_3$) 9.115 (s, 2H), 7.971 (dd, 2H), 7.438 (dd, 2H),

0.495 (s, 18H). ^{13}C-NMR (δ in $CDCl_3$) 152.408, 133.126, 132.552, 128.558, 126.954, 126.669, 112.137, 112.109, 100.544, 0.119. Accurate mass for $C_{24}H_{24}N_2SSi_2$: *m*/*e* = 428.11978 [M^+], calc. *m*/*e* = 428.11981.

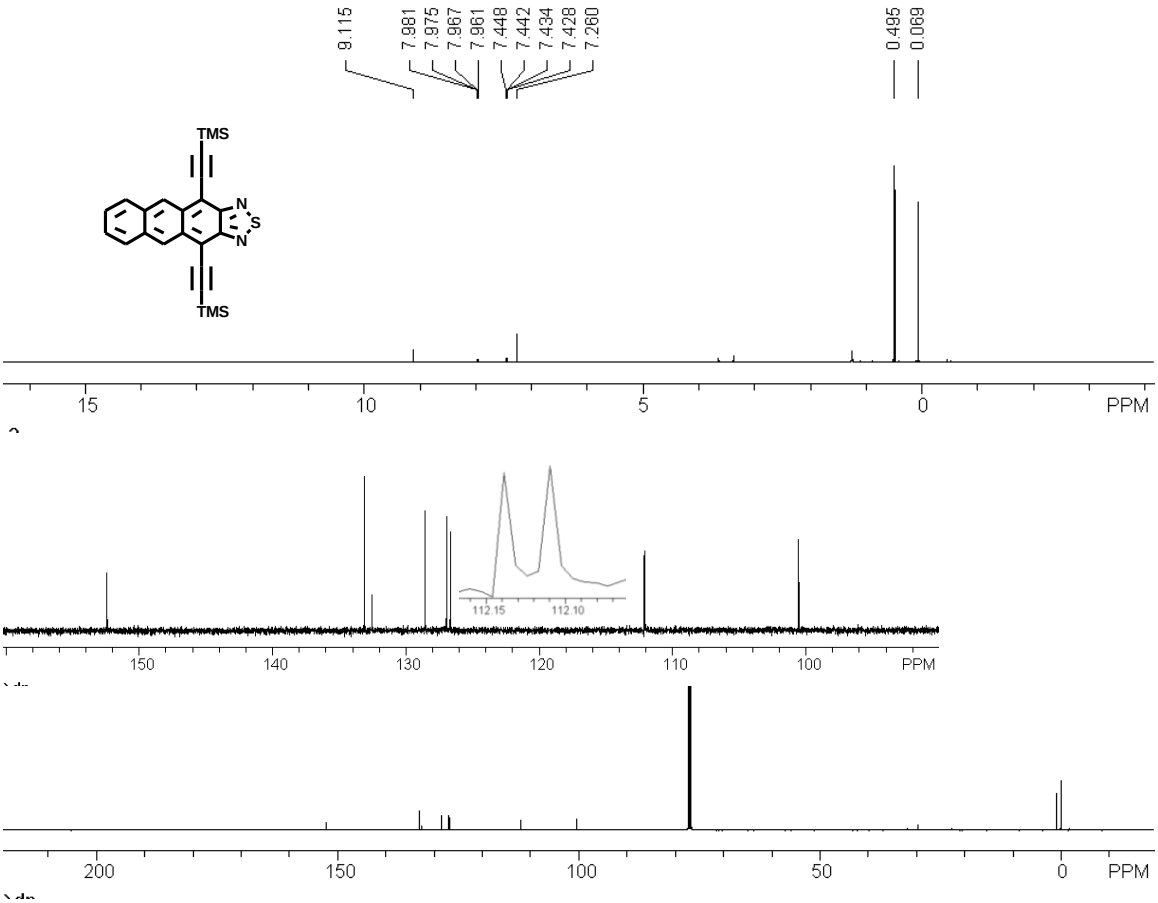

Figure 2.9. ^{1}H (top) and ^{13}C (bottom) NMR of **2.3a** with structure inset

2.4.10 4,11-Bis(triethylsilylethynyl)anthra[2,3-*c*][1,2,5]thiadiazole, **2.3b**.

In a procedure identical to **2.3a**, **2.3b** was synthesized in 18% yield and isolated as dark-blue crystals. m.p. = 139 °C (decompose). **2.3b**: IR (ATR, cm^{-1}) 3048, 2954, 2878, 2807, 2729, 2691, 2639, 2155, 2117, 1923, 1891, 1787, 1374, 1299, 1267, 1228, 1184, 1148, 1136. ^{1}H-NMR (δ in $CDCl_3$): 9.174 (s, 2H), 7.93 (dd, 2H), 7.413 (dd, 2H), 1.248 (t,

18H), 0.918 (q, 12H). ^{13}C-NMR (δ in $CDCl_3$): 152.646, 133.069, 132.563, 128.520, 126.850, 126.702, 112.241, 109.858, 101.812, 7.741, 4.588. Accurate mass for $C_{30}H_{36}N_2SSi_2$: *m*/*e* = 512.20859 [M^+], calc. *m*/*e* = 512.20795.

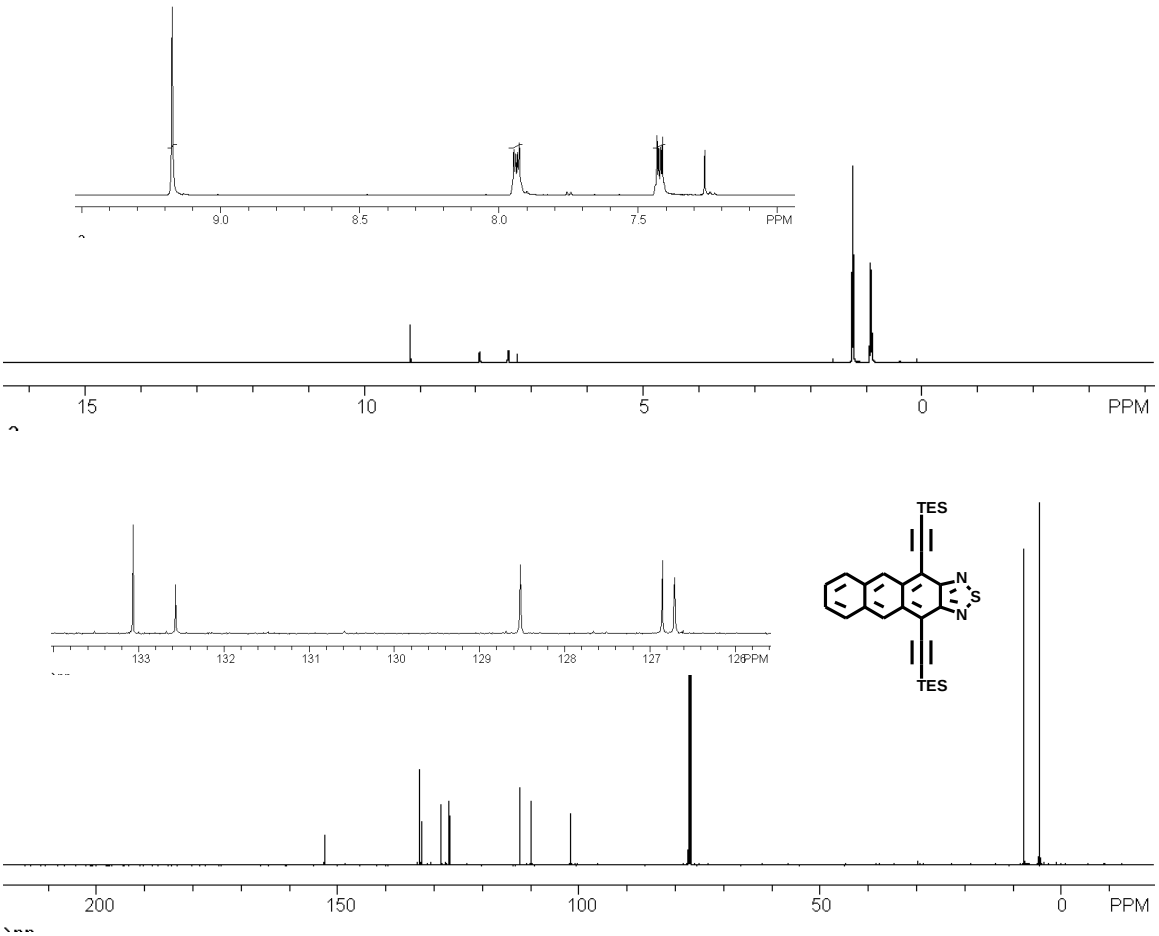

Figure 2.10. ^{1}H (top) and ^{13}C (bottom) NMR of **2.3b** with structure inset

2.4.11 4,11-Bis(triisopropylsilylethynyl)anthra[2,3-*c*][1,2,5]thiadiazole, **2.3c**.

In a procedure identical to **2.3a**, **2.3c** was synthesized in 92% yield and isolated as dark-blue crystals. m.p. = 172-174 °C (decompose). **2.3c**: IR (KBr, cm^{-1}) 2941, 2863, 2122, 1526, 1462, 1373, 1069, 1013, 993, 879, 734, 672. ^{1}H-NMR (δ in $CDCl_3$) 9.23 (s, 2H),

7.94-7.91 (q, 2H), 7.44-7.41 (q, 2H), 1.32-1.31 (m, 42H). ^{13}C-NMR (δ in $CDCl_3$) 152.93, 133.02, 132.63, 128.54, 126.80, 126.78, 112.34, 108.87, 102.61, 18.90, 11.53. Accurate mass for $C_{36}H_{48}N_2SSi_2$: *m*/*e* = 596.30700 [M^+], calc. *m*/*e* = 596.30768.

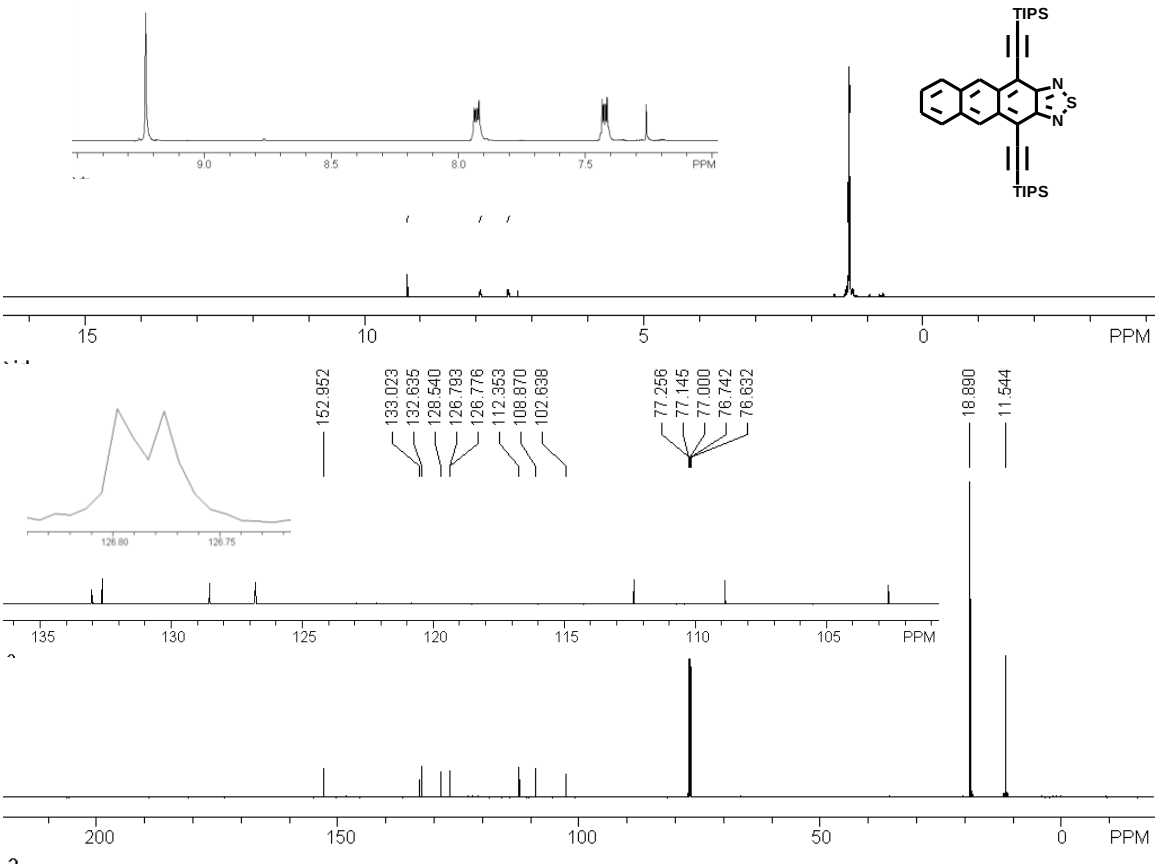

Figure 2.11. ^{1}H (top) and ^{13}C (bottom) NMR of **2.3c** with structure inset

2.4.12 Spectroscopic Characterization Data of **2.1a-2.3c**.

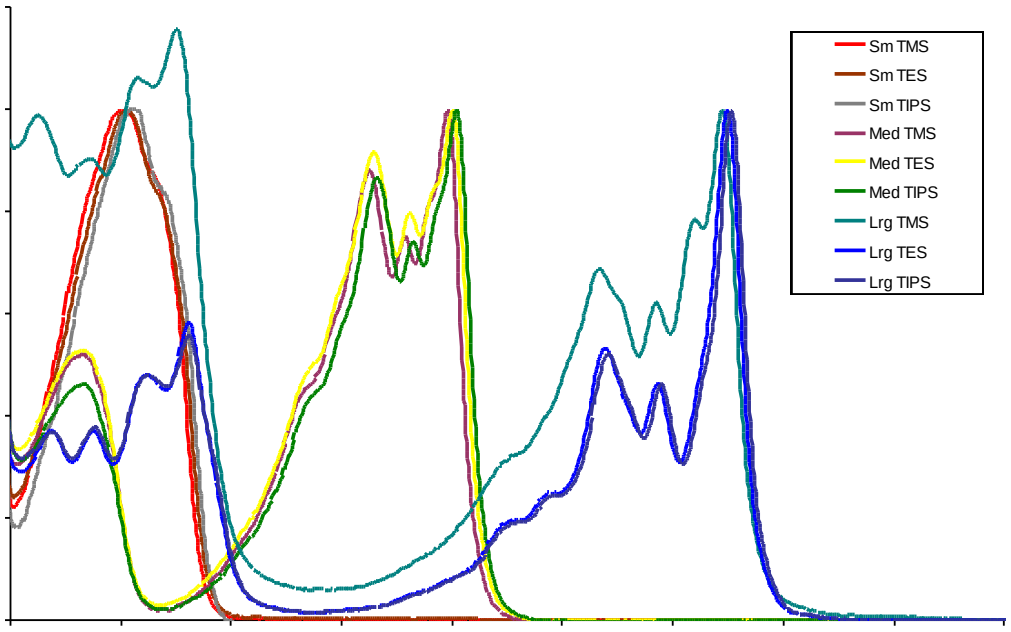

Figure 2.12. Absorption spectra of compounds **2.1a-2.3c**

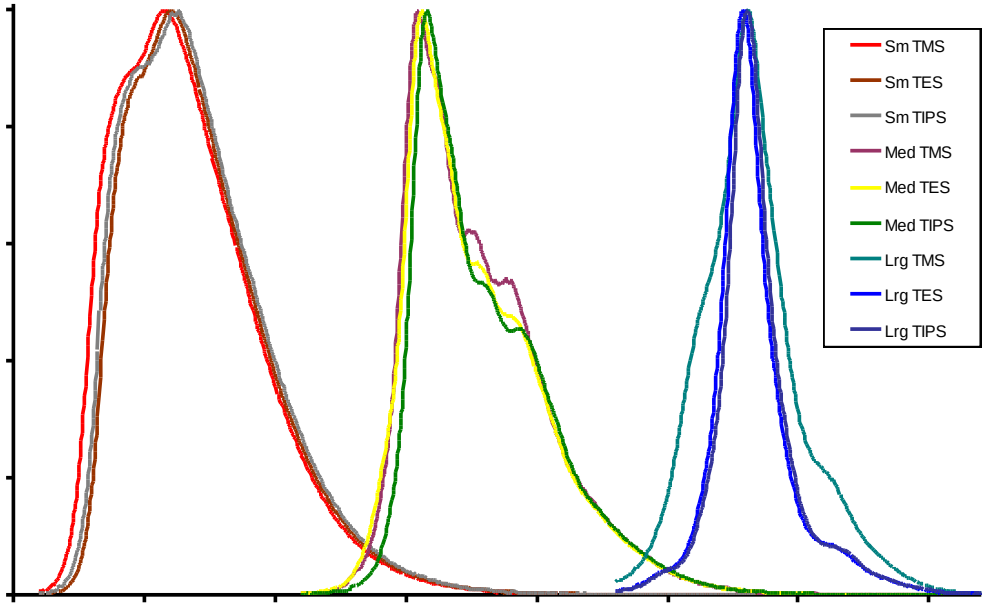

Figure 2.13. Emission spectra of compounds **2.1a-2.3c**

2.5 References

[1] (a) Forrest, S. R.; *Nature* **2004**, *428*, 911. (b) Bao, Z. N.; ACS Symp. Ser. **2004**, *874*, 1.

[2] (a) Neher, D. Adv. *Mater*. **1995**, *7*, 691. (b) Gross, M.; Müller, D. C.; Nothofer, H. G.; Scherf, U.; Neher, D.; Bräuchle, C.; Meerholz, K. *Nature*, **2000**, *405*, 661-665. (c) Kraft, A.; Grimsdale, A. C.; Holmes, A. B. *Angew. Chem. Int. Ed. Engl.* **1998**, *37*, 402.

[3] (a) Katz, H. E.; Bao, Z. N.; Gilat, S. L. *Acc. Chem. Res*. **2001**, *34*, 359. (b) Dimitrakopoulos, C. D.; Malenfant, P. R. L. *Adv. Mater.* **2002**, *14*, 99. (c) Duan, X. F.; Niu, C. M.; Sahi, V.; Chen, J.; Parce, J. W.; Empedocles, S.; Goldman, J. L. *Nature* **2003**, *425*, 274.

[4] (a) Spanggaard, H.; Krebs, F. C. *Solar Cells* **2004**, *83*, 125. (b) Hoppe, H.; Sariciftci, N. S. *J. Mater. Res.* **2004**, *19*, 1924. (c) Gunes, S.; Neugebauer, H.; Sariciftci, N. S. *Chem. Rev.* **2007**, *107*, 1324.

[5] (a) Anthony, J. E. *Angew. Chem. Int. Ed.* **2008**, *47*, 452. (b) Anthony, J. E. in Functional Organic Materials (Müller, T. J. J.; Bunz, U. H. F. Eds), Wiley-VCH, Weinheim 2007, Chapter 14, pp 511-546. (c) Anthony, J. E. *Chem. Rev.* **2006**, *106*, 5028-5048.

[6] Miao, Q.; Nguyen, T. Q.; Someya, T.; Blanchet, G. B.; Nuckolls, C. *J. Am. Chem. Soc.* **2007**, *125*, 10284.

[7] Swartz, C. R.; Parkin, S. R.; Bullock, J. E.; Anthony, J. E.; Mayer, A. C.; Malliaras, G. G. *Org. Lett*. **2005**, *7*, 3163.

[8] (a) Wudl, F.; Koutentis, P. A.; Weitz, A.; Ma, B.; Strassner, T.; Houk, K. N.; Khan S. I., *Pure Appl. Chem.* **1999**, *71*, 295-302. (b) Hutchison, K.; Srdanov, G.; Hicks, R.; Yu, H. N.; Wudl, F.; Strassner, T.; Nendel, M.; Houk, K. N. *J. Am. Chem. Soc.* **2001**, *120*, 2989. (c) Winkler, M.; Houk, K. N. *J. Am. Chem. Soc.* **2007**, *129*, 1805.

[9] (a) Usta, H.; Facchetti, A.; Marks, T. J. *J. Am. Chem. Soc.* **2007**, *130*, 8580. (b) Wang, Z.; Kim, C.; Facchetti, A.; Marks, T. J. *J. Am. Chem. Soc.* **2007**, *129*, 13362. (c) Yoon, M. H.; Facchetti, A.; Stern, C. E.; Marks, T. J. *J. Am. Chem. Soc.* **2006**, *128*, 5792. (d) Yoon, M. H.; DiBenedetto, S. A.; Facchetti, A.; Marks, T. J. *J. Am. Chem. Soc.* **2005**, *127*, 1348.

[10] (a) Babel, A.; Jenekhe, S. A. *J. Am. Chem. Soc.* **2003**, *125*, 13656. (b) Jenekhe, S. A.; Yi, S. J. *Appl. Phys. Lett.* **2000**, *77*, 2635. (c) Babel, A.; Zhu, Y.; Cheng, K. F.; Chen, W. C.; Jenekhe, S. A. *Adv. Funct. Mater. 17*, **2007**, 2542.

[11] Bangcuyo, C. G.; Evans, U.; Myrick, M. L.; Bunz, U. H. F. *Macromolecules* **2001**, *34*, 7592.

[12] (a) Miao, S.; Brombosz, S. M.; Schleyer, P. v. R.; Wu, J. I.; Barlow, S.; Marder, S. R.; Hardcastle, K. I.; Bunz, U. H. F. *J. Am. Chem. Soc.* **2008**, *130*, 7339. (b) Miao, S.; Appleton, A. L.; Berger, N.; Barlow, S.; Marder, S. R.; Hardcastle, K. I.; Bunz, U. H. F. *Chem. Eur. J.* **2009**, *20*, 5222-5225.

[13] (a) Barranco, E.; Martin, N.; Segura, J. L.; Seoane, C.; de la Cruz, P.; Langa, F.; Gonzalez, A.; Pingarron, J. M. *Tetrahedron* **1993**, *49*, 4881. (b) Bedworth, P. V.; Perry, J. W.; Marder, S. R. *Chem. Commun.* **1997**, 1353.

[14] Payne, M. M.; Odom, S. A.; Parkin, S. R.; Anthony, J. E. *Org. Lett.* **2004**, *6*, 3325.

[15] Bendikov, M.; Wudl, F.; Perepichka, D. F. *Chem. Rev.* **2004**, *104*, 4891, see ref. 406.

Chapter 3: Acidochromicity of Bisarylethynylbenzenes: Hydroxy versus Dialkylamino Substituents

3.1 Introduction

It can easily be seen that the free ethynyl groups in the acenothiadiazoles discussed in the previous section could be used as a handle for functionalization to produce responsive fluorophores. In the subsequent section, we will discuss the synthesis and characterization of dibutylamino and hydroxy substituted bis(arylethynyl)benzothiadiazoles. However, it is prudent to first examine the more simple example of substituted bis(arylethynyl)benzenes in order to fully understand the effects seen in these systems before exploring the more complicated systems.

Reactive chromophores or fluorophores change color, emission wavelength, and/or emission intensity upon exposure to analytes and are potentially useful as sensors. They contain a chromophoric π-conjugated core with embedded functionality possessing free electron pairs before or after addition of an analyte.[1] The interaction of the free electron pairs of functional fluorophores with suitable analytes or stimuli influences the position of the HOMO, LUMO, or both and elicits changes in absorption and emission.

The concept of isolobality of molecules was set forth by Hoffmann[2] and contends that molecules of similar Frontier Molecular Orbital (FMO) structure and geometry display similar reactivity and properties. One should be able to use the isolobal principle to predict – at least qualitatively – the expected responses of classes of

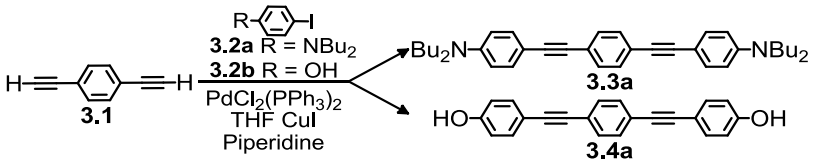

Scheme 3.1. Synthesis of compounds **3.3a** and **3.4a** via Sonogashira coupling of substituted *p*-iodobenzenes **3.2a-b**

consanguine fluorophores towards change of pH or metal coordination. Superficially, one might expect hydroxy substituents should be isolobal to amino groups. However, a simple application of the isolobal principle will not always suffice in such organic systems, as the relative orbital ordering results in systems where (in a formal sense) free electron pairs interact predominately with either the σ- or the π-system. If the free electron pairs are energetically low lying, we expect them to interact predominately with the σ-system, while energetically higher lying electron pairs should have a larger interaction with the π-system.

A simple test bed for this hypothesis would be compounds **3.3a** and **3.4a**, bis(arylethynyl)benzenes functionalized with dibutylamino and hydroxy groups respectively. Though synthetically simple, their sensory responses have not been examined. Comparison of **3.3a** and **3.4a** with their analogous distyrylbenzenes **3.5a** and **3.6a** permit the expansion of this study to investigate differences that arise when alkenyl groups are exchanged for alkynyl groups. Probing the acidochromicity and photophysical properties of **3.3a**-**3.6a** should offer insight into the application of the isolobal principle and provide an understanding of fundamental physical-organic issues in these systems.

3.2 Results and Discussion

Distyrylbenzene compounds **3.5a** and **3.6a** were synthesized according to literature procedures.[3,4] Surprisingly, **3.4a**[5] has been reported only once and **3.3a** is unreported, although the dimethyl[6] and dihexyl[7] substituted compounds are known. Heck-Cassar-Sonogashira-Hagihara (HCSH) coupling of **3.2a** to **3.1** furnishes **3.3a**. Similarly, **3.4a** was synthesized from the HCSH coupling of **3.2b** with **3.1** (Scheme 1).[8] Upon protonation with trifluoroacetic acid or deprotonation with tetrabutylammonium hydroxide, compounds **3.3b**, **3.4b**, **3.5b** and **3.6b** are obtained.

For ease of discussion, isolobal pairs have been placed into sets (**A**-**D**, Figures 3.1, 3.2). These compounds were examined through UV-vis and fluorescence spectroscopy (dilute solutions in diethyl ether, 1,4-dioxane, chloroform, dichloromethane, methanol, ethanol, isopropanol, *tert*-butyl alcohol, acetonitrile, dimethylformamide, and dimethylsulfoxide; see Section 3.4.2 and Figure 3.2).

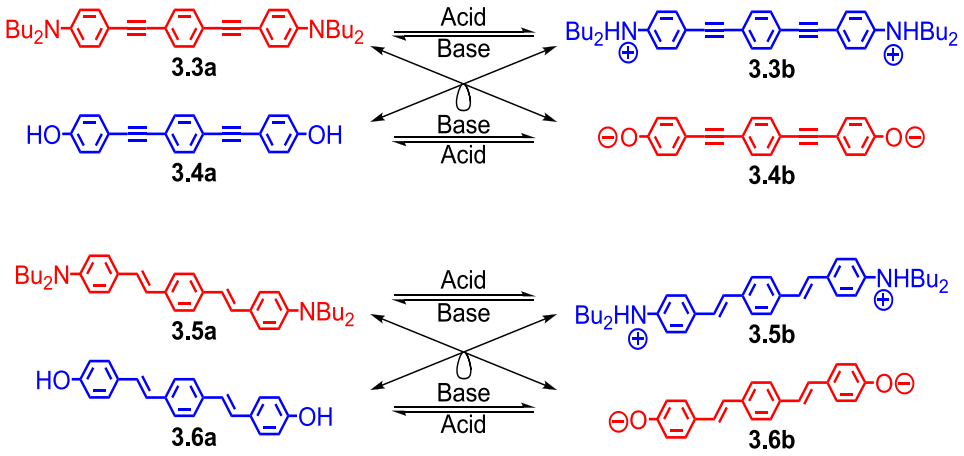

Figure 3.1. Acid/Base equilibrium relationships of **3.3a**-**3.6b** are shown. Diagonal isoelectronic relationships are indicated.

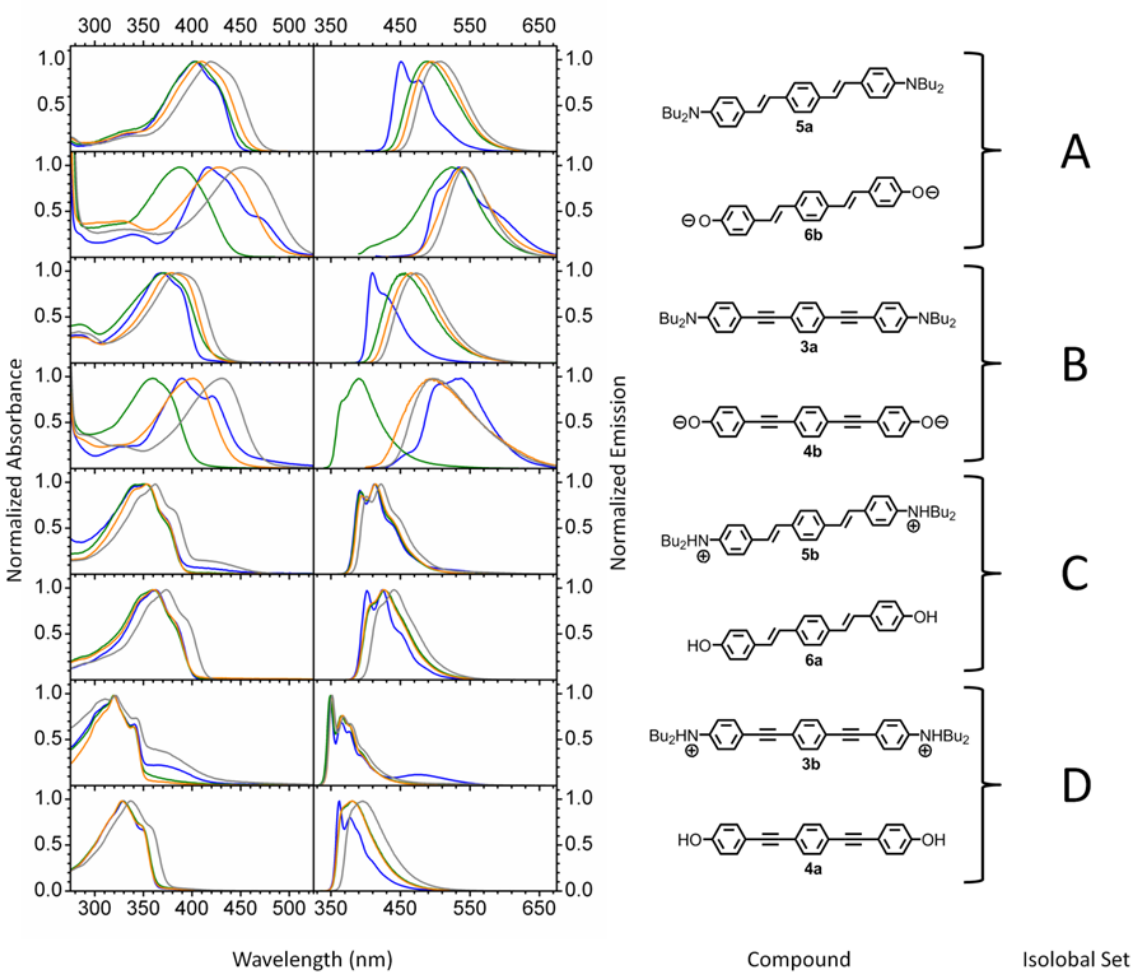

Figure 3.2. Absorption (left) and emission (right) spectra of **3.3a**-**3.6b** in diethyl ether (blue), methanol (green), acetonitrile (orange) and dimethylsulfoxide (grey). Compounds are grouped by electronic structure into isolobal sets **A**-**D** (far right).

Figure 3.2 displays the absorption and emission of sets **A**-**D** in four representative solvents to permit a qualitative examination of solvent effects upon each compound. Diethyl ether, methanol, acetonitrile and dimethylsulfoxide were chosen because they represent non-polar, polar protic, and polar aprotic solvents. In the case of sets **C** and **D**, with the exception of **3.4a** in the very polar solvent DMSO, the absorption spectra for both compounds are nearly each superimposable in a range of solvents. The absorption spectra of **3.3b** and **3.4a** are only ~10 nm apart and display similar

vibronic features. Similarities are also observed in the emission spectra of set **D**; **3.3b** displays nearly overlapped, highly structured emissions in a range of solvents. **3.4a** exhibits a similarly featured emission in diethyl ether; however, as solvent polarity increases, the vibronic features give way to a broadened, smooth lineshape. Once again, the emission λ_{max} of **3.4a** is similar to that of **3.3b**. Set **C** behaves in a nearly identical fashion to **D**; however, the absorption and emission spectra are red-shifted approximately by 30 and 40 nm, respectively. In sets **C** and **D**, the chromophores lack available lone pairs; as a result, we would expect little solvent dependence in their absorption or emission λ_{max}. Furthermore, the isolobal principle suggests all four chromophores should exhibit similar photophysical properties. Indeed, this is what is observed.

Surprising differences were observed in sets **A** and **B**, where the chromophores possess available lone pairs. The isolobal principle predicts that pairs **3.5a** and **3.6b** and **3.3a** and **3.4b** should exhibit similar photophysical properties; furthermore, we expect sets **A** and **B** to behave in a similar fashion. While sets **A** and **B** are similar, differences appear in the pairs **3.5a** and **3.6b** and **3.3a** and **3.4b**. In the case of dibutylamino-functionalized **3.5a** and **3.3a**, the absorption spectra in variety of solvents are similarly featured and exhibit a minimal (~25 nm) solvent dependence. Greater solvent dependence is observed in the emission spectra. The emission of **3.5a** and **3.3a** in ether is highly featured; as solvent polarity increases, the emission is redshifted (~60 nm) and vibronic definition disappears.

In **3.6b** and **3.4b**, methanol exhibits the highest energy absorption, and dramatic solvent dependence (~80 nm) is observed in the absorption maxima. Divergence is

also observed in the emission spectra. The emission of **3.6b** and **3.4b** in diethyl ether is considerably redshifted relative to their alkylamino counterparts (~80-100 nm). Little solvent dependence is observed in the emission of **3.6b** (~20 nm), while in the case of **3.4b**, a large solvent effect is seen. Here, the emission of **3.4b** varies by more than 150 nm, ranging from MeOH at lowest energy to ether at highest energy.

The compounds in sets **C** and **D** behave as isolobal pairs; however, the surprising lack of 'isolobality' in the case of **A** and **B** requires an explanation. Previously, we have analyzed solvent dependent absorption and emission spectra of similar compounds utilizing the Lippert-Mataga equation:[4a] A solvent's dielectric constant and refractive index are used to calculate an orientation polarizability value (Δf) for a given solvent; Δf is then plotted against the energy of the Stokes shift for each measured solvent.[9] Generally, a linear plot is obtained with the magnitude of the slope reflecting the change in a fluorophore's dipole moment upon excitation.

A Lippert-Mataga analysis of **3.3a**-**3.6b** proved difficult; whereas the dibutylamino compounds (**3.3a**, **3.3b**, **3.5a**, and **3.5b**) were well correlated, the phenolic compounds (**3.4a**, **3.4b**, **3.6a**, and **3.6b**) showed no meaningful relationship. The Lippert-Mataga equation only considers non-specific effects related to solvent reorganization. Solvent-fluorophore interactions may, however, play a critical role in understanding the behavior of the phenolates.

We subjected **3.3a**-**3.6b** to a Kamlet-Taft (KT) solvent analysis accounting for solvent-specific interactions due to hydrogen bonding or acid/base reactions.[10] KT relies on a multivariate linear regression analysis of the absorption λ_{max} of a chromophore in a variety of solvents (Eq. 3.1).

Eq 3.1. Kamlet-Taft multivariate approach:

$$\nu\,(1000/\mathrm{cm}) = \nu_0 + s \cdot \pi^* + a \cdot \alpha + b \cdot \beta$$

The KT approach correlates the solvent-dependent spectral shifts observed (ν) for a chromophore with three solvent-dependent parameters (α, β, and π*). Here, ν_0 corresponds to the absorption or emission energy of the chromophore in a vacuum while *s*, *a*, and *b* are fitted coefficients obtained from the linear regression analysis. The index π* expresses the ability of the solvent to stabilize the chromophore's charge and/or dipole via nonspecific dielectric interactions. α and β incorporate solvent-solute interactions; β describes the proton accepting character of the solvent while α corresponds to the hydrogen donating character of the solvent. By analyzing the coefficients, it is possible to determine the degree to which each mode of interaction (α, β, and π*) affect the absorption λ_{max} of a chromophore.

Table 3.1 shows the results of the Kamlet-Taft analysis. The calculated ν_0 values range from 25.1 to 31.2 x 10^3 cm^{-1}; the compounds within isolobal set **A** have similar

Table 3.1. Coefficient Values Obtained from Kamlet-Taft Analysis

	A		**B**		**C**		**D**	
Compound	**3.5a**	**3.6b**	**3.3a**	**3.4b**	**3.5b**	**3.6a**	**3.3b**	**3.4a**
ν_0 [a]	25.1	25.4	27.4	26.8	28.8	27.9	31.2	30.7
s	-1.2	-1.4	-1.5	-2.5	-0.76	-0.76	-0.26	-0.52
a	0.29	2.7	0.17	2.9	0.60	0.52	-0.07	0.32
b	0.16	-2.7	0.14	-1.5	-0.63	-0.31	0.30	-0.55
R [b]	0.95	0.90	0.95	0.80	0.83	0.77	0.58	0.80

[a] Units of ν_0 are in 10^3 cm^{-1}. [b] R is the correlation coefficient.

ν_0 values as do those in sets **B**, **C** and **D**. As one would expect, the values of ν_0 for the styryl isolobal set **A** are slightly lower, indicating a redshift in the gas phase absorption relative to their arylethynyl congeners in set **B**. The same relationship holds true for the styryl compounds in **C** relative to their arylethynyl analogues in **D**. The *s* coefficient of the π^* term reflects the contribution of nonspecific dielectric interactions of the solvent with the fluorophore and is somewhat analogous to the slope obtained from a Lippert-Mataga analysis; it is related to the fluorophore's dipole. In all cases, this term is negative, inducing a spectral redshift. Isolobal pairs behave similarly and as we would expect. In sets **C** and **D**, electron pairs are involved in proton bonding. As a consequence, *s* is less significant, suggesting a smaller dipole. In sets **A** and **B**, where free electron pairs are more available, *s* is larger, suggesting a greater dipole.

The *a* and *b* coefficients for the isolobal sets **C** and **D** are modest. The lack of available free electron pairs results in minimal solvent-specific interaction. Similarly, in the case of dibutylamino compounds **3.3a** and **3.5a**, the *a* and *b* values are also relatively small. The *s* term is the predominant influence on the observed absorption. However, in the case of the deprotonated phenols **3.4b** and **3.6b**, *a* and *b* become significant, with *a* inducing a hypsochromic shift and *b* resulting in a bathochromic shift. This results in the divergent photophysical behavior observed in **3.4b** and **3.6b** relative to their isolobal counterparts.

Why is this pronounced solvent effect observed exclusively in **3.4b** and **3.6b** and not in their isolobal counterparts **3.3a** and **3.5a**? One might attribute this differential behavior to the increased basicity of a phenolate ($pK_a \sim 10$) as compared to a

Table 3.2. Selected Photophysical Data of Compounds **3a-6b** in CH_3CN

	A		**B**		**C**		**D**	
Compound	**3.5a**	**3.6b**	**3.3a**	**3.4b**	**3.5b**	**3.6a**	**3.3b**	**3.4a**
λ_{max} Absorption (nm)	410	431	378	408	353	364	321	328
λ_{max} Emission (nm)	494	542	466	496	414	426	351	380
ε ($M^{-1}\cdot cm^{-1}$)	7774	17515	6799	9632	4712	24191	6089	10230
Φ	0.60[a]	0.13	0.51	<0.01	0.73[a]	0.43	0.54	0.43

[a] Previously reported in reference 4a.

dialkylamino group ($pK_a \sim 6.6$).[1] A look into the Hammett σ-values[11] is instructive, as here the σ-values of $-O^-$, $-N(C_3H_7)_2$, -OH and $-NMe_2H^+$ are $\sigma = -0.81$, $\sigma = -0.93$, $\sigma = -0.37$, and $\sigma \approx 0.70$.[12] The Hammett values testify to the apparent electronic similarity of the phenolate to the dialkylamino groups but of course do not take into account the hydrogen bonding contributions that will undoubtedly be much stronger in the case of a phenolate than in a neutral amine. More surprising is the similarity of the spectroscopic properties of the phenols and the ammonium salts (where hydrogen bonding apparently does not play a significant role), given the larger differences in their respective Hammett parameters. While the correlation with Hammet σ_p-parameters is appealing and grossly correct, they clearly cannot explain the subtleties in this interesting system.

An important additional point is the quantum yields of these eight compounds, which we determined in acetonitrile. Generally, in the pairs **A** and **B**, the aniline always has a significantly higher quantum yield than the phenolate. In the case of **3.4b**, the quantum yield is below 0.01. For the pairs **C** and **D**, the differences are

much smaller and the quantum yields are generally quite substantial. In both cases, the ammonium species display a higher quantum yield than the phenols. The differences in the quantum yields are somewhat intransparent, as it is often observed, the only rough trend is that the higher the emission wavelength, the lower the emission quantum yield is; a notable exception is **3.4b** with its vanishing emission. Generally, the amines do better with respect to emission quantum yield than the phenols and phenolates, for subtle reasons that are not easily divined.

3.3 Conclusions

We examined the photophysical properties and acidochromicity of hydroxy- and dibutylamino-functionalized distyrylbenzenes and arylethynylbenzenes. While sets **C** and **D** exhibit similar photophysical behavior as expected, and do not possess effective lone pairs, sets **A** and **B** – possessing lone pairs that interact effectively with the π-system of the fluorophore– show different behavior in absorption and emission. These differences stem from fluorophore-solvent interactions which disproportionally affect the phenolate-substituted dyes.

The true electronic similarity of **3.3a**-**3.6b** can be appreciated when viewing their absorption and emission in acetonitrile – a solvent possessing small and similar α and β parameters (Figure 3.3, Table 3.2). The contribution of solute-specific effects is minimized; the isolobal similarity of **A** and **B** as well as **C** and **D** becomes readily apparent. This highlights the fact that although the phenolate and dibutylamino groups are isolobal, the difference in their pK_as and the presence of the ionic phenolate results in

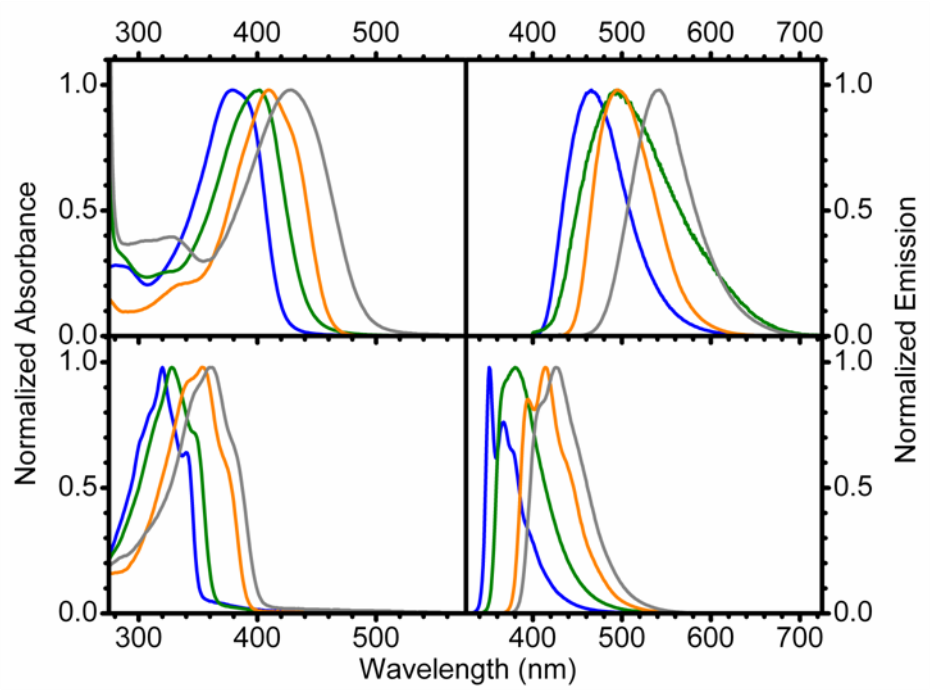

Figure 3.3. Absorption (left) and emission (right) spectra of **3.3a-3.6b** in acetonitrile. Top: **3.3a** (blue), **3.4b** (green), **3.5a** (orange), **3.6b** (grey). Bottom: **3.3b** (blue), **3.4a** (green), **3.5b** (orange), **3.6a** (grey).

dyes that are electronically isolobal but which behave very differently in practice particularly in hydrogen bonding solvents.

An interesting and somewhat unexpected is the finding that free electron pairs in the hydroxy compounds **3.4a** and **3.6a** are *not* available for conjugation with the π-system. Apparently, these electrons are too low in energy to permit efficient interaction. The other, somewhat expected trend is that dyes containing alkene bridges display redshifted spectral features when compared to analogous fluorophores featuring alkyne groups. While the gas phase absorption is redshifted in all of the alkene compounds relative to the corresponding alkyne compounds, the degree to which a solvent effects the absorption of a molecule is nearly identical among an alkene-alkyne pair as can be seen through similar values of *s*, *a*, and *b*.

This work has been published in *The Journal of Organic Chemistry*:

Brombosz, Scott M.; Zucchero, Anthony J.; McGrier, Psaras L.; Bunz, Uwe H. F. *Journal of Organic Chemistry*, **2009**, *74*, 8909-8913.

3.4 Experimental and Supplementary Information

3.4.1 4,4'-(1,4-Phenylenebis(ethyne-2,1-diyl))bis(N,N-dibutylaniline), **3.3a**.

To a stirring solution of 0.150 g of 1,4-diethynylbenzene (**3.1**) (1.19 mmol, 1 eq.) in 10 mL of degassed THF/Piperidine (3:1 v/v) under nitrogen was added 0.867 g of **3.2a** (2.62 mmol, 2.2 eq.), 8.3 mg of $PdCl_2(PPh_3)_2$ (0.012 mmol, 0.01 eq.) and 2.3 mg of CuI (0.012 mmol, 0.01 eq.). The vessel was sealed and allowed to stir for 24 hours. The solution was then poured into dichloromethane, followed by extraction with brine (x2) and water (x2). The organic layer was dried with magnesium sulfate, filtered and concentrated under reduced pressure. The crude compound was then purified by column chromatography utilizing DCM:Hexane (2:3) furnishing **3.3a** in 48% yield as a yellow solid. (0.342 g, 0.643 mmol). ^{1}H-NMR (500 MHz, $CDCl_3$) d 0.96 (t, 12H J=9 Hz), 1.36 (m, 8H), 1.57 (m, 8H), 3.28 (t, 8H J=12 Hz), 6.57 (d, 4H J=9 Hz), 7.35 (d, 4H J=9 Hz), 7.42 (s, 4H); ^{13}C-NMR (125 MHz, $CDCl_3$) 114.41, 20.74, 51.10, 87.61, 92.87, 108.99, 111.60, 123.53, 131.43, 133.29, 148.41; IR (KBr) $\tilde{\nu}$ 3798 (w), 3333 (w), 3196 (w), 3092 (w), 3043 (w), 2953 (s), 2868 (s), 2727 (w), 2561 (w), 2207 (s), 2160 (m), 1902 (w), 1884 (w), 1688 (w), 1609 (s), 1523 (s), 1468 (m), 1400 (m), 1371 (m), 1285 (m), 1198 (m), 1144 (s), 1109 (m), 926 (m), 833 (s), 814 (s), 525 (m).

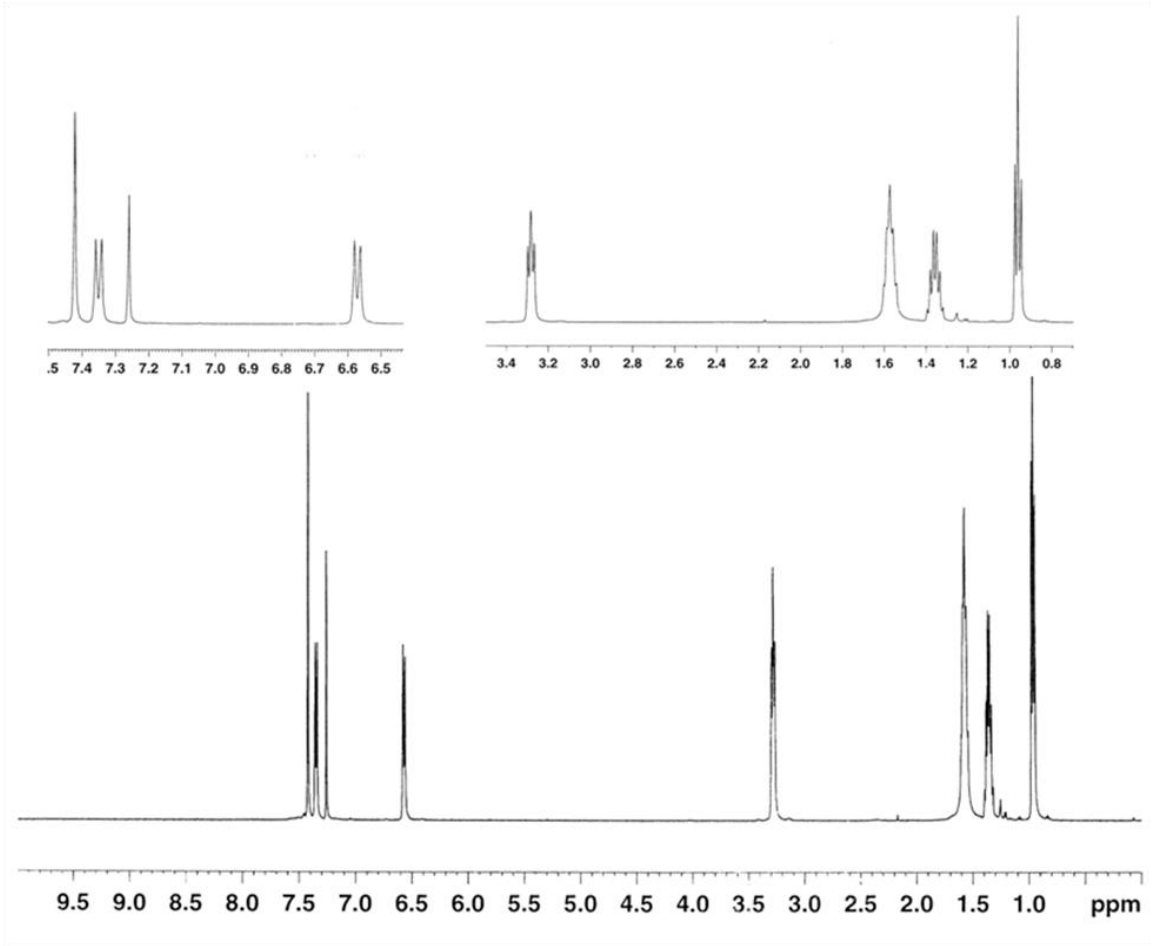

Figure 3.4. 1H-NMR spectrum of **3.3a** ($CDCl_3$)

3.4.2 Spectroscopic Data of Compounds **3.3a-3.6b**.

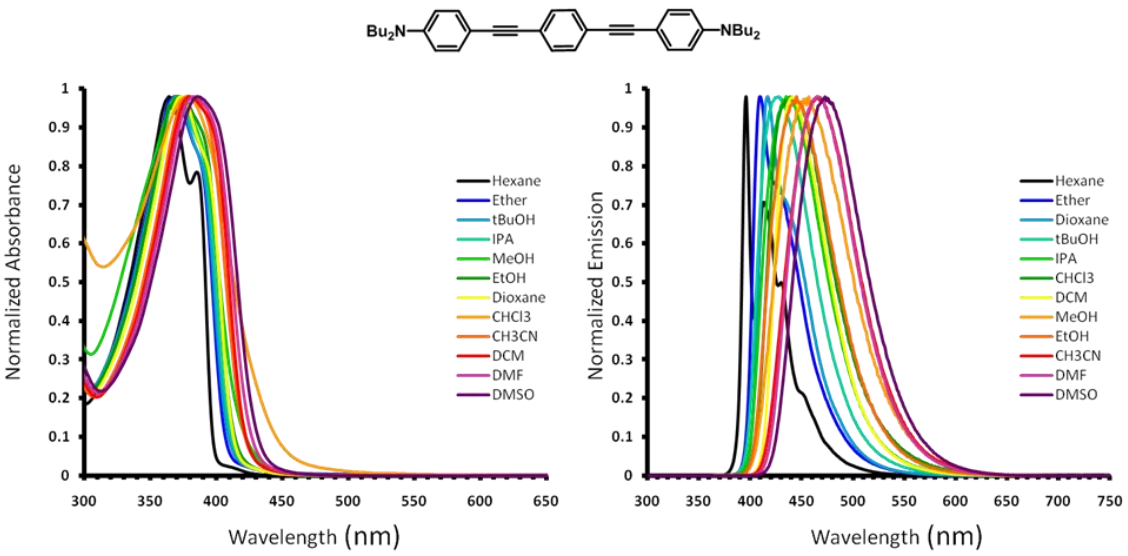

Figure 3.5. Absorption (left) and emission (right) spectra of **3.3a** in a variety of solvents.

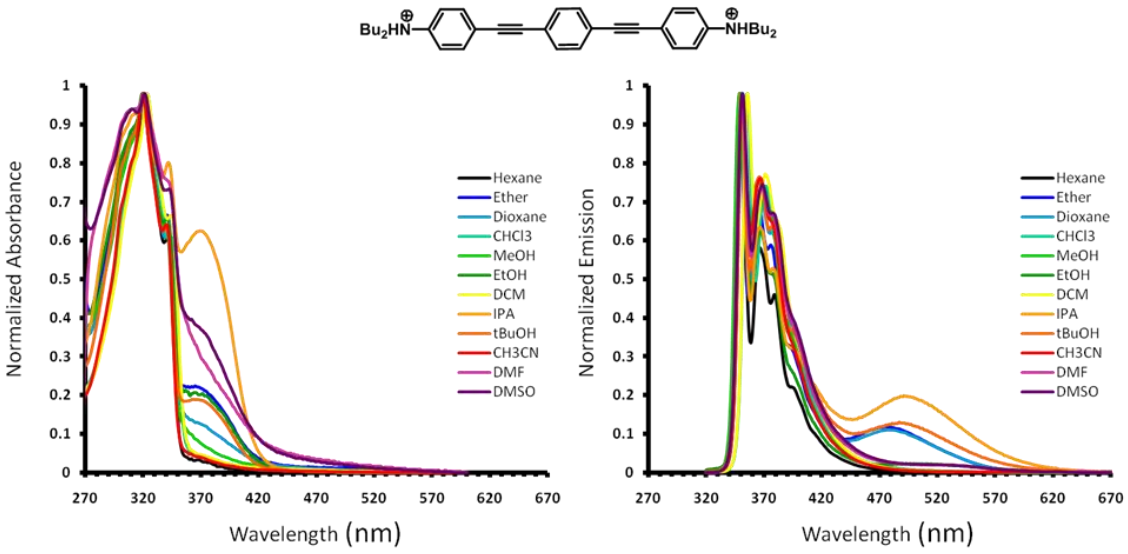

Figure 3.6. Absorption (left) and emission (right) spectra of **3.3b** in a variety of solvents.

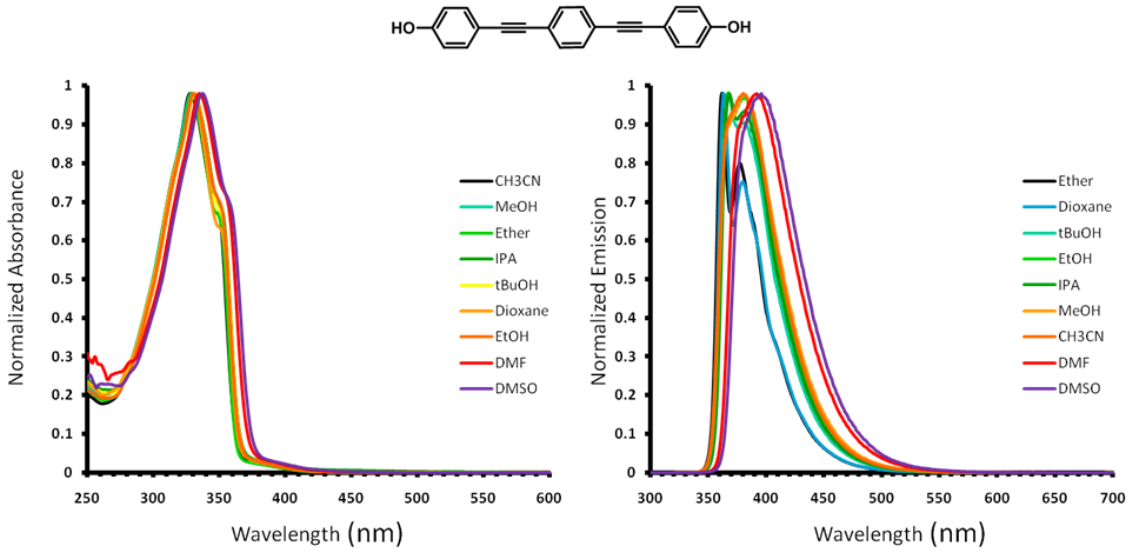

Figure 3.7. Absorption (left) and emission (right) spectra of **3.4a** in a variety of solvents.

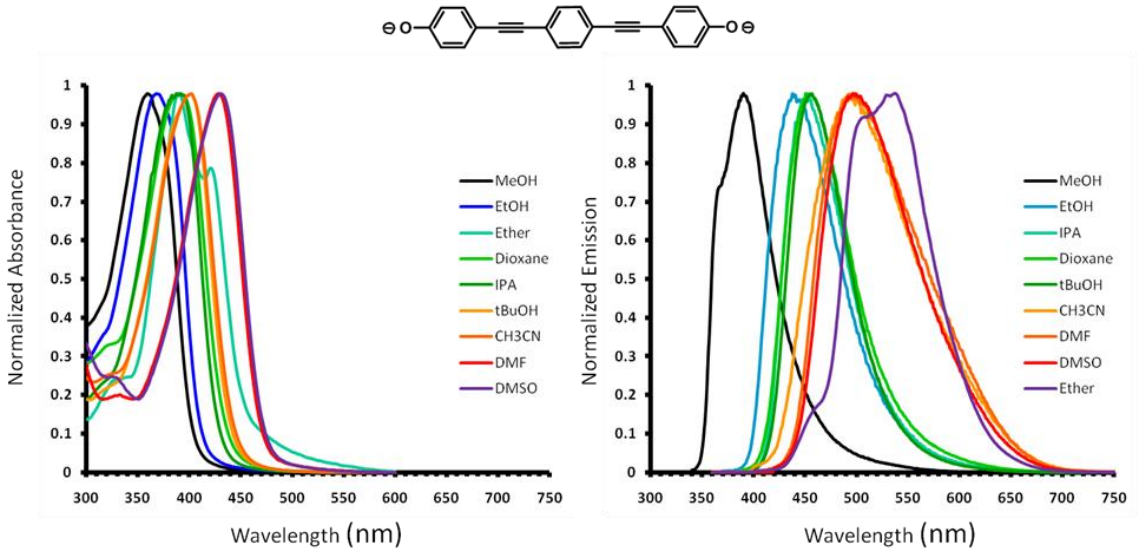

Figure 3.8. Absorption (left) and emission (right) spectra of **3.4b** in a variety of solvents.

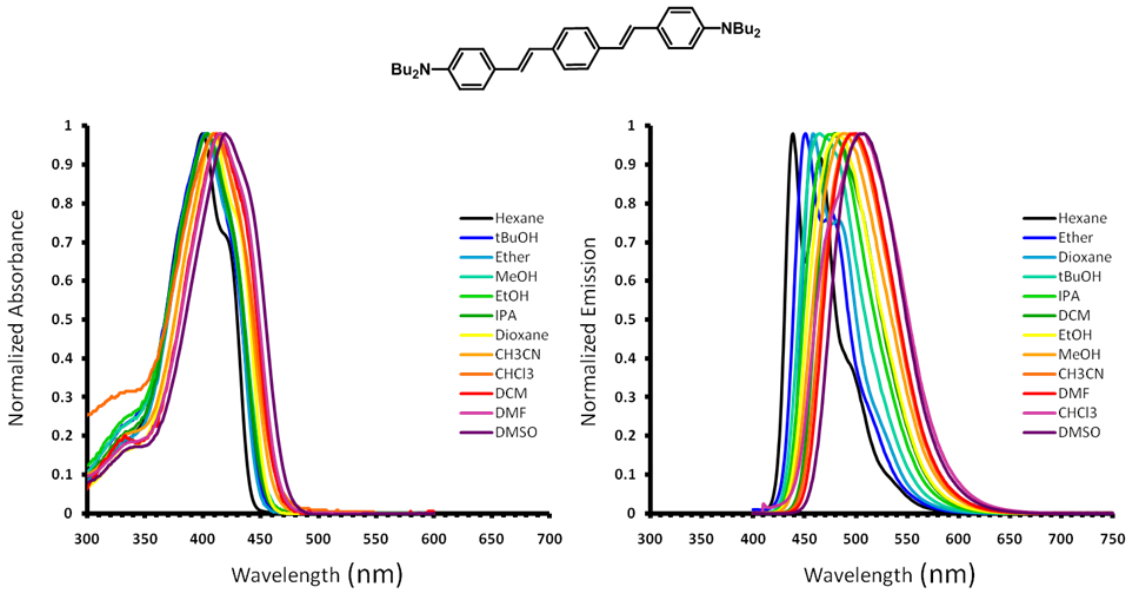

Figure 3.9. Absorption (left) and emission (right) spectra of **3.5a** in a variety of solvents.

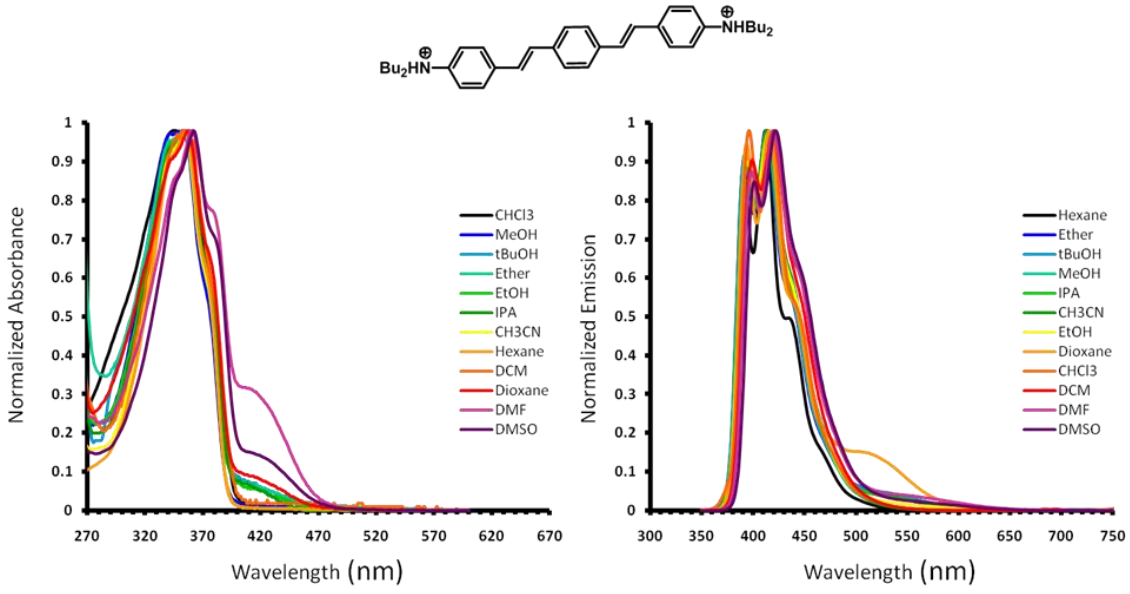

Figure 3.10. Absorption (left) and emission (right) spectra of **3.5b** in a variety of solvents.

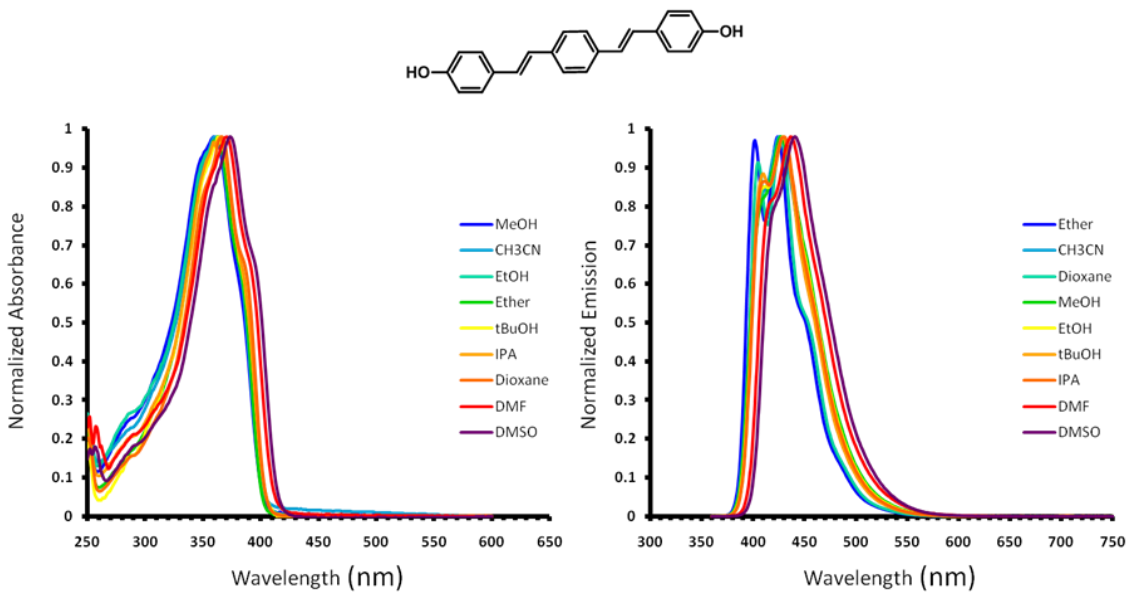

Figure 3.11. Absorption (left) and emission (right) spectra of **3.6a** in a variety of solvents.

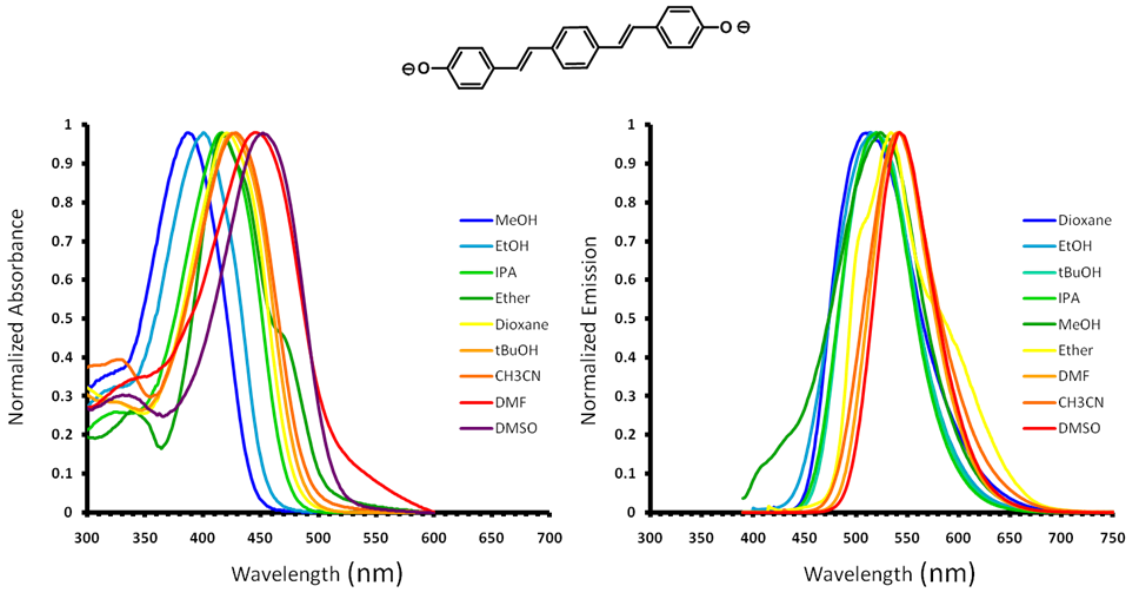

Figure 3.12. Absorption (left) and emission (right) spectra of **3.6b** in a variety of solvents.

3.4.3. Kamlet-Taft Analysis Data

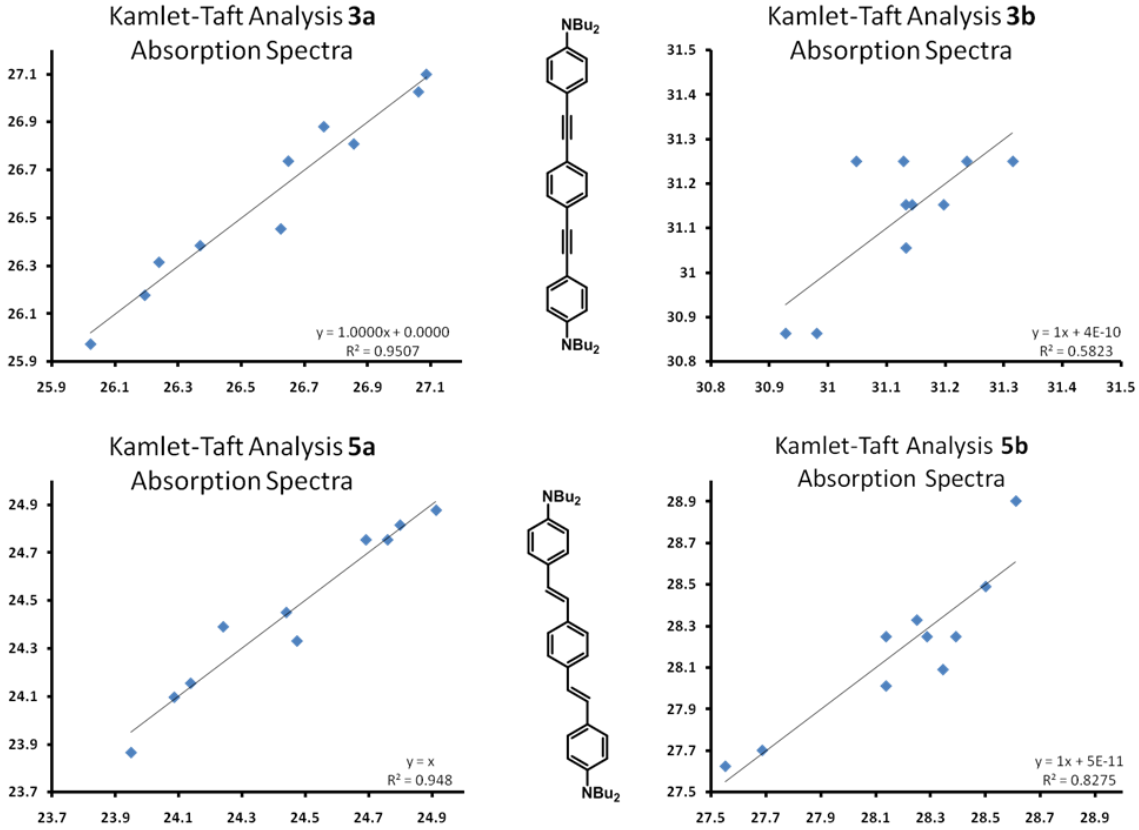

Figure 3.13. Kamlet-Taft multivariate linear regression analysis plots of **3.3a** (top left), **3.3b** (top right), **3.5a** (bottom left), and **3.5b** (bottom right).

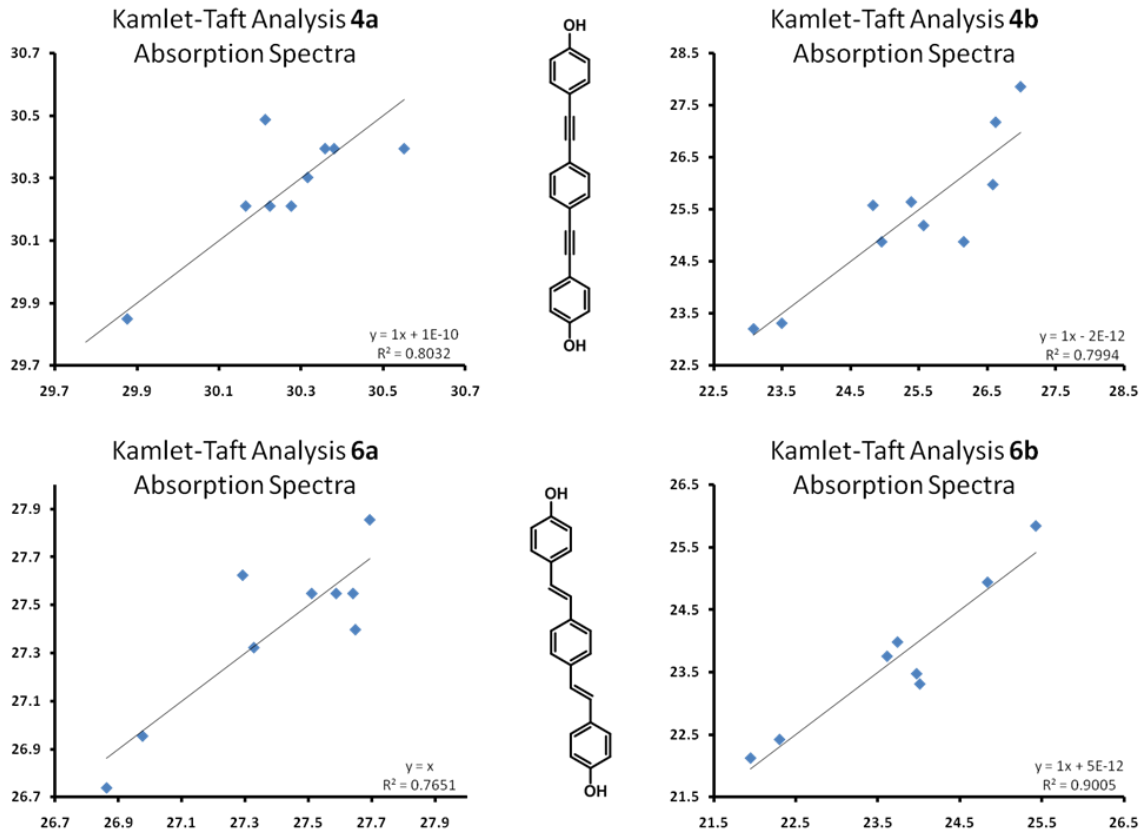

Figure 3.14. Kamlet-Taft multivariate linear regression analysis plots of **3.4a** (top left), **3.4b** (top right), **3.6a** (bottom left), and **3.6b** (bottom right).

3.5 References

[1] Zucchero, A. J.; Wilson, J. N.; Bunz, U. H. F. *J. Am. Chem. Soc.* **2006**, *128*, 11872-11881.

[2] (a) Hoffmann, R. *Angew. Chem. Int. Ed.* **1982**, *21*, 711-724. (b) Evans, D. G.; Mingos, D. M. P. *J. Organomet. Chem.* **1982**, *232*, 171-191.

[3] Solntsev, K. M.; McGrier, P. L.; Fahrni, C. J.; Tolbert, L. M.; Bunz, U. H. F. *Org. Lett.* **2008**, *10*, 2429-2432.

[4] (a) Zucchero, A. J.; Tolosa, J.; Tolbert, L. M.; Bunz, U. H. F. *Chem. Eur. J.* **2009**, *47*, 13075-13081. (b) Albota, M.; Beljonne, D.; Bredas, J.-L.; Ehrlich, J. E.; Fu, J.-Y.; Heikal, A. A.; Hess, S. E.; Kogej, T.; Levin, M. D.; Marder, S. R.; McCord-Maughon, D.; Perry, J. W.; Rockel, H.; Rumi, M.; Subramaniam, G.; Webb, W. W.; Wu, X.-L.; Xu, C. *Science.* **1998**, *281*, 1653-1656. (c) Cumpston, B. H.; Ananthavel, S. P.; Barlow, S.; Dyer, D. L.; Ehrlich, J. E.; Erskine, L. L.; Heikal, A. A.; Kuebler, S. M.; Lee, I.-Y. S.; McCord-Maughon, D.; Qin, J.; Rockel, H.; Rumi, M.; Wu, X.-L.; Marder, S. R.; Perry, J. W. *Nature.* **1999**, *398*, 51-54. (d) Rumi, M.; Ehrlich, J. E.; Heikal, A. A.; Perry, J. W.; Barlow, S.; Hu, Z.; McCord-Maughon, D.; Parker, T. C.; Roeckel, H.; Thayumanavan, S.; Marder, S. R.; Beljonne, D.; Bredas, J.-L. *J. Am. Chem. Soc.* **2000**, *122*, 9500-9510.

[5] Yam, C. M.; Kakkar, A. K. *Langmuir.* **1999**, *15*, 3807-3815.

[6] (a) Kivala, M.; Boudon, C.; Gisselbrecht, J.-P.; Seiler, P.; Gross, M.; Diederich, F. *Chem. Commun.* **2007**, 4731-4733. (b) Nguyen, P.; Yuan, Z.; Agocs, L.; Lesley, G.; Marder, T. B. *Inorg. Chim. Acta.* **1994**, *220*, 289-296.

[7] (a) Michinobu, T.; Boudon, C.; Gisselbrecht, J.-P.; Seiler, P.; Frank, B.; Moonen, N. N. P.; Gross, M.; Diederich, F. *Chem. Eur. J.* **2006**, *12*, 1889-1905. (b) Liu, B.; Liu, J.; Wang, H.-Q.; Zhao, Y.-D.; Huang, Z.-L. *J. Mol. Struct.* **2007**, *833*, 82-87.

[8] (a) Negishi, E.; Anastasia, L. *Chem. Rev.* **2003**, *103*, 1979-2017. (b) Sonogashira, K. J. *Organomet. Chem.* **2002**, *653*, 46-49. (c) Bunz, U. H. F. *Chem. Rev.* **2000**, *100*, 1605-1645.

[9] (a) Von Lippert, E. *Z. Electrochem.* **1957**, *61*, 962-975. (b) Mataga, N.; Kaifu, Y.; Koizumi, M. *Bull. Chem. Soc. Jpn.* **1956**, *29*, 465-470.

[10] (a) Kamlet, M. J.; Abboud, J.-L.; Abraham, M. H.; Taft, R. W. *J. Org. Chem.* **1983**, *48*, 2877-2887. (b) Dong, J.; Solntsev, K. M.; Tolbert, L. M. *J. Am. Chem. Soc.*

2006, *128*, 12038-12039. (c) Wu, Y.; Lawson, P. V.; Henary, M. M.; Schmidt, K.; Brédas, J.-L.; Fahrni, C. J. *J. Phys. Chem. A.* **2007**, *111*, 4584-4595.

[11] (a) Hammett, L. P. *Chem. Rev.* **1935**, *17*, 125-136. (b) Hansch, C.; Leo, A.; Taft R. W. *Chem. Rev.* **1991**, *91*, 165-195.

[12] Interpolated from the σ_p-values for $-NH_3^+$ (0.60) and NMe_3^+ (0.82); the other values are directly from Table 1 in reference.[11 b]

Chapter 4: Bis(arylethynyl)benzothiadiazoles: Enhancing the Dynamic Range of Simple Senory Materials Through Enforcement of FMO Separation

4.1 Introduction

Responsive chromophores exhibiting changes in color, emission wavelength, and/or emission intensity invesitgated for applications in sensory schemes. Important are efforts to improve the selectivity, sensitivity, or dynamic range of responsive dyes.[1] Bis(arylethynyl)benzenes and distyrylbenzenes bearing either *para*-hydroxy or -dibutylamino substituents behave as simple functional fluorophores; protonation of the alkylamino nitrogen or deprotonation of the phenol elicit observable spectroscopic shifts.[2]

An investigation of the neutral and protonated/deprotonated states reveals both the

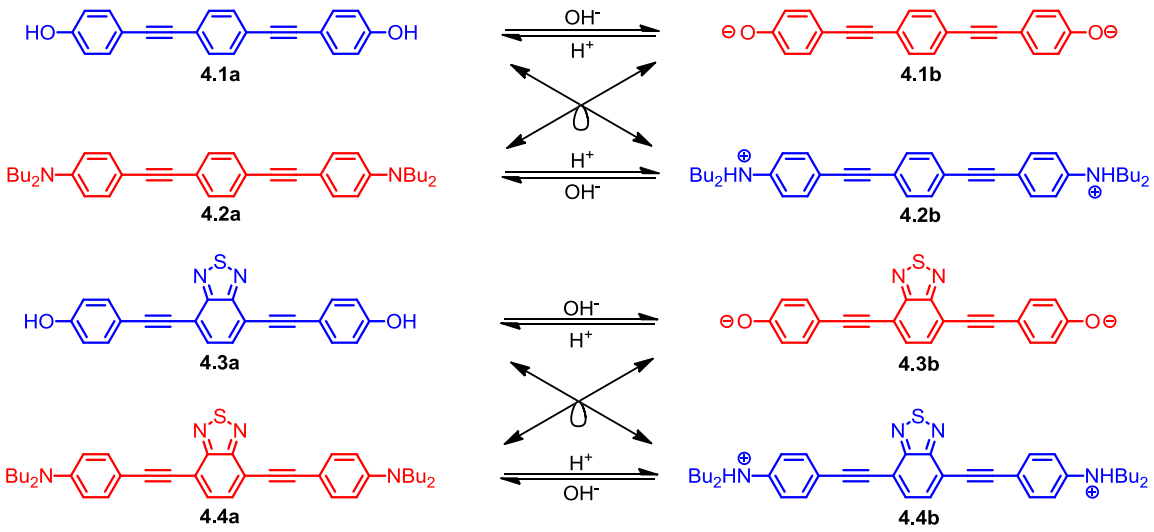

Scheme 4.1. Acid/base equilibrium relationships of **4.1a**-**4.4b**. The underlying electronic similarity of functional groups are indicated by diagonal lines as well as paired colors.

underlying electronic simililarity of phenolate/alkylamino- and phenol/alkylammonium- groups and the interplay of these electronic structures with solvents. A superficial examination of the Lewis structures of **4.1a**-**4.2b** (Scheme 4.1) suggests the similar electronic structure of the phenol and protonated dibutylammonium compounds (**4.1a** and **4.2b, A**) as well as the phenolate and neutral dibutylamino compounds (**4.1b** and **4.2a, B**). The spectroscopic properties of **4.1a** and **4.2b** in a range of solvents are nearly identical, owing to their electronic similarity. However, varied spectroscopic properties were observed in **4.1b** and **4.2a**; Kamlet-Taft[3] solvent analysis suggests this results from different interaction of **4.1b** and **4.2a** with proton donating and accepting solvents.

Owing to their relatively small π-systems, **4.1a** and **4.2a** exhibit absorption maxima ranging from 300-450 nm and are blue to blue-green emissive depending upon the solvent utilized. While these fluorophores are responsive, the spectral range upon exposure to acid, base, or metal cations was small; shifts of only 50 nm in absorption and 100 nm in emission were observed. (See Chapter 3)

4.2 Results and Discussion

In an effort to enhance the spectral range of bis(arylethynyl)benzenes upon exposure to analytes, we prepared **4.3a** and **4.4a**. Benzothiadiazoles are strong electron acceptors; we explored the introduction of a π-acceptor core would result in strong intramolecular charge transfer, enhancing their photophysical properties. Related beznothiadiazole-based molecules have been examine for senory[4] and solid phase luminescence[5] studies. However, the interaction of solvents and the pH

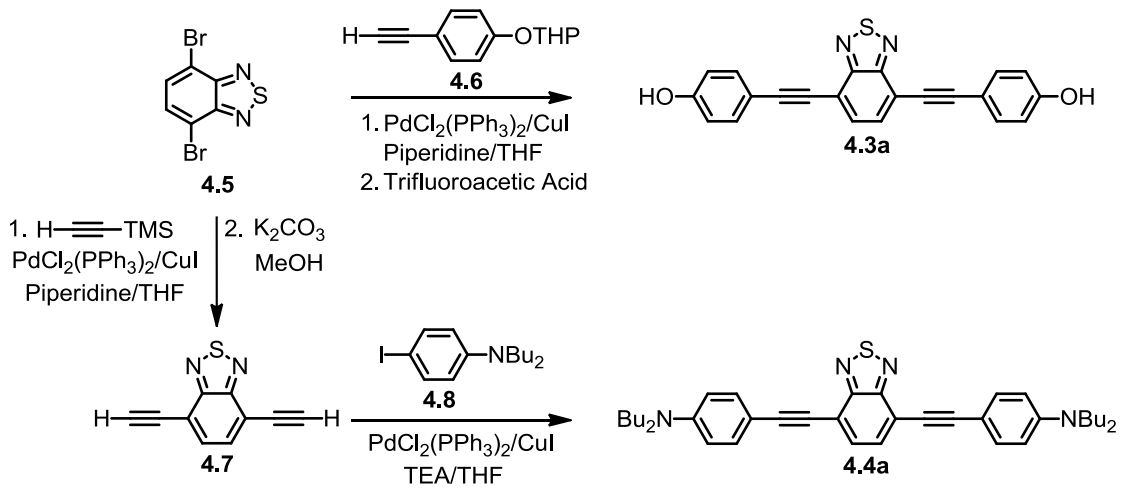

Scheme 4.2. Synthesis of **4.3a** and **4.4a**.

dependent response has been neglected.

Pd-catalyzed Sonogashira coupling[6] of the ethynylphenol **4.6** to **4.5** results in the THP protected benzothiadiazole. Deprotection (trifluoroacetic acid) furnishes bis(*p*-hydroxyphenyl-ethynyl)benzothiadiazole (**4.3a**, 58%). Sonogashira coupling of **4.7** with known **4.8** yielded bis(*p*-dibutylanilinoethynyl)benzo-thiadiazole (**4.4a**, 85%).

We explored their photophysical behavior of **4.3a** and **4.4a** in a variety of solvents (tetrahydrofuran, 1,4-dioxane, ether, dichloromethane, chloroform, acetonitrile, methanol, ethanol, isopropanol, *tert*-butanol, dimethylformamide, and dimethylsulfoxide). The selection of the solvent plays a significant role in the chromic and fluorescent appearance of **4.3a**, **4.3b**, **4.4a**, and **4.4b** in solution. (Figure 4.1)

The spectroscopic properties of **4.1a-4.4b** in CH_3CN are tabulated in Table 4.1. Significant bathochromic shifts in absorption profiles are observed in compounds **4.3a**-**4.4b** relative to the corresponding bisarylethynylbenzenes **4.1a**-**4.2b**. Large

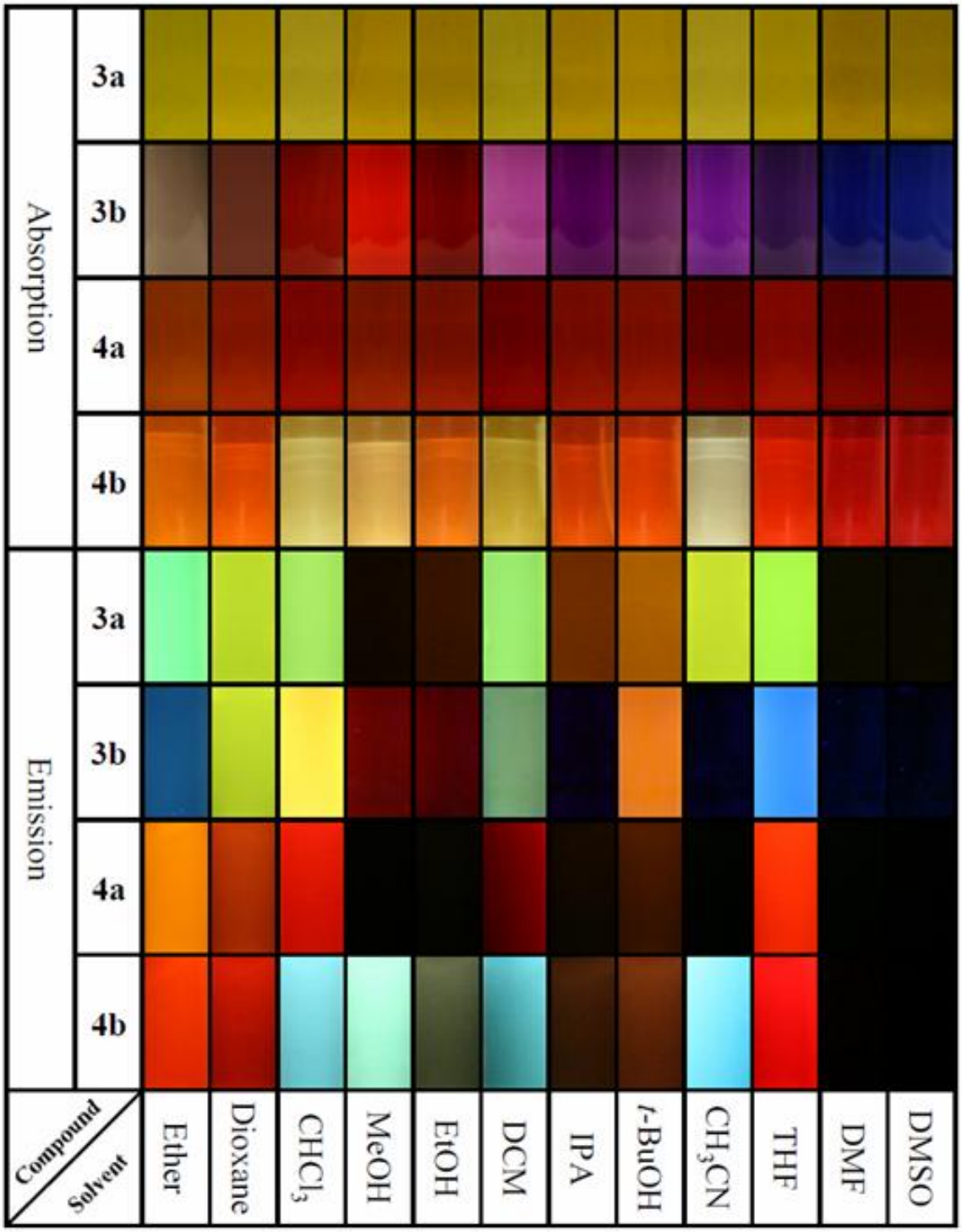

Figure 4.1. Absorption (top) and emission (bottom) of **4.1a-4.4b** in a variety of solvents. All photographs were taken using a Canon EOS Digital Camera equipped with an EFS 18-55mm lens. Emission photos were taken under a blacklight (ex = 365 nm).

Table 4.1. Tabulated spectroscopic data of compounds **4.1a-4.4b** in acetonitrile.

Compound	**4.1a**	**4.2b**	**4.2a**	**4.1b**	**4.3a**	**4.4b**	**4.4a**	**4.3b**
λ_{max} Abs (nm)	328	321	378	408	427	396	502	553
λ_{max} Em (nm)	380	351	466	496	539	479	634	-[b]
ε (M^{-1}•cm^{-1})	10230	6089	6799	9632	24015	29437	32230	28335
Φ	0.43	0.54	0.51	<0.01	0.41	0.78	<0.01	-[b]
τ (ns)[a]	0.91	0.48	1.81	1.49	6.65	3.19	2.56	-[b]

[a]Monoexponential decay. [b]Emission too faint to be measured.

extinction coefficients, hallmarks of ICT[7] were measured (~2.4-3.2 x 10^4 $M^{-1}cm^{-1}$). These values are approximately 2-5 times larger in magnitude than ε for **4.1a**-**4.2b**.

Similarly, the emission λ_{max} of **4.3a**-**4.4b** were redshifted realtive to compounds **4.1a**-**4.2b** except in the case of **4.3b** which was quenched in acetonitrile. The quantum yield (QY) of **4.4a** was less than 1% while **4.3b** was completely quenched. Upon protonation of **4.3b** and **4.4a**, both blueshift and increase their emission intensity. QYs of **4.3a** and **4.4b** were high (41%, 78%). The introduction of the thiadiazole core in **4.3a**, **4.4a**, and **4.4b** provides fluorescent materials which exhibit long fluorescent lifetimes. We have shown previously that these long lifetimes are typical of systems containing arylthiadiazoles (See chapter 5).[8]

FMOs were calculated for compounds **4.1**-**4.4** (Figure 4.2). If we compare compounds **4.1** and **4.3**, we observe that the HOMO and LUMO of **4.1a** are distributed across the molecule and are nearly overlapped whereas the in the case of **4.3a**, the LUMO is localized on the benzothiadiazole ring. Upon deprotonation of **4.1**, the HOMO and LUMO are destabilized to a similar degree (slightly moreso for

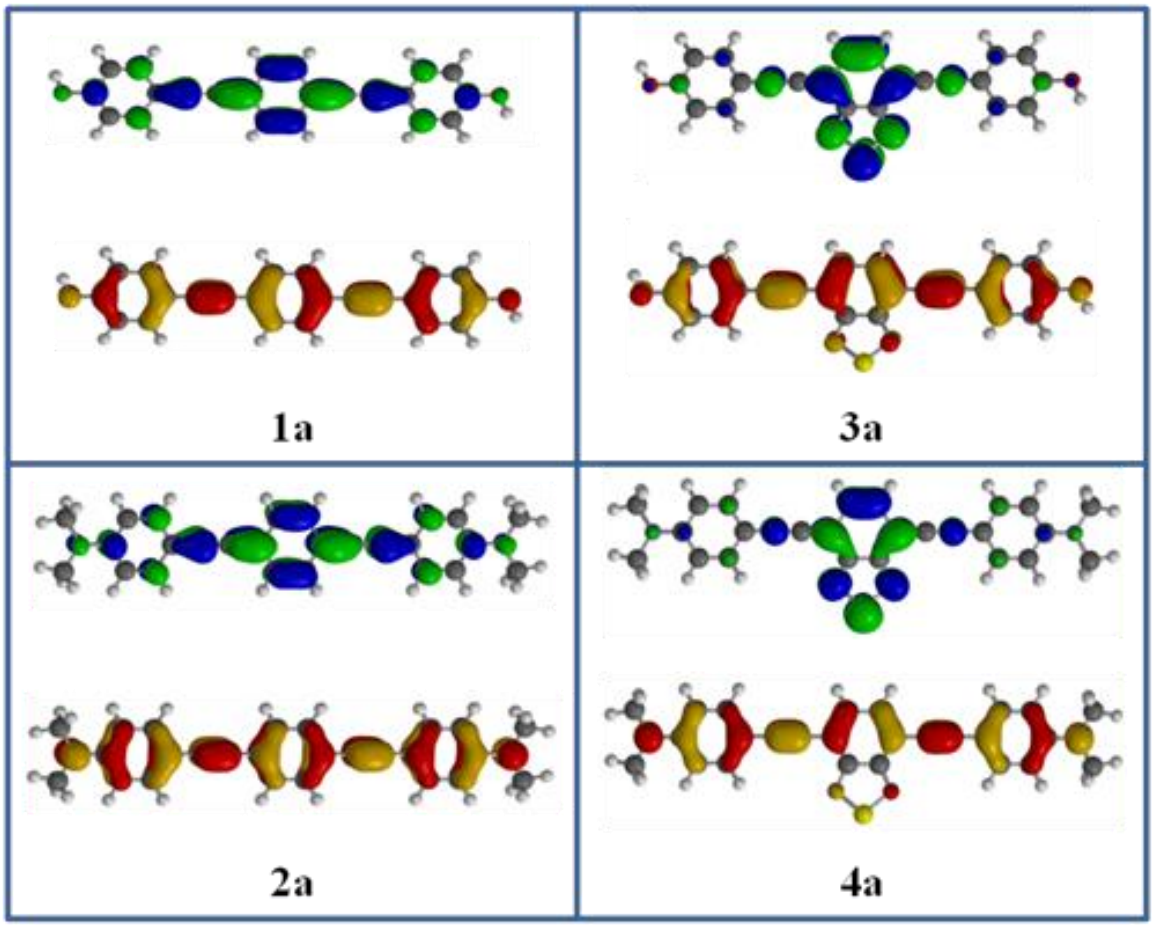

Figure 4.2. HOMO (Red and Yellow) and LUMO (Green and Blue) of **4.1a-4.4a**. FMOs were calculated with B3LYP 6-31G**//6-31G** using Spartan.

the HOMO) resulting in only a slight redshift in absorption onset. In the case of **4.3**, however, the HOMO and LUMO are disproportanatly affected. The HOMO is destabilized to a greater extent than the LUMO. This results in a large redshift in the absorption onset.

In the case of the dibutyl compound **4.4**, a similar but opposite effect is observed. Compound **4.4a** is more similar to **4.3a** with the LUMO localized again on the benzothiadiazole ring. Upon protonation, the FMOs of **4.2** are equally stabilized (the HOMO slightly moreso) resulting in a slight blueshift in absorption onset. As for **4.4a**, the HOMO is much more stabilized than the LUMO resulting in a compound

Table 4.2 Coefficient values obtained from KT analysis.

	A		**B**		**C**		**D**	
Compound	**4.1a**	**4.2b**	**4.2a**	**4.1b**	**4.3a**	**4.4b**	**4.4a**	**4.3b**
v_0[a]	30.7	31.2	27.4	26.8	23.3	24.7	20.6	21.5
s	-0.52	-0.26	-1.5	-2.5	-0.02	0.31	-1.1	-3.0
a	0.32	-0.07	0.17	2.9	-0.07	-0.34	-0.24	2.1
b	-0.55	0.30	0.14	-1.5	-0.71	1.4	0.02	-3.1
R[b]	0.80	0.58	0.95	0.80	0.72	1.0	0.82	0.78

[a]Units of v_0 are in 10^3 cm^{-1}. [b]R is the correlation coefficient.

that has a significantly hypsochomically shifted absorption profile.

Kamlet-Taft (KT) solvent analysis correlates the solvent-dependent spectral shifts (υ) observed for a chromophore with solvent parameters – α, β, and π* (eq. 4.1). By performing a multivariate linear regression analysis of the λ_{max} absorption of a chromophore in a variety of solvents the KT provides *s*, *a*, *b*, and υ_0, the projected absorption of a chromophore in a vacuum (Table 4.2). KT describes the impact of non-specific dielectric (π*), hydrogen-bond donating (α), and hydrogen-bond accepting (β) modes of interaction between a solvent and a chromophore:

$$\nu\ (1000/\mathrm{cm}) = \nu_0 + s \cdot \pi^* + a \cdot \alpha + b \cdot \beta \qquad (4.1)$$

4.4a was unable to be protonated in several solvents; The introduction of the stongly electron-withdrawing thiadiazole group lowers the pK_a of the dialkylaniline sufficently that only solvent protonation was observed. Given this limitation, KT analysis of **4.4b** was accomplished using data obtained in dichloromethane, chloroform, acetonitrile and methanol.

The *s* coefficient of the π* term quantifies the importance of dielectric interactions of the solvent with the chromophore; as such, it is correlated with the chromophore's dipole. Once again, we observe similar behavior in the case of electronically analogous pairs. In the case of **A** and **C**, we observe small values of s, suggesting these four chromophores possess relatively small dipoles. However, **B** and **D** possess much larger, negative *s* values, indicating the presence of a significant dipole. This can be rationalized as **B** and **D** possess available electron pairs on the alkylamino nitrogens and phenolates; protonation of these positions in the case of **A** and **C** decreases potential dipole contribution.

The *a* and *b* coefficients quantify solvent specific interactions with the chromophore via proton donation or proton acceptance. In Chapter 3 we detailed the surprising differential influence of these interactions on **4.1a-4.2b**. As expected, in the case of set **A**, we observe similar small values for *a* and *b*. However, in spite of their apparent electronic similarity, **4.1b** displays large values for *a* and *b* while **4.2a** exhibits very small values for these coefficients. We attributed this unexpected divergence to the increased bascitiy of the phenolate as compared the dialkylamino group. This previous finding for **B** is mirrored in the benzothiadiazole analogues **D**. The values obtained for *a* and *b* are small in the case of **4.4a**; however, they are large for phenolate **4.3b**.

Surprisingly, sets **A** and **C** show some unexpected differences. In the case of **4.4b**, we now observe a substantial value for *b*, suggesting that the absorption of this chromophore is heavily influenced by solvent basicity. Presumably, the introduction of the electron-accepting benzothiadiazole increases the acidity of **4.3a** and **4.4b**. As

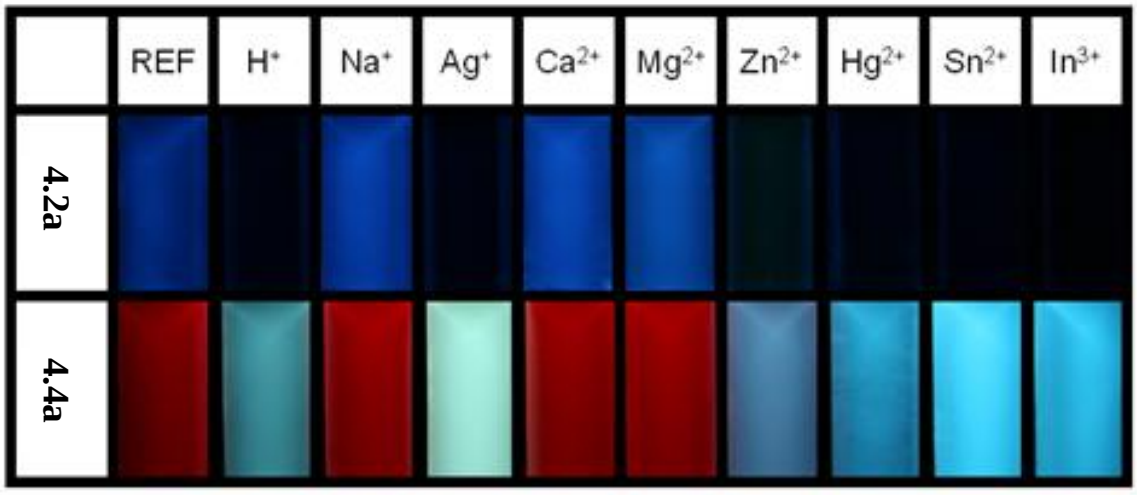

Figure 4.3. Fluorescence response of **4.2a** and **4.4a** towards a variety of metal cations and protons in CH_2Cl_2. All photos were taken under a blacklight (ex = 365 nm) using a Canon EOS Digital Camera equipped with an EFS 18-55mm lens.

a result, this compound is now sensitive to solvent basicity.

We exposed **4.4a** (in DCM) towards protons and metal triflate salts (Na^+, Ag^+, Ca^+, Mg^{2+}, Zn^{2+}, Hg^{2+}, Sn^{2+}, and In^{3+}). While in the presence of sodium, calcium and magnesium there was no response, there was a blueshift of about 110 nm in the absorption onset and 160 nm in the emission λ_{max} upon binding to silver, zinc, mercury, tin and indium (See Figures 4.3,4.8). These responses were identical to those observed upon protonation. Similar selectivity was observed in **4.2a**, but only quenching was observed rather than the dramatic red→blue emission shift seen in **4.4**. This is indicative that the introduction of the thiadiazole core does not affect the nature of the binding ability of the dibutylamino group.

4.3 Conclusions

Phenol- and alkylamino-substituted bis(phenylethynyl)-benzothiadiazoles, while

synthetically simple to prepare, hold promise as robust sensory chromophoric and fluorophoric materials. Compounds **4.3** and **4.4** possess well understood solvatochromic properties very similar to fluorophores **4.1** and **4.2** as noted in the in the general trends of the coefficent values from the KT analysis. Simple functionalization with a thiadiazole group imbues these compounds with dramatic turn-on and turn-off emissive properties, as well as large ε values and absorptions in the visible region of the spectrum, leading to intense coloration. In particular, compound **4.4** is ripe to be utilized in cation sensing applications due to it excellent sensory dynamic range. The general design of these materials allows for modular construction of a library of fluorophores with various recognition units. We are currently persuing the construction of benzothiadiazole based fluorophores with selective binding sites for analyte specific sensory materials.

4.4 Experimental and Supplementary Information

4.4.1 4,4'-(benzo[c][1,2,5]thiadiazole-4,7-diylbis(ethyne-2,1-diyl))diphenol, **4.3a**.

To a vacuum degassed solution of THF (10 mL) and triethylamine (10 mL) was added $PdCl_2(PPh_3)_2$ (0.02 g, 0.03 mmol, 0.003 eq.), CuI (0.01 g, 0.05 mmol, 0.05 eq.) and PPh_3 (0.015 g, 0.06 mmol, 0.06 eq.) followed by **4.5** (0.30 g, 0.001 mol, 1 eq.) and **4.6** (0.40 g, .002 mol, 2 eq.). The flask was sealed and heated to 80 ^oC under N_2 for 24 h. The mixture was then dissolved into DCM and filtered. The solvent was removed under vacuum and the residue was separated on silca (DCM). The protected product was immediately dissolved in DCM and cooled in a dryice/acetone bath. 2 mL of TFA was added. The solution was allowed to stir for 2 h. The organic layer was then washed it water (x3) and dried over magnesium sulfate. The residue was recrystallized to yield a red powder (0.21g, 58%). ^{1}H-NMR (500 MHz, DMSO-*d*6) 6.85 (d, 4H, J=8.6 Hz), 7.47 (d, 4H, J=8.6 Hz), 7.85 (S, 2H), 10.08 (S, 2H); ^{13}C-NMR (125 MHz, DMSO-*d*6) 84.14, 97.72, 111.90, 115.98, 116.17, 132.16, 133.40, 153.75, 158.75;

4.4.2 4,4'-(benzo[c][1,2,5]thiadiazole-4,7-diylbis(ethyne-2,1-diyl))bis(N,N-dibutylaniline), **4.4a**.

To a vacuum degassed solution of THF (10 mL) and triethylamine (10 mL) was added $PdCl_2(PPh_3)_2$ (0.02 g, 0.03 mmol, 0.01 eq.) and CuI (0.006 g, 0.03 mmol, 0.01 eq.) followed by **4.7** (0.56 g, 0.003 mol, 1 eq.) and **4.7** (2.22 g, .0067 mol, 2.2 eq.). The flask was sealed and heated to 80 ^oC under N_2 for 24 h. The mixture was then

dissolved in DCM and washed with water (x3), dried with magnesium sulfate and concentrated under reduced pressure. The crude mixture was separated on silica (gradient hexane to 1:1 hexane:DCM to DCM). The fractions containing product were concentrated under vacuum and suspended in methanol. The solution was brought to reflux for 3 h and then cooled. Filtration of the precipitate furnished compound **4.4b** (1.53 g, 85%) as a red powder. ^{1}H-NMR (500 MHz, $CDCl_3$) 0.971 (t, 12H), 1.37 (m, 8H), 1.59 (m, 8H), 3.30 (t, 8H), 6.60 (d, 4H), 7.49 (d, 4H), 7.68, (s, 2H); ^{13}C-NMR (125 MHz, $CDCl_3$) 13.84, 20.24, 29.29, 50.60, 84.04, 99.38, 107.91, 111.06, 116.87, 131.44, 133.33, 148.34, 154.41;

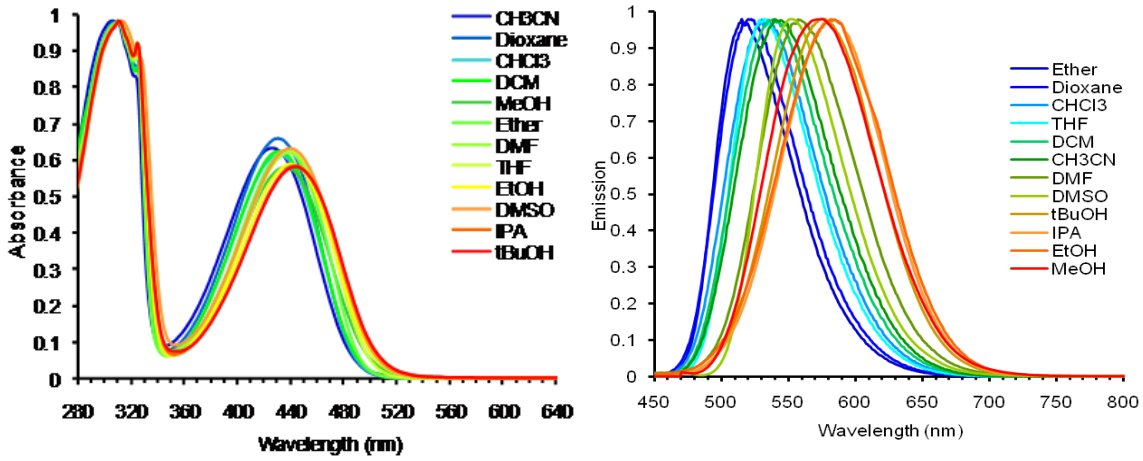

Figure 4.4. Absorption (left) and emission (right) spectra of **4.3a** in a variety of solvents.

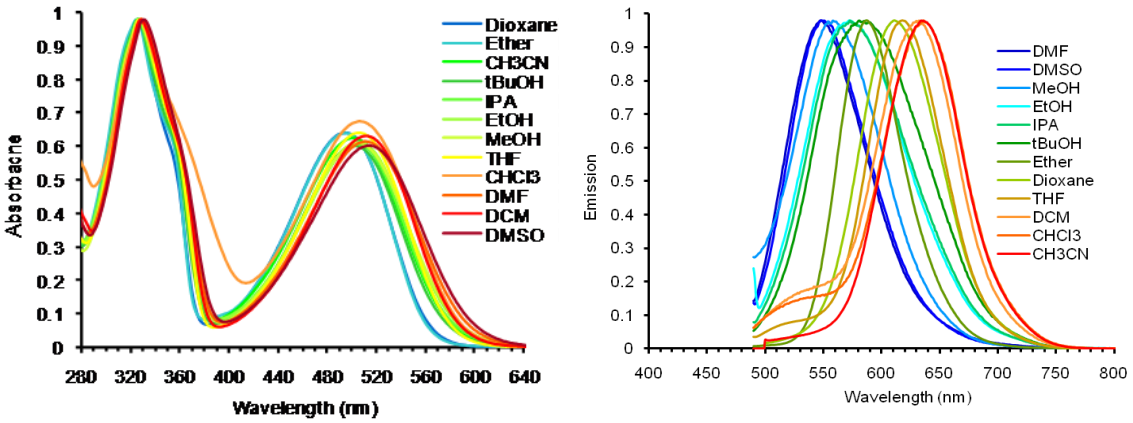

Figure 4.5. Absorption (left) and emission (right) spectra of **4.4a** in a variety of solvents.

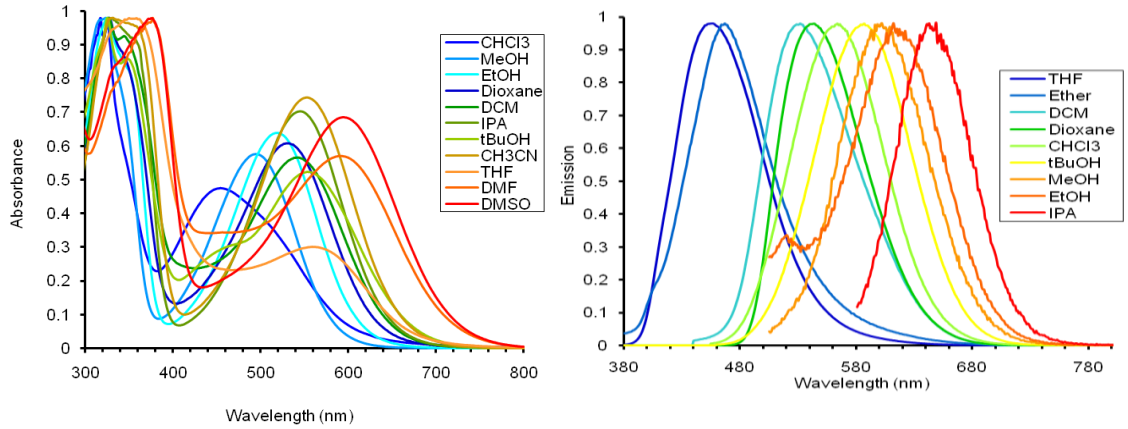

Figure 4.6. Absorption (left) and emission (right) spectra of **4.3b** in a variety of solvents.

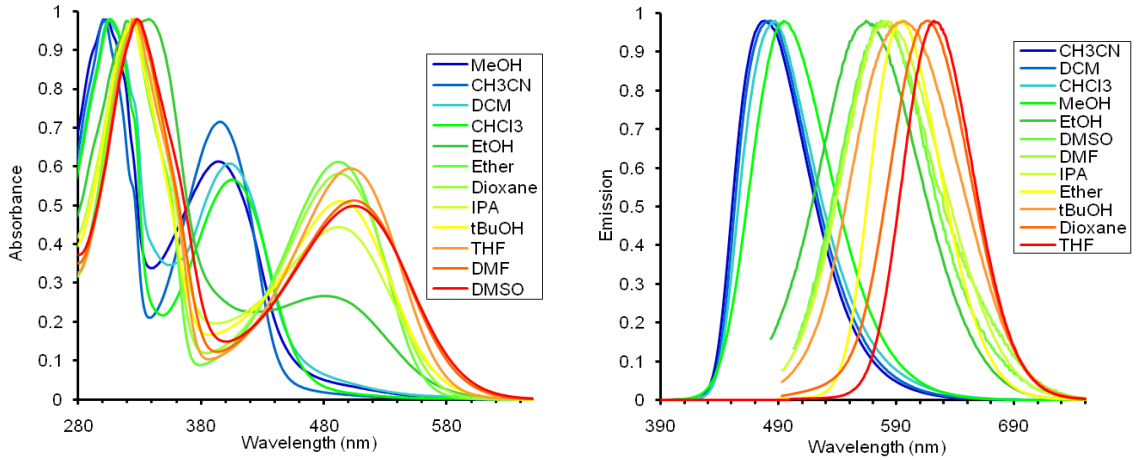

Figure 4.7. Absorption (left) and emission (right) spectra of **4.4b** in a variety of solvents.

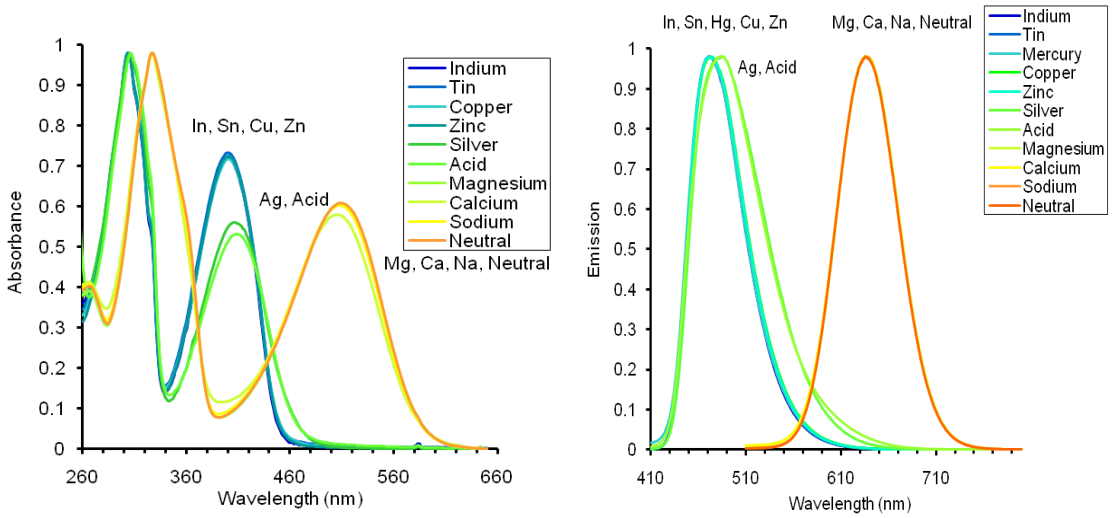

Figure 4.8. Absorption (left) and emission (right) spectra of **4.3a** in the presence of metal triflate salt in DCM.

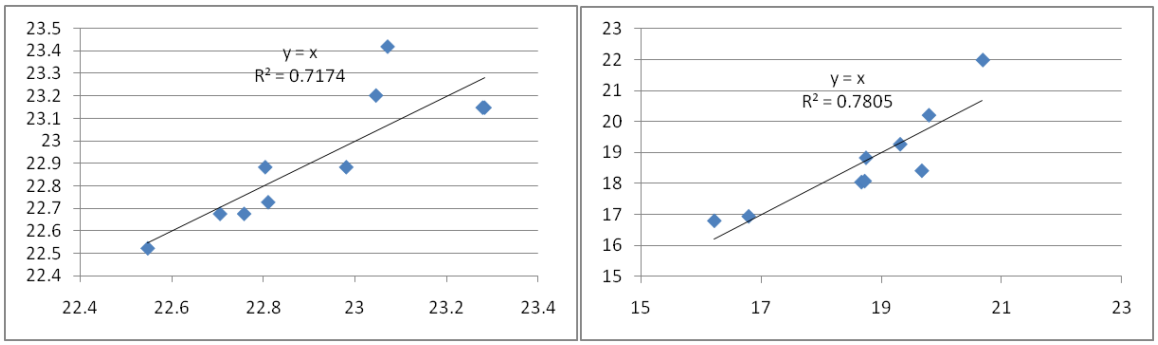

Figure 4.9. Kamlet-Taft plots of **4.3a** (left) and **4.3b** (right).

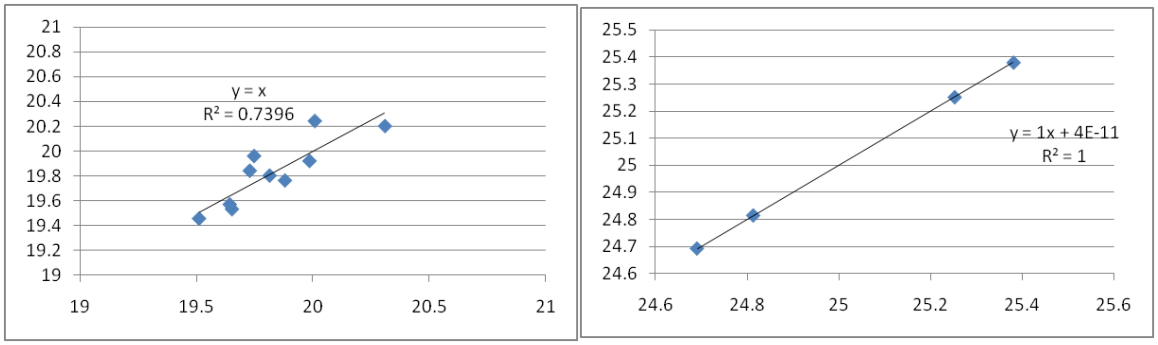

Figure 4.10. Kamlet-Taft plots of **4.4a** (left) and **4.4b** (right).

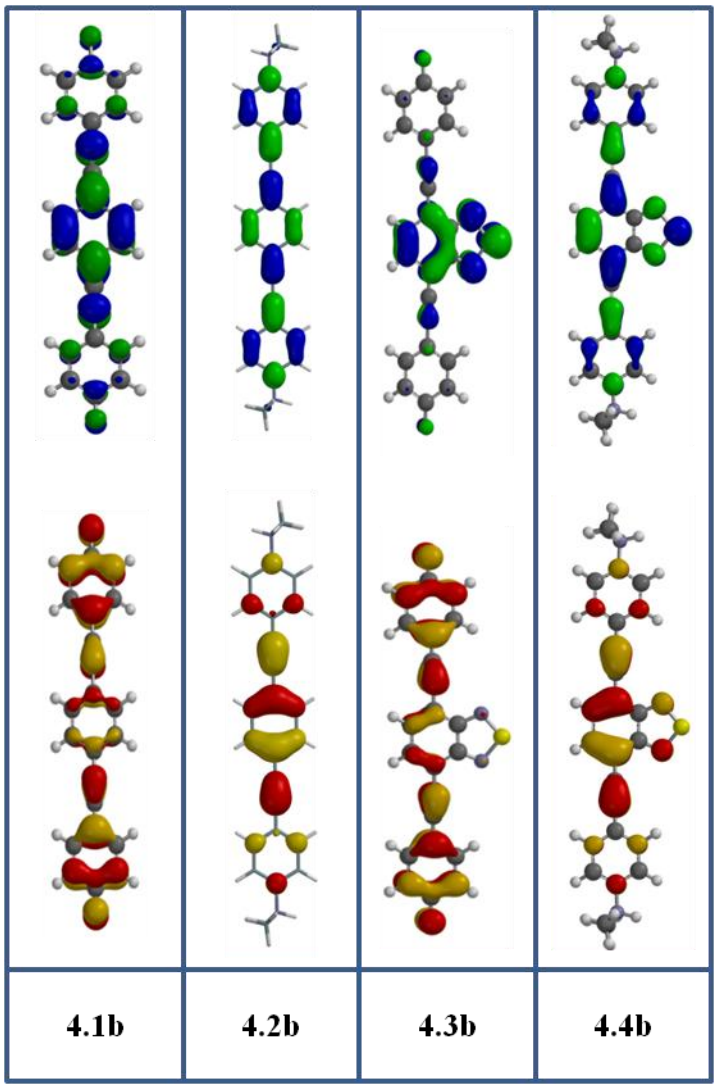

Figure 4.11. HOMO (Red and Yellow) and LUMO (Green and Blue) of **4.1b**-**4.4b**. FMOs were calculated with B3LYP 6-31G**//6-31G** using Spartan.

4.5 References

[1] (a) Martinez-Manez, R.; Sancenon, F. *Chem. Rev.* **2003**, *103*, 4419-4476. (b) Beer, P.D.; Gale, P.A. *Angew. Chem. Int. Ed.* **2001**, *40*, 486-516. (c) Haryley, J.H.; James, T.D.; Ward, C.J. *J. Chem. Soc. Perkin Trans.* **2000**, *1*, 3155-3184.

[2] (a) Rumi, M.; Ehrlich, J. E.; Heikal, A. A.; Perry, J. W.; Barlow, S.; Hu, Z.; McCord-Maughon, D.; Parker, T. C.; Roeckel, H.; Thayumanavan, S.; Marder, S. R.; Beljonne, D.; Bredas, J.-L. *J. Am. Chem. Soc.* **2000**, *122*, 9500-9510. (b) Zucchero, A. J.; Tolosa, J.; Tolbert, L. M.; Bunz, U. H. F. *Chem. Eur. J.* **2009** 15(47), 13075-13081. (c) Brombosz, Scott M.; Zucchero, Anthony J.; McGrier, Psaras L.; Bunz, Uwe H. F. *Journal of Organic Chemistry*, **2009**, 74, 8909-8913.

[3] Kamlet, M. J.; Abboud, J.-L.; Abraham, M. H.; Taft, R. W. *J. Org. Chem.* **1983**, *48*, 2877-2887.

[4] Neto, Brenno A. D.; Lapis, Alexandre A. M.; Mancilha, Fabiana S.; Vasconcelos, Igor B.; Thum, Caroline; Basso, Luiz A.; Santos, Diogenes S.; Dupont, Jaierton. *Organic Letters*, **2007**, *20*, 4001-4004.

[5] (a) Marcelo, N. F.; Vieira, A. A.; Cristiano, R.; Gallardo, H.; Bechtold, I. H. *Synthetic Metals*, **2009**, *7-8*, 675-680. (b) Vieira, Andre A.; Cristiano, Rodrigo; Bortoluzzi, Adailton J.; Gallardo, Hugo *Journal of Molecular Structure*, **2008**, *1-3*, 364-371. (c) Yao, Yung-Hsin; Kung, Liang-Rern; Hsu, Chain-Shu *Journal of Polymer Research*, **2006**, *4*, 277-283.

[6] Sonogashira, K. J. *Organomet. Chem.*, **2002**, *653*, 46-49.

[7] Grabowski, Z. R.; Krystyna, R.; Wolfgang, R. *Chemical Reviews* **2003**, 103(10), 3899-4031.

[8] Brombosz, Scott M.; Appleton, Anthony Lucas; Zappas, Andrew J.; Bunz, Uwe H. F. *Chemical Communications*, 2010, **46**, 1419 – 1421.

Chapter 5: Water Soluble Benzo- and Naphtho-thiadiazole Bistriazoles And Their Metal-Binding Properties

5.1 Introduction

In addition to the Sonogashira coupling of the terminal alkyne of the acenothiadiazoles, it is possible to react these free ethynyl groups utilizing click chemistry. As discussed below, this one reaction efficiently provides water-soluble, relatively redshifted, and metal-binding fluorophores.

The 1,3-dipolar cycloaddition of alkynes to azides was first investigated by Szeimies and Huisgen,[1] and was later retooled as a copper catalyzed process for the easy access towards 1,4-disubstituted triazoles.[2] While intended by Sharpless[3] for the construction of biologically active molecules, the "click" reaction is now popular for the construction of polymers and materials.[4]

A generally attractive but less explored aspect of the triazole formation is their incorporation, as functional modules, into fluorophores and/or chromophores; the triazole group could either work as an auxochromic group or a conjugative bridge between two chromophores or π-systems.[5] Herein we report that triazoles are quite powerful auxochromes, i.e., functional groups that red-shift the absorption and emission of acenothiadiazole-types.

We[6,7] and others[8] are interested in metallo-responsive fluorophore systems, and we have recently disclosed that a dipolar 1,3-cycloadduct containing a 2-pyridyl residue leads to turn-on fluorescence when exposed towards metal cations. In this

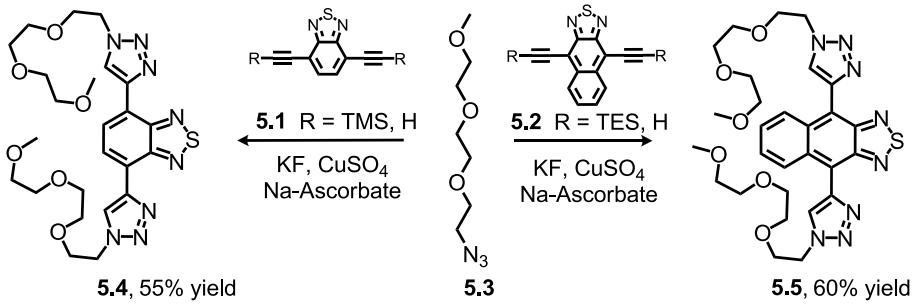

Scheme 5.1. Synthesis of compounds **5.4** and **5.5**.

communication we present attractive, novel water-soluble and fluorescent bis-cycloadducts **5.4** and **5.5** that display binding pockets for metal cations.

5.2 Results and Discussion

Table 5.1. Photophysical Properties of Compounds **5.1**, **5.2**, **5.4**, and **5.5** in Dichloromethane and Water

Cpd	Abs. λ_{max}		Emission λ_{max}		Φ^a		Fluor-escence Lifetime (ns, τ)		Stokes Shift (cm^{-1})		Gap Calcd eV (nm) [b]	FMO positions Calculated (eV)[b]	
	DCM	H_2O	DCM	H_2O	DCM	H_2O	DCM	H_2O	DCM	H_2O		HOMO	LUMO
1.5[c]	386	NA	443	NA	0.85	NA	7.9	NA	3334	NA	3.41 (364)	-6.15	-2.74
4.5	406	385	508	519	0.72	0.13	14.0	7.0	4946	6706	3.10 (399)	-5.64	-2.54
2.5[c]	528	NA	534	NA	0.28	NA	15.2	NA	212	NA	2.50 (496)	-5.55	-3.05
5.5	505	475	610	602	0.09	0.013	18.4	5.3	3409	4442	2.35 (527)	-5.13	-2.78

[a] Quinine sulfate in 0.1 M H_2SO_4 (aq.) used as a reference standard. [b] B3LYP 6-31G**//6-31G** SPARTAN [c] In the case of **5.1** and **5.2**, the TIPS protected analogue was utilized due to its greater stability than the corresponding TMS or TES analogues

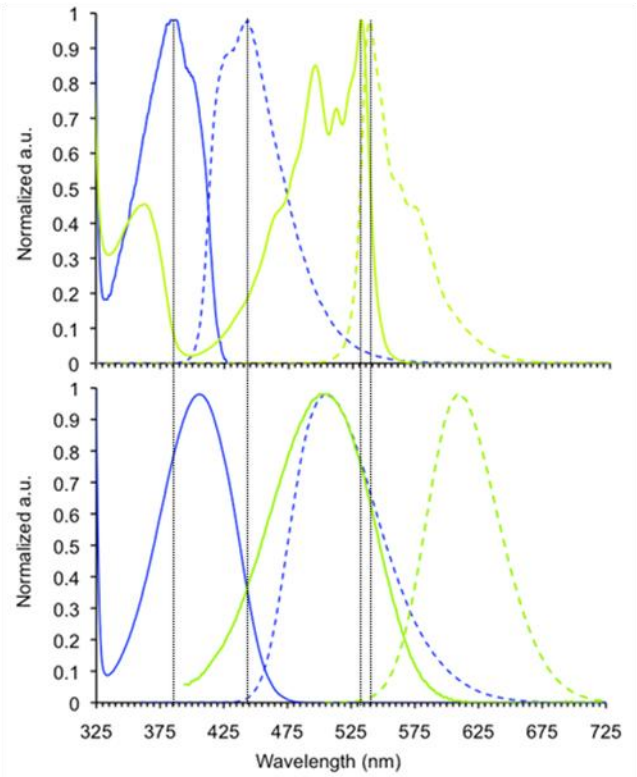

Figure 5.1. Normalized absorption and emission spectra of **5.1** (blue), and **5.2** (green, both Top) and **5.4** (blue) and **5.5** (green, both Bottom) in dichloromethane. Solid lines depict absorption spectra while broken lines depict emission spectra. In the case of **5.1** and **5.2**, the TIPS protected analogue was utilized due to its greater stability than the corresponding TMS or TES analogues.

The TMS-protected diethynylbenzothiadiazole (**5.1**)[9] is deprotected *in situ* by KF; the azide **5.3**, $CuSO_4$ (2.5 eq) and sodium ascorbate (2.5 eq) are added to give **5.4** in 55% yield. The same approach works for **5.5** which is formed analogously in 60% yield by reaction of **5.2** with **5.3** under identical conditions. The use of a large excess of copper sulfate was necessary to catalyze this reaction, as the products **5.4** and **5.5** bind copper salts quite efficiently. We selected the oligoethylene azide **5.3** as substituent, as it a) confers water solubility and b) is known for its "biophobic" properties, i.e., it suppresses non-specific interactions with proteins, etc. Table 5.1

summarizes the relevant photophysical properties of **5.1, 5.2**, **5.4** and **5.5**. There are several noteworthy trends. In dichloromethane (DCM) the emissive quantum yields of all investigated species (**5.1**, **5.2**, **5.4**, **5.5**) are high. Generally, the quantum yields of the precursor alkynes are somewhat higher than those of their 1,3-dipolar azide adducts. As the precursor alkynes do not dissolve in water, only the quantum yields of **5.4** and **5.5** were obtained for aqueous solutions. While **5.4** displays a quite robust quantum yield of 13% in water, in the case of **5.5** the quantum yield in water drops to 1.3%. With its emission wavelength of 525 nm and a quantum yield of 13%, **5.4** is potentially a very useful fluorophore core as it is quite stable towards photobleaching. In addition, the emissive lifetimes of **5.4** in DCM (14 ns) and in water (7 ns) solutions are unusually high. The larger congener **5.5** displays similarly large fluorescence lifetimes of 18 ns and 5 ns in DCM and water, respectively. This is testimony to the photophysical properties of the benzothiadiazole core, as the precursor alkynes also display relatively long emissive lifetimes, although not as long as those observed for the 1,3-cycloadducts.

The long fluorescence lifetime of the cycloadduct **5.4** is promising for potential applications as a bio-fluorophore. As complex biological matrices such as cells,

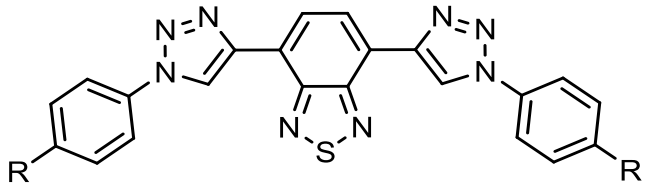

5.6a R = Hex-
5.6b R = H-

Scheme 5.2. Compounds **5.6a** and **5.6b**.

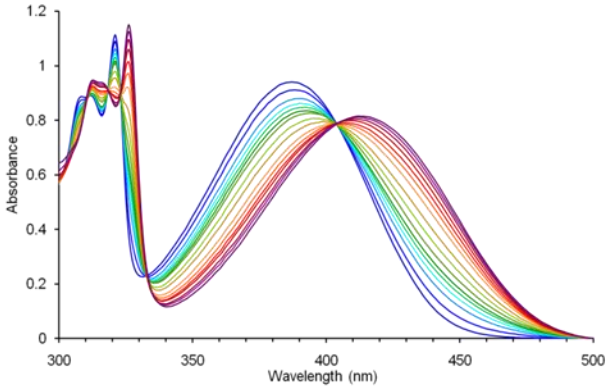

Figure 5.2. Representative absorption titration of **5.4** (blue trace; 151.5 μM) with $CuSO_4$ in water. [Cu] ranges from 0-6.26 x 10^{-1} M (red trace **5.4**-Cu^{2+} complex).

serum, etc. are always fraught with background fluorescence[10] with an emissive half life of around 3 ns, fluorophores such as **5.4** should shine if time-gated detection is used. Quite unusual is also that the emission and absorption wavelengths of **5.4** and **5.5** are not very solvent dependent and that we actually see a slight blue-shift in the absorption features for both **5.4** and **5.5** when going from DCM into water.

The emission of **5.4** displays a slight red-shift when going from DCM to water, while **5.5** displays a slight blue-shift upon the same solvent change. The similarity of the spectral properties in water and in DCM suggests that these fluorophores do not exhibit a large degree of charge transfer character in the ground or excited states. This is reasonable because **5.4** and **5.5** are electron poor due to both building blocks, the triazole and the thiadiazole, being electron acceptors.

Surprising is the quite significant red-shifts in absorption and particularly emission wavelengths of the 1,3-diploar cycloadducts **5.4** and **5.5** in comparison to their diyne precursors **5.1** and **5.2**.[11] Quantum chemical calculations (B3LYP 6-31G**//6-31G** as implemented by SPARTAN for Windows) also support this trend

(Table 5.1) and show that the HOMO and the LUMO positions are both raised, however the destabilization of the HOMO is more pronounced than the destabilization of the LUMO when going from alkyne to triazole. The absorption and emission profiles for **5.6a** (DCM; $\lambda_{max\ abs}$ = 409 nm, $\lambda_{max\ emission}$ = 507 nm) are very similar to those obtained for **5.4** and Spartan computes (B3LYP 6-31G**//6-31G**) HOMO and LUMO of the model compound **5.6b** at -5.69 eV and -2.66 eV. Consequently, while the triazole unit has a strong auxochromic effect, it is poor at transmitting electronic communication between two π-systems.

Adducts **5.4** and **5.5** display a binding pocket that should readily bind to metal analytes of appropriate charge and atomic radius as previously demonstrated by us and by Xie *et al.* for similar types of 1,3-dipolar cycloadducts, but only in non-aqueous solutions.[12]

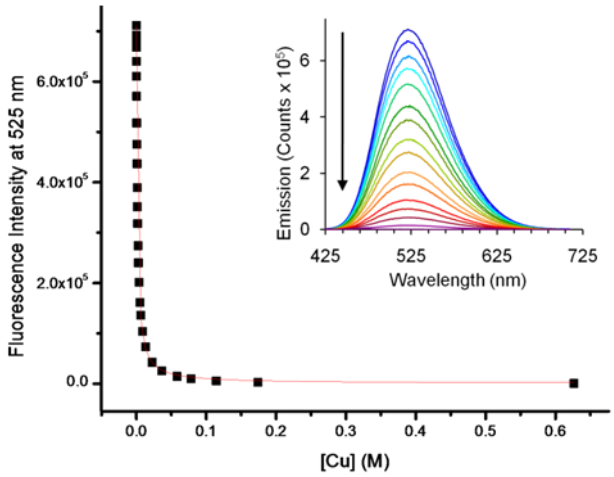

Figure 5.3. Emission data (black dots) of the titration of **5.4** (151.5 μM) with $CuSO_4$ in water. Red line indicates the fitted equation used to determine binding constant. [Cu] ranges from 0-6.26 x 10^{-1} M. Inset: Representative emission titration of **5.4** with $CuSO_4$ in water.

Table 5.2. Binding Data of **5.4** and **5.5** with Copper (II) and Nickel (II) in Water

Compound	**5.4**	**5.4**	**5.5**
Metal [a]	Cu(II)	Ni(II)	Cu(II)
Log *K* from absorption [b]	2.83	3.18	2.96
Log *K* from emission [c]	2.70 ± 0.01	3.17 ± 0.01	2.71 ± 0.03

[a] The sulfate salt was used in all cases. [b] Values obtained from the deconvolution of the absorption spectra utilizing Datan software.[12] [c] Values obtained from fitting the quenching of the emission spectra with Equation 1.

Our adducts (**5.4**, **5.5**) allow the screening of metal binding in water. Upon addition of the triflate salts of Li^+, Na^+, K^+, Ca^{2+}, Zn^{2+}, Mg^{2+}, and Sn^{2+} to an aqueous solution of **5.4**, no change in the absorption or emission spectra is observed. Upon addition of Hg^{2+} and trifluoroacetic acid (TFA) no change in the absorption spectra is observed,

however the emission of **5.4** becomes quenched. Upon the addition of Cu^{2+} or Ni^{2+} the charge transfer band in the absorption spectra redshifts (~20-30 nm) and the emission also quenches. Titrations of **5.4** and **5.5** with copper sulfate and **5.4** with nickel sulfate in water were performed to determine the strength of the binding.

Attempting to plot the fluorescence quenching spectra according to the standard Stern-Volmer equation resulted in significant deviation from linearity. However, the data was well correlated when Equation 5.1 is employed,

$$I_q = I_o + \frac{I_{final} - I_o}{2} * \left\{ 1 + \frac{[Q]}{[F]} + \frac{1}{K_{sv}[F]} - \left[\left(1 + \frac{[Q]}{[F]} + \frac{1}{K_{sv}[F]} \right)^2 - 4\frac{[Q]}{[F]} \right]^{\frac{1}{2}} \right\} \quad (5.1)$$

where I_q is the intensity of the fluorescence at a given quencher concentration, I_o is

the initial fluorescence intensity of the fluorophore, I_{final} is the final intensity of the fluorescence of the quenched fluorophore, [Q] is the concentration of the quencher added, [F] is the concentration of the fluorophore and K_{sv} is the apparent Stern-Volmer constant.

The results of the titration are summarized in Table 5.2. The binding of **5.4** to Ni(II) in water resulted in a binding constant of log K = 3.17 $\pm$ 0.01. The lower binding constant in comparison to Xie's (log K = 4.48 $\pm$ 0.03) is expected as the titration was performed in water, which is a more competitive ligating solvent than acetonitrile. The binding constant for Cu(II) in water was slightly smaller in magnitude than that of nickel with log K = 2.70 $\pm$ 0.01. The binding constant for the binding of copper to **5.5** was determined to be log K = 2.71 $\pm$ 0.03. This binding constant was nearly identical to that of **5.4** which demonstrated the independence of the binding upon the size of the aceno portion of the core. Interestingly, the necessity of a stoichiometric amount of copper in the synthesis of **5.4** and **5.5** can be attributed to this high binding constant as once the triazole group is formed; the effective concentration of free copper available to catalyze the reaction is drastically reduced. Binding constants were also obtained from the deconvolution of the absorption spectra from the titration of the metal utilizing Datan software.[13] In all cases, the constants obtained from the absorption spectra were in good to excellent agreement with the values obtained from the Stern-Volmer plots of the emission spectra. Assuming a 1:1 complex agrees very well with the obtained data.

Apparently upon coordination to one copper ion, the second binding pocket becomes too electron poor to effectively bind another copper ion in aqueous solution.

5.3 Conclusions

In conclusion, we have prepared water soluble bistriazoles **5.4** and **5.5** and the model compound **5.6a**. From the combination of spectroscopic and computational data, we can conclude that the triazole-ring has a strong auxochromic effect and leads to red-shifted spectroscopic features for the connected arene in the 4-position, but at the same time is a poor electronic conduit, as the spectroscopic properties of **5.6a** are almost identical to that of **5.4**. The adducts **5.4** and **5.5** do not show large solvent dependencies of their spectroscopic properties, and **5.4** is surprisingly fluorescent in water and binds both copper and nickel in aqueous solution. Overall, the 1,3-dipolar cycloaddition of alkynes to azides is a superb tool to prepare functional, metallo-responsive fluorophores.

This work has been published in *Chemical Communications*:

Brombosz, Scott M.; Appleton, Anthony Lucas; Zappas, Andrew J.; Bunz, Uwe H. F. *Chemical Communications*, **2010**, *46*, 1419 – 1421.

5.4 Experimental and Supplementary Information

5.4.1 4,7-Bis(1-(2-(2-(2-methoxyethoxy)ethoxy)ethyl)-1H-1,2,3-triazol-4-yl)benzo[c][1,2,5]thiadiazole, **5.4**.

To a stirring solution of 0.150 g (1.0 eq, 4.57×10^{-4} mol) of 4,7-bis((trimethylsilyl) ethynyl)benzo[c][1,2,5]thiadiazole (**5.1**) in 10 mL of 5:1 THF:H_2O was added 0.139 g (4.0 eq, 1.826×10^{-3} mol) of KF hydrate was added and the solution was allowed to stir for 30 minutes. After the addition of 0.216 g (2.5 eq, 1.14×10^{-3} mol) of **5.3** the solution was freeze-pump-thawed three times to remove any oxygen. While under a flow of N_2, 0.182 g (2.5 eq, 1.14×10^{-3} mol) of copper sulfate and 0.226 g (2.5 eq, 1.14×10^{-3} mol) of sodium ascorbate was added. After stirring overnight, the crude mixture was filtered through celite with dichloromethane. The solvent was removed under vacuum. The product was filtered through a short silica column with dichloromethane followed by ethyl acetate as the eluent to elute any thiadiazole starting material. The product (**5.4**) was then eluted with acetone. After concentration, the recovered oil was dissolved in water and lyophilized for two days to yield a yellow/green solid in 55% yield (0.141 g). ^{1}H-NMR (500 MHz, $CDCl_3$) 3.30 (s, 6H), 3.46 (m, 4H), 3.59 (m, 4H), 3.65 (m, 8H), 3.98 (t, 4H J=5 Hz), 4.68 (t, 4H J=5 Hz), 8.63 (s, 2H), 8.85 (s, 2H); ^{13}C-NMR (125 MHz, $CDCl_3$) 50.44, 58.95, 69.56, 70.54, 70.73, 71.83, 122.67, 125.02, 125.97, 143.00, 152.25; IR (KBr) $\tilde{\nu}$ 3500 (w), 3175 (m), 3113 (w), 2870 (s), 2291 (w), 1946 (w), 1580 (w), 1539 (w), 1456 (s), 1366 (s), 1271 (s), 1227 (s), 1142 (s), 1045 (s), 981 (s), 879 (s), 825 (s), 692 (s), 619 (s), 500 (s); HRMS Calc. for $C_{24}H_{35}O_6N_8S$ (FAB **5.4** + H) 563.24003, found 563.24070.

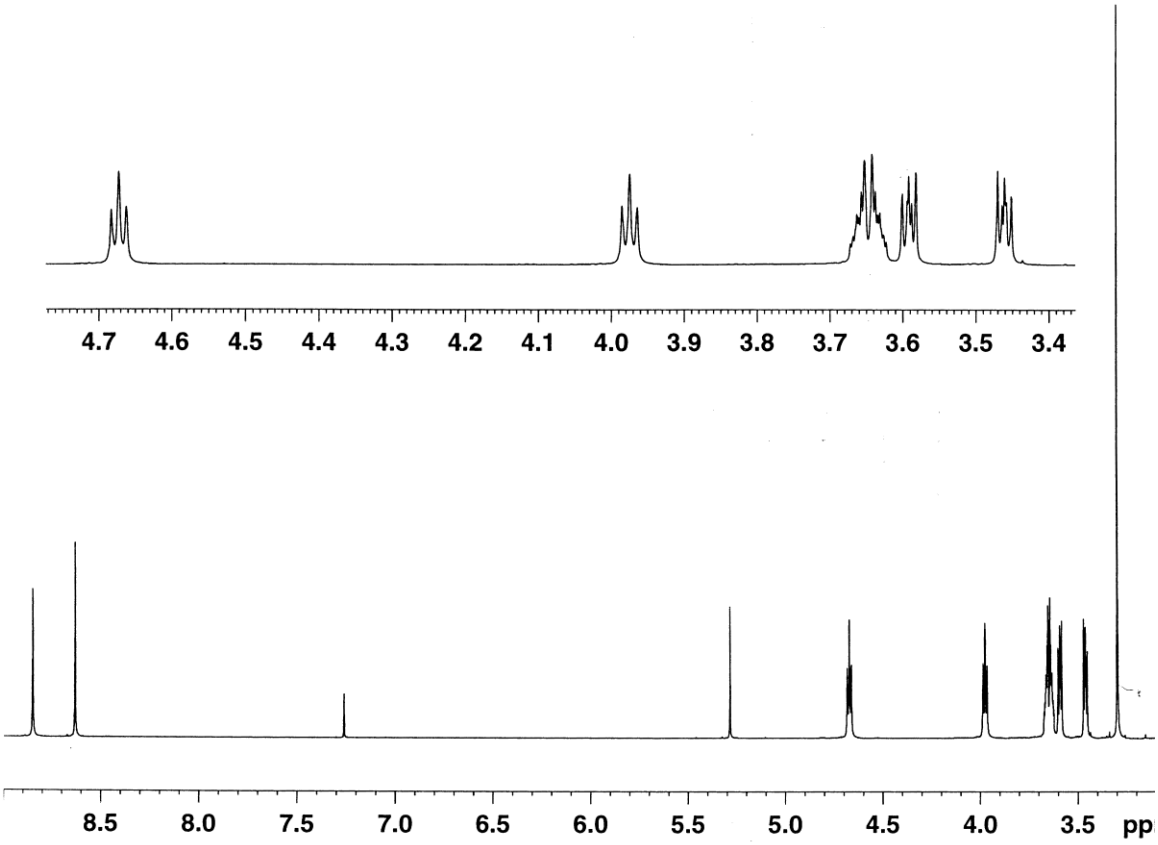

Figure 5.4. ^{1}H-NMR spectrum ($CDCl_3$) of compound **5.4**.

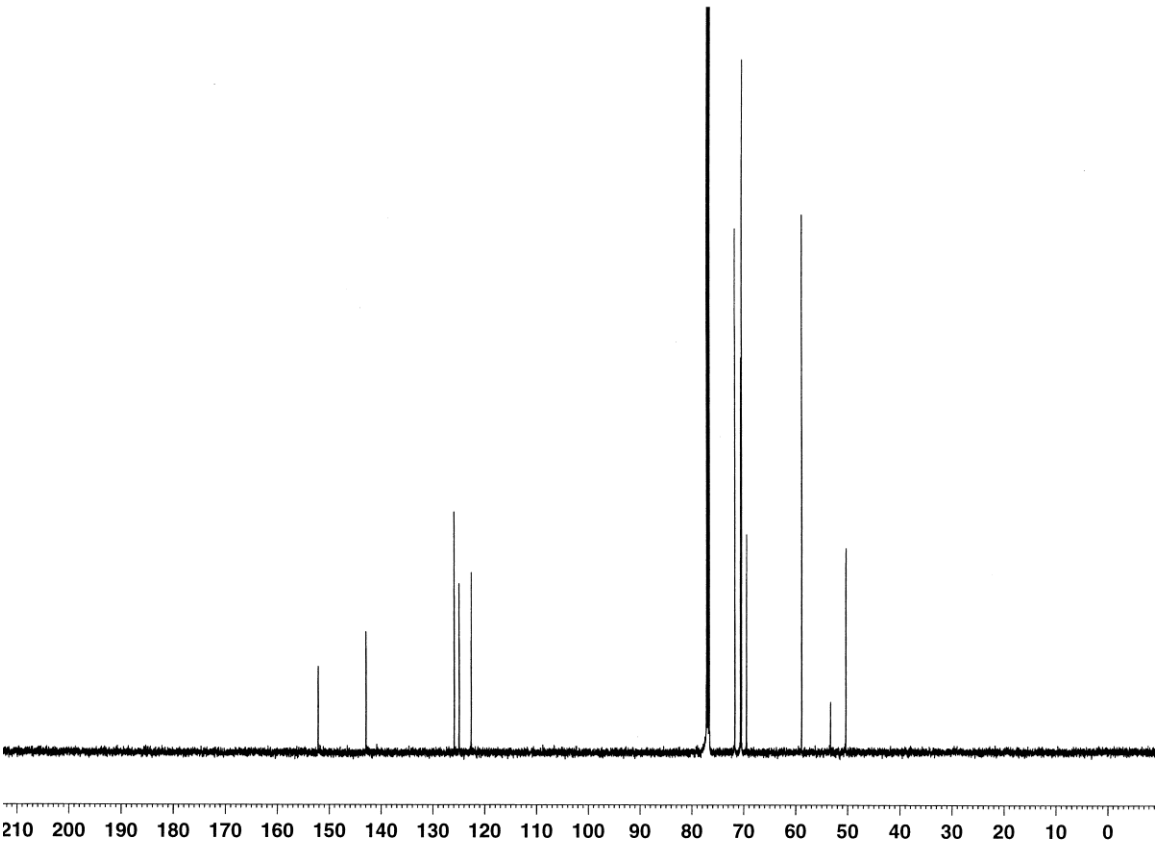

Figure 5.5. ^{13}C-NMR spectrum ($CDCl_3$) of compound **5.4**.

5.4.2. 4,9-Bis(1-(2-(2-(2-methoxyethoxy)ethoxy)ethyl)-1H-1,2,3-triazol-4-yl)naphtho [c][1,2,5]thiadiazole, **5.5**.

To a stirring solution of 0.150 g (1.0 eq, $3.24x10^{-4}$ mol) of 4,9-bis((triethylsilyl)ethynyl)-naphtho[2,3-c][1,2,5]thiadiazole (**5.2**) in 10 mL of 5:1 THF:H_2O was added 0.099 g (4.0 eq, $1.3x10^{-3}$ mol) of KF hydrate was added and the solution was allowed to stir for 30 minutes. After the addition of 0.153 g (2.5 eq, $8.10x10^{-4}$ mol) of **5.3** the solution was freeze-pump-thawed three times to remove any oxygen. While under a flow of N_2, 0.129 g (2.5 eq, $8.10x10^{-4}$ mol) of copper sulfate and 0.161 g (2.5 eq, $8.10x10^{-4}$ mol) of sodium ascorbate was added. After stirring overnight, the crude mixture was filtered through celite with dichloromethane. The solvent was removed under vacuum. The product was filtered through a short silica column with dichloromethane followed by ethyl acetate as the eluent to elute any thiadiazole starting material. The product (**5.5**) was then eluted with 20% acetone in ethyl acetate. After concentration, the recovered oil was dissolved in water and lyophilized for two days to yield a red solid in 60% yield (0.119 g). ^{1}H-NMR (500 MHz, $CDCl_3$) 3.24 (s, 6H), 3.41 (m, 4H), 3.58 (m, 4H), 3.69 (m, 8H), 4.05 (t, 4H J=5 Hz), 4.78 (t, 4H J=5 Hz), 7.52 (dd, 2H J=6Hz), 8.66 (s, 2H), 9.03 (dd, 2H J=6Hz); IR (KBr) $\tilde{\nu}$ 3497 (w), 3148 (m), 2870 (s), 1950 (w), 1647 (w), 1533 (w), 1458 (s), 1352 (s), 1259 (s), 1109 (s), 1051 (s), 893 (s), 822 (s), 765 (s), 721 (s), 529 (s); HRMS Calc. for $C_{28}H_{37}O_6N_8S$ (FAB **5.5** + H) 613.25568, found 613.25273.

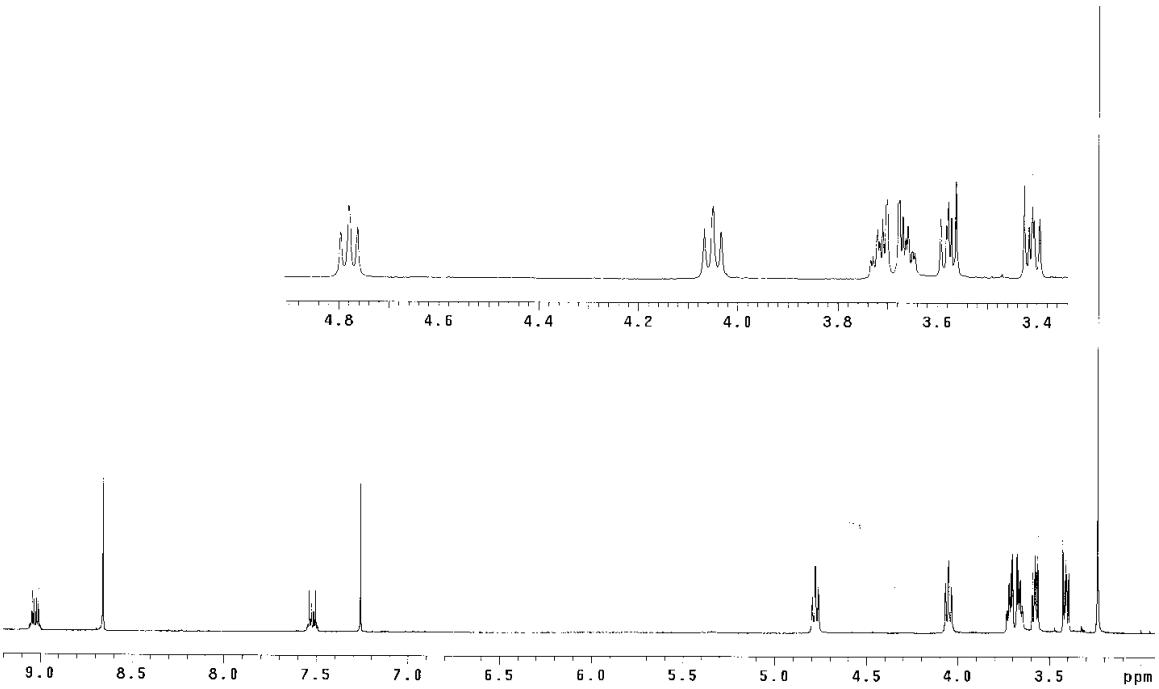

Figure 5.6. ^{1}H-NMR spectrum ($CDCl_3$) of compound **5.5**.

5.4.3. 4,7-Bis(1-(4-hexylphenyl)-1H-1,2,3-triazol-4-yl)benzo[c]

[1,2,5]thiadiazole, **5.6a**.

To a stirring solution of 0.150 g (1.0 eq, $4.57x10^{-4}$ mol) of 4,7-bis((trimethylsilyl) ethynyl)benzo[c][1,2,5]thiadiazole (**5.1**) in 10 mL of 5:1 THF:H_2O was added 0.139 g (4.0 eq, $1.826x10^{-3}$ mol) of KF hydrate was added and the solution was allowed to stir for 30 minutes. After the addition of 0.232 g (2.5 eq, $1.14x10^{-3}$ mol) of **7** the solution was freeze-pump-thawed three times to remove any oxygen. While under a flow of N_2, 0.182 g (2.5 eq, $1.14x10^{-3}$ mol) of copper sulfate and 0.226 g (2.5 eq, $1.14x10^{-3}$ mol) of sodium ascorbate was added. After stirring overnight, the crude mixture was filtered through celite with dichloromethane. The solvent was removed under vacuum. The product was filtered through a short silica column with dichloromethane to elute any thiadiazole starting material. The product (**5.6a**) was then eluted with 5% ethyl acetate in DCM.

Concentration under reduced pressure provided **5.6a** as a yellow solid (0.070g, 26% yield). ^{1}H-NMR (300 MHz, $CDCl_3$) 0.89 (t, 6H), 1.32 (m, 12H), 1.63 (m, 4H), 2.65 (t, 4H), 7.29 (d, 4H J=5 Hz), 7.68 (d, 4H =5 Hz), 8.59 (s, 2H), 9.00 (s, 2H); ^{13}C-NMR (125 MHz, $CDCl_3$) 14.41, 22.85, 29.14, 31.54, 31.92, 35.73, 120.44, 121.77, 122.49, 126.13, 129.76, 134.91, 143.54, 144.08, 152.16; IR (KBr) $\tilde{\nu}$ 3167 (m), 3051 (w), 2955 (s), 2924 (s), 2853 (s), 2280 (w), 1909 (m), 1728 (m), 1580 (m), 1517 (s), 1466 (m), 1410 (m), 1240 (s), 1177 (m), 1040 (s), 989 (s), 885 (s), 837 (s), 802 (s), 519 (s); HRMS Calc. for $C_{34}H_{38}N_8S$ (EI **6b** + H) 590.2940, found 590.2925.

5.4.4. Spectroscopic Response Data of **5.4** in Water

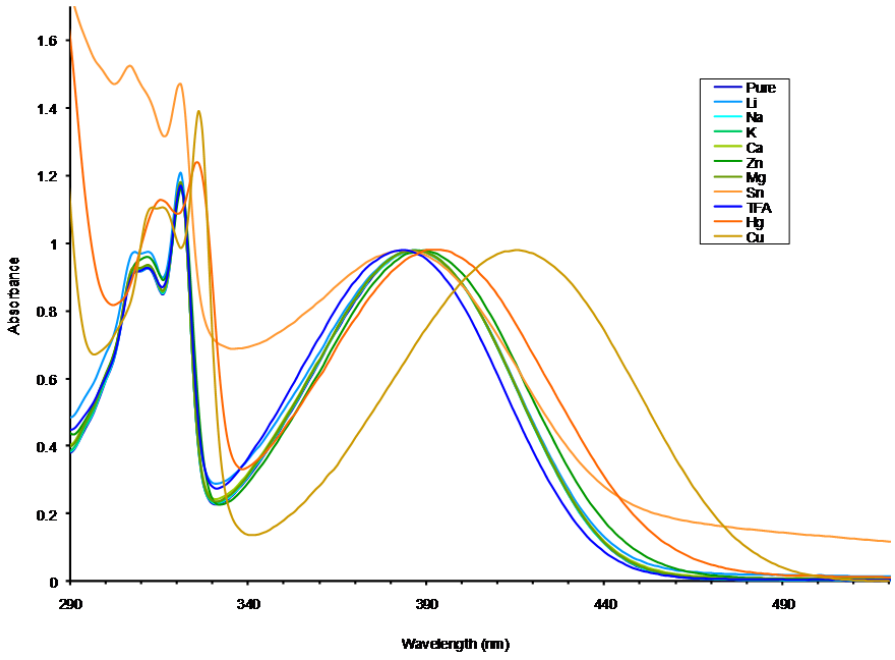

Figure 5.7. Absorption spectra of **5.4** before and after the addition of metal triflates and TFA in water. All fluorophore concentrations were at 89 μM.

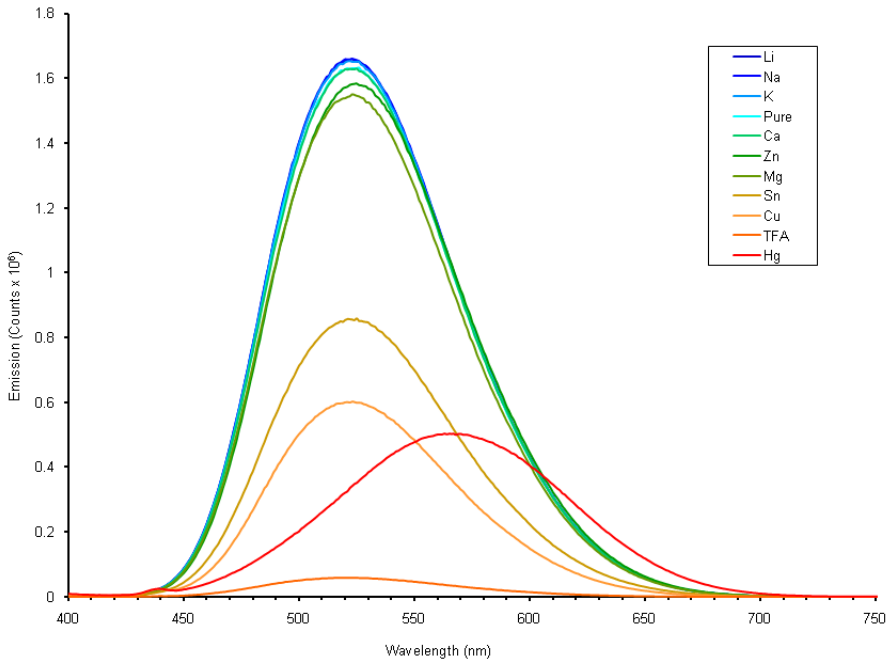

Figure 5.8. Emission spectra of **5.4** before and after the addition of metal triflates and TFA in water. All fluorophore concentrations were at 89 μM.

5.4.5 Stern-Volmer Plots of **5.4** and **5.5**

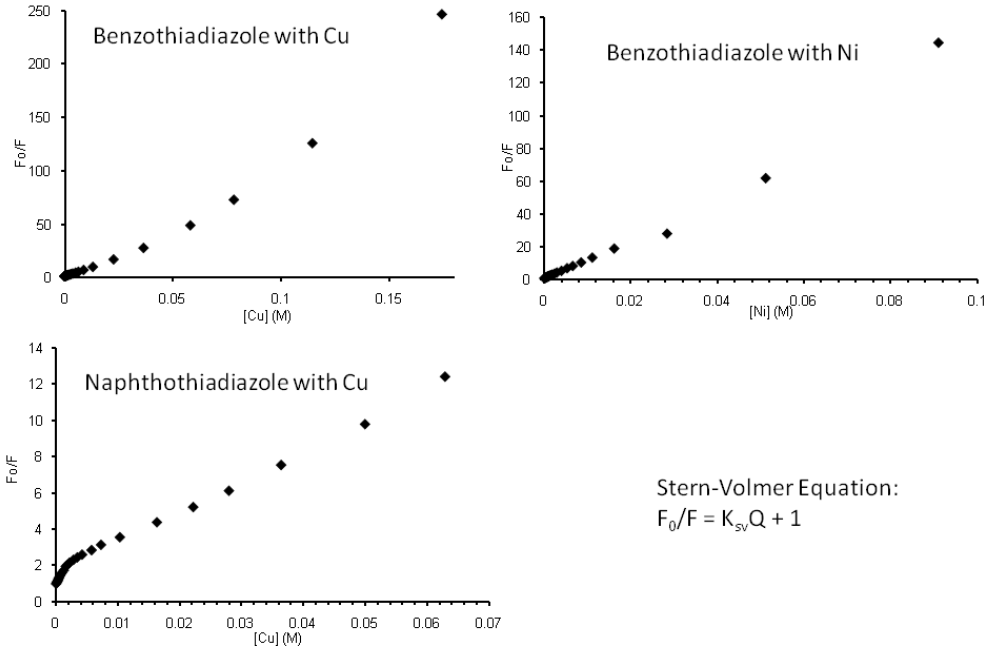

Figure 5.9. Emission quenching data plotted according to the standard Stern-Volmer equation showing the non-linear behavior of the quenching. Compound **5.4** with Cu(II) (Top Left), compound **5.4** with Ni (II) (Top Right), **5.5** with Cu(II) (Bottom Left).

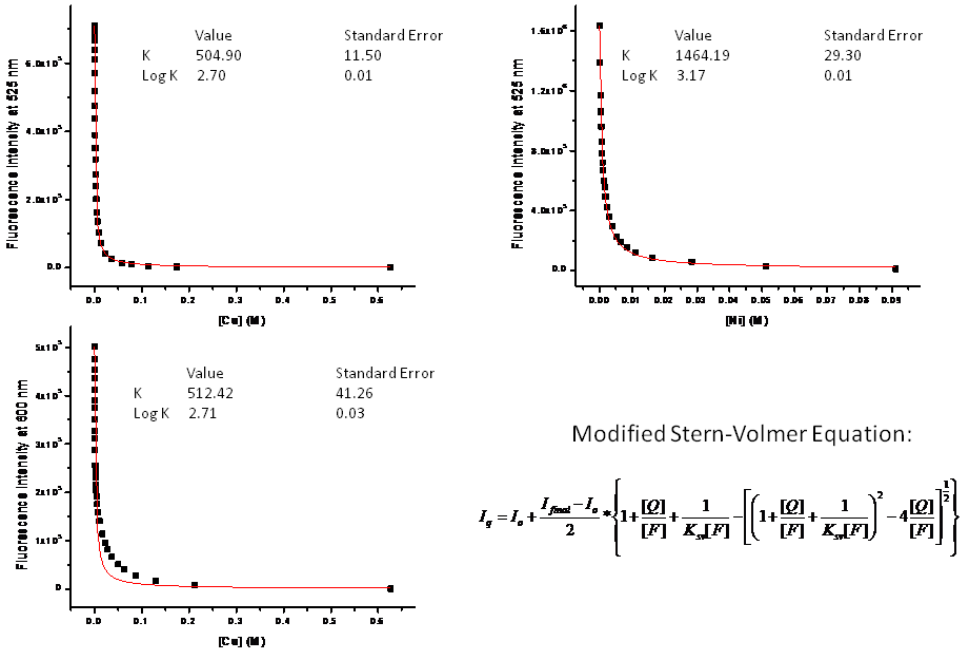

Figure 5.10. Emission quenching data plotted according to the modified Stern-Volmer equation. Compound **5.4** with Cu(II) (Top Left), compound **5.4** with Ni (II) (Top Right), **5.5** with Cu(II) (Bottom Left).

5.4.6 Absorption and Emission Titrations of **5.4** and **5.5**.

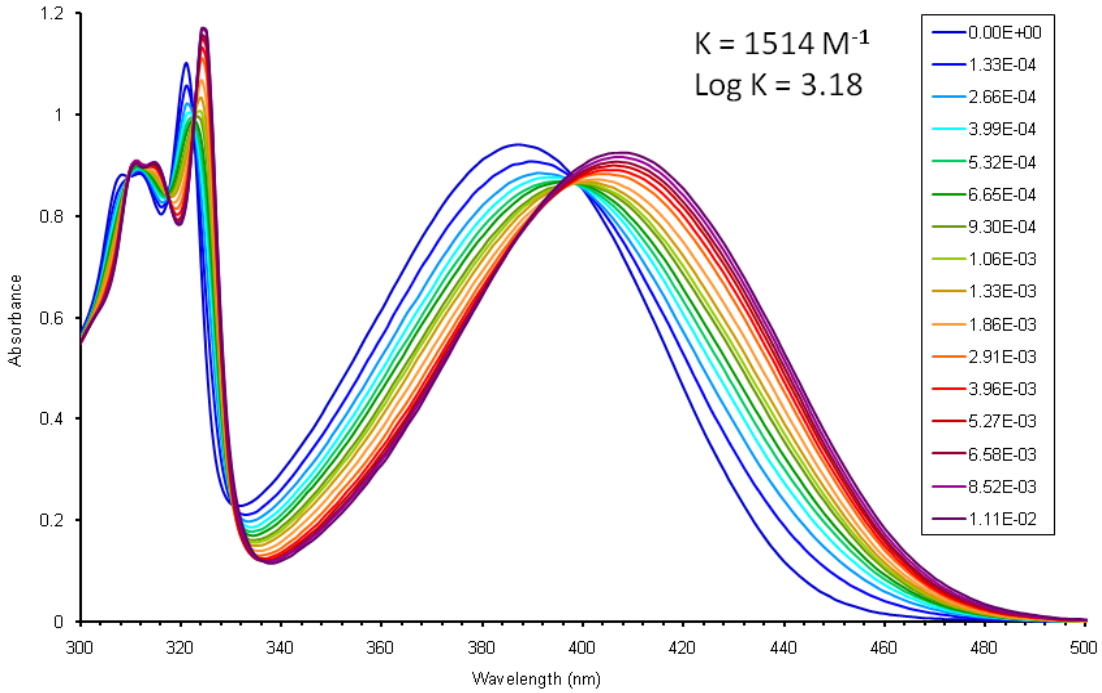

Figure 5.11. Absorption spectra of the titration of **5.4** (151 μM) with $NiSO_4$ in water.

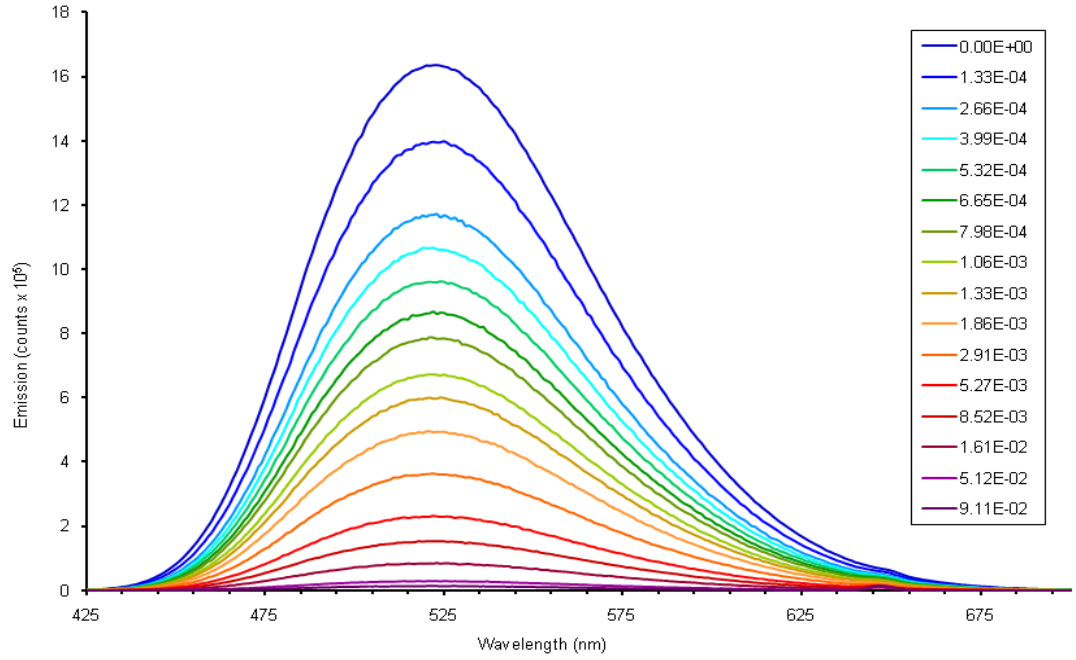

Figure 5.12. Emission spectra of the titration of **5.4** (151 μM) with $NiSO_4$ in water.

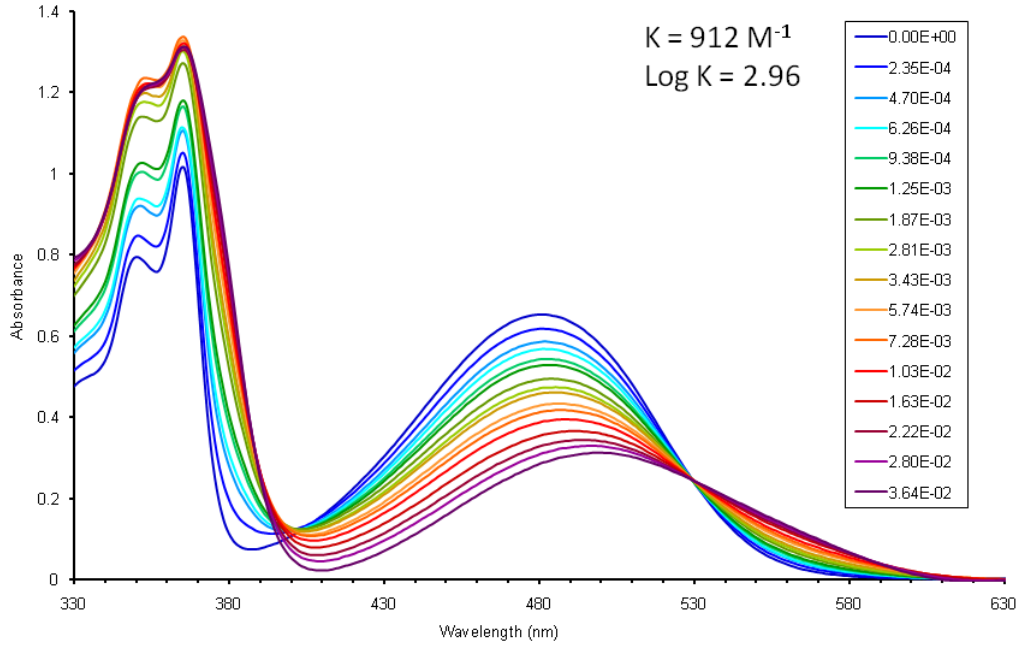

Figure 5.13. Absorption spectra of the titration of **5.5** (166 μM) with $CuSO_4$ in water.

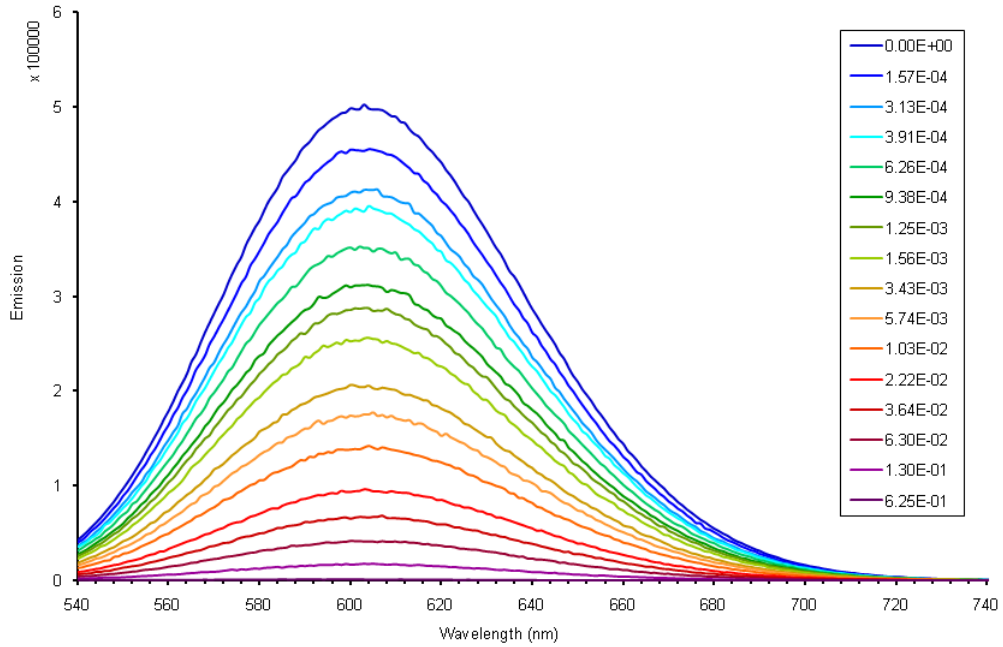

Figure 5.14. Emission spectra of the titration of **5.5** (166 μM) with $CuSO_4$ in water.

5.5 References

[1] (a) Huisgen, R.; Szeimies, G.; Moebius, L. *Chem. Ber.* **1967**, *100*, 2494. (b) R. Huisgen, R. Knorr, L. Moebius, G. Szeimeis, *Chem. Ber.* **1965**, *98*, 4014.

[2] (a) Lutz, J. F. *Angew. Chem.* **2007**, *46*, 1018. (b) Binder, W. H.; Sachsenhofer, R. *Macromol. Rapid. Commun.* **2007**, *28*, 15. (c) Meldal, M.; Tornoe, C. W.; *Chem. Rev.* **2008**, *108*, 2952.

[3] (a) Kolb, H. C.; Sharpless K. B. *Drug Discovery Today* **2003**, *8*, 1128. (b) Phillips, R. L.; Kim, I. B.; Tolbert, L. M.; Bunz U. H. F. *J. Am. Chem. Soc.* **2008**, *130*, 6952. (c) Phillips, R. L.; Kim, I. B.; Carson, B. E.; Tidbeck, B.; Bai, Y.; Lowary, T. L.; Tolbert, L. M.; Bunz, U. H. F. *Macromolecules* **2008**, *41*, 7316.

[4] (a) Engert, B. C.; Bakbak, S.; Bunz, U. H. F. *Macromolecules* **2005**, *38*, 5868. (b) Bakbak, S.; Leech, P. J.; Carson, B. E.; Saxena, S.; King, W. P.; Bunz, U. H. F. *Macromolecules* **2006**, *39*, 6793. (c) Erdogan, B.; Song, L. L.; Wilson, J. N.; Park, J. O.; Srinivasarao, M.; Bunz, U. H. F. *J. Am. Chem. Soc.* **2004**, *126*, 3678.

[5] Opsteen, J. A.; van Hest, J. C. M. *Chem. Commun.* **2005**, 57-59.

[6] Schweinfurth, D.; Hardcastle, K. I.; Bunz, U. H. F. *Chem. Commun.* **2008**, 2203.

[7] (a) Wilson, J. N. Bunz, U. H. F. *J. Am. Chem. Soc.* **2005**, *127*, 4124. (b) Zucchero, A. J.; Wilson, J. N.; Bunz, U. H. F. *J. Am. Chem. Soc.* **2006**, *128*, 11872. (c) Tolosa, J.; Zucchero, A. J.; Bunz, U. H. F. *J. Am. Chem. Soc.* **2008**, *132*, 6498.

[8] (a) Wang, X. Y.; Kimyonok, A.; Weck, M. *Chem. Commun.* **2006**, 3933. (b) Happ, B.; Friebe, C.; Winter, A.; Hager, M. D.; Hoogenboom, R.; Schubert, U. S. *Chem. Asian J.* **2009**, *4*, 154.

[9] Bangcuyo, C. G.; Evans, U.; Myrick, M. L.; Bunz, U. H. F. *Macromolecules* **2001**, *34*, 7592.

[10] Lakowicz, J.R. *Principles of Fluorescence Spectroscopy*, 3rd ed.; Springer, 2006.

[11] Gonzlez-Vera, J. A.; Lukovi, E.; Imperiali, B. *J. Org. Chem.* **2009**, *74*, 7309-7314.

[12] Maisonneuve, S.; Fang, Q.; Xie, J. *Tetrahedron* **2008**, *64*, 8716.

[13] http://www.iss.com/products/components/datan/

Chapter 6: Are N,N-Dihydrodiazatetracene-Derivatives Antiaromatic?

6.1 Introduction

Having explored the unique properties of the acenothiadiazoles, we turned our attention to producing N-heteroacenes. These compounds can be easily produced through the condensation reaction of an *ortho*-diamine and an *ortho*-dione and due to the ease of synthesis of *o*-diones, a wide variety of N-heteroacenes can be produced. In this initial examination, we will produce the relatively simple diazatetracene and study its photophysical, electrochemical, and antiaromatic properties.

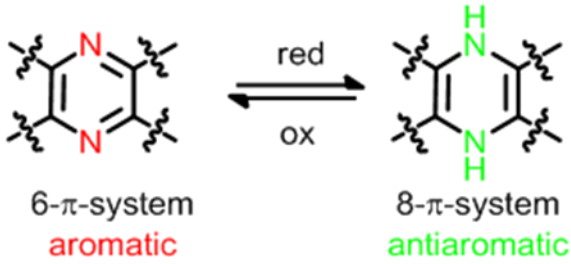

Scheme 6.1. Interconversion of an aromatic 6-π-pyrazine module into an antiaromatic 8-π-dihydropyrazine module.

The higher acenes have been widely used in organic electronics, due to their high charge carrier mobilities.[1] Pentacene in particular has potential applications as thin-film p-channel transistors.[2] Its crystal packing exhibits significant π-π intermolecular overlap, which contributes to its high mobility.[2,3] Anthony has demonstrated that pentacenes, hexacenes, and heptacenes with strategically placed, sterically demanding alkyne substituents are stable and can be easily processed.[3] Their crystal structures can be manipulated predictably by the choice of appropriate substituents to maximize π-π-

stacking in the solid state.[4] We now explore the potential elaboration of these systems by synthesizing and studying the properties of a pair of soluble, redox-related diaza and dihydrodiaza- tetracenes.

The considerable interest in pentacene (~2000 papers, Web of Science) has only recently been extended to the larger nitrogen-containing heteroacenes, even though these have been known since the late 19th century.[5] Houk,[6] Wudl,[7] Nuckolls,[8] Tadokoro[9] Jenekhe[10] and Yamashita[11] have rejuvenated the field. Large heteroacenes show potential as electron-transport materials.

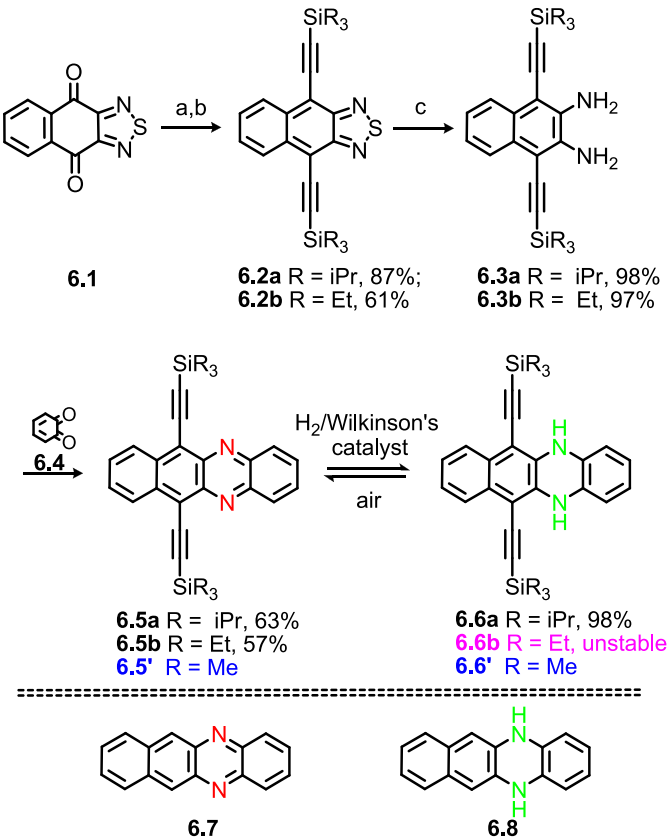

Scheme 6.2. Synthesis of the heteroacenes **6.5a,b** and dihydroheteroacenes **6a,b**. a: R_3Si-CC-Li, then wet ether; **a** R = isopropyl, **b** R = ethyl; b: KI, NaH_2PO_2, AcOH, c: $LiAlH_4$, THF.

An underappreciated and rarely discussed aspect of the chemistry of the larger diazaacenes is their potential to be reduced (hydrogenated) into to their formally antiaromatic congeners (Scheme 6.1). Indeed, the dihydro-forms of the diaza- and tetraazapentacenes seem to be remarkably viable.[4] Hinsberg reported that both the parent and the dihydro forms of diaza- and tetraazatetracenes to be persistent, and he contended that the dihydro forms of the larger azaacenes were even more stable.[12] The notions of aromaticity and particularly of antiaromaticity[13] had not yet been developed in 1901. Consequently, the behavior of the formally antiaromatic dihydronaphthophenazine did not seem surprising at the time. This contribution illuminates the stabilities and spectroscopic properties of **6.5-6.8** in relationship to their aromatic/antiaromatic character.

6.2 Results and Discussion

The addition of the lithium salt of (triisopropylsilyl)acetylene or (triethylsilyl)acetylene to quinone **6.1**[14] forms an intermediate diol which reacts with potassium iodide and sodium hypophosphite in acetic acid into the naphthothiadiazole derivatives **6.2a,b**.[15] $LiAlH_4$ reduction of **6.2a,b** in THF afforded diamine **6.3a,b** in close to quantitative yields as blue-fluorescent, almost colorless powders. *ortho*-Quinone (**6.4**), obtained by oxidation of catechol in dichloromethane by acidic aqueous dichromate, was coupled with **6.3a,b** to furnish **6.5a,b** after flash chromatography (hexanes/dichloro-methane 1/1) as dark-red, air-stable, crystalline materials.

The packing of **6.5a,b, 6.7** and **6.8** is of interest, as it determines the existence of short π-π-intrastack interactions, which is a necessary, although not sufficient,

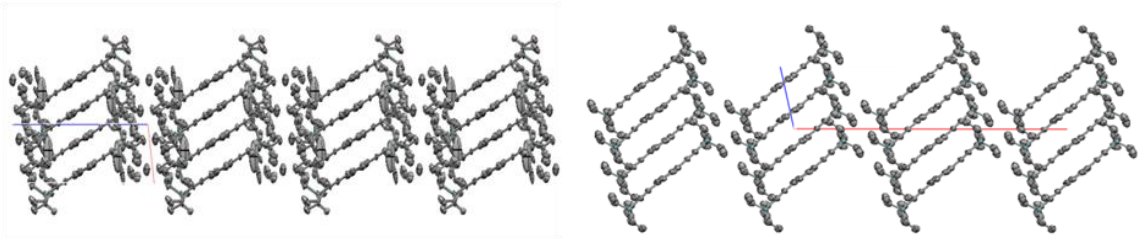

Figure 6.1. Packing of **6.5a** (left) and **6.5b** (right); view along the *b*-axis.

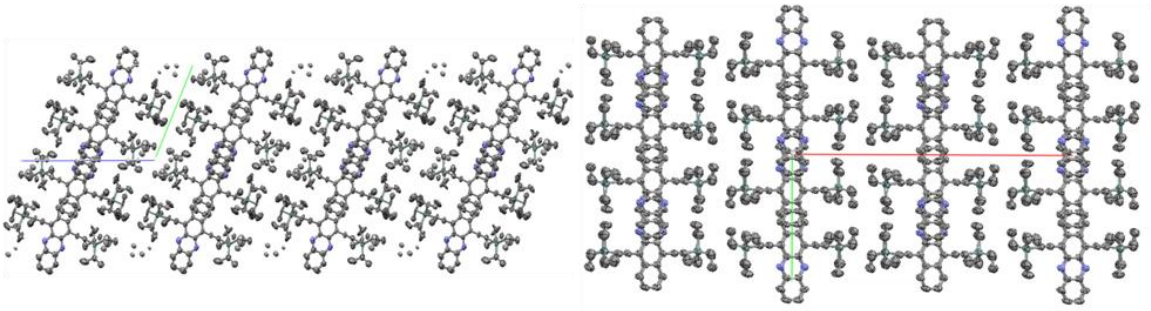

Figure 6.2. Packing of **6.5a** (left) and **6.5b** (right); view along the *a*-axis.

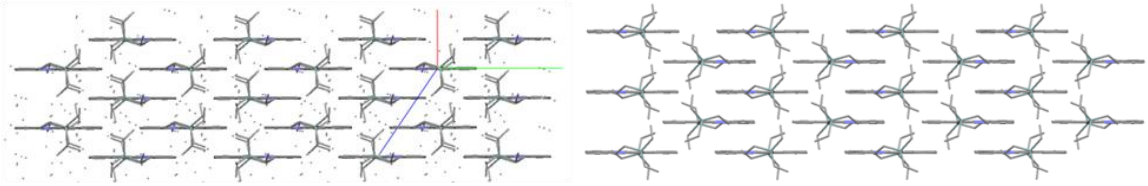

Figure 6.3. Stacking of **6.5a** (left) and **6.5b** (right), viewed along the axis that is formed by the two ethynyl substituents. Note that this view is *not* along any viable crystallographic main axis.

prerequisite for their successful incorporation into thin-film transistors or other organic electronic devices. Crystalline specimens of **6.5a**, **6.5b, 6.7** and **6.8** were subjected to X-ray crystal-structure analysis; **6.5a**, **6.5b,** and **6.7** are stable under the crystallization conditions (dichloromethane/hexanes for **6.5a**,**b** and DMSO for **6.7)**. Initial attempts to crystallize **6.8** from DMSO under ambient conditions gave red single crystals that had a crystallographic cell identical to **6.7**. But when crystallized from DMF in a dry box under exclusion of air, **6.8** was found to produce yellow platelets. Table 6.1 shows details of the four X-ray crystal structures. The structure of **6.5b** is better resolved, as the TIPS groups in **6.5a** are disordered, resulting in a high R-value to 15%; however, the packing is clearly discernable. The parent compounds **6.7** and **6.8** are well-behaved and the crystal structures could be refined to give low R-values. Table 6.1 displays cell parameters and R-values.

While **6.5a** and **6.8** are triclinic, **6.5b** and **6.7** pack in a monoclinic cell. Figures 6.1-6.4 display the packing patterns of **6.5a** and **6.5b**. *Despite their quite different unit cells, the packing of* **6.5*a*** *and* **6.5*b*** *is similar.* The most significant difference is illustrated in Figure 6.2; **6.5a** is arranged in a tilted fashion, while **6.5b** forms a rectangular pattern. The most likely reason for the subtle difference in packing is the increased steric demand of the TIPS group in comparison to that of the triethylsilyl substituent. A subtle difference in the tilt angle of the molecules within one stack differentiates **6.5a** from **6.5b**. The best description of the overall packing is perhaps that of a tilted brick wall, i.e. heteroacenes **6.5a,b** pack in a 2-D-stack but with significant short-axis offset, similar to acceptor-substituted tetracene derivatives prepared by Anthony *et al.*[16] The short intra-stack distance of two molecules of **6.5a**, 3.35 Å, equals the combined van der Waals radii

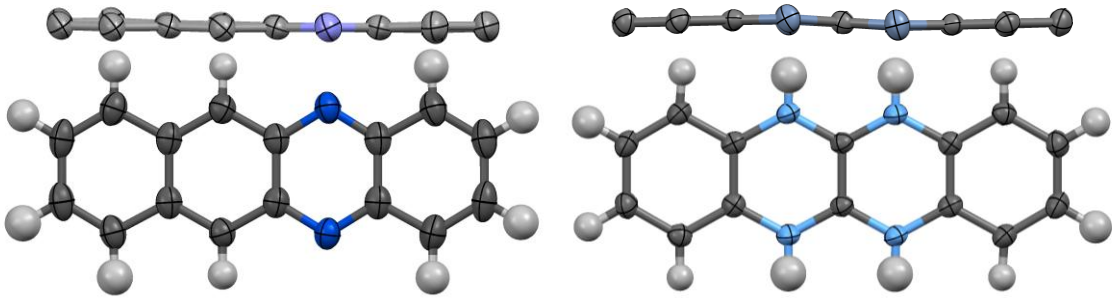

Figure 6.4. Molecular structures of **6.7** (left) and of **6.8** (right). The top view displays the planarity of both **6.7** and **6.8**. The four powder blue colored positions in **6.8** contain overall two nitrogen atoms in either the 5,12- or the 6,11-position as a consequence of the disorder of **6.8** where it can take on two different orientations.

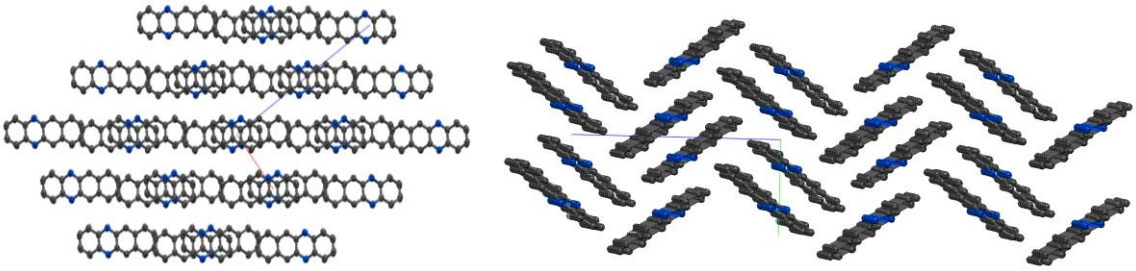

Figure 6.5. Packing of **6.7**. View along the *b*-axis (left) and along the *a*-axis (right).

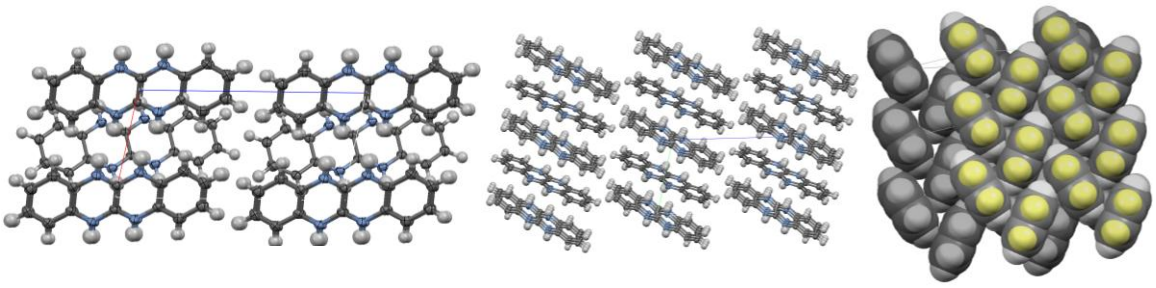

Figure 6.6. Packing of **6.8**. View along the *b*-axis (left) and along the *a*-axis (middle). View along the diagonal of the crystallographic *b* and *c* axes (right).

Table 6.1. Crystallographic Parameters of **6.5a**, **6.6a**, **6.7**, and **6.8**

Compound	*a* (Å)	*b* (Å)	*c* (Å)	α (°)	β (°)	γ (°)	Space Group	Z	R (%)
6.5a	7.40	13.89	18.43	112	95.6	90.5	P-1	2	15
6.5b	7.21	13.69	30.89	90	102	90	C2/c	4	8.8
6.7	7.07	8.44	18.52	90	95.2	90	$P2_1/c$	4	4.0
6.8	5.83	7.85	12.51	101	101	94	P-1	2	4.5
TC[a]	6.06	7.84	13.01	77.0	72.1	85.8	P-1	2	5.7

[a] TC = Tetracene, data from: Holmes, D.; Kumaraswamy, S.; Matzger, A. J.; Vollhardt, K. P. C. *Chem. Eur. J.***1999**, *5*, 3399-3412.

of carbon. A virtually identical value, 3.33 Å is found for **6.5b**, which suggests that both heteroacenes have a packing arrangement desirable for molecular electronics applications. The size of the substituents on the alkynes has in this case only a relatively small effect on the overall packing of the heteroacenes **6.5a** and **6.5b**.

The crystal packing of the two parent heteroacenes **6.7** (Figure 6.5) and **6.8** (Figure 6.6), differs from that of **6.5a,b** (Figures 6.1-6.3) and tetracene.[17] Both **6.7** and **6.8** are nearly planar, but the NH-groups in **6.8** are slightly puckered and the structure is disordered with respect to the relative position of the dihydropyrazine ring in the molecule. As the CH- and NH-groups are of similar size and steric bulk, the molecules of **6.8** pack as if they possess an inversion center (Figure 6.4). The planarity of **6.8** is relevant to discussion of the question of aromaticity and/or antiaromaticity (vide infra). As shown in Figure 6.5, **6.7** displays a herringbone packing, in which the intrastack distance is approximately 3.8 Å along the *b*-axis. But **6.8** exhibits a face-to-edge arrangement, in which the π–π stacking is absent (see Figure 6.6). Both **6.7** and **6.8** have unfavorable packing for high charge carrier mobility, since they have only modest (**6.7**)

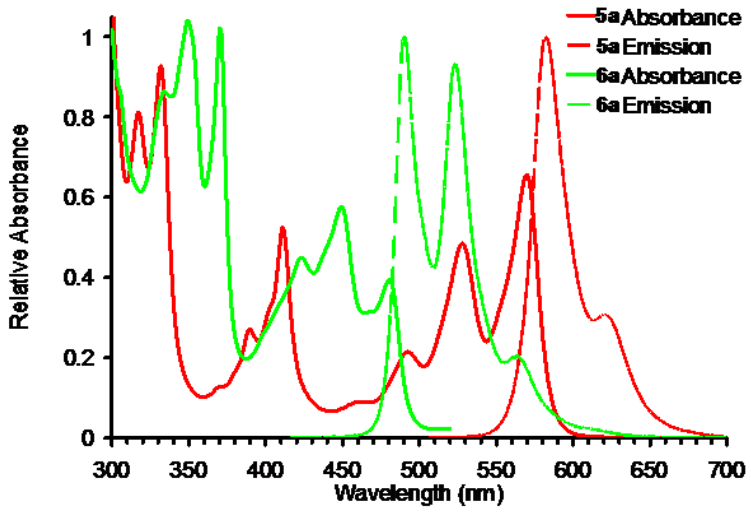

Figure 6.7. UV-vis and emission spectra of **6.5a** and **6.6a** in dichloromethane.

or absent (**6.8**) intrastack π–π-interactions. However, the packing of **6.5a,b** (Figures 6.1-6.3) enforces the intrastack π–π-interactions due to the presence of the silylated alkyne substituents. We were unable to obtain an X-ray crystal structures for **6.6a**, since **6.6a** oxidized quickly to **6.5a**, even in the crystalline state.

While 6,11-bis(triisopropylsilylethynyl)benzo[b]phenazine (**6.5a**) is non-fluorescent in the solid state, due to its intra-stack interactions, it is red-fluorescent in solution with acene-type vibronic progressions both in absorption and emission (λ_{max} abs = 571 nm, λ_{max} emission = 583 nm, Figure 6.7);[18] **6.5a** is persistent and melts at 186 ^{o}C without decomposition. It can be hydrogenated at 2500 psi H_2 pressure using Wilkinson's catalyst ($(Ph_3P)_3RhCl$) to give a new, brightly yellow-green fluorescent compound (assigned structure **6.6**) in 98% yield. The absorption and emission spectra of **6.6a** are shown in Figure 6.7 (λ_{max} abs = 482 nm, λ_{max} emission = 491 nm). The NH units gave a distinct, sharp IR band at 3396 cm^{-1} and a single broad ^{1}H NMR peak. Otherwise, the NMR spectrum of **6.6a** is similar to that of **6.5a**, except that all the ^{1}H signals are shifted

to higher field. Dihydro-heteroacene **6.6a** is isolable, but quickly reverts to **6.5a** on exposure to air, both in solution and in the solid state. The compound **6.6b** is so unstable that it oxidizes back to **6.5b** almost immediately. Interestingly, the acetylene substituents seem to decrease the persistence of **6.6a**, compared to Hinsberg's parent diazadihydro-tetracene **6.8**.[12]

6.3 Electrochemistry and Computational Analysis

We performed cyclic voltammetry (CV) of **6.5a** and **6.6a** in THF / 0.1 M $^{n}Bu_4NPF_6$ to examine their redox relationships in an electron-transfer rather than hydrogen-transfer sense. Sample voltammograms are shown in Figure 6.8 and their potentials are summarized in Table 6.2; **6.5a** undergoes a fully reversible first molecular reduction, at a similar potential as **6.7**. Both compounds also exhibit less chemically reversible reductions to the dianion at more negative potential.

For **6.7**, the reduction is irreversible. Heteroacene **6.5a** shows the characteristics of an EC-type process, in which a reversible electron transfer is followed by chemical reaction on a comparable timescale and displays a reversible molecular oxidation at +0.95 V vs. ferrocenium / ferrocene. The voltammograms of **6.6a** and **6.8** are different from one another: while the oxidation of **6.6a** is irreversible, **6.8** undergoes two successive more-or-less reversible oxidations.[19] The similarities between **6.5a** and **6.7** are obvious from the close values of their first and second reduction potentials as well as the reversibility of their electrochemistry. For **6.6a** and **6.8**, the origin of their differences in chemical reversibility is unknown, however, the irreversibility of $\mathbf{6.6a}^{+/0}$ may be related to its tendency to be oxidized (in the sense of hydrogen loss).

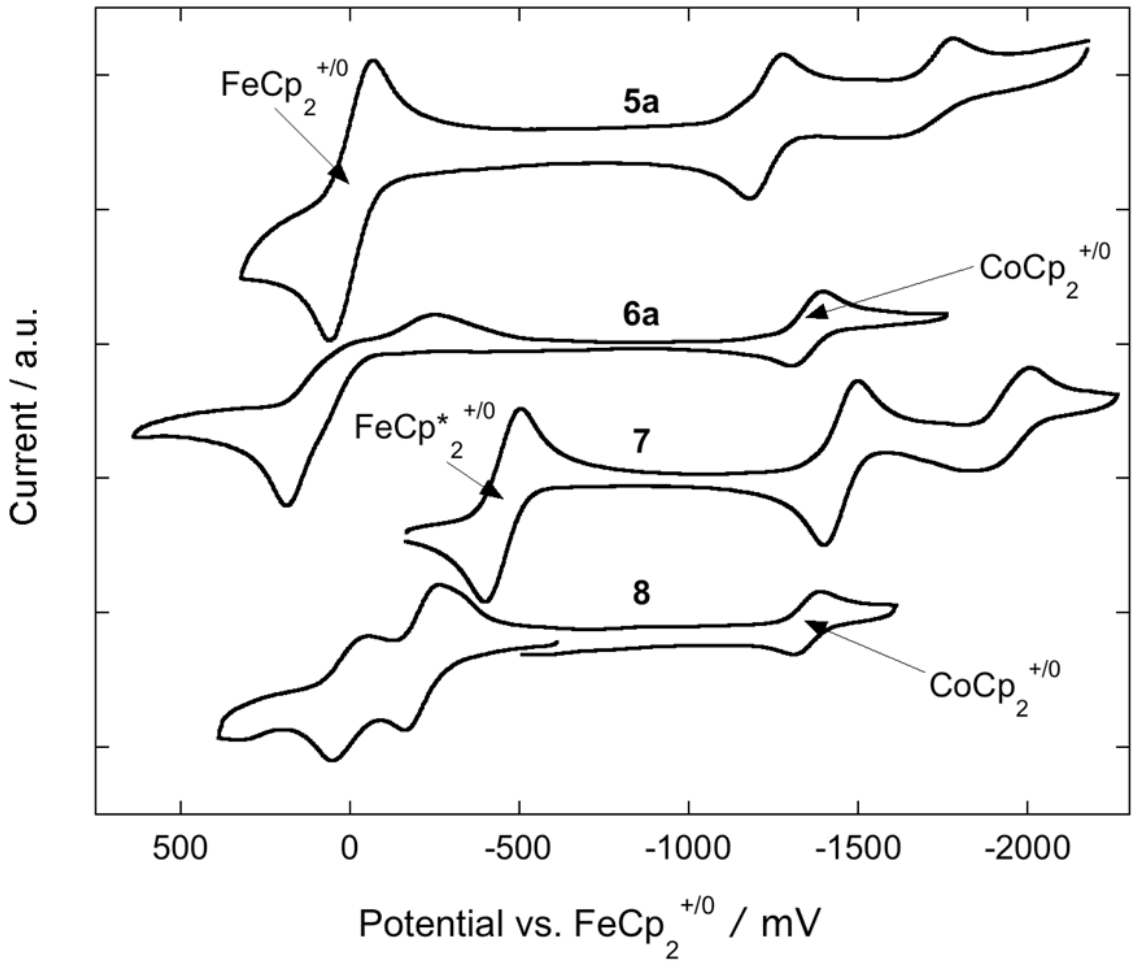

Figure 6.8. Cyclic voltammograms of **6.5a**, **6.6a**, **6.7** and **6.8** (right) in THF / 0.1 M $^{n}Bu_4NPF_6$ recorded at 50 mVs^{-1}. Signals due to internal reference couples are indicated, different couples having been chosen for different compounds to avoid overlap. In all cases, the data have been plotted relative to the ferrocenium / ferrocene redox couple.

The electrochemical data also make possible a rough estimate of the solid-state ionization potentials and electron affinities, parameters important for potential applications in organic electronics. The solid-state electron affinity of **6.5a** can be estimated (as described in reference 20) as ca. –3.4 eV, approaching those estimated in the same way for well-established electron-transport materials with facile electron injection including perylene diimides (ca. –3.6 eV)[20a-c] and C_{60} (ca. –3.7 eV), and considerably more exothermic than that of Alq_3 [20d] (ca. –2.3 eV), which is widely used as

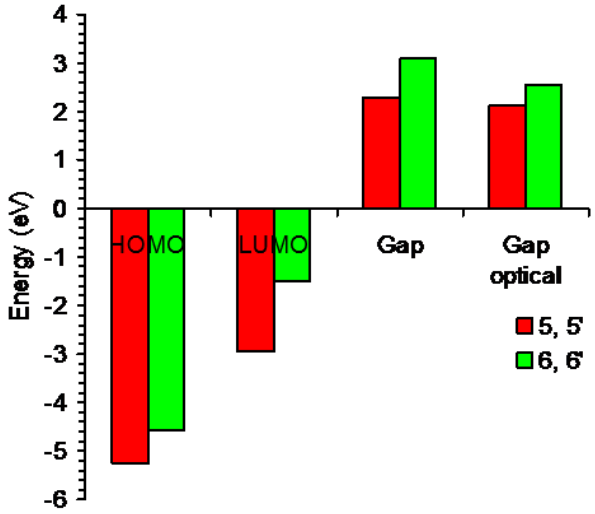

Figure 6.9. HOMO/LUMO energies and band gaps, computed at B3LYP/6-31G*// B3LYP/6-31G*, for **6.5'** (red) and **6.6'**(green), and optical data (Gap optical) for **6.5** and **6.6**.

an electron-transport material in organic light-emitting diodes. The solid-state ionization potential of **6.5a** is estimated at ca. 6.1 eV (see SI), significantly higher than that of well-established hole-transport materials such as TIPS-pentacene (ca. 5.5 eV estimated by the same method from the potential given in reference 3a in the SI), and TPD (directly measured at 5.4 eV),[20e] suggesting a large barrier to hole injection from typical electrode materials used in organic electronics. The reversible reductions of **6.5a** and **6.7** reveal that the radical anions of these species are relatively stable. Moreover, their reduction potentials are in the vicinity of the solution reduction potential of molecular oxygen (for which we observe E_{red} at ca. –1.3 V vs. $FeCp_2^{+/0}$ in THF / 0.1 M $^nBu_4NPF_6$), suggesting the possibility of air-stable electron-transport of these materials.

Despite the formally 4n π perimeter of **6.6a,b**, **6.6'**, and **6.8**, the computed heats of hydrogenation of **6.7** to **6.8** (ΔH_H = -20.8 kcal/mol at B3LYP/6-311+G** with ZPE correction) is 5.8 kcal/mol more exothermic than that of the inner ring of tetracene (ΔHH

= -15.0 kcal/mol). *Hence, **6.8** is destabilized only modestly by its antiaromatic dihydropyrazine subunit.*

Table 6.2. Electrochemical Half-Wave Potentials (V vs. Ferrocenium / Ferrocene) for **6.5a**, **6.6a**, **6.7**, and **6.8** in THF / 0.1 M $^{n}Bu_4PF_6$

Cpd (M)	$E_{1/2}$ ($M^{2+/+}$) (V)	$E_{1/2}$ ($M^{+/0}$) (V)	$E_{1/2}$ ($M^{0/-}$) (V)	$E_{1/2}$ ($M^{-/2-}$) (V)
6.5a	-	a	-1.23[a]	-1.78[a]
6.7	-	-	-1.44	-2.00[b]
6.6a	-	+0.19[b]	-	
6.8	0.00	-0.21	-	-

[a] In CH_2Cl_2 / 0.1 M $^{n}Bu_4NPF_6$ a reversible oxidation is observed at +0.95 V; reversible and EC-type reductions are seen at –1.21 and –1.68 V, respectively, in the same solvent. [b] Irreversible, the given values correspond to the peak potentials of E_{red} (for **6.7**) and E_{ox} (for **6.6a**).

This comparison is influenced by the difference in CH vs. NH bond energies. Thus, the computed heat of hydrogenation involving non-aromatic models, 2,3-dihydropyrazine and 1,2,3,4-tetrahydropyrazine (ΔH_H= –18.8 kcal/mol), is nearly the same as that of **6.7** to **6.8**. In contrast, the hydrogenation of 2,3-cyclohexadiene to cyclohexene (ΔH_H= –22.5 kcal/mol) is 7.5 kcal/mol more exothermic than that of tetracene to dihydrotetracene. Evidently, the loss of aromatic stabilization energy (ASE) upon the hydrogenation of **6.7** to **6.8** is less than that of tetracene to 5,12-dihydrotetracene, despite the 4n-π-perimeter of **6.8**.

Moreover, the HOMO-LUMO gap of *aromatic* **6.5a,b** is smaller than that of the *formally antiaromatic* **6.6a,b**. As shown in Figure 9 for **6.5'** and **6.6'**, the computed LUMO energy difference (-3.0 eV for **6.5'** vs. -1.5 eV for **6.6'**) is greater than that of the HOMO (-5.2 eV for **6.5'** to -4.6 eV for **6.6'**). Hence, the band gap increases from 2.3 eV for **6.5'** to 3.1 eV in **6.6'**. The experimentally obtained optical band gaps, obtained from

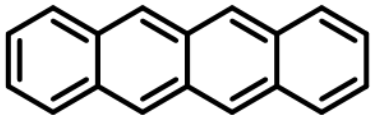

Remote	-1.6	-3.4	-	-	$\Sigma_{NICS,\,zz}$	-10.0
Local	-28.4	-39.2	-	-	$\Sigma_{NICS,\,zz}$	-135.5
Total	-30.0	-42.6	-	-	$\Sigma_{NICS,\,zz}$	-145.2

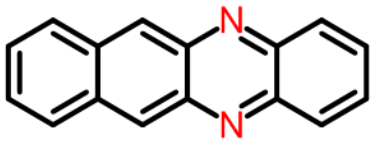

Remote	-2.0	-3.8	-3.6	-2.8	$\Sigma_{NICS,\,zz}$	-12.2
Local	-28.0	-39.1	-38.2	-27.9	$\Sigma_{NICS,\,zz}$	-133.2
Total	-30.0	-42.9	-41.8	-30.4	$\Sigma_{NICS,\,zz}$	-145.4

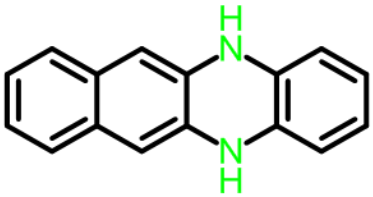

Remote	7.9	15.1	15.7	15.7	$\Sigma_{NICS,\,zz}$	40.8
Local	-35.1	-29.9	27.6	-33.4	$\Sigma_{NICS,\,zz}$	-70.8
Total	-27.2	-18.8	29.7	-17.7	$\Sigma_{NICS,\,zz}$	-30.0

Figure 6.10. IGLO-LMO (localized molecular orbital) and GIAO-CMO (canonical molecular orbital) $NICS(0)_{\pi zz}$ computed at PW91/IGLO-III//B3LYP/6-311+G**. "Local" refers to the π LMO contributions of individual localized double bonds and lone pairs associated with the designated individual rings (when appropriate, localized exocyclic π bonds are included). "Remote" refers to the remaining π MO contributions. Note also that the sum of the remote and local total LMO contributions matches the CMO total closely. (The planar C_{2v} form of **6.8** had one imaginary frequency, but has essentially the same energy as the C_s minimum).

the intersection of absorption and emission traces, of **6.5a,b** and **6.6a** (2.1 eV and 2.6 eV, respectively) agree reasonably well. For comparison, the solution electrochemical HOMO-LUMO gap is 2.16 eV.

Diazatetracenes, like **6.5a,b** and **6.7**, certainly are aromatic, but are their 4n π dihydro derivatives really antiaromatic? NICS (nucleus independent chemical shifts) computations at the centers of the individual rings of **6.7** and **6.8** (as well as tetracene for comparison) are revealing (Figure 6.10).[21] Our analysis employs the $NICS(0)_{\pi zz}$ index,[22] which is based on the out-of-plane tensor components of both the canonical (CMO) and the localized (LMO) π molecular orbital contributions to the isotropic NICS. $NICS(0)_{\pi zz}$ data for both the dissected IGLO-LMO method (with Pipek-Mezey localization as implemented in the deMon program)[23,24] and the GIAO-CMO[25] method are computed at PW91/IGLO-III//B3LYP/6-311+G** for uniformity.

As expected, all the individual local $NICS(0)_{\pi zz}$ values of **6.7** and the overall $\Sigma NICS(0)_{\pi zz}$ sums are highly diatropic and are similar to those of tetracene (Figure 6.10).[23] Both their total LMO and total CMO $NICS(0)_{\pi zz}$ data are almost identical. The LMO details are instructive. Note that the "local" and "total" LMO $NICS(0)_{\pi zz}$ data, for both **6.7** and tetracene are very similar. Evidently, the large negative $NICS(0)_{\pi zz}$ values of the individual rings are due to their "local" diatropicity (i.e., the π contributions involving each ring itself). The "remote" π contributions (from the other rings) are rather small. Hence, the diamagnetic contributions of the aromatic subunits of both **6.7** and tetracene are localized. This is in line with Clar's rule that structures with a maximum number of localized sextet rings are advantageous energetically. Hence, $NICS(0)_{\pi zz}$ is a relatively uncontaminated measure of the magnetic aromaticity of individual rings in a polycyclic

aromatic system. The inner rings of **6.7** and of tetracene are more diatropic than the outer rings.[26]

The behavior of **6.8** is different. Both LMO and CMO $\Sigma NICS(0)_{\pi zz}$ (–28±2 ppm) reveal **6.8** to be *weakly aromatic* despite its 4n π perimeter (Figure 6.10). Note that the dihydropyrazine ring is highly paratropic (see both LMO and CMO $NICS(0)_{\pi zz}$ of the dihydropyrazine ring of **6.8** in Figure 6.10), but its paramagnetic contributions are rather delocalized. Unlike **6.7**, the "remote" LMO contributions of the individual aromatic rings of **6.8** (shown in green) are distinctly paratropic. Hence, the $\Sigma NICS(0)_{\pi zz}$ of both tetracene and **6.7** (approximately –145 ppm) are much greater in magnitude than **6.8**. Remarkably, the benzenoid rings of **6.8** have significantly less diatropic individual "total" LMO $NICS(0)_{\pi zz}$ values compared to their corresponding rings in **6.7**, but their "local" LMO $NICS(0)_{\pi zz}$ values are similar (see Figure 6.10). Evidently, the "local" aromaticites of the benzenoid rings of **6.8** are preserved, despite the presence of the antiaromatic dihydro ring.

The magnetic criteria suggest that **6.8** and its derivatives **6.6a,b** are aromatic, even though less so than **6.7** and **6.5a,b**, at least when aromaticity is viewed as a *global* property. If one considers aromaticity as a local ring-by-ring rather than a global molecular property, **6.6** and **6.8** can be viewed as overall aromatic, yet the central dihydropyrazine ring in both is strongly (locally) antiaromatic, with an additional global component. However, upon dehydrogenation the strong local antiaromaticity disappears. On the other hand, part of the relative stability of **6.6** and **6.8** comes from the increased HOMO-LUMO gap, another experimental and calculational observation is at odds with both simple Hückel theory and the expectations fuelled by antiaromatic compounds such

as cyclobutadiene. Particularly compared to the latter one the persistability of **6.8** is high as it is easily isolated and characterized. In the case of **6.6a** and **6.6b** the persistability is decreased, yet **6.6b** is sufficiently stable allowing its characterization.

6.4 Conclusions

In conclusion, we have prepared a redox interconvertible pair of heterocyclic tetracene derivatives, the aromatic **6.5a,b** and **6.7** and their dihydro-derivatives **6.6** and **6.8**. These compounds are potentially useful as active layers in thin-film transistors. The formation of the requisite films for **6.5-6.8** is challenging and under current investigation. While **6.5a,b** is persistent, **6.6a,b** is readily oxidized to **6.5a,b** in air. The 4n+2 π species, **6.5a,b** and **6.7**, have small band gaps and are red-fluorescent. In contrast, their 4n π dihydro derivatives, **6.6a,b** and **6.8**, are green-fluorescent and have significantly larger band gaps. The 4n π compounds, **6.6a,b** and **6.8**, display significantly reduced aromaticity when compared to **6.5a,b** and **6.7**. The paratropicity of the antiaromatic (4n π) dihydropyrazine subunits is *delocalized* throughout the system. Thus, although they are easily oxidized, large 4n π compounds like **6.6a,b, 6.6'** and **6.8** are not appreciably destabilized relative to their 4n+2 π congeners, **6.5a,b, 6.5'** and **6.7**.

This work was published in the *Journal of the American Chemical Society*:

Miao, Shaobin; Brombosz, Scott M.; Schleyer, Paul v. Rague; Wu, Judy I.; Barlow, Stephen; Marder, Seth R.; Hardcastle, Kenneth I.; Bunz, Uwe H. F. *Journal of the American Chemical Society* **2008**, *23*, 7339-7344.

6.5 Experimental and Supplementary Information

6.5.1 2,3-Diaminonaphthalene-1,4-dione

A mixture of 2,3-dichloronaphthalene-1,4-dione (5.00 g, 22.0 mmol) and potassium phthalimide (8.60 g, 46.4 mmol) in CH_3CN (250 mL) was refluxed for 18 h. The mixture was then filtered and the precipitates were washed with water until the filtrate was colorless. The yellowish solid was collected and dried *in vacuo*. The solid and NH_2NH_2 (15.0 mL) were suspended in H_2O (150 mL) at 60 ºC for 12 h. The mixture was filtered and the precipitate was washed with H_2O (3 x 100 mL), dried *in vacuo*. 2,3-Diaminonaphthalene-1,4-dione was obtained as a dark-purple solid in 3.28 g yield (79%, two steps).

6.5.2 Naphtho[2,3-*c*][1,2,5]thiadiazole-4,9-dione, **6.1**.

The mixture of 2,3-diaminonaphthalene-1,4-dione (2.40 g, 12.8 mmol) in $SOCl_2$ (15 mL) was refluxed for 12 h. The mixture was filtered and the precipitate was washed with CH_2Cl_2 (3 x 20 mL). The solid was collected and dried *in vacuo*; naphtho[2,3-c][1,2,5]thiadiazole-4,9-dione was obtained as light yellow solid (2.06 g, 75%).

6.5.3 4,9-bis(triisopropylsilylethynyl)naphtho[2,3-c][1,2,5]thiadiazole, **6.2a**.

To an oven-dried Schlenk flask was added triisopropylsilylacetylene (2.60 mL, 11.6 mmol) and dry THF (10 mL), followed by butyllithium (5.70 mL, 9.12 mmol) at 0 °C. The solution was stirred at room temperature for 1 h, and then compound **6.1** (0.500 g, 2.31 mmol) was added to the solution. The mixture was stirred at ambient temperature for 12 h and then quenched with wet ethyl ether. After evaporation of the solvent, the residue was filtered over silica gel using hexane/ethyl acetate (v/v, 5:1) to yield the

corresponding diol. After the solvent was evaporated, the crude diol was, without further characterization, suspended in acetic acid (20 mL) and potassium iodide (3.80 g, 22.9 mmol) and NaH_2PO_2 (2.00 g, 22.8 mmol) were added. The mixture was heated to reflux for 1 h. After cooling to room temperature, H_2O (100 mL) was added to the mixture and the aqueous solution was extracted with hexanes (3 x 100 mL). The combined organic layers were dried *in vacuo*. The solids were further purified by chromatography on silica gel using a hexane/CH_2Cl_2 (v/v, 6:1) solvent mixture. Compound **6.2a** (1.10 g, 87% yield, two steps) was isolated as red crystals. m.p. = 182-184 °C. **6.2a**: IR (KBr, cm^{-1}) 2943, 2863, 2136, 1533, 1458, 1387, 1241, 1041, 925, 882, 767, 734. ^{1}H-NMR (δ in $CDCl_3$) 8.58-8.56 (q, 2H), 7.57-7.55(q, 2H), 1.28-1.27 (m, 42H). ^{13}C-NMR (δ in $CDCl_3$) 153.20, 135.05, 127.81, 127.56, 112.89, 107.36, 101.64, 18.82, 11.44. Accurate mass for $C_{32}H_{46}N_2SSi_2$: *m*/*e* = 546.28598 [M+], calc. *m*/*e* = 546.29203.

6.5.4 4,9-Bis(triethylsilylethynyl)naphtho[2,3-c][1,2,5]thiadiazole, **6.2b**.

In a synthesis identical to **6.2a**, **6.2b** was synthesized in 61 % yield as red crystals. m.p. = 115-117 °C. **6.2b**: IR (KBr, cm^{-1}) 2954, 2873, 2132, 1534, 1457, 1383, 1237, 1041, 973, 924, 742, 726. ^{1}H-NMR (δ in $CDCl_3$) 8.55-8.52 (q, 2H), 7.58-7.55(q, 2H), 1.20-1.16 (t, 18H), 0.88-0.82 (q, 12H). ^{13}C-NMR (δ in $CDCl_3$) 152.86, 135.12, 127.93, 127.54, 112.76, 108.35, 100.78, 7.67, 4.48. Accurate mass for $C_{26}H_{34}N_2SSi_2$: *m*/*e* = 462.19902 [M+], calc. *m*/*e* = 462.19813.

6.5.5 1,4-Bis(triisopylsilylethynyl)naphthalene-2,3-diamine, **6.3a**.

To the solution of **6.2a** (1.00 g, 1.83 mmol) in THF (20 mL) was added $LiAlH_4$ (0.600 g, 15.8 mmol) at 0 °C and the mixture was stirred at room temperature for 12 h. The mixture was quenched with saturated NH_4Cl solution and extracted with ethyl ether (3 x

200 mL). The combined organic layers were dried over Na_2SO_4 and the solvent was removed *in vacuo* to give a light yellow solid **6.3a** (0.930 g, 98%). m.p. = 165-167 °C. **6.3a**: I.R. (KBr) 3407, 3326, 3227, 3065, 2941, 2863, 2136, 1508, 1458, 1259, 1150, 1073, 1015, 882, 758. ^{1}H-NMR (δ in $CDCl_3$) 8.12-8.09 (q, 2H), 7.40-7.37(q, 2H), 4.35 (s, 4H), 1.23 (s, 42H). ^{13}C-NMR (δ in $CDCl_3$) 138.68, 128.43, 124.77, 124.41, 103.72, 102.44, 101.87, 18.81, 11.32. Accurate mass for $C_{32}H_{50}N_2Si_2$: *m*/*e* = 518.35152 [M+], calc. *m*/*e* = 518.35126.

6.5.6 1,4-Bis(triethylsilylethynyl)naphthalene-2,3-diamine, **6.3b**.

In a synthesis identical to **6.3a**, **6.3b** was synthesized in 97 % yield as light yellow solid. **6.3b**: I.R. (KBr) 3443, 3358, 2953, 2873, 2136, 1618, 1507, 1444, 1235, 1015, 973, 837, 726. ^{1}H-NMR (δ in $CDCl_3$) 8.07-8.04 (q, 2H), 7.37-7.34 (q, 2H), 4.35 (s, 4H), 1.15-1.10 (t, 18H), 0.81-0.73 (q, 12H). ^{13}C-NMR (δ in $CDCl_3$) 138.62, 128.34, 124.74, 124.43, 103.61, 103.57, 101.10, 7.70, 4.59. Accurate mass for $C_{26}H_{38}N_2Si_2$: *m*/*e* = 434.25890 [M+], calc. *m*/*e* = 434.25736.

6.5.7 6,11-Bis(triisopropylsilylethynyl)benzo[b]phenazine, **6.5a**.

To a solution of $K_2Cr_2O_7$ (3.40 g, 11.6 mmol) in 2n H_2SO_4 was added CH_2Cl_2 (200 mL) and catechol (0.640 g, 5.81 mmol). The mixture was stirred at room temperature for 10 min and the organic layer was then separated with aqueous layer. To the organic layer was added **6.3a** (1.00 g, 1.93 mmol) and acetic acid (1 mL) and the mixture was heated to reflux for 4 h. The solvent was removed *in vacuo* and the residue was separated by a column (flash silica gel, Hex:CH_2Cl_2, v/v, 3:1) to give **6.5a** as red solid (0.720 g, 63%). m.p. = 185-186 °C. **6.5a**: I.R. (KBr) 2941, 2864, 2129, 1521, 1458, 1389, 1101, 1041, 882, 747. ^{1}H-NMR (δ in $CDCl_3$) 8.75-8.73 (q, 2H), 8.23-8.21 (q, 2H), 7.82-7.80 (q, 2H),

7.66-7.64 (q, 2H), 1.33-1.32 (m, 42H). ^{13}C-NMR (δ in $CDCl_3$) 144.58, 141.24, 135.17, 131.03, 130.33, 127.92, 127.63, 120.85, 108.09, 102.86, 18.93, 11.60. Accurate mass for $C_{38}H_{50}N_2Si_2$: *m*/*e* = 590.35100 [M+], calc. *m*/*e* = 590.35126.

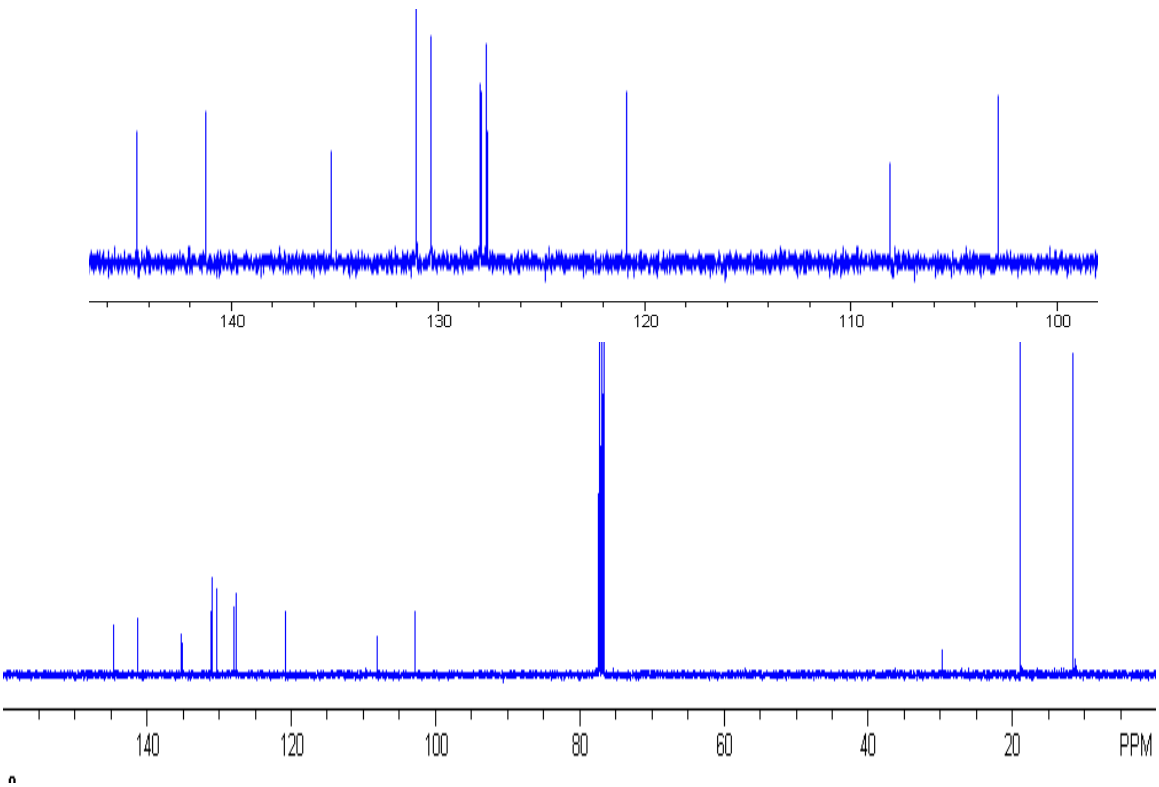

Figure 6.11. ^{13}C-NMR ($CDCl_3$) of compound **6.5a**.

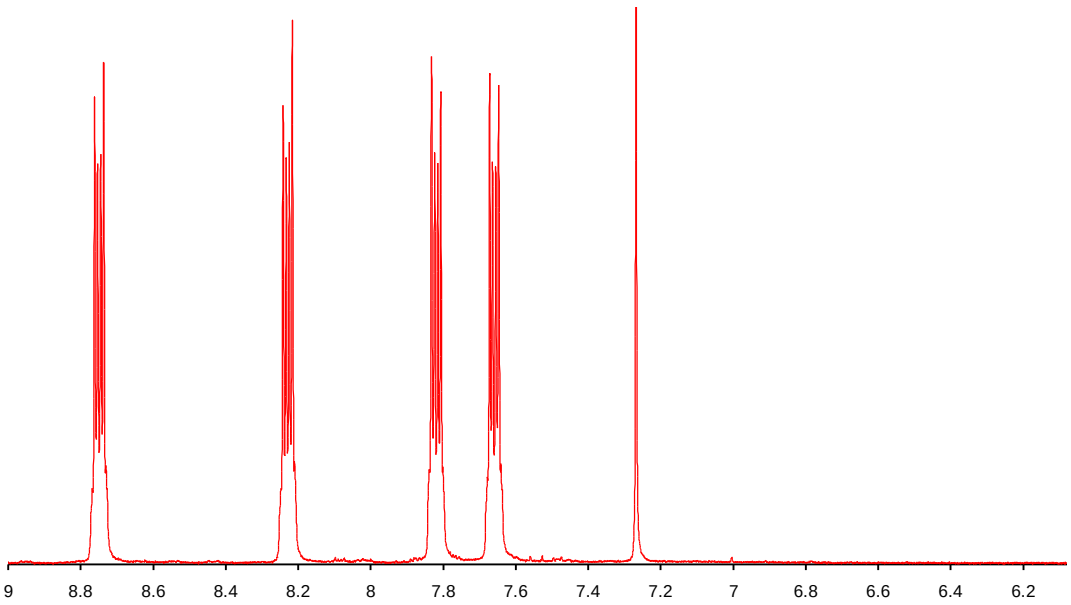

Figure 6.12. ^{1}H-NMR ($CDCl_3$) of compound **6.5a**.

6.5.8 6,11-Bis(triethylsilylethynyl)benzo[b]phenazine, **6.5b**.

In a synthesis identical to **6.5a**, **6.5b** was synthesized in 57 % yield as red solid. m.p. = 156-158 °C. **6.5b**: I.R. (KBr) 2955, 2877, 2132, 1522, 1457, 1391, 1042, 1014, 858, 752. ^{1}H-NMR (δ in $CDCl_3$) 8.77-8.73 (q, 2H), 8.29-8.25 (q, 2H), 7.84-7.81 (q, 2H), 7.69-7.66 (q, 2H), 1.31-1.25 (t, 18H), 0.95-0.87 (q, 12H). ^{13}C-NMR (δ in $CDCl_3$) 144.57, 140.90, 135.25, 131.16, 130.32, 128.04, 127.64, 120.72, 109.08, 102.05, 7.79, 4.62. Accurate mass for $C_{32}H_{38}N_2Si_2$: *m*/*e* = 506.25756 [M+], calc. *m*/*e* = 506.25736.

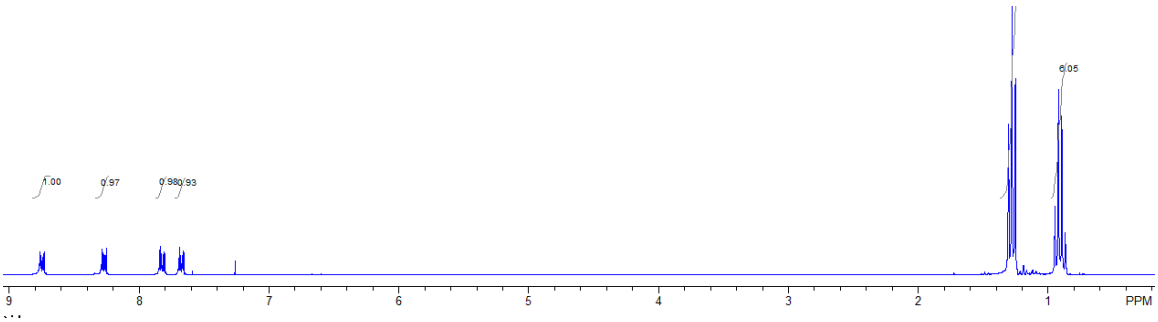

Figure 6.13. ^{1}H-NMR ($CDCl_3$) of compound **6.5b**.

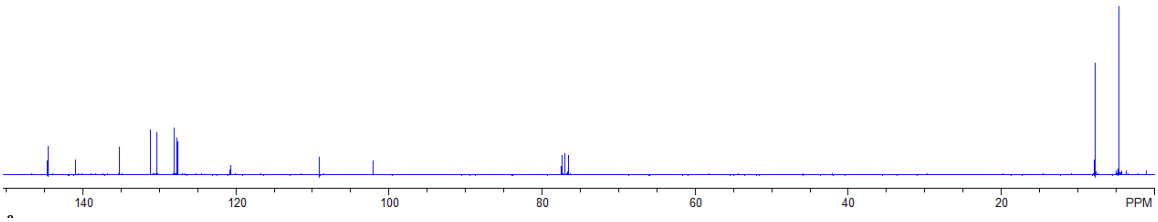

Figure 6.14. ^{13}C-NMR ($CDCl_3$) of compound **6.5b**.

6.5.9 6,11-Bis(triisopropylsilylethynyl)-5,-12-dihydrobenzo[b]phenazine, **6.6a**.

Diyne **6.5a** (50 mg, 0.085 mmol) and $(Ph_3P)_3RhCl$ (3.0 mg, 0.0032 mmol) in a mixture of CH_2Cl_2/EtOH (v/v, 1:2) were stirred at 40 °C under a hydrogen atmosphere (2500 psi) for 12 h. The mixture was filtered over celite and the solvent was removed *in vacuo* to give **6.6a** as yellow solid (49 mg, 98%). **6.6a**: I.R. (KBr) 3396, 2934, 2863, 2124, 1479, 1299, 882, 745. ^{1}H-NMR (δ in $CDCl_3$) 7.72-7.69 (q, 2H), 7.18-7.15 (q, 2H), 6.59-6.56 (q, 2H), 6.29 (s, 2H), 6.24-6.21 (q, 2H), 1.21-1.20 (m, 42H). ^{13}C-NMR (δ in $CDCl_3$) 136.04, 129.82, 129.31, 124.70, 124.18, 121.95, 112.59, 102.96, 100.52, 97.84, 18.77, 11.23. Accurate mass for $C_{38}H_{52}N_2Si_2$: *m*/*e* = 592.36714 [M+], calc. *m*/*e* = 592.36691.

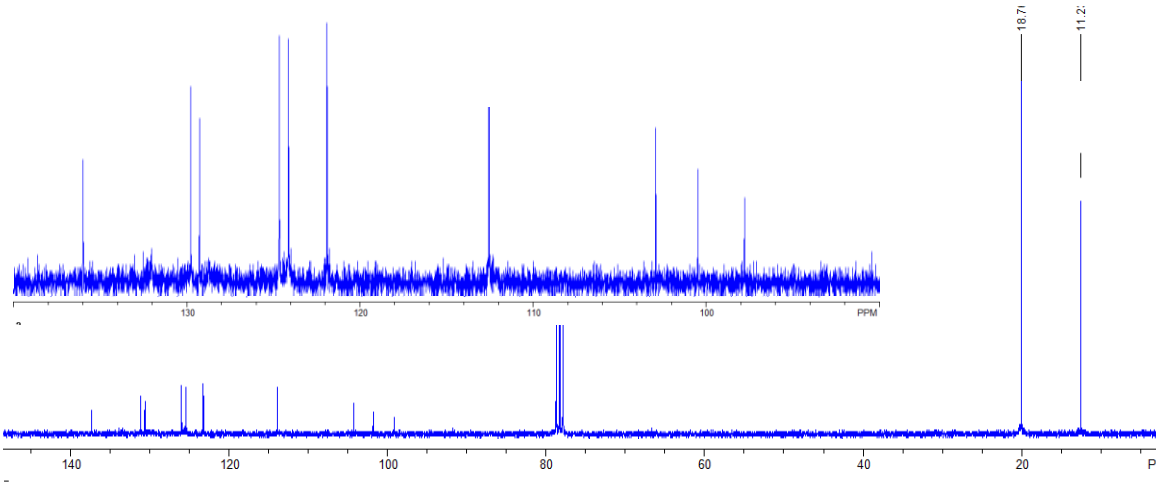

Figure 6.15. ^{13}C-NMR ($CDCl_3$) of compound **6.6a**.

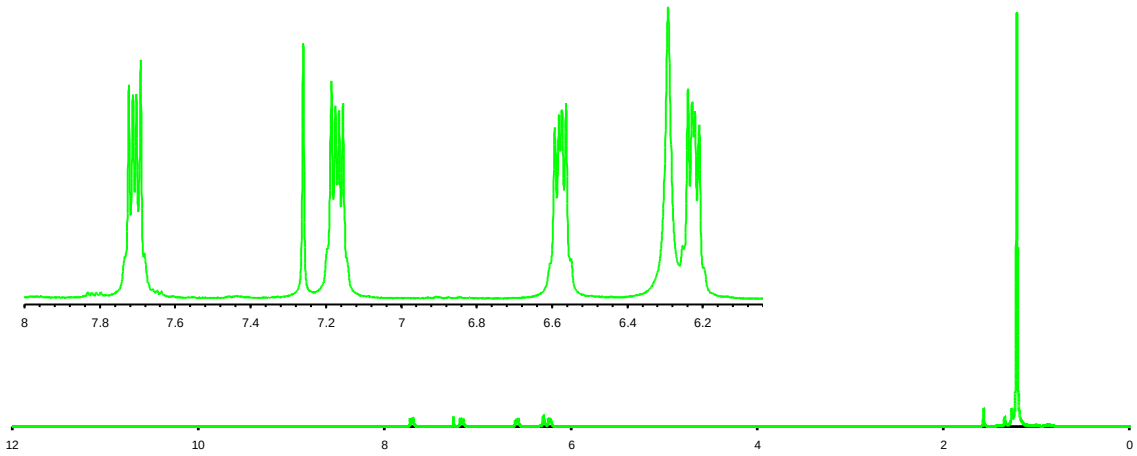

Figure 6.16. ^{1}H-NMR ($CDCl_3$) of compound **6.6a**.

6.5.10 5,12-Dihydrobenzo[b]phenazine, **6.8**.

Naphthalene-2,3-diol (6.00 g, 37.5 mmol) and *o*-phenylenediamine (4.05 g, 37.5 mmol) were stirred together in a 100 mL round-bottom flask. The flask was heated to 180 ^{o}C and stirring continued for 30 minutes. After cooled down to room temperature, the material was then washed on a filter with methanol, acetone and then diethyl ether. The resulting material was collected and dried *in vacuo* to give **6.8** as a yellow solid (7.34 g, 84%). **6.8**: I.R. (KBr): 3397, 3051, 1629, 1585, 1507, 1465, 1403, 1308, 1243, 1178, 1108, 948, 856. ^{1}H-NMR (δ in DMSO-d_6) 8.11 (s, 2H), 7.14 (m, 2H), 6.89 (m, 2H), 6.33 (m, 2H), 6.21 (s, 2H), 6.15 (m, 2H). ^{13}C-NMR (δ in DMSO-d_6) 134.49, 131.62, 130.78, 124.78, 122.81, 120.20, 111.67, 104.26. Accurate mass for $C_{16}H_{12}N_2$: *m/e* = 232.09924 [M+], calc. *m/e* = 232.10005. CV (vs. Cp_2Fe): $E_{1/2}^{0/+}$ = 0.0025 V, $E_{1/2}^{+/2+}$ = -0.209 V.

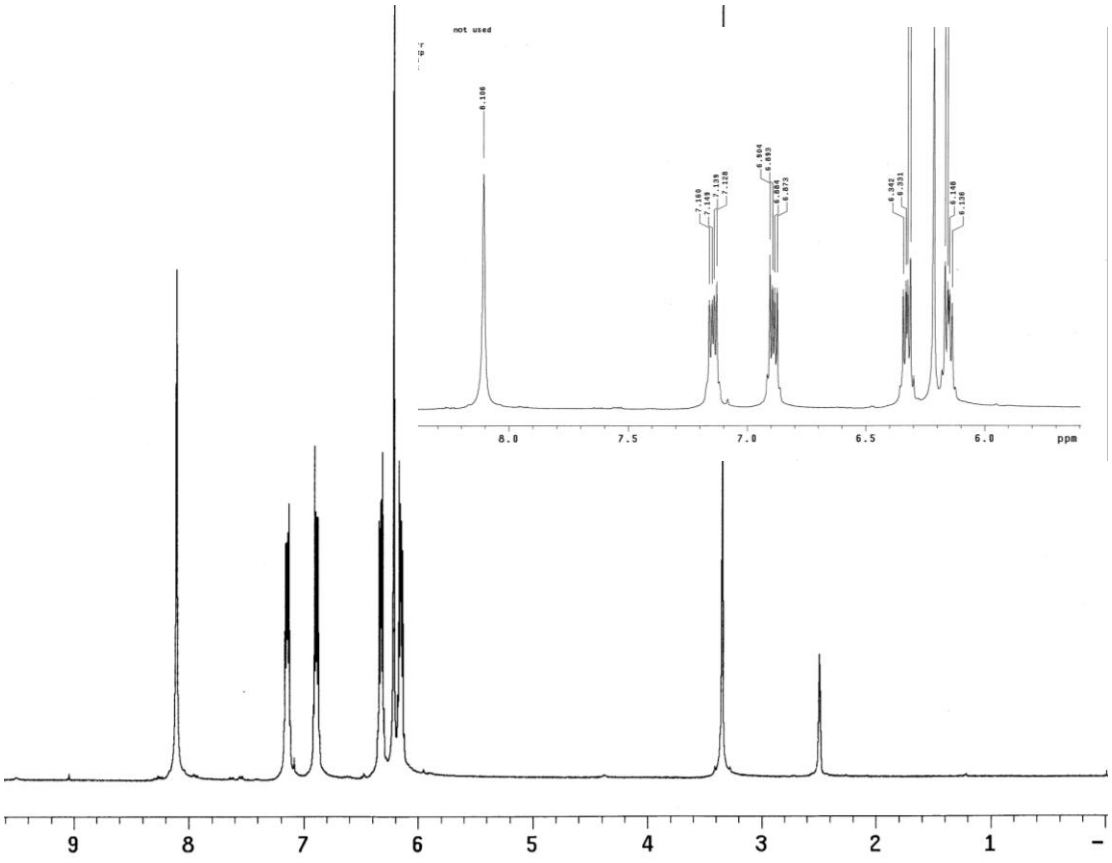

Figure 6.17. ^{1}H-NMR (DMSO-*d*6) of compound **6.8**.

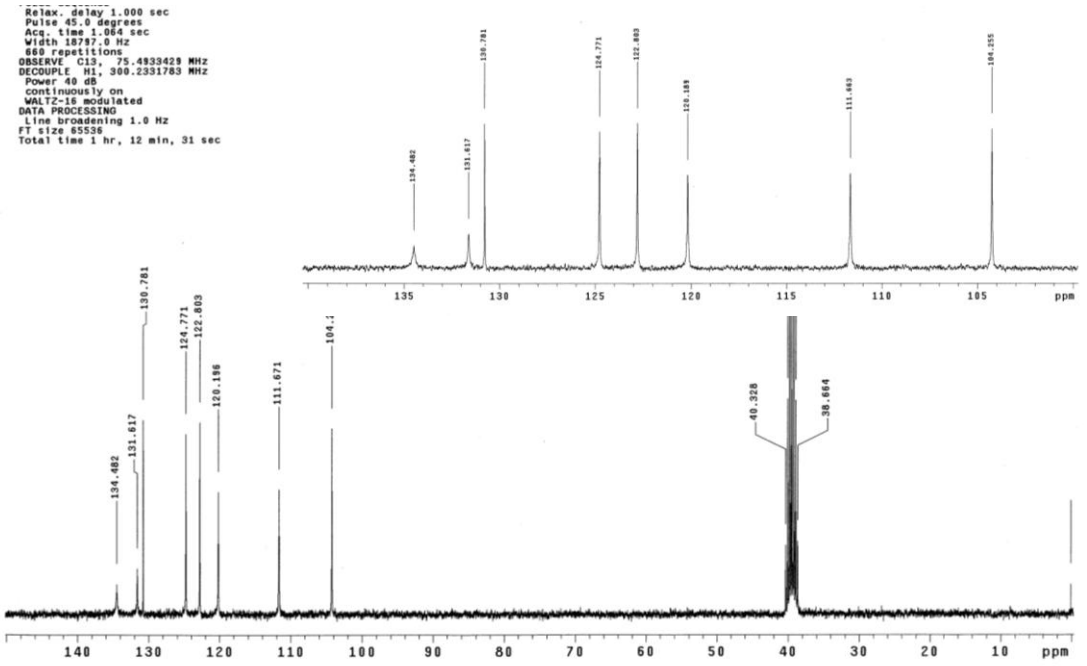

Figure 6.18. ^{13}C-NMR (DMSO-*d*6) of compound **6.8**.

6.5.11 Benzo[b]phenazine, **6.7**.

To a suspension of 5,12-dihydrobnzo[b]phenazine (4.00 g, 17.2 mmol) in acetic acid (100 mL) was added a 2n solution of $K_2Cr_2O_7$ (8.34 g, 34.4 mmol). The mixture was allowed to stir for one hour at room temperature during which time the solution became clear and red. The solution was then poured into water and extracted with chloroform (3x100ml). The organic layers were combined, dried *in vacuo* to give **6.7** as a dark red solid (3.67g, 93%). **6.7**: I.R. (KBr): 3046, 1582, 1528, 1459, 1383, 1109, 878, 749. ^{1}H-NMR (δ in $CDCl_3$) 8.90 (s, 2H), 8.22 (m, 2H), 8.11 (m, 2H), 7.78 (m, 2H), 7.51 (m, 2H). ^{13}C-NMR (δ in $CDCl_3$) 144.73, 140.27, 134.66, 130.57, 130.04, 128.59, 127.74, 126.80. Accurate mass for $C_{16}H_{10}N_2$: *m/e* = 230.08493 [M+], calc. *m/e* = 230.08440. CV (vs. Cp_2Fe): $E^{0/+}_{1/2}$ = -1.444 V, $E^{+/2+}_{1/2}$ = -1.912 V.

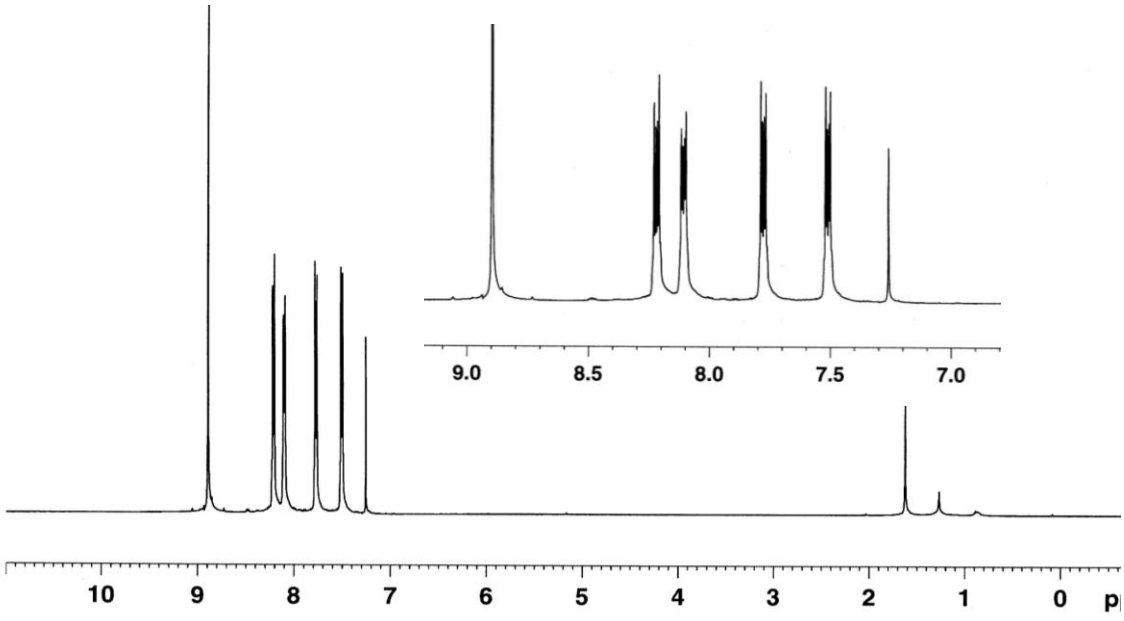

Figure 6.19. ^{1}H-NMR ($CDCl_3$) of compound **6.7**.

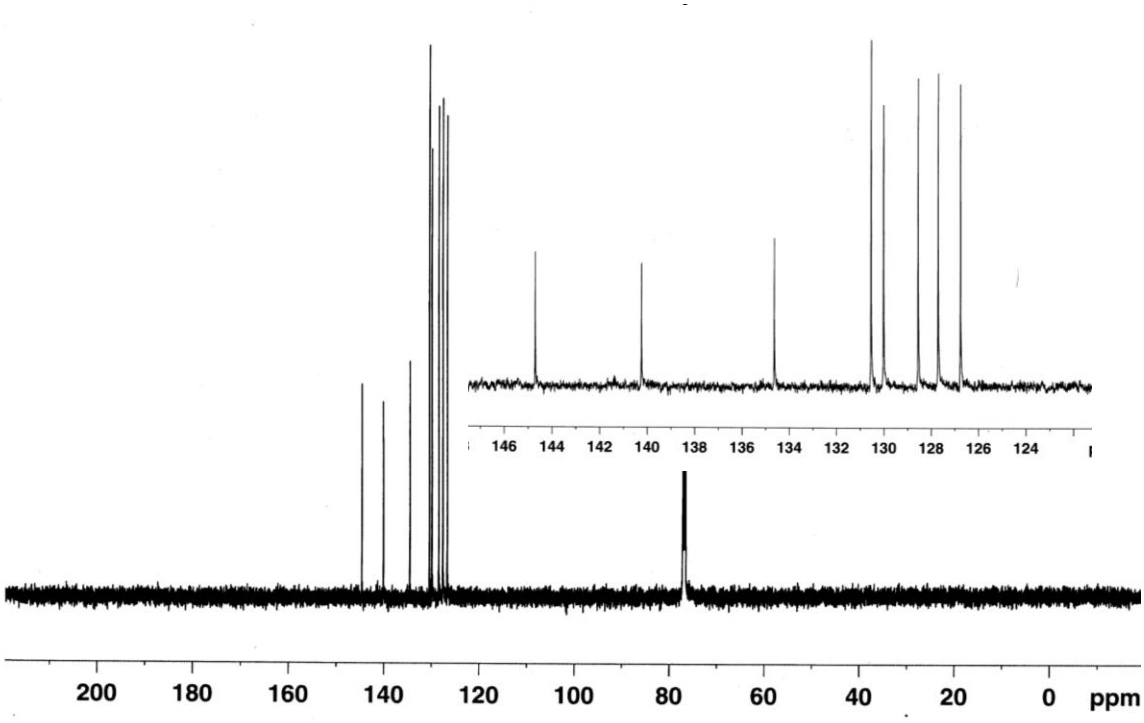

Figure 6.20. ^{13}C-NMR ($CDCl_3$) of compound **6.7**.

6.5.12 IR Spectral Comparison

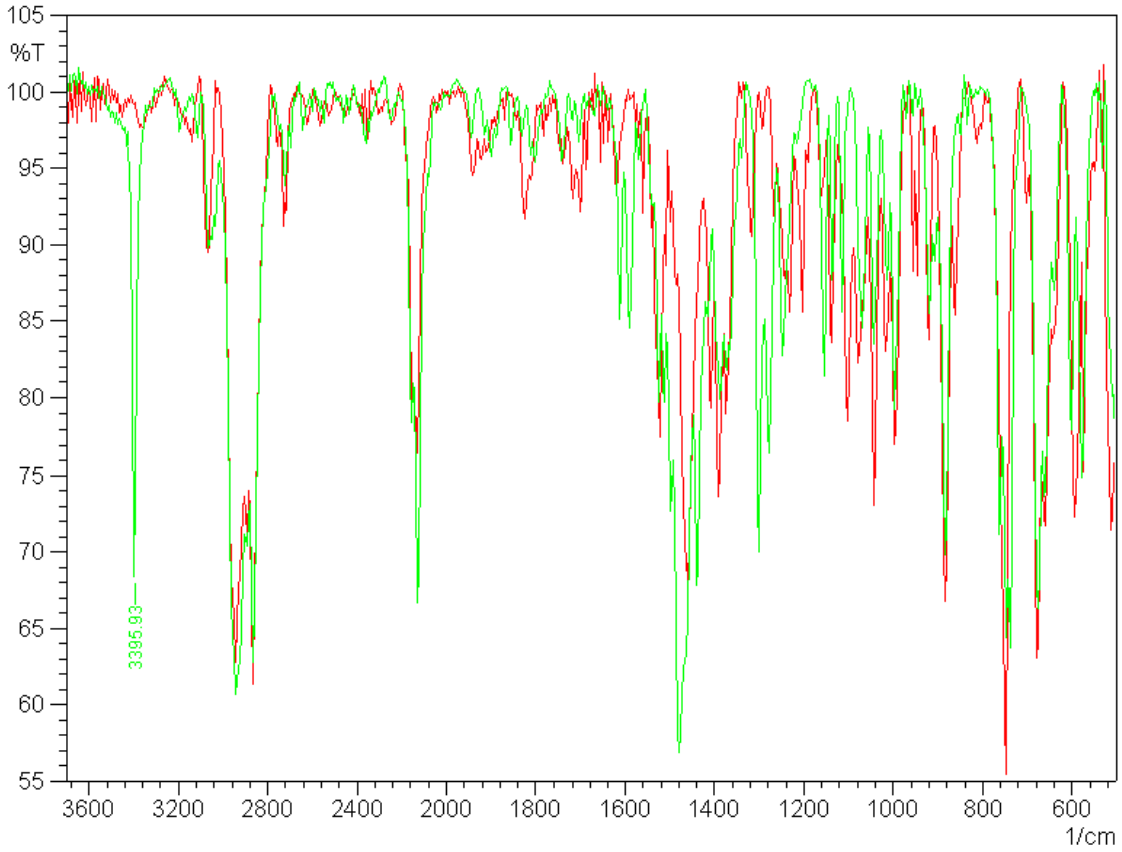

Figure 6.21. Overlaid IR Spectra of **6.5a** and of **6.6a**. The spectrum of **6.5a** is colored red and the spectrum of **6.6a** is colored green. Visible is the strong N-H-band for **6.6a** at 3396 cm^{-1}.

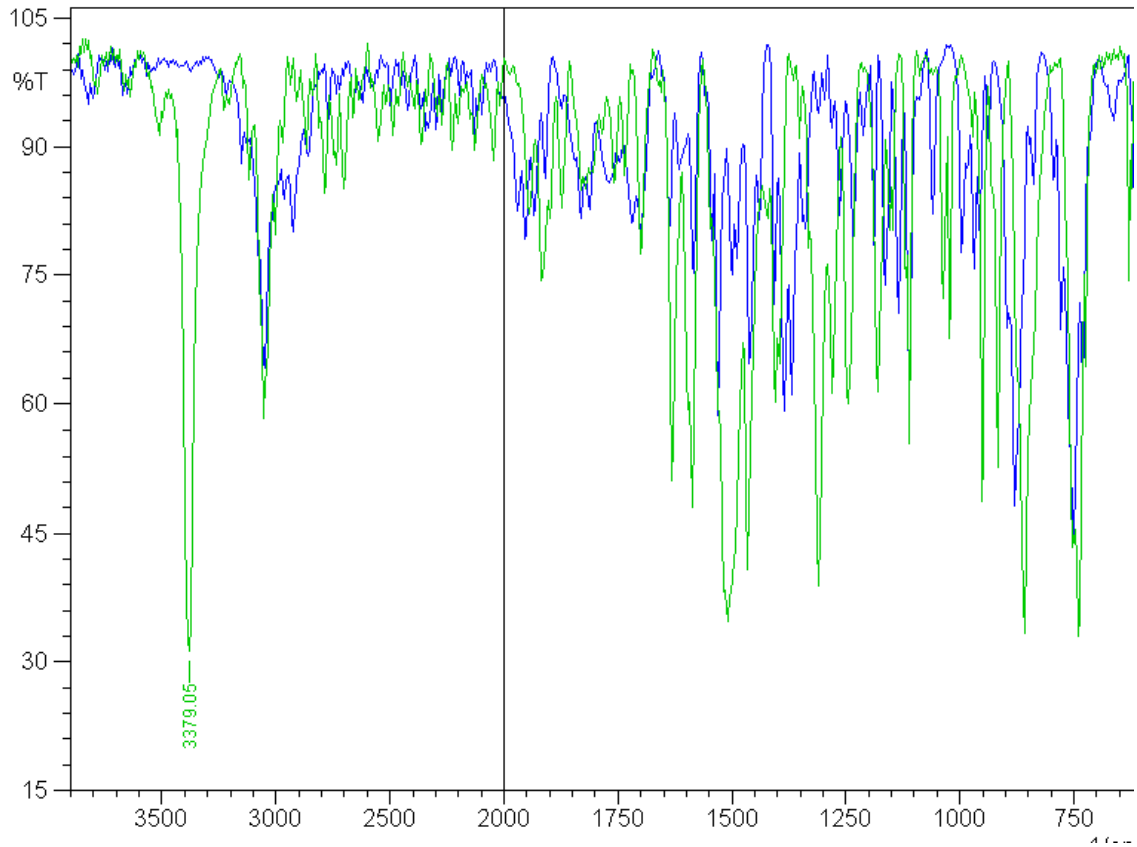

Figure 6.22. Overlaid IR Spectra of **6.7** and of **6.8**. The spectrum of **6.7** is colored blue and the spectrum of **6.8** is colored green. Visible is the strong N-H-band for **6.8** at 3379 cm^{-1}.

6.5.13 Spectroscopic Characterization of **6.5-6.8**.

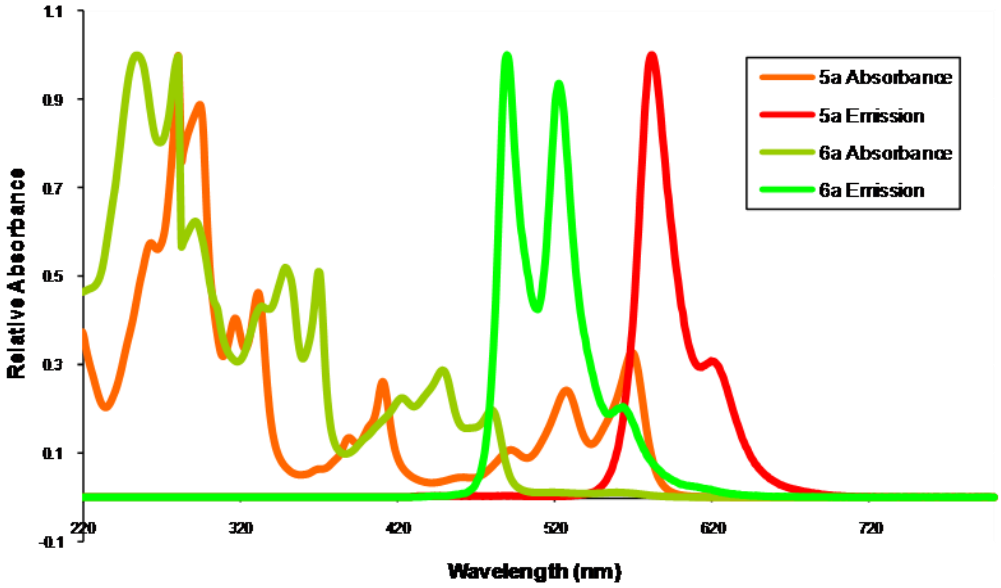

Figure 6.23. Overlaid UV-Vis and Emission-Spectra of **5a** and of **6a** in Hexane.

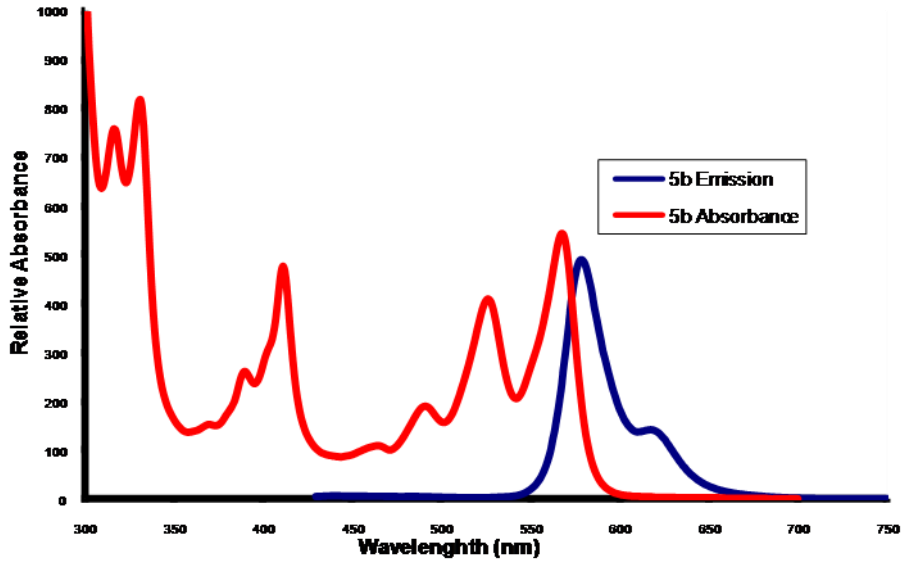

Figure 6.24. Overlaid UV-Vis and Emission-Spectra of **6.5b** in Hexane.

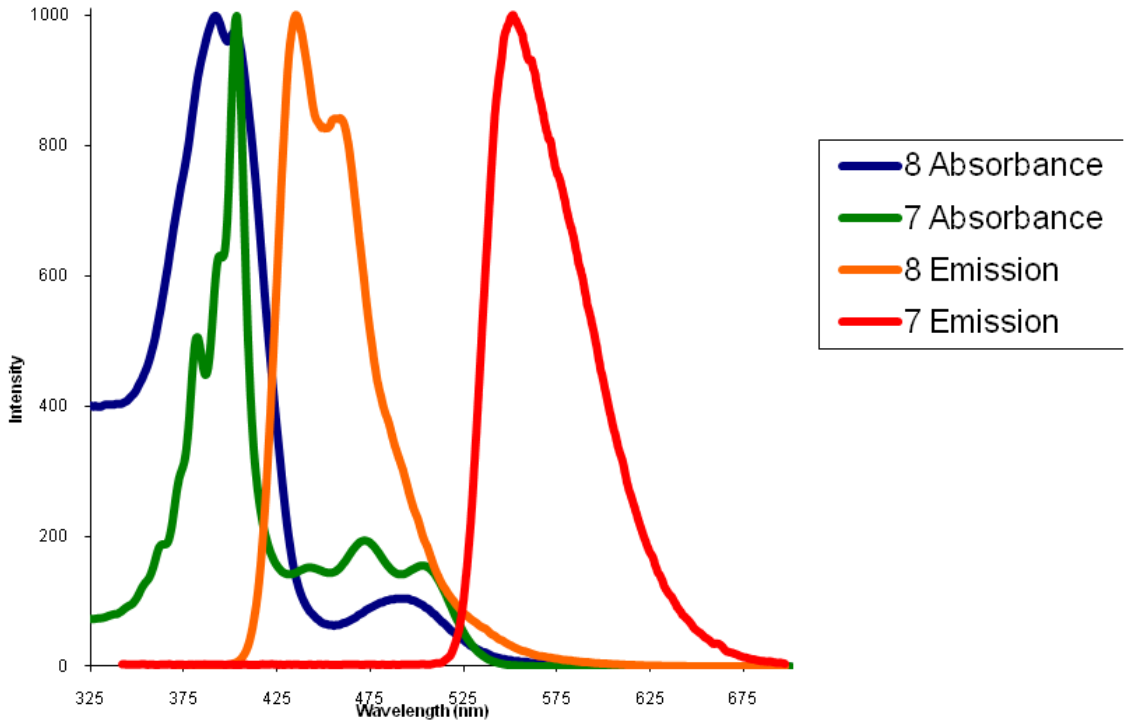

Figure 6.25. Overlaid UV-Vis and Emission-Spectra of **6.7** and of **6.8** in CH_2Cl_2.

6.5.14 Archive of Computed Structures

$C_{16}H_{10}N_2$ (6.7)

1\1\ GINC-UGA-PVRS-PC13PVRS\Freq\RB3LYP\6-311+G(d,p)\C16H10N2\JIWU\26-Jul-2007\0\\#P GEOM=ALLCHECK GUESS=TCHECK RB3LYP/6-311+G(D,P) FREQ\\diazanaphthacene c2v\\0,1\C,-0.0595570893,-0.7255720913,0.\C,-0.0595570893,0.7255720913,0.\C,1.1682229615,-1.4127102749,0.\C,1.1682229615,1.4127102749,0.\N,-1.2151272252,-1.423239784,0.\N,-1.2151272252,1.4232397784,0.\C,2.3772811355,-0.726326197,0.\C,2.3772811355,0.726326197,0.\C,-2

.3477550441,-0.7273758082,0.\C,-2.3477550441,0.7273758082,0.\C,3.63796
90722,-1.4088791401,0.\C,3.6379690722,1.4088791401,0.\C,-3.6035884522,
-1.4169035213,0.\C,-3.6035884522,1.4169035213,0.\C,4.8120928763,-0.714
8432239,0.\C,4.8120928763,0.7148432239,0.\C,-4.7732658774,-0.716039063
6,0.\C,-4.7732658774,0.7160390636,0.\H,1.1440038479,-2.4966465619,0.\H
,1.1440038479,2.4966465619,0.\H,3.6374504735,-2.4935068459,0.\H,3.6374
504735,2.4935068459,0.\H,-3.5806677705,-2.5001180409,0.\H,-3.580667770
5,2.5001180409,0.\H,5.7576878112,-1.2450500282,0.\H,5.7576878112,1.245
0500282,0.\H,-5.7209812806,-1.2425642144,0.\H,-5.7209812806,1.24256421
44,0.\\Version=x86-Linux-G98RevA.5\State=1-A1\HF=-725.4142859\RMSD=6.8
18e-10\RMSF=1.428e-04\ZPE=135.2523816\Dipole=0.1217958,0.,0.\DipoleDer
009,0.1398131\Polar=432.5915261,0.0005031,194.9469308,-0.0000262,-0.00
05617,95.9561063\PG=C02V [SGV(C16H10N2)]\NImag=0\\0.70429771,-0.015677
002,0.02538504\\-0.00038656,-0.00053385,0.,-0.00038656,0.00053385,0.,0
01952,-0.00005044,0.,0.00001952,0.00005044,0.\\\@

$C_{16}H_{12}N_2$ (6.8)

1\1\ GINC-UGA-PVRS-PC20PVRS\Freq\RB3LYP\6-311+G(d,p)\C16H12N2\JIWU\30-
Jul-2007\0\\#P GEOM=ALLCHECK GUESS=TCHECK RB3LYP/6-311+G(D,P)
FREQ\\dihydrodiazanaphthacene cs\\0,1\C,0.0224522184,-0.7164712018,0.168903919

7\C,0.0224522184,0.7164712018,0.1689039197\C,1.210999637,-1.3976133673
,0.0760806705\C,1.210999637,1.3976133673,0.0760806705\N,-1.2094833007,
-1.3625756188,0.2979265942\N,-1.2094833007,1.3625756188,0.2979265942\C
,2.45602049,-0.7144541248,-0.0045581932\C,2.45602049,0.7144541248,-0.0
045581932\C,-2.4263298947,-0.7042271123,0.0881463328\C,-2.4263298947,0
.7042271123,0.0881463328\C,3.6924419084,-1.3981182162,-0.0877546355\C,
3.6924419084,1.3981182162,-0.0877546355\C,-3.6246916858,-1.3908042767,
-0.0862235247\C,-3.6246916858,1.3908042767,-0.0862235247\C,4.881946428
5,-0.7051437479,-0.1684439676\C,4.8819464285,0.7051437479,-0.168443967
6\C,-4.8252743118,-0.6950427969,-0.2493729241\C,-4.8252743118,0.695042
7969,-0.2493729241\H,1.206285781,-2.4836198502,0.0734453079\H,1.206285
781,2.4836198502,0.0734453079\H,-1.2097092519,-2.366507494,0.205207395
6\H,-1.2097092519,2.366507494,0.2052073956\H,3.6922008831,-2.483533966
7,-0.0872910638\H,3.6922008831,2.4835339667,-0.0872910638\H,-3.6185298
054,-2.4762697031,-0.0872549761\H,-3.6185298054,2.4762697031,-0.087254
9761\H,5.8205701516,-1.2439996667,-0.2324315003\H,5.8205701516,1.24399
96667,-0.2324315003\H,-5.7498233942,-1.2447984124,-0.3778273895\H,-5.7
498233942,1.2447984124,-0.3778273895\\Version=x86-Linux-G98RevA.5\Stat
e=1-A'\HF=-726.6401956\RMSD=2.129e-10\RMSF=1.217e-05\ZPE=149.8134107\D

ipole=-0.4411467,0.,-0.1161278\DipoleDeriv=1.613956,0.1799634,-0.10091

.0257897,0.0105371,-0.0308649,0.010474,0.1429209\Polar=403.4843454,0.0

00341,195.9361695,-0.0327947,0.0019603,102.2223903\PG=CS [X(C16H12N2)]

\NImag=0\\0.73477868,-0.05422908,0.65327372,-0.04081833,0.00272214,0.1

.00066727,0.00005837,-0.00406866,0.03496393,-0.01808892,0.02885361\\-0

28,-0.00000016,0.00000002,0.00000028,-0.00000016\\\@

$C_{18}H_{12}$ (tetracene)

1\1\GINC-SHERIDAN\FOpt\RB3LYP\6-311+G(d,p)\C18H12\SCHLEYER\17-Jun-

1999\0\\#BECKE3LYP/6-311+G**OPT\\NAPHTHACENE

D2h\\0,1\C,0.,0.,0.7250608473\C,0.,0.,0.72506

08473\C,1.2340451474,0.,-1.4048549355\C,1.2340451474,0.,1.4048549355\C,-1.23404

51474,0.,-1.4048549355\C,-1.2340451474,0.,1.4048549355\C,2.4472132061,0.,-0.724

9115469\C,2.4472132061,0.,0.7249115469\C,-2.4472132061,0.,-0.7249115469\C,-2.44

72132061,0.,0.7249115469\C,3.7073763833,0.,-1.4076509535\C,3.7073763833,0.,1.40

76509535\C,-3.7073763833,0.,-1.4076509535\C,-3.7073763833,0.,1.4076509535\C,4.8

828170671,0.,-0.7147531904\C,4.8828170671,0.,0.7147531904\C,-4.8828170671,0.,-0

.7147531904\C,-4.8828170671,0.,0.7147531904\H,1.2344368323,0.,-2.4906415352\H,1

.2344368323,0.,2.4906415352\H,-1.2344368323,0.,-2.4906415352\H,-1.2344368323,0.

,2.4906415352\H,3.7072258379,0.,-2.4926998832\H,3.7072258379,0.,2.4926998832\H,

-3.7072258379,0.,-2.4926998832\H,-3.7072258379,0.,2.4926998832\H,5.8281928369,0

.,-1.2454983785\H,5.8281928369,0.,1.2454983785\H,-5.8281928369,0.,-1.2454983785

\H,-5.8281928369,0.,1.2454983785\\Version=x86-Linux-G98RevA.5\State=1-AG\HF=-

69

3.3293112\RMSD=6.744e-09\RMSF=3.719e-05\Dipole=0.,0.,0.\PG=D02H

[C2"(C1.C1),SG(C16H12)]\\@

6.6 References

[1] Nelson, S. F.; Lin, Y. Y.; Gundlach, D. J.; Jackson, T. N. *Appl. Phys. Lett.* **1998**, *72*, 1854-1856.

[2] (a) Dimitrakopoulos, C. D.; Malenfant, P. R. L. *Adv. Mater*. **2002**, *14*, 99-117. (b) Dimitrakopoulos, C. D.; Mascaro, D. J. *IBM J. Res. Develpment* **2001**, *45*, 11-27. (b) Reese, C.; Bao, Z. N. *J. Mater. Chem.* **2006**, *16*, 329-333. (d) Roberson, L. B.; Kowalik, J.; Tolbert, L. M.; Kloc, C.; Zeis, R.; Chi, X. L.; Fleming, R.; Wilkins, C. *J. Am. Chem. Soc.* **2005**, *127* , 3069-3075.

[3] (a) Anthony, J. E. *Chem. Rev.* **2006,** *106*, 5028-5048. (b) Anthony, J. E.; Brooks, J. S.; Eaton, D. L.; Parkin, S. R. *J. Am. Chem. Soc.* **2001**, *123*, 9482-9483. (c) Payne, M. M.; Parkin, S. R.; Anthony, J. E. *J. Am. Chem. Soc.* **2005**, *127*, 8028-8029.

[4] Anthony, J. E.; Eaton, D. L.; Parkin, S. R. *Org. Lett.* **2002**, *4*, 15-18.

[5] (a) Fischer, O.; Hepp, E. *Chem. Ber.* **1890**, *23*, 2789-2798. (b) Fischer, O.; Hepp, E. *Chem. Ber.* **1900**, *33*, 1485-1498. (c) Kehrmann, F. *Chem. Ber.* **1890**, *23*, 2446-2454.

[6] Winkler, M.; Houk, K. N. *J. Am. Chem. Soc.* **2007**, *129*, 1805-1815.

[7] Wudl, F.; Koutenis, P. A.; Weitz, A.; Ma, B.; Strassner, T.; Houk, K. N.; Khan, S. I. *Pure Appl. Chem.* **1999**, *71*, 295-302.

[8] Miao, Q.; Nguyen, T. Q.; Someya, T.; Blanchet, G. B.; Nuckolls, C. *J. Am. Chem. Soc.* **2003**, *125*, 10284-10287.

[9] Tadokoro, M.; Yasuzuka, S.; Nakamura, M.; Shinoda, T.; Tatenuma, T.; Mitsumi, M.; Ozawa, Y.; Toriumi, K.; Yoshino, H.; Shiomi, D.; Sato, K.; Takui, T.; Mori, T.; Murata, K. *Angew. Chem. Int. Ed.* **2006**, *45*, 5144-5147.

[10] Jenekhe, S. A. *Macromolecules* **1991**, *24*, 1-10.

[11] Nishida, J.; Naraso; Murai, S.; Fujiwara, E.; Tada, H.; Tomura, M.; Yamashita, Y. *Org Lett.* **2004**, *6*, 2007-2010.

[12] Hinsberg, O. *Liebigs Ann. Chem.* **1901**, *319*, 257-286.

[13] Breslow, R.; Brown, J.; Gajewski J. J. *J. Am. Chem. Soc.* **1967**, *89*, 4383-4390.

[14] Cava, M. P.; Schlessinger, R. H. *Tetrahedron Lett.* **1964**, 3815-3817.

[15] Miao, S.; Smith, M. D.; Bunz, U. H. F. *Org. Lett.* **2006**, *8*, 757-760. (b) Miao, S.; Schleyer, P. v. R.; Wu, J. I.; Hardcastle, K. I.; Bunz, U. H. F. *Org. Lett.* **2007**, *9*, 1073-1076.

[16] (a) Odom, S. A.; Parkin, S. R.; Anthony, J. E. *Org. Lett.* **2003**, *5*, 4245-4248. (b) Anthony J. E. in Functional Organic Materials, Ed. Bunz U. H. F., Müller T. J. J., Wiley-VCH, Weinheim 2007, 511-545.

[17] Holmes, D.; Kumaraswamy, S.; Matzger, A. J.; Vollhardt, K. P. C. *Chem. Eur. J.* **1999**, *5*, 3399-3412.

[18] Perkampus H.-H., UV-Vis Atlas of Organic Compounds, 2nd ed. VCH, Weinheim 1992.

[19] (a) The overall process is chemically reversible; however, integration of the reduction wave for the $\mathbf{8}^{2+/+}$ process corresponds to less than one electron, while the $\mathbf{8}^{+/0}$ reduction wave corresponds to more than one electron. This may suggest coupled electron and proton transfer processes as has been seen for other phenazine derivatives; however, we have not investigated this aspect in detail. (b) Laviron, E.; Roullier, L. *J. Electroanal. Chem.* **1983**, *157*, 7-18. (c) Sawyer, D. T.; Komai, R. Y. *Anal. Chem.* **1972**, 44, 715-721.

[20] (a) These estimates were made as previously described using Alq_3 and TPD as references for EA and IP, respectively. As discussed, alternative less conservative (more exothermic) estimates of EA can be obtained using other comparisons. (b) Zhan, X.; Risko, C.; Amy, F.; Chan, C.; Zhao, W.; Barlow, S.; Kahn, A.; Brédas, J. L.; Marder, S. R. *J. Am. Chem. Soc.* **2005**, *127*, 9021-9029. (c) An, Z.; Yu, J.; Jones, S. C.; Barlow, S.; Yoo, S.; Domercq, B.; Prins, P.; Siebbeles, L. D. A.; Kippelen, B.; Marder, S. R. *Adv. Mater.* **2005**, *17*, 2580-2583 and references cited therein. (d) Cahen, D.; Kahn, A. *Adv. Mater.* **2003**, *15*, 271-277. (e) Anderson, J. D.; McDonald, E. M.; Lee, P. A.; Anderson, M. L.; Ritchie, E. L.; Hall, H. K.; Hopkins, T.; Nash, E. A.; Wang, J.; Padias, A.; Thayumanavan, S.; Barlow, S.; Marder, S. R.; Jabbour, G.; Shaheen, S.; Kippelen, B.; Peyghambarian, N.; Wightman, R. M.; Armstrong, N. R., *J. Am. Chem. Soc.* **1998**, *120*, 9646-9655.

[21] Schleyer, P. v. R.; Maerker, C.; Dransfeld, A.; Jiao, H. J.; Hommes, N. J. R. V. *J. Am. Chem. Soc.* **1996**, *118*, 6317-6318.

[22] (a) Corminboeuf, C.; Hein, T.; Seifert, G.; Schleyer, P. v. R. *J. Phys. Chem. Chem. Phys.* **2004**, *6*, 273-276. (b) Chen, Z. F.; Wannere, C. S.; Corminboeuf, C.; Puchta, R.; Schleyer, P. v. R. *Chem. Rev.* **2005**, *105*, 3842-3888. (c) Fallah-Bagher-Shaidaei,

H.; Wannere, C. S.; Corminboeuf, C.; Puchta, R.; Schleyer, P. v. R. *Org. Lett.* **2006**, *8*, 863-866.

[23] Schleyer, P. v. R.; Manoharan, M.; Wang, Z. X.; Kiran, B.; Jiao, H.; Puchta, R.; Hommes, N. J. R. V. *Org. Lett.* **2001**, *3*, 2465-2468.

[24] (a) Kutzelnigg, W. *Isr. J. Chem.* **1980**, *19*, 193-200. (b) Pipek, J.; Mezey, P. G. *J. Chem. Phys.* **1989**, *90*, 4916-4926. (c) Malkin, V. G.; Malkina, O. L.; Casida, M. E.; Salahub, D. R. *J. Am. Chem. Soc.* **1994**, *116*, 5898-5908.

[25] (a) Corminboeuf, C.; Heine, T.; Weber, J. *Org. Lett.* **2003**, *5*, 1127-1130 (b) Moran, D.; Manoharan, M.; Heine, T.; Schleyer, P. v. R. *Org. Lett.* **2003**, *5*, 23-26. (c) Heine, T.; Schleyer, P. v. R.; Corminboeuf, C.; Seifert, G.; Reviakine, R.; Weber, J. *J. Phys. Chem. A*, **2003**, *107*, 6470 -6475.

[26] Schleyer, P. v. R.; Manoharan, M.; Jiao, H.; Stahl, F. *Org. Lett.* **2001**, *3*, 3643-3646.

Chapter 7: From Acenes to Diazaacenes: Enabling Electronegative Substitution as a Tool for Engineering Optical and Electronic Properties

7.1 Introduction

The larger acene cores provide a particularly attractive framework for the design of molecules with tunable properties that can be useful for organic electronic applications. Pentacenes such as **7.1** or **7.5**, but also **7.2** (first prepared by Hinsberg 1901[1]), are of major interest as hole-transport materials in thin-film transistors[2,3] and have high charge-

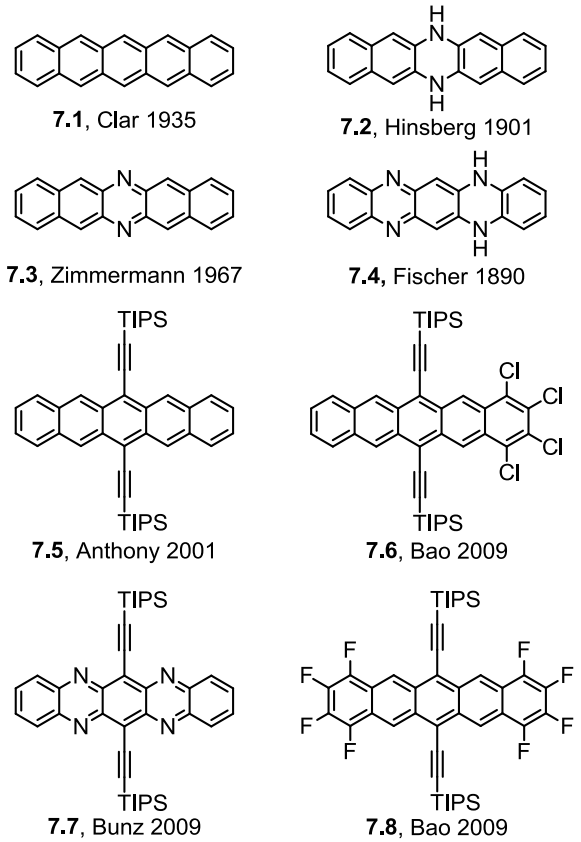

Figure 7.1 Different types of acene compounds.

carrier mobilities, due to their favorable solid-state packing and small reorganization energies;[3,4,5] pentacene is also a component of reference for systems in the development of small-molecule organic solar cells.[6] While Houk suggested that larger N-heteroacenes could behave as electron-transport materials when suitably substituted,[7] to date acenes have generally functioned as hole-transport materials. Only few acenes have exhibited appreciable electron mobilities.[8,910,11] To realize the full potential of acenes and heteroacenes, it is essential to expand the scope of materials available. Figure 7.1 shows recent and historical members in the series of pentacenes.[12,13] Chlorinated pentacenes such as **7.6** were processed into ambipolar transistors. Chlorination lowers both HOMO and LUMO, but with the former effect insufficient to preclude hole injection, while the latter effect facilitates electron injection; however, the optical gap does not change to any appreciable extent.[14] The tetrachloro substitution only led to a slight shift in the absorption maximum going from 643 nm for **5**[15] to 654 nm for **7.6** in solution, suggesting that chlorine substitution had comparable impact on both the ground and first excited state in both compounds.[16,17,18,19] Lowering the absorption energies can be useful in the context of organic solar cells when looking for acene derivatives displaying absorption into the near-IR as observed in Anthony's hexacenes and heptacenes.[20,21]

We report here the simple synthesis of novel heteroacenes, viz. diazapentacene **7.15a**, the halogenated diazatetracene **7.11b** and the tetrahalodiazapentacenes **7.15b**,**c**. Electronegative substitution, i.e. transforming **7.11a→7.11b** and **7.15a→7.15b,c** causes surprising bathochromic shifts in absorption, in addition to the improved reducibility, expected to originate from the stabilization of the LUMOs by electronegative substitution.[22] We expect the halogenated heteroacenes presented herein to generate

materials that exhibit a highly tunable optical absorption in the red part of the visible or in the near-IR.

7.2 Results and Discussion

Condensation of **7.9** (Figure 7.2) with **7.10b** gave tetrachlorodiazatetracene **7.11b** smoothly and in good yields. For comparison purposes we also re-synthesized **7.11a**.[23] The diamine **7.13** is obtained by $LiAlH_4$-reduction of **7.12**[24] and was reacted with **7.10a-c** to furnish the N,N-dihydrodiazapentacenes **7.14a-c** in moderate yields. It has been noted in the past that the formation of the formally antiaromatic **7.14a-c** (diazapentacene series) occurs, but the same is not observed in the diazatetracene series (**7.11**). [1, 25,26]

The intermediates **7.14a-c** are oxidized by manganese dioxide to give **7.15a-c** after chromatography as green-black, environmentally stable crystalline materials in high yield. Figure 3a displays the long-wavelength features of the UV-vis spectra of a selection of the diazatetracenes and diazapentacenes and, as a comparison, the UV-vis spectrum of the tetraazapentacene **7.7**.[7]

The significant spectral red shift observed when going from **7.11a** to **7.11b** and from **7.15a** to **7.15b** or **7.15c** is evident in Figure 7.3; while bathochromic shifts have precedence upon substitution of molecules with electronegative groups, the contrast of the pairs **7.11a→b/7.15a→b** and **7.5/7.6** was unanticipated and is somewhat unusual. The absorption spectrum of **7.11b** (in hexane) shows a λ_{max} of 617 nm, while **7.11a,** the parent, displays a λ_{max} of 571 nm; i.e., the tetrachloro substitution leads to a red shift of 1306 cm^{-1} or 0.16 eV, while, in comparison, tetrachloropentacene **7.6** exhibits an

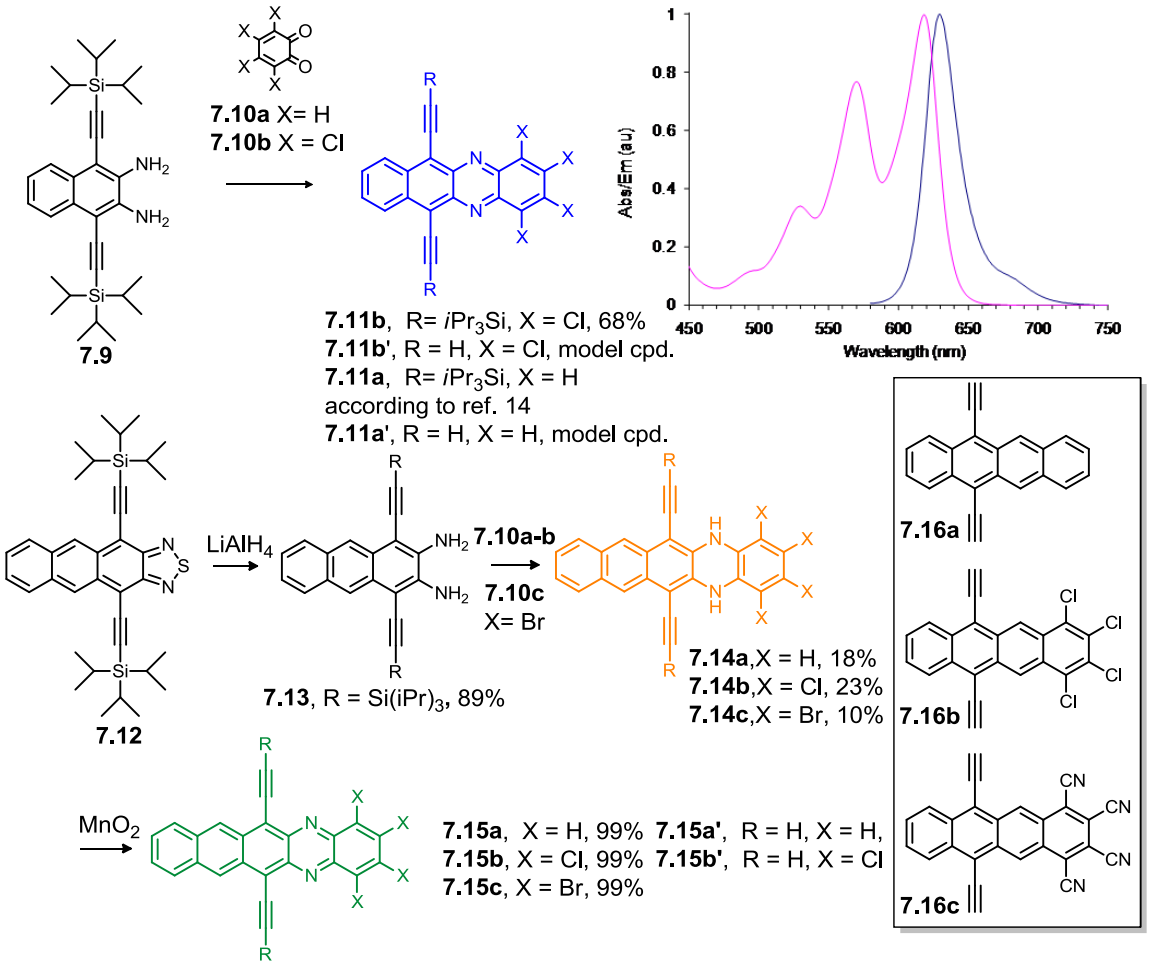

Figure 7.2. Synthesis of **7.11a** and **7.11b**, UV-vis and fluorescence spectra of diazatetracene **7.11b** in hexanes, synthesis of the diazaacene-types **7.14-7.15**, depiction of the model compounds **7.16a-c** and **7.15a'**,**b'**. The condensation of the diamine **7.9** with the *ortho*-quinones **7.10a** and **7.10b** furnished the diazaacenes **7.11a** and **7.11b** in excellent yield; **7.11a'** and **7.11b'** are used in computational studies. Upon reacting **7.13** with **7.10**, the NH-intermediates **7.14a-c** are isolated and oxidized efficiently to **7.15a-c**, respectively, by manganese dioxide. Azaacene **7.11b** is fluorescent and its absorption (λ_{max} 617 nm) is bathochromically shifted compared to that of the non-chlorinated analog **7.11a** (λ_{max} of 571 nm).

absorption maximum only 0.032 eV lower in energy than that of the parent compound **7.5** according to published UV-vis spectra.[27,28]

By change of substituent/size of the acene framework, an absorption range from 561-758 nm can be "tuned in" in **7.11** and **7.15**. The expected acene-type vibronic fine structure is observed for all of the compounds. Table 7.1 displays the numerical values for the absorption spectra and the results of the cyclic voltammetry and quantum chemical calculation using Density Functional (DFT) and Time-Dependent Density Functional Theory (TD-DFT). In Figure 7.3a the spectra of **7.15a** and **7.15c** are shown to demonstrate that bromine has an effect on the absorption properties of diazaacenes almost indistinguishable from that of chlorine substituents (Table 7.1), consistent with the similar inductive and mesomeric properties of these two halogens (Br: F = +0.45, R = –0.22; Cl: F = +0.42, R = –0.19; F = field effect parameter, R = resonance parameter) i.e., both substituents act as moderately inductive (σ) electron-withdrawing groups and as weak π-donors, as indicated by the Swain-Lupton parameters quantifying these two effects.[29]

TD-DFT values of the vertical transition energies (S_1^{vert}) for the lowest-lying singlet excited states of model compounds **7.11a'**, **7.11b'**, **7.15a'** and **7.15b'** reproduce the trends observed in the experimental data of **7.11a,b** and **7.15a,b**; TD-DFT calculations for the tetracenes **7.16a** and **7.16b** predict only a very small red shift in absorption as a result of chlorination, which is also consistent with experimental data for the corresponding homolog pentacenes, **7.5** and **7.6**. Moreover, the calculations indicate in all cases that the transitions are predominantly HOMO-to-LUMO in character. The trends in the electrochemical gaps between the half-wave potentials corresponding to molecular

A

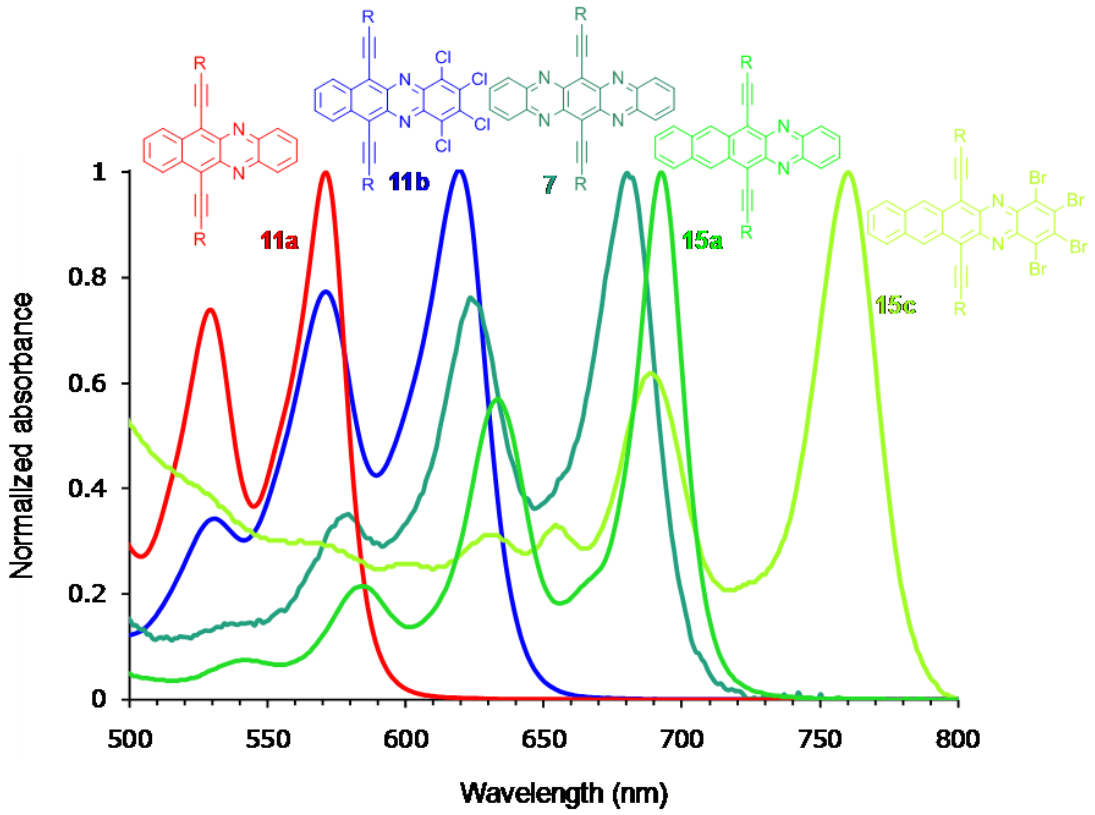

B

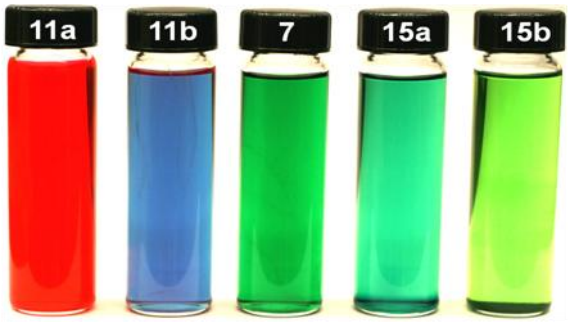

Figure 7.3. UV-vis spectra of selected heteroacenes. (a) Long-wavelength normalized UV-vis spectra in hexane. (b) Photograph of solutions of heteroacenes in hexane. The combined effects of annulation and halogenation leads to a shift of absorption from 571 to 758 nm. The spectrum of **7.15b** (see Figure 7.25) is almost superimposable onto that of **7.15c.** It is clear that the halo-substitution in both tetracenes and in pentacenes leads to significant red shifts in absorption. Chlorine and bromine substituents are equally effective. The UV-vis spectrum of **7.7** was taken from ref 12.

oxidation and reduction closely follow those in the experimental and TD-DFT optical transition energies and the DFT HOMO-LUMO gaps (Table 7.1).[30] Accordingly, we have examined the frontier molecular orbitals in order to explain the origin of the unexpected large red shifts observed in the spectra of the azaacenes upon halogenation.

Table 7.1. Absorption and Emission Maxima and Electrochemistry of the Investigated Heteroacenes

Acene	**7.11a**	**7.11b**	**7.11c**	**7.15a**	**7.15b**	**7.15c**	**7.16a**	**7.16b**	**7.16c**
λ_{max} abs (nm)	571	617	-	692	756	759	-	-	-
$E_{1/2}^{0/-}$(V)[b]	-1.19	-0.92	-	-1.05	-0.79	-0.79	-	-	-
$E_{1/2}^{+/0}$(V)[b]	+0.99	+1.11	-	+0.68	+0.83	+0.80	-	-	-
elchem. gap (V)	2.18	2.03	-	1.73	1.62	1.59	-	-	-
opt. gap (eV) [a]	2.17	2.01	-	1.79	1.64	1.63	-	-	-
S_1^{vert} [c]	2.07	1.91	1.38	1.58	1.44	nd	2.16	2.13	1.61
calcd. HOMO-LUMO gap (eV)[d]	2.37	2.25	1.81	1.87	1.77	nd	2.41	2.39	2.00
HOMO (eV)	-5.72	-6.03	-6.66	-5.37	-5.66	nd	-5.28	-5.68	-6.38
LUMO (eV)	-3.35	-3.78	-4.84	-3.50	-3.89	nd	-2.87	-3.30	-4.38

a) From absorption maxima. *b)* In a 1:1 v/v mixture of a 0.1 M acetonitrile solution of $^{n}Bu_4NPF_6$ and toluene, vs. $FeCp_2^{+/0}$. *c)* Time-Dependent Density Functional Theory (TD-DFT) calculations at the B3LYP/6-311+G* level. The transitions are all one-electron transitions with a > 80% HOMO-LUMO contribution. *d)* The desilylated model compounds **7.11a', 7.11b', 7.15a'** and **7.15b'** were used for the calculations to reduce the computation time.

Figure 7.4 displays the frontier molecular orbitals (energy in eV) of **7.11a'**/**7.11b'** and **7.16a**/**7.16b**. In both pairs, stabilization of the LUMOs results when attaching four chlorine substituents. The stabilization is 0.43 eV in both **7.11b'** and **7.16b**. More importantly, upon going from **7.11a'** to **7.11b'** the HOMO is only stabilized by 0.31 eV, while in the case of **7.16a/7.16b** the HOMO stabilization is 0.40 eV, very similar to that

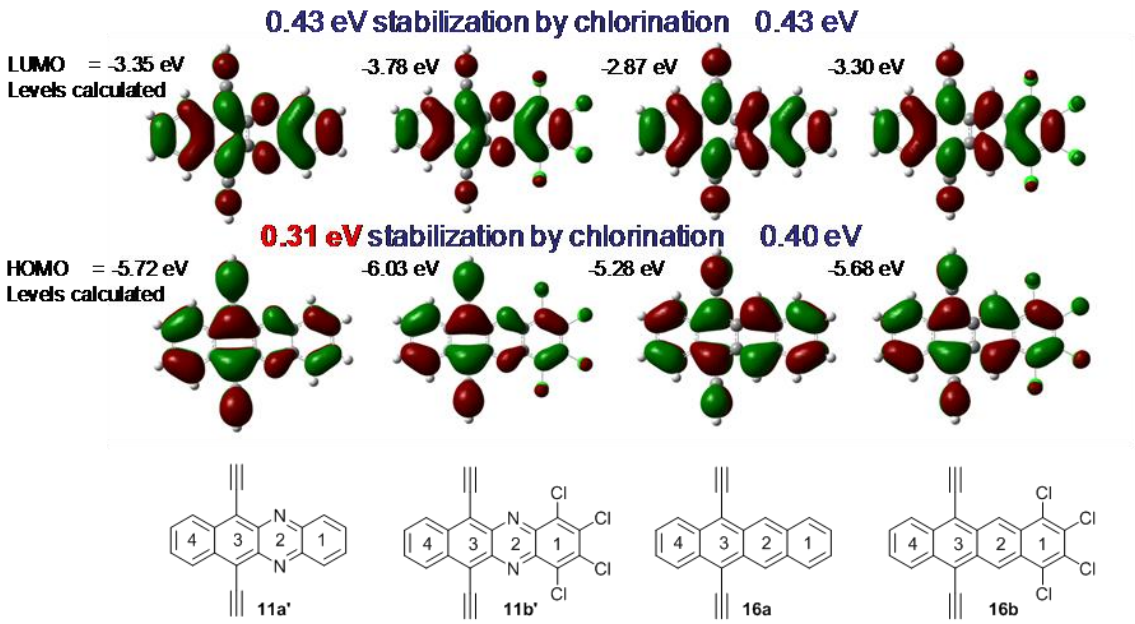

Figure 7.4. Frontier molecular orbitals (HOMO, middle, LUMO, top) of acene derivatives. The bottom shows the structural formulae and numbering of the rings. The LUMOs of the four compounds are very similar to each other. Both **7.11b'** and **7.16b** experience a stabilization of 0.43 eV through the chlorine substitution. The HOMOs of **7.11a** and **7.11b** and **7.16a** and **7.16b** resemble each other qualitatively but are pair wise (**7.11**/**7.16**) different. The differences are pronounced in the rings 1 and 2 as particularly in the HOMO of **7.11a'** the orbital coefficients (see SI) on the rings 1 and 2 are small; as a consequence the chlorine substituents are less effective in stabilizing the HOMO (going from **7.11a'** to **7.11b'**)**,** mirroring the optical behavior seen in compound **7.11b**.

observed for the LUMO. The LUMOs of all four compounds are similar in appearance (Figure 7.4), explaining the consistent effect of halogenation. In contrast, the geometric shape of the HOMOs differs between the two classes of molecule; **7.11a**/**7.11b** display smaller orbital coefficients on rings 1 and 2 (Figure 7.4), while in pair **7.16a**/**7.16b** the HOMOs have roughly similar coefficients on all rings. The smaller HOMO coefficients on rings 1 and 2 in **7.11b'** lead to its diminished stabilization by the four chlorine substituents when compared to the pair **7.16a,b**, in which the HOMO coefficients are larger on these rings (Figure 7.4). Based upon the computational results, the contribution

(sum of the squared orbital coefficients) from rings 1 and 2 is about three times as large in **7.16a** as in the heteroacene **7.11a**'. The diminished stabilization of the HOMO when going from **7.11a**' to **7.11b**' is the reason for the induced red-shift in the diazaacenes. The same effect is also operative for the larger diazapentacenes **7.15a** and **7.15b** where identical effects are observed according to calculations, electrochemistry, and optical spectroscopy (Table 7.1).

If the proposed explanation is correct, stronger acceptors such as cyano should have a larger effect and reduce the energy of the optical transitions (and the band gap) further. In such compounds the HOMO should have vanishing coefficients on rings 1 and 2. To test

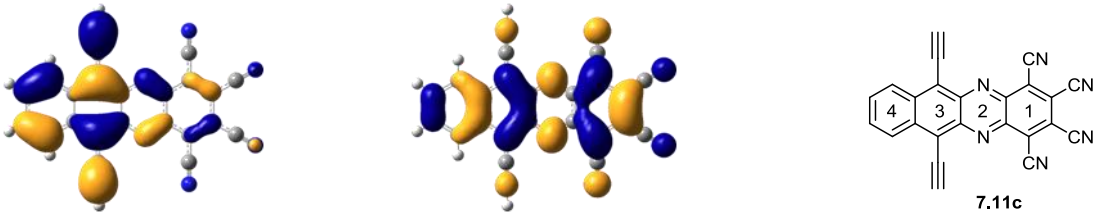

7.11c

Figure 7.5. Frontier molecular orbitals (HOMO -6.30 eV, left, LUMO -4.49 eV, right, gap = 1.81 eV) of tetracyanodiazaacene **7.11c.** Calculated by DFT using B3LYP/6-311+G* basis sets. Compared to **7.11a** calculated on the same level of theory, the optical band gap (S_0-S_1 transition) shrinks from 2.07eV to 1.38 eV.

this hypothesis, we performed quantum chemical calculations on model **7.11c** (Figure 7.5). The HOMO of 7.**11c** is predominantly localized on rings 3 and 4, while the LUMO is extended over all four rings; as a result, the calculated optical gap shrinks to 1.38 eV. When compared to the parent **7.11a**, this is a decrease of almost 0.7 eV. A disjoint orbital structure,[13] i.e. spatially separated frontier molecular orbitals, with the disjointing effect further amplified by electronegative substituents, decreases the transition energies for diazaacenes, an effect less observed in acenes which have more congruent frontier

molecular orbitals.[13] When computationally comparing **7.16a** with cyano-substituted **7.16c**, there also occurs a lowering of the optical gap; however, with 0.55 eV, it is smaller than the effect seen when going from **7.11a** to **7.11c**.

The disjoint frontier MOs in diazaacenes is one of their defining features and opens the door to amplified substituent effects in the engineering of electronic and optical properties. N-Heteroacenes in which optical absorption and electron affinity can be tuned independently are within reach. Some of these materials might prove to be promising electron-transport materials.

7.3 Conclusions

In conclusion, we have prepared halogenated azaacenes **7.11b** and **7.15b,c**, which display bathochromically shifted absorptions when compared to their non-halogenated congeners **7.11a** and the previously unknown **7.15a**. Bathochromic shift upon chlorination is not observed in the acene/tetrachloroacene series, indicating that the pyrazines are a necessary ingredient for this engineering of optical properties. Quantum-chemical calculations reveal that this difference in behavior can be attributed to the substituent-induced disjoint frontier molecular orbitals of the azaacenes. The interplay between pyrazines and electronegative substituents serves as a uniquely useful tool to manipulate the absorption characteristics of N-heteroacenes. This effect will enhance the design and tuning of acene-type materials for organic electronics and other applications.

This work has been submitted to *Nature Chemistry*:

Appleton, Anthony L.; Brombosz, Scott M.; Barlow, Stephen; Sears, John; Brédas, Jean-Luc.; Marder, Seth R.; Bunz, Uwe H. F. **Submitted**.

7.4 Experimental and Supplementary Information

7.4.1 1,2,3,4-Tetrachloro-6,11-bis((triisopropylsilyl) ethynyl)benzo[*b*] phenazine, **7.11b**.

To a dry 50 mL round bottom flask was added compound **7.9**[1] (0.200 g, 3.85 x 10^{-4} mol, 1 equiv.), compound **7.10b** (0.0950 g, 3.85 x 10^{-4} mol, 1 equiv.), ethanol (10 mL) and acetic acid (3 mL). The solution was brought to reflux and stirred overnight. The reaction was cooled on an ice bath and quenched with water. The precipitate was filtered with water, washed with cold methanol (10 mL) and allowed to dry. The product was purified by column chromatography (10:1, hexane : dichloromethane). Compound **7.11b** was isolated as green-black crystals (0.190 g, 67.6% yield). **7.11b**: m.p. = 179 °C (decomp.); IR (KBr, cm^{-1}) 3116, 3062, 2939, 2889, 2862, 2754, 2723, 2360, 2129, 1461, 1438, 1388, 1361, 1238, 1180; ^{1}H-NMR (δ in $CDCl_3$) 8.76 (dd, $^{3}J_{HH}$ = 3.2 Hz, $^{4}J_{HH}$ =6.8 Hz, 2H), 7.70 (dd, $^{3}J_{HH}$ = 3.2 Hz, $^{4}J_{HH}$ = 6.8 Hz, 2H), 1.29-1.27 (m, broad, 42H); ^{13}C-NMR (δ in $CDCl_3$) 140.52, 139.27, 136.58, 134.60, 132.26, 129.03, 127.82, 121.35, 109.68, 101.90, 18.94, 11.56; accurate mass for $C_{38}H_{46}Cl_4N_2Si_2$: *m/e* = 726.19656 [M+], calc. *m/e* = 726.19537; elemental analysis for $C_{38}H_{46}Cl_4N_2Si_2$ [C] = 62.69, calc. [C] = 62.63.

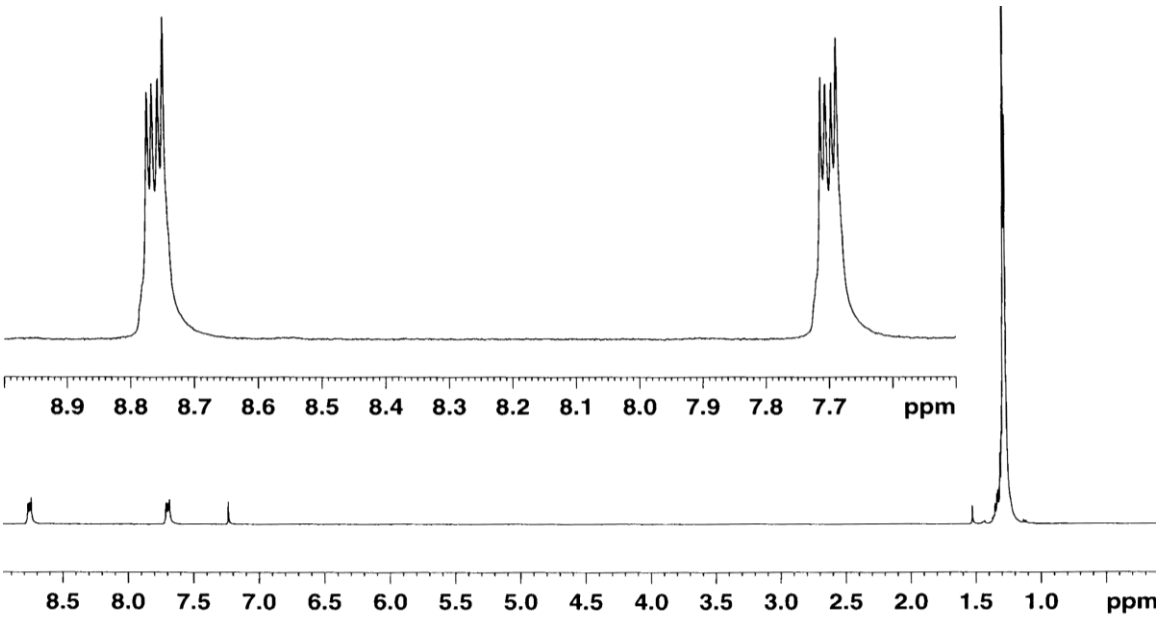

Figure 7.6. ^{1}H-NMR of **7.11b**.

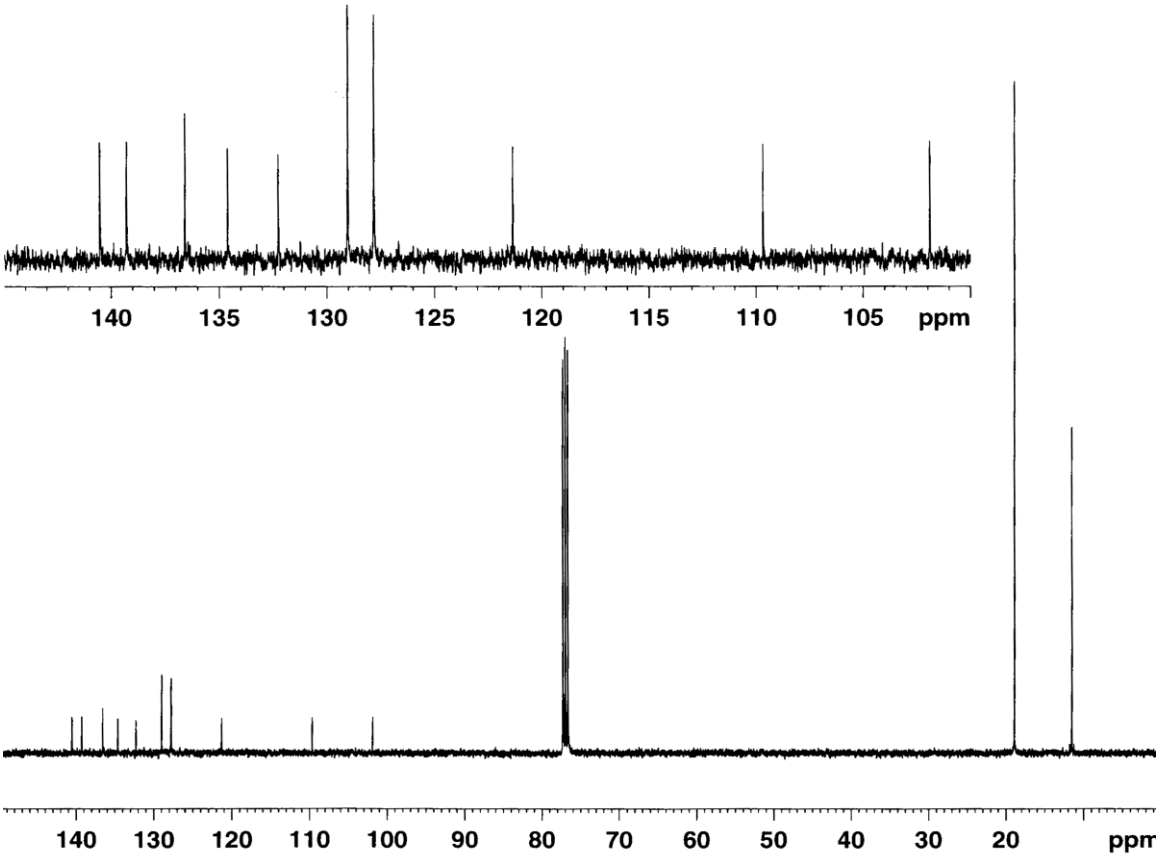

Figure 7.7. ^{13}C-NMR of **7.11b**.

7.4.2 1,4-Bis((triisopropylsilyl)ethynyl)anthracene-2,3-diamine, **7.13**.

To an oven dried 1 L Schlenk flask was added compound **7.12**[2] (5.20 g, 8.71 x 10^{-3} mol) and dry THF (100 mL). The mixture was purged with nitrogen for 5 min and cooled on an ice bath to 0 °C. Lithium aluminum hydride (3.31 g, 8.71 x 10^{-2} mol, 10 equiv.) was added over 1 h. The reaction was again purged with nitrogen for 5 min and sealed from the atmosphere with a bubbler. The reaction was stirred for 12 h, while the ice was allowed to melt. The reaction was placed back on an ice bath and allowed to cool to 0 °C. The reaction was quenched with aqueous ammonium chloride solution and extracted with diethyl ether (5 x 150 mL). The organic layer was dried with sodium sulfate, filtered, and the solvent was removed *in vacuo*. The product was purified by column chromatography (3:1, hexane : dichloromethane). Compound **7.13** was obtained as a golden solid (4.41 g, 89% yield). **7.13**: m.p. = stable to 250 °C; IR (KBr, cm^{-1}) 3448, 3355, 3228, 3163, 3047, 2962, 2862, 2719, 2136, 1932, 1913, 1620, 1550, 1539, 1454, 1392, 1307, 1238, 1180; ^{1}H-NMR (δ in $CDCl_3$) 8.60 (s,2H), 7.91 (dd, $^{3}J_{HH}$ = 3.2, $^{4}J_{HH}$ = 6.4 Hz, 2H), 7.39 (dd, $^{3}J_{HH}$ = 3.2, $^{4}J_{HH}$ = 6.4 Hz, 2H), 4.49 (s, 4H), 1.25 (s, 42H); ^{13}C-NMR (δ in $CDCl_3$) 139.67, 130.93, 127.82, 127.53, 124.57, 122.81, 102.75, 102.13, 101.74, 18.70, 11.28; accurate mass for $C_{36}H_{52}N_2Si_2$: *m/e* = 568.36863 [M+], calc. *m/e* = 568.36691.

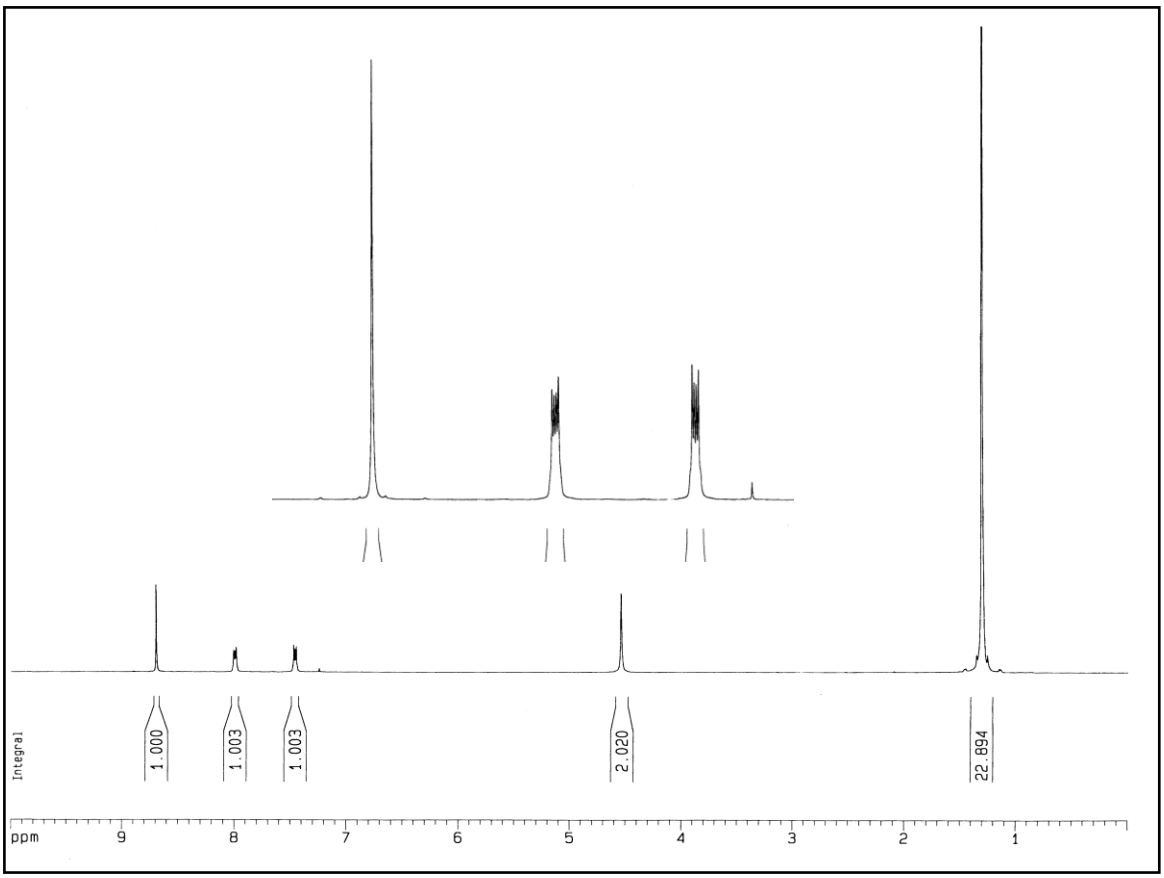

Figure 7.8. ^{1}H-NMR of **7.13**.

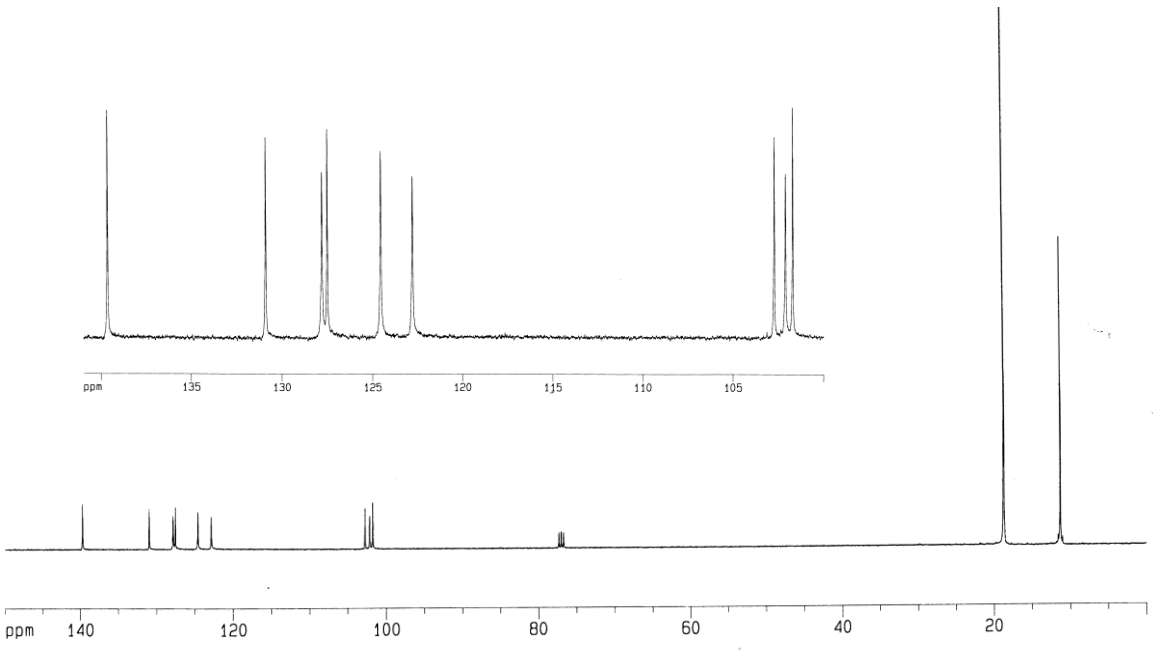

Figure 7.9. ^{13}C-NMR of **7.13**.

7.4.3 6,13-Bis((triisopropylsilyl)ethynyl)-5,14-dihydronaphtho [2,3-*b*]phenazine, **7.14a**.

Compound **7.13** (0.435 g, 7.65 x 10^{-4} mol) and **7.10a**[1] (0.245 g, 2.29 x 10^{-3} mol, 3 eqiv) were heated to reflux in DCM (50 mL) and acetic acid (3 mL) for 12 h. The reaction mixture was washed with water (2 x 250 mL); the organic layer was dried with sodium sulfate, filtered, and the solvent removed *in vacuo*. The product was purified by column chromatography (hexane). Compound **7.14a** was obtained as a metallic red-green solid (0.0853 g, 17.5%). **7.14a**: m.p. = 263 °C (decomp.); IR (KBr, cm^{-1}) 3488, 3400, 3199, 3147, 3120, 3055, 3028, 2956, 2923, 2864, 2752, 2721, 2360, 2198, 2135, 2030, 1870, 1737, 1589, 1461, 1315, 1261, 1182; ^{1}H-NMR (δ in $CDCl_3$) 8.169 (s, 2H), 7.75 (dd, $^{3}J_{HH}$ = 3.2 Hz, $^{4}J_{HH}$ = 6.3 Hz, 2H), 7.30 (dd, $^{3}J_{HH}$ = 3.2 Hz, $^{4}J_{HH}$ = 6.4 Hz, 2H), 6.64 (dd, $^{3}J_{HH}$ = 3.3 Hz, , $^{4}J_{HH}$ = 5.7 Hz, 2H), 6.33 (dd, $^{3}J_{HH}$ = 3.4 Hz, $^{4}J_{HH}$ = 5.6 Hz, 2H), 6.614 (s, 2H), 1.253 (s, 42H); ^{13}C-NMR (δ in $CDCl_3$) 136.25, 131.55, 129.07, 128.46, 127.66, 124.82, 122.15, 122.13, 112.98, 103.52, 100.93, 96.01, 18.90, 11.41; accurate mass for $C_{42}H_{54}N_2Si_2$: *m/e* = 642.3849 [M+], calc. *m/e* = 642.3826.

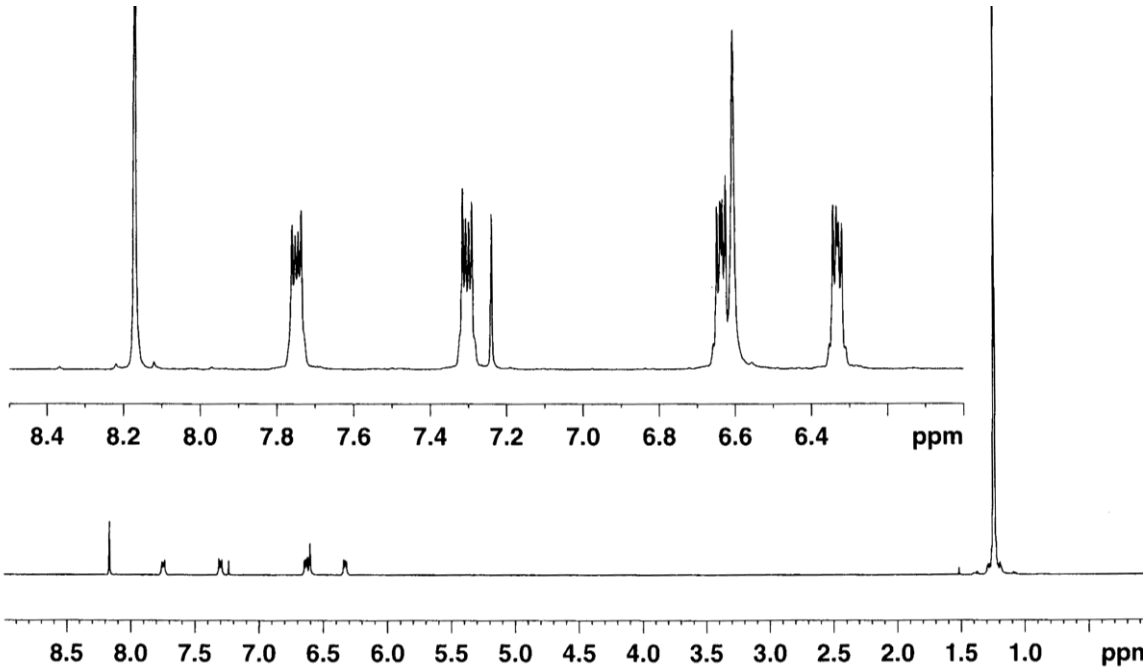

Figure 7.10. ^{1}H-NMR of **7.14a**.

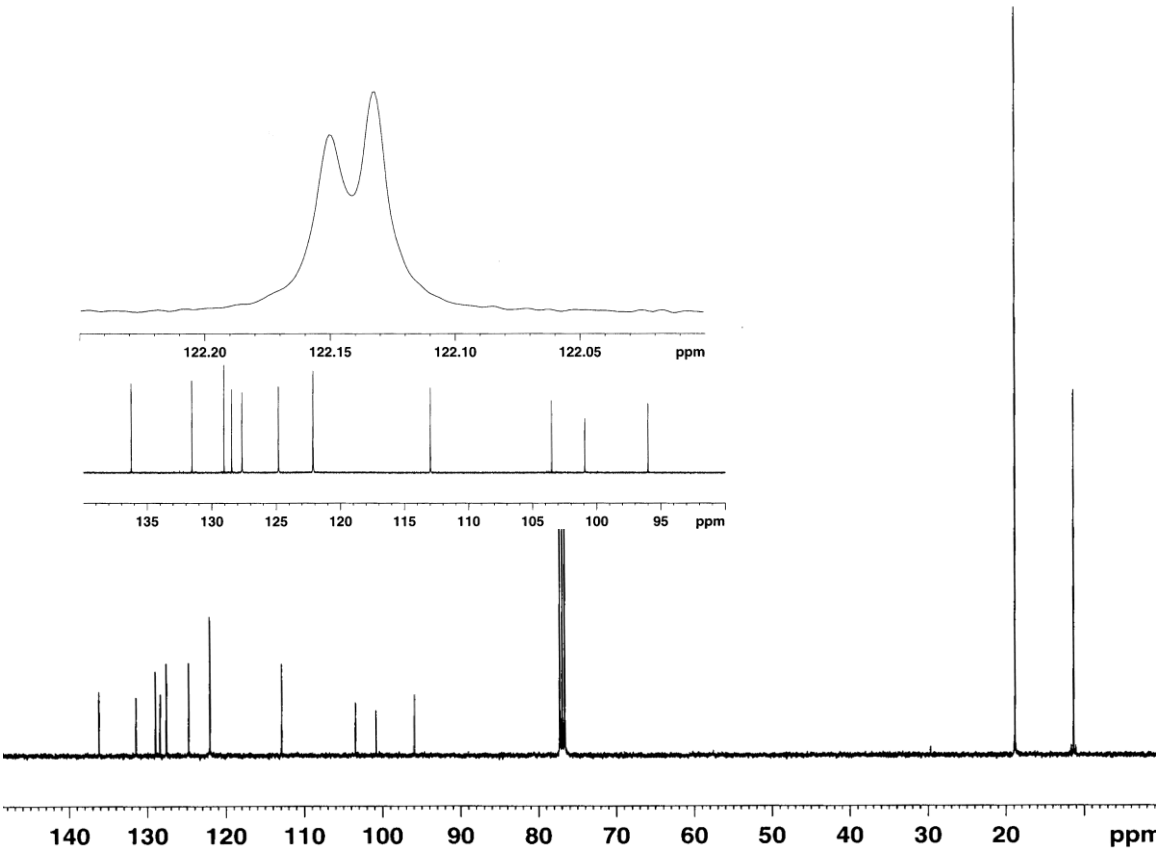

Figure 7.11. ^{13}C-NMR of **7.14a**.

7.4.4 6,13-Bis(triisopropylsilyl)ethynyl)naptho[2,3-*b*]phenazine, **7.15a**.

Compound **7.14a** (0.100 g, 1.56 x 10^{-4} mol) was dissolved in DCM (25 mL) and stirred for 4 h with an excess of MnO_2. The solvent was removed *in vacuo*. The product was purified by column chromatography (3:1, hexane : DCM). Compound **7.15a** was obtained as a green solid (0.0995 g, 99% yield). **7.15a**: m.p. = 265 °C (decomp.); IR (KBr, cm^{-1}) 3145, 3118, 3047, 3024, 2956, 2939, 2923, 2862, 2752, 2721, 2136, 2111, 1731, 1600, 1521, 1461, 1377, 1259, 1103; ^{1}H-NMR (δ in $CDCl_3$) 9.411 (s, 2H), 8.16 (dd, $^{3}J_{HH}$ = 3.4 Hz, $^{4}J_{HH}$ = 6.9 Hz, 2H), 8.02 (dd, $^{3}J_{HH}$ = 3.2 Hz, $^{4}J_{HH}$ = 6.6 Hz, 2H), 7.75 (dd, $^{3}J_{HH}$ = 3.4 Hz, $^{4}J_{HH}$ = 6.9 Hz, 2H), 7.46 (dd, $^{3}J_{HH}$ = 3.2 Hz, $^{4}J_{HH}$ = 6.6 Hz, 2H), 1.360-1.350 (m, broad, 42H); ^{13}C-NMR (δ in $CDCl_3$) 145.01, 140.98, 132.92, 132.57, 131.21, 130.48, 128.71, 126.80, 126.75, 120.75, 109.52, 103.81, 18.98, 11.69; accurate mass for $C_{42}H_{52}N_2Si_2$: *m/e* = 640.3674 [M+], calc. *m/e* = 640.3669; elemental analysis for $C_{42}H_{52}N_2Si_2$ [C] = 78.69, [H] = 8.18 calc. [C] = 78.11, [H] = 8.14 found

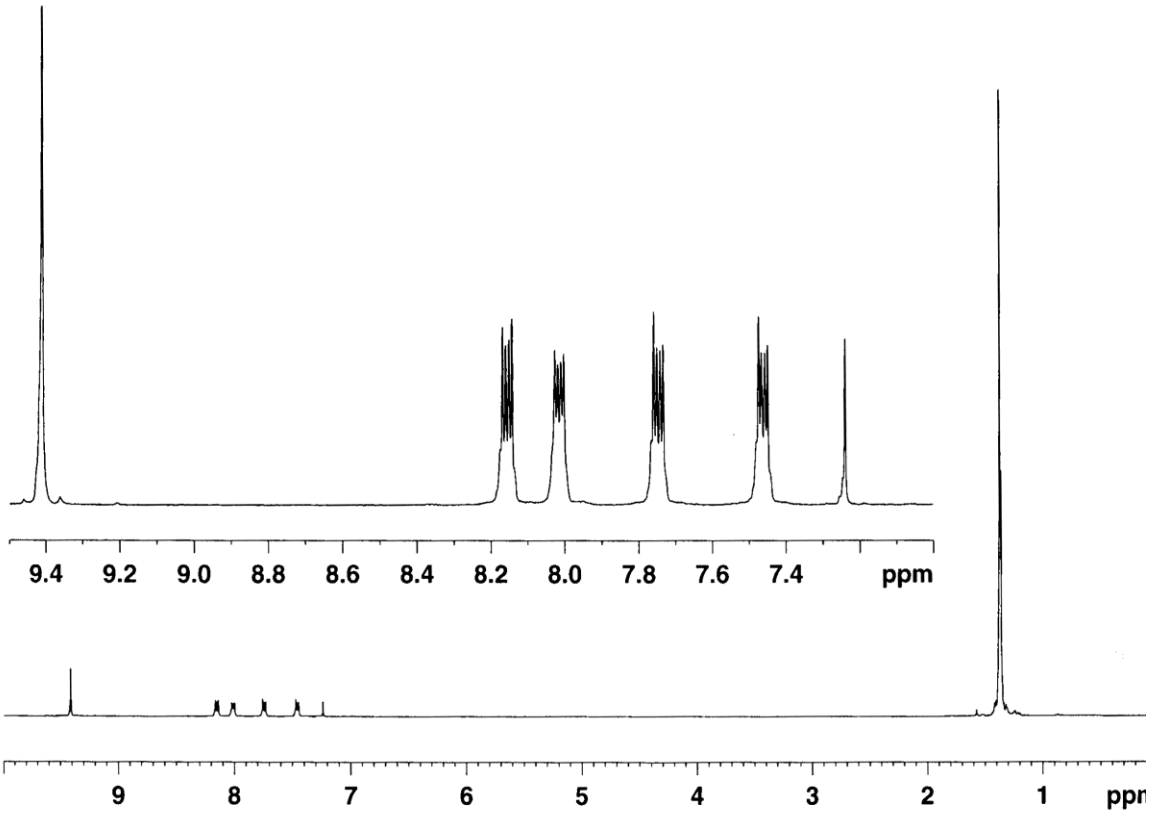

Figure 7.12. ^{1}H-NMR of **7.15a**.

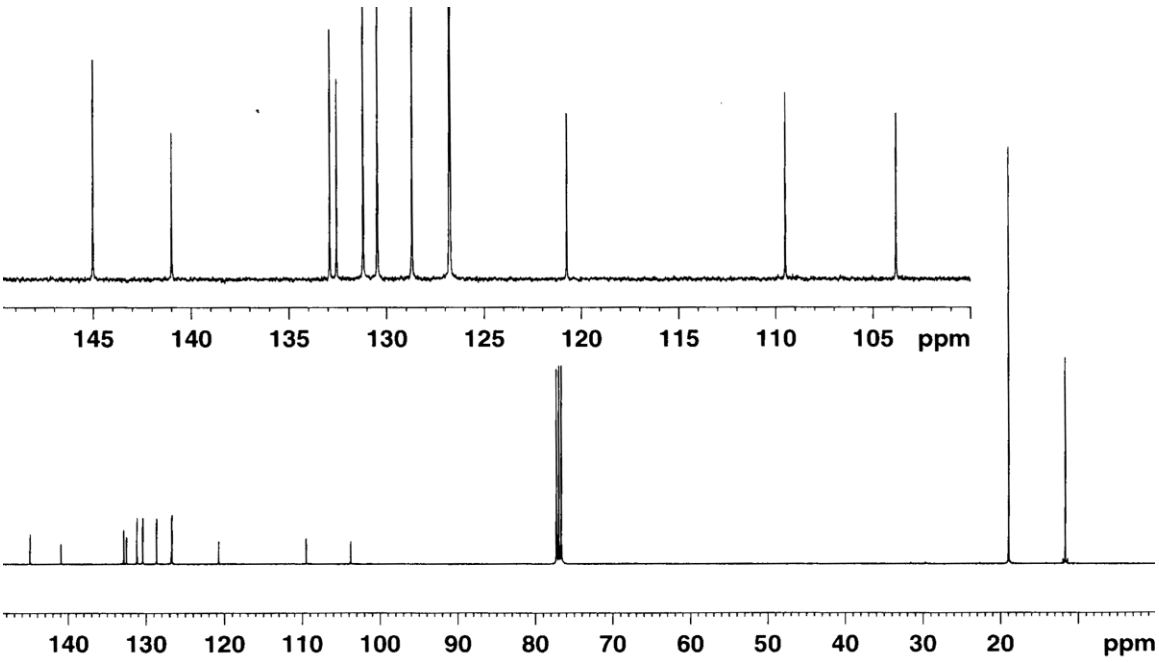

Figure 7.13. ^{13}C-NMR of **7.15a**.

7.4.5 1,2,3,4-Tetrachloro-6,13-bis((triisopropylsilyl)ethynyl)-5,14-dihydronaphtho[2,3,*b*]phenazine, **7.14b**.

Compound **7.13** (0.200 g, 3.52×10^{-4} mol) and **7.10b** (0.0864 g, 3.52×10^{-4} mol, 1 equiv.) were dissolved in a mixture of ethanol (3 mL) and acetic acid (1.5 mL) and reacted under microwave irradiation at 120 °C for 10 min. The reaction was extracted with water (50 mL) and dichloromethane (50 mL). The organic layer was dried with sodium sulfate and the solvent was removed *in vacuo*. The product was purified by column chromatography (9:1, hexane : dichloromethane) to give **7.14b** as a metallic red-green solid (0.0631 g, 23%). **7.14b**: m.p. = stable up to 350 °C; IR (KBr, cm^{-1}) 3382, 3186 3168, 3155, 3048, 2927, 2918, 2891, 2863, 2853, 2722, 2554, 2129, 1928, 1888, 1797, 1750, 1579, 1553, 1488, 1463, 1429, 1421, 1387, 1365, 1313, 1275, 1180, 1144; ^{1}H-NMR (δ, $CDCl_3$) 8.34 (s, 2H), 7.81 (dd, $^{3}J_{HH}$ = 3.2 $^{4}J_{HH}$ = 6.4 Hz, 2H), 7.39 (dd, $^{3}J_{HH}$ = 3.2, $^{4}J_{HH}$ = 6.4 Hz, 2H), 7.181 (s, 2H), 1.27-1.27 (m, broad, 42H); ^{13}C-NMR (δ,$CDCl_3$) 133.29, 131.86, 128.34, 127.84, 126.89, 125.49, 123.57, 123.21, 114.93, 105.40, 99.52, 99.13, 18.86, 11.35; accurate mass for $C_{42}H_{50}N_2Si_2Cl_4$: m/e = 778.22852 [M+], calc. m/e = 778.22667.

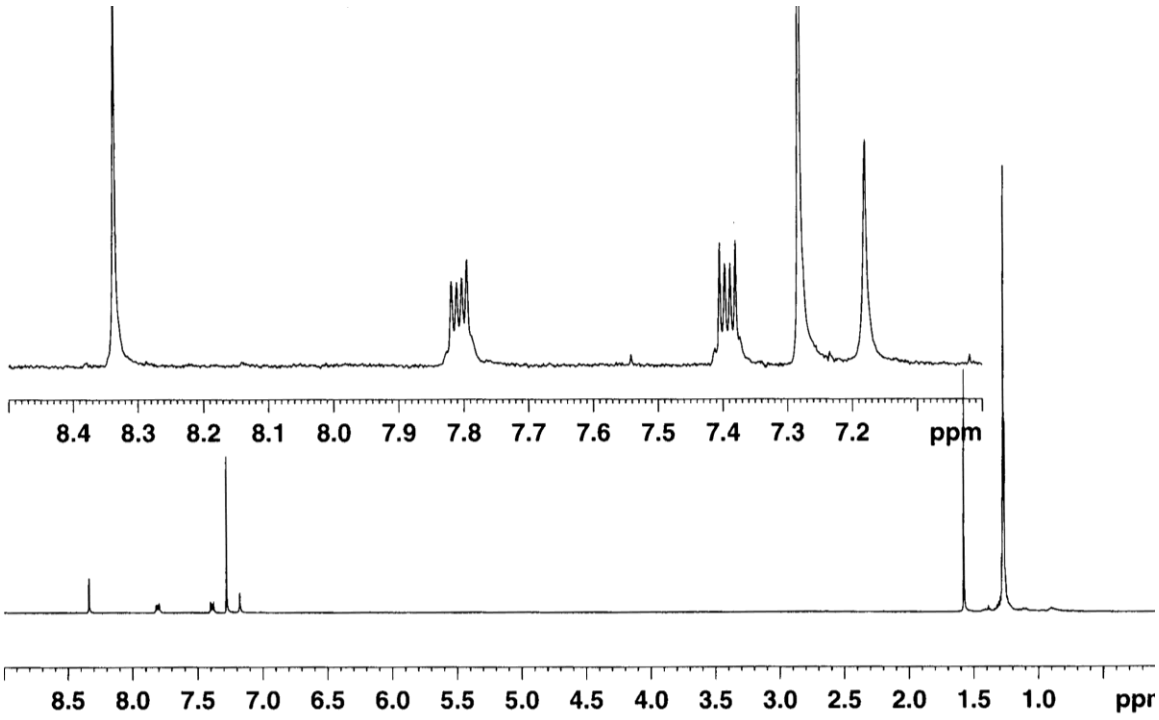

Figure 7.14. ^{1}H-NMR of **7.14b**.

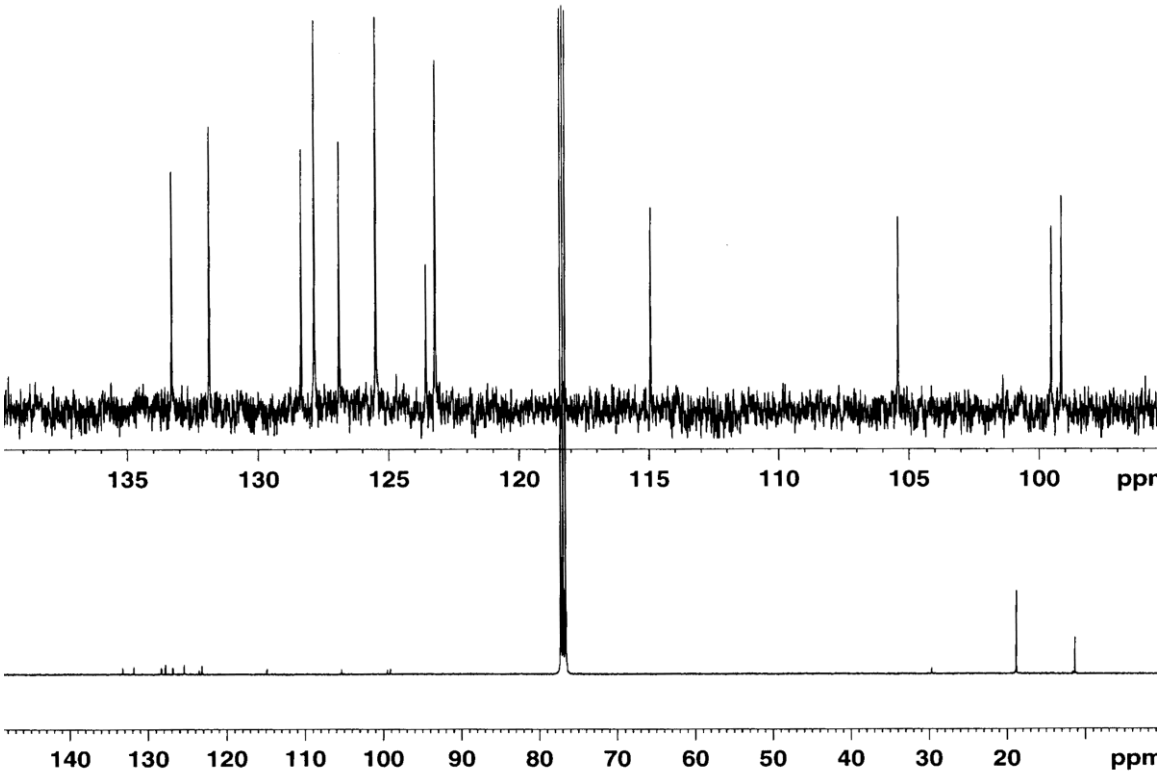

Figure 7.15. ^{13}C-NMR of **7.14b**.

7.4.6 1,2,3,4-Tetrachloro-6,13-bis((triisopropylsilyl)ethynyl) naphtho [2,3-*b*]phenazine, **7.15b**.

Compound **7.14b** (0.0631 g, 8.08×10^{-5} mol) was dissolved in dichloromethane (25 mL) and stirred for 4 h with an excess of activated MnO_2. The solvent was removed *in vacuo*. The product was purified by column chromatography (3:1, hexane : dichloromethane) to furnish **7.15b** (0.061 g, 99% yield) as a dark green solid. m.p. = 243 °C; IR (KBr, cm^{-1}) 3068, 3045, 2953, 2940, 2926, 2920, 2889, 2863, 2756, 2722, 2136, 1538, 1462, 1437, 1374, 1355, 1110; ^{1}H-NMR (δ, $CDCl_3$) 9.45 (s, 2H), 8.05 (dd, $^{3}J_{HH}$ = 3.1 Hz, $^{4}J_{HH}$ = 6.6 Hz, 2H), 7.56 (dd, $^{3}J_{HH}$ = 3.1 Hz, $^{4}J_{HH}$ = 6.6, 2H), 1.35-1.33 (m, broad, 42H); ^{13}C-NMR (δ, $CDCl_3$) 139.93, 139.42, 134.59, 133.52, 133.45, 132.27, 128.73, 127.42, 127.23, 121.43, 111.14, 102.91, 18.95, 11.61; accurate mass for $C_{42}H_{48}N_2Si_2Cl_4$: m/e = 776.21004 [M+], calc. m/e = 776.21102; elemental analysis for $C_{42}H_{48}N_2Si_2Cl_4$ [C] = 64.56, calc. [C] = 64.77.

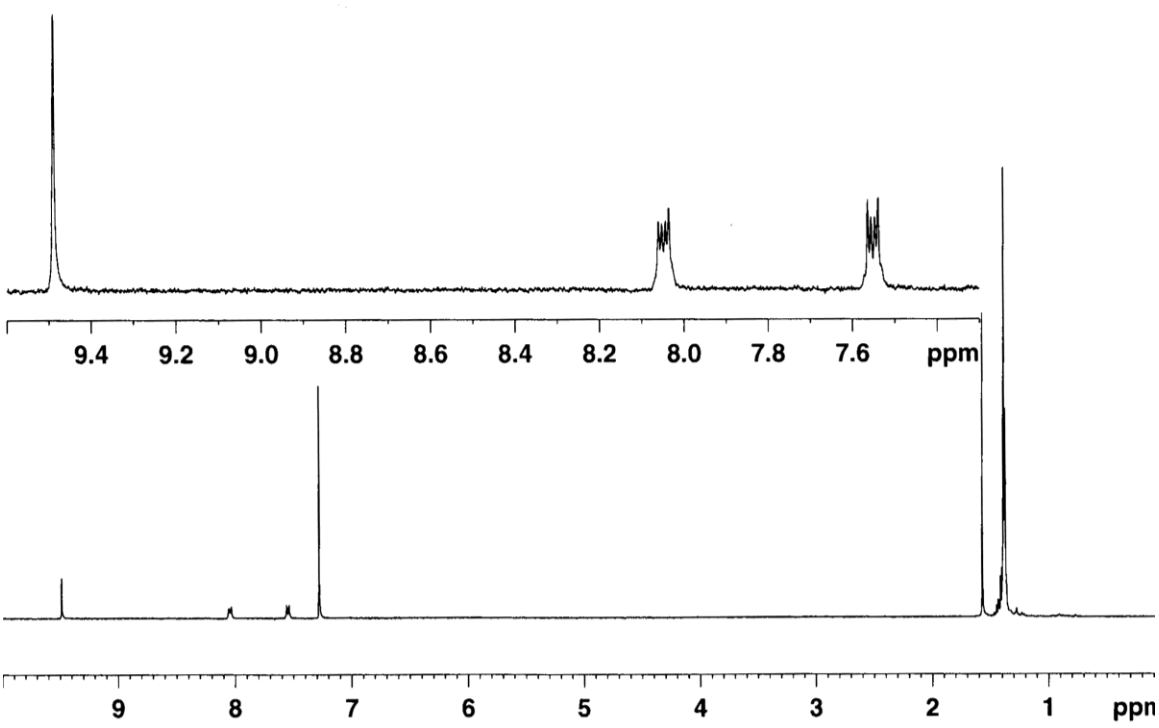

Figure 7.16. ^{1}H-NMR of **7.15b**.

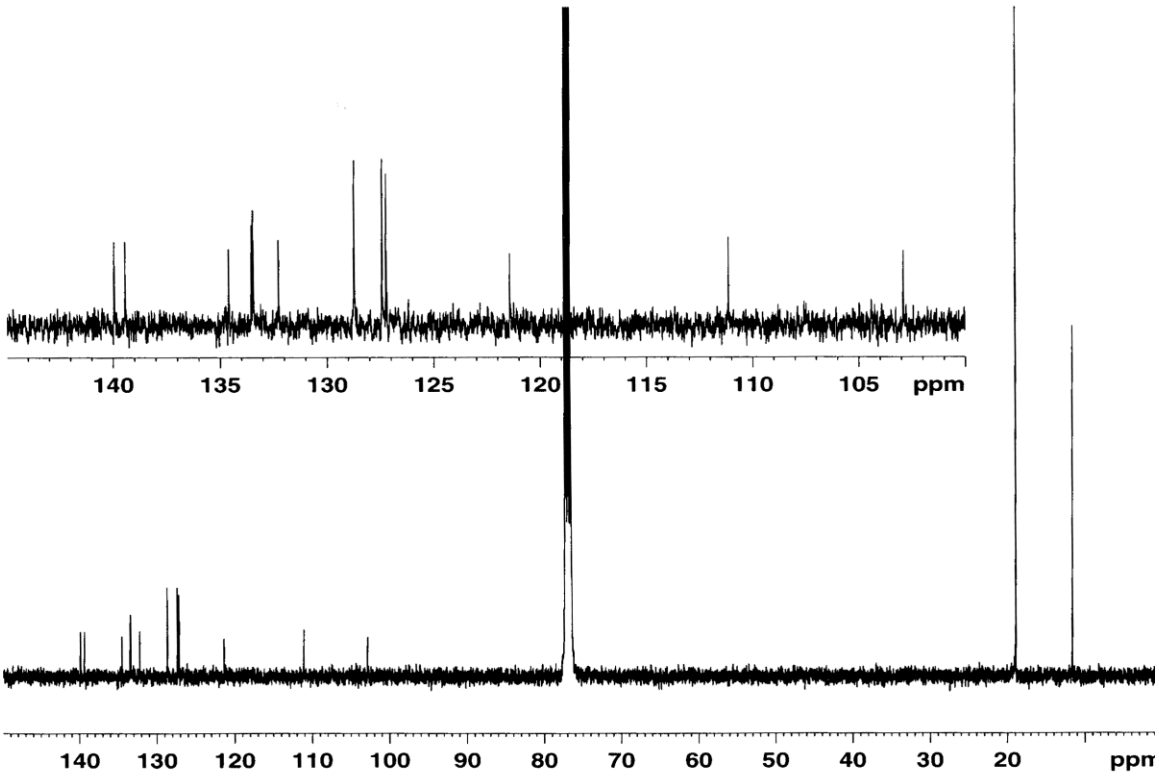

Figure 7.17. ^{13}C-NMR of **7.15b**.

7.4.7 1,2,3,4-Tetrabromo-6,13-bis((triisopropylsilyl)ethynyl)-5,14-dihydronaphtho[2,3,*b*]phenazine, **7.14c**.

Compound **7.13** (0.073 g, 1.28 x 10^{-4} mol) and compound **7.10c** (0.0544 g, 1.28 x 10^{-4}, 1 equiv.) were dissolved in ethanol (5 mL) and acetic acid (1.5 mL) and refluxed for 12 h. The reaction was extracted with water (50 mL) and DCM (50 mL). The organic layer was dried with sodium sulfate and the solvent was removed *in vacuo*. The product was purified by column chromatography (hexane). Compound **7.14c** was obtained as dark red-green solid (0.0172 g, 14% yield). **7.14c**: m.p. = 275 °C (decomp.); IR (KBr, cm^{-1}) 3361, 3045, 2939, 2926, 2920, 2887, 2862, 2721, 2534, 2360, 2143, 2127, 1580, 1556, 1485, 1462, 1455, 1431, 1421, 1389, 1361, 1311, 1265, 1229, 1181, 1143; ^{1}H-NMR (δ in $CDCl_3$) 8.30 (s, 2H), 7.75 (dd, $^{3}J_{HH}$ = 3.4 Hz, $^{4}J_{HH}$ = 6.4 Hz, 2H), 7.34 (dd, $^{3}J_{HH}$ = 3.1 Hz, $^{4}J_{HH}$ = 6.4 Hz, 2H), 7.27 (s, 2H), 1.23-1.22 (m, broad, 42H); ^{13}C-NMR (δ in $CDCl_3$) 133.79, 131.87, 128.82, 128.45, 127.83, 125.47, 123.21, 118.41, 109.09, 105.42, 99.64, 98.93, 18.91, 11.41; accurate mass for $C_{42}H_{50}N_2Si_2Br_4$: *m/e* = 954.02184 [M+], calc. *m/e* = 954.02460.

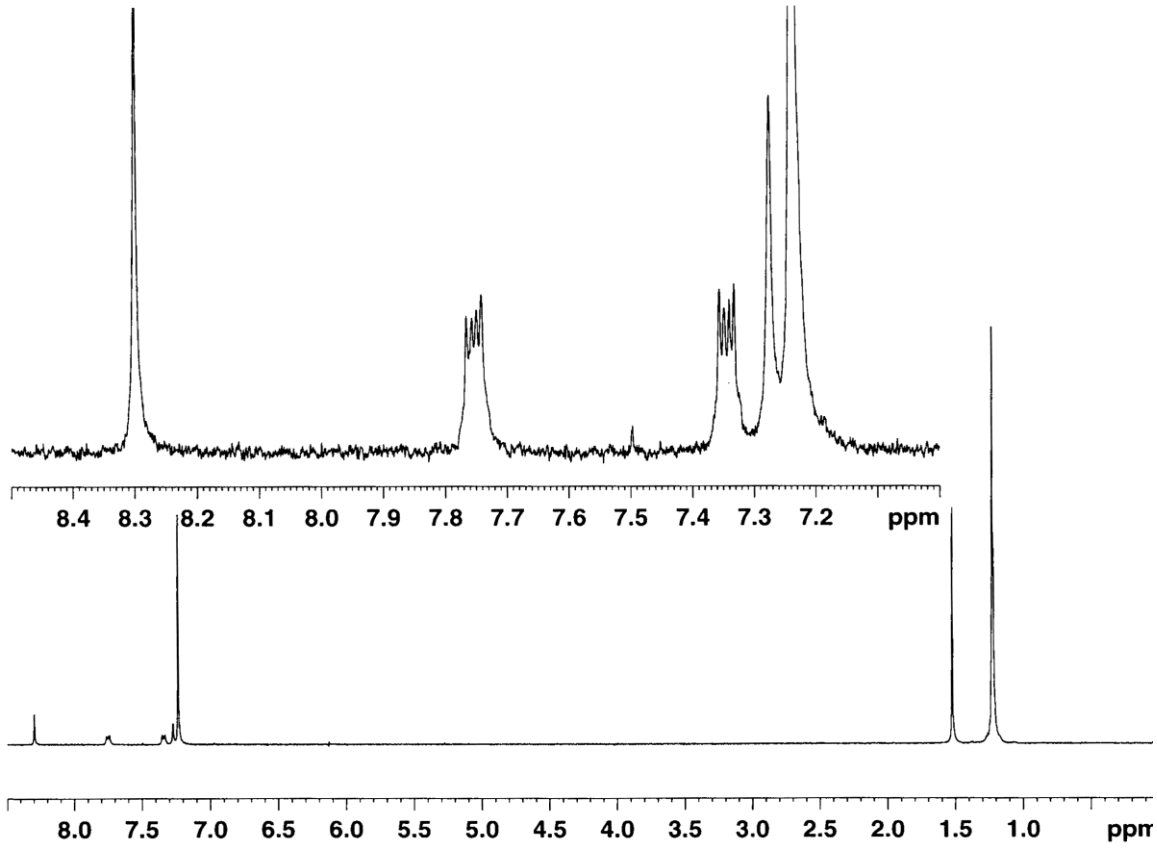

Figure 7.18. [1]H-NMR of **7.14c**.

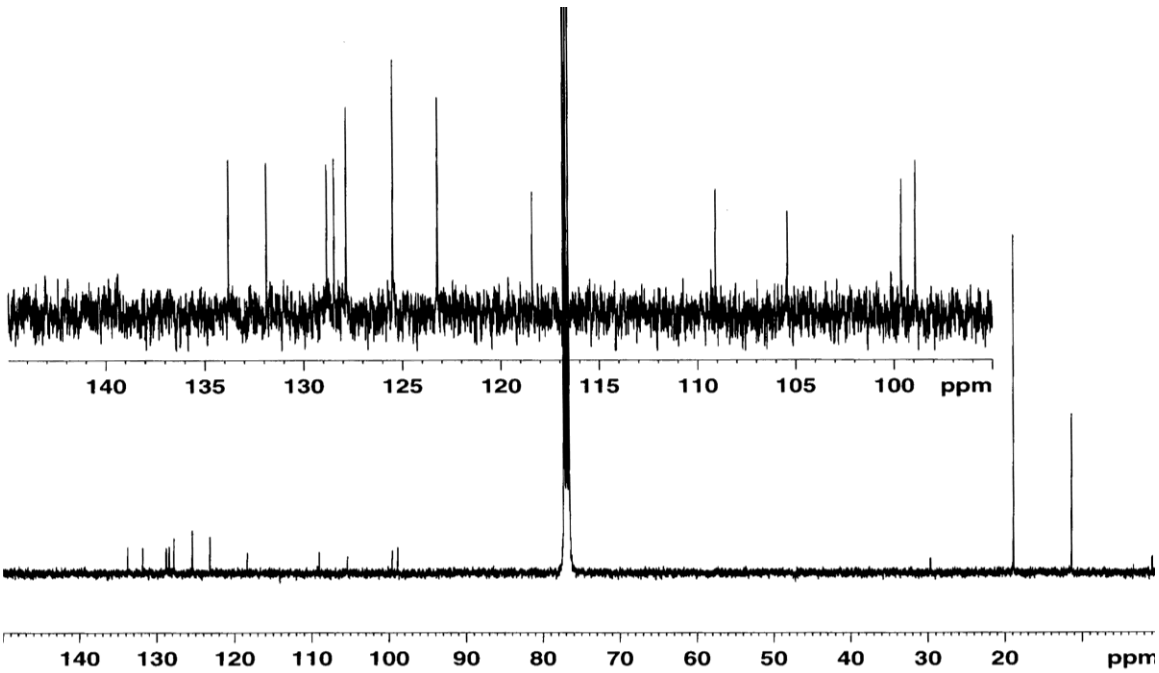

Figure 7.19. [13]C-NMR of **7.14c**.

7.4.8 1,2,3,4-Tetrabromo-6,13-bis((triisopropylsilyl)ethynyl)

naphtho [2,3-*b*]phenazine, **7.15c**.

Compound **7.14c** (0.0172 g, 1.79 x 10^{-5}) was dissolved in DCM (25 mL) and stirred for 4 h with an excess of MnO_2. The solvent was removed *in vacuo*. The product was purified by column chromatography (3:1, hexane : DCM). Compound **7.15c** was obtained as a dark-green solid (0.0171 g, 100%). **7.15c**: m.p. = 275 °C (decomp.); IR (KBr, cm^{-1}) 3045, 2954, 2939, 2925, 2889, 2861, 2753, 2722, 2143, 2125, 1531, 1486, 1463, 1433, 1422, 1407, 1375, 1359, 1344, 1163, 1137, 1108; ^{1}H-NMR (δ in $CDCl_3$) 9.459 (s, 2H), 7.99 (dd, $^{3}J_{HH}$ = 3.2 Hz, $^{4}J_{HH}$ = 6.5 Hz, 2H), 7.50 (dd, $^{3}J_{HH}$ = 3.2 Hz, $^{4}J_{HH}$ = 6.7 Hz, 2H), 1.343-1.331 (m, broad, 42H); ^{13}C-NMR (δ in $CDCl_3$) 140.52, 140.48, 133.63, 133.55, 131.68, 128.96, 128.75, 127.45, 127.29, 121.27, 111.11, 103.11, 19.04, 11.69; Mass Spectra Analysis (ESI) for $C_{42}H_{48}N_2Si_2Br_4$: *m/e* = 952 [M+], calc. *m/e* = 952. Due to poor ionization, accurate mass could not be determined. The isotopic splitting pattern was consistent with a tetrabrominated compound.

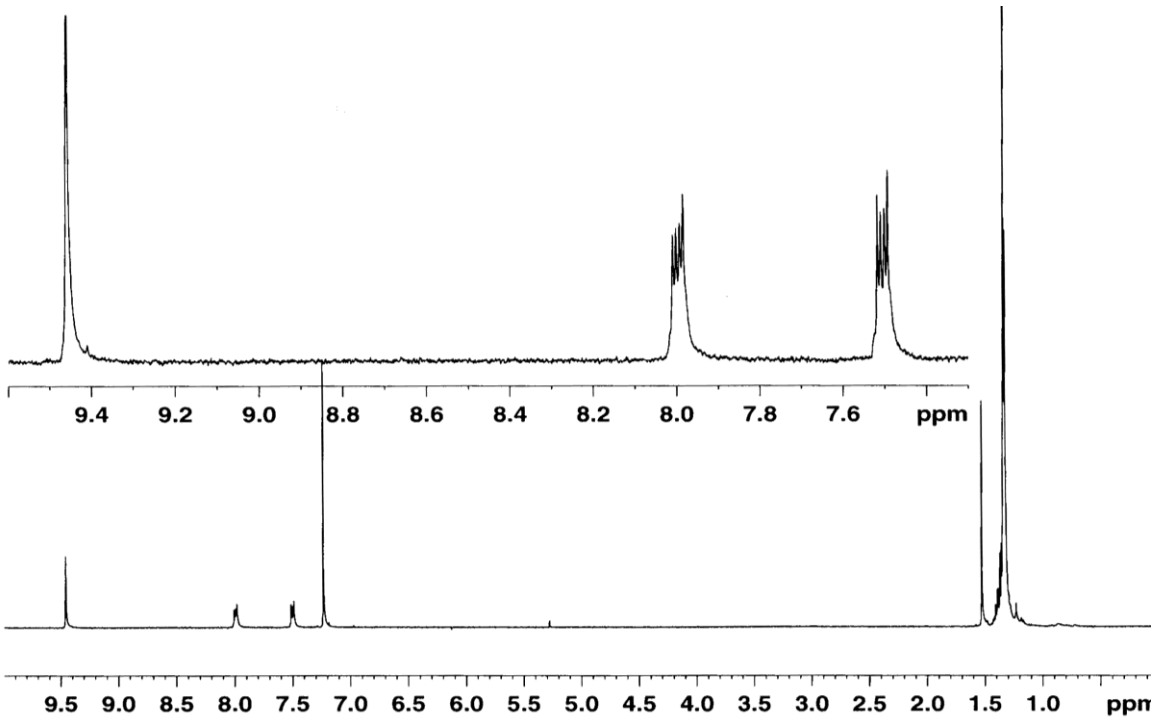

Figure 7.20. ^{1}H-NMR of **7.15c**.

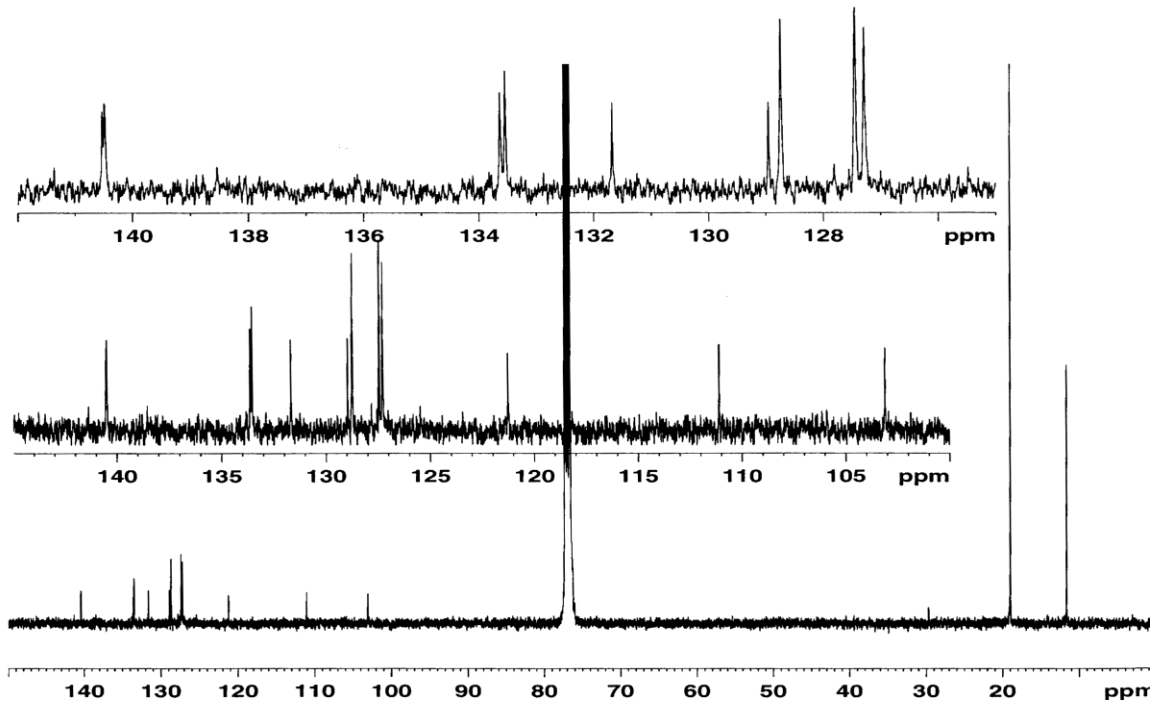

Figure 7.21. ^{13}C-NMR of **7.15c**.

7.4.9 Spectroscopic Data

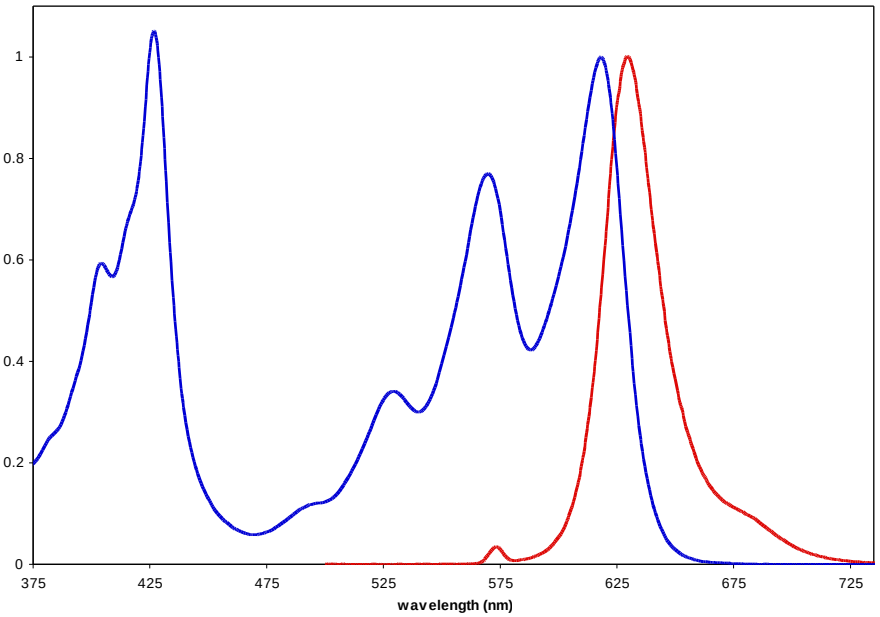

Figure 7.22. Normalized absorption (blue) and emission (red) spectra of **7.11b**.

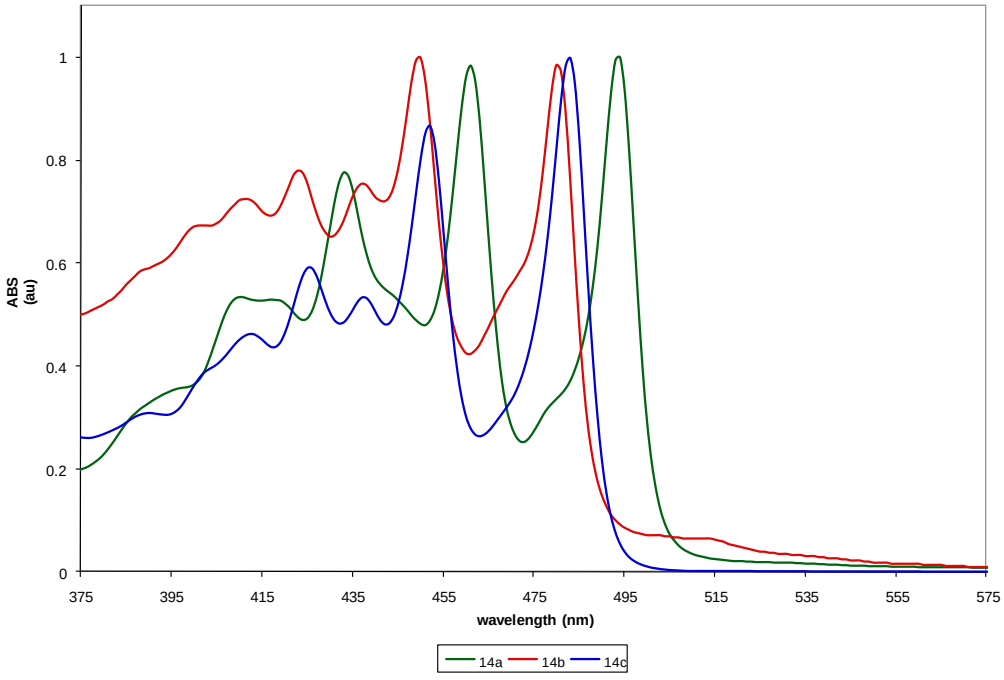

Figure 7.23. Normalized absorption spectra of **7.14a-c**.

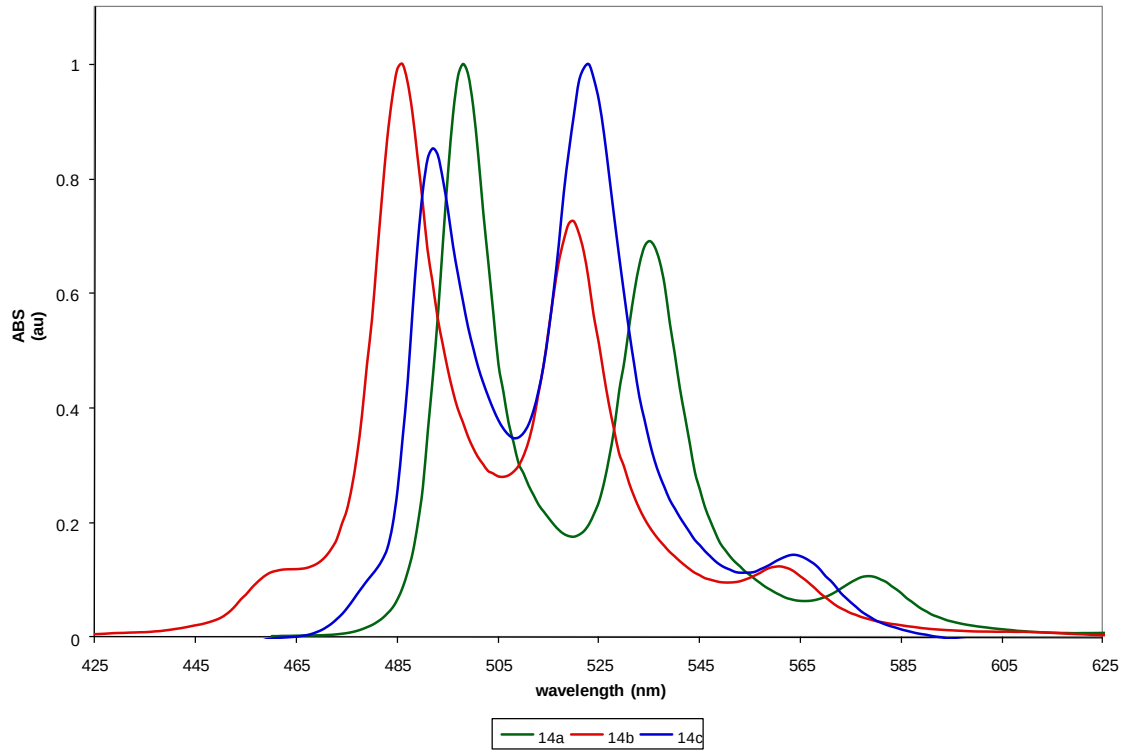

Figure 7.24. Normalized emission spectra of **7.14a-c**.

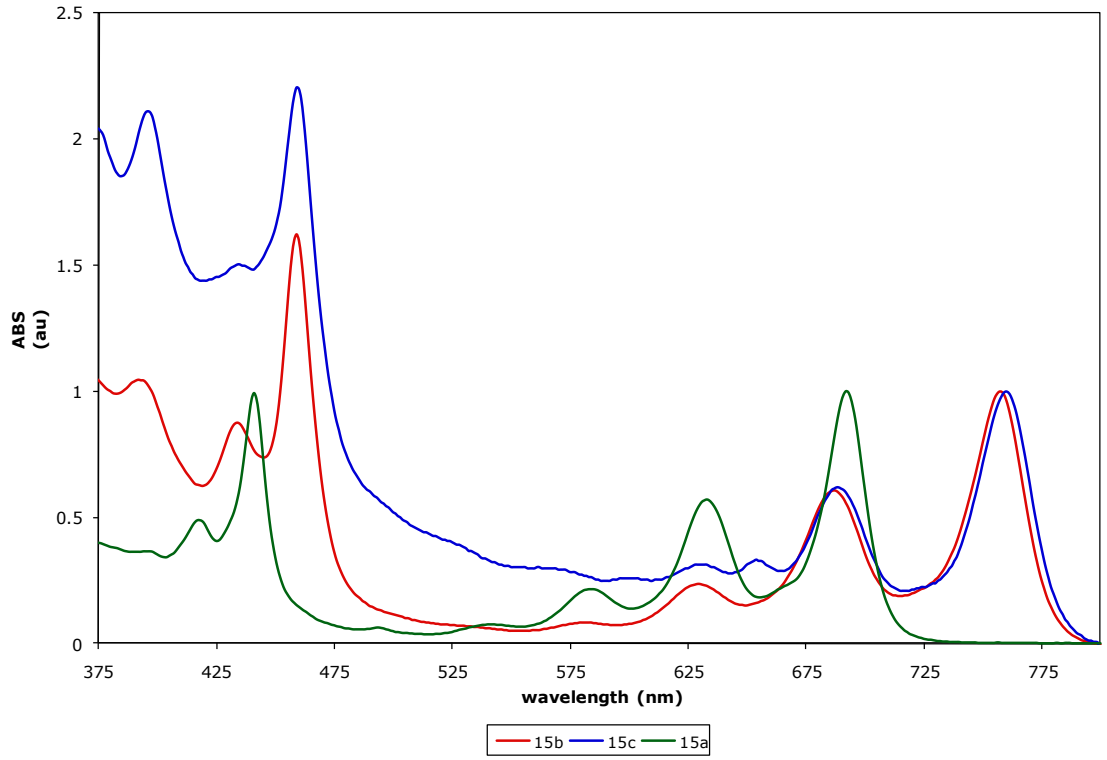

Figure 7.25. Normalized emission spectra of **7.15a-c**.

7.4.10 Computational Results and Details

Electronic structure computations were performed at the DFT level employing the three-parameter hybrid exchange functional from Becke[31] and the correlation functional from Lee, Yang, and Parr[32] (the combination commonly referred to as B3LYP). All computations were carried out with a 6-311+G* Pople basis set with the Gaussian 2009 program.[3329] Geometries of the ground singlet states were completely optimized (RMS gradient 3×10^{-4}, RMS displacement 1.2×10^{-3}). Vertical and adiabatic ionization potentials were computed from the unrestricted B3LYP computations of the corresponding ionic states. Vertical and adiabatic excitation energies were computed within the time-dependent (TD-) DFT approach. The first excited electronic state was completely optimized at the TD-DFT level. The totality of the theoretical characterizations (vertical and adiabatic ionization potentials, electron affinities, and excitation energies) along with the B3LYP/6-311+G* optimized geometries for the ground state are included in the supplementary material.

B3LYP/6-311+G* optimized ground-state geometries

7.11a' B3LYP/6-311+G* optimized geometry

C	2.193697	0.723308	-0.000001
C	3.452493	1.402902	0.000001
C	4.629960	0.711915	-0.000002
C	4.629963	-0.711899	-0.000005
C	3.452497	-1.402891	-0.000007
C	2.193700	-0.723301	-0.000004
H	3.450903	2.486015	0.000003
H	5.573260	1.248207	-0.000001
H	5.573265	-1.248188	-0.000007
H	3.450911	-2.486003	-0.000009

C	0.976025	1.435820	0.000002
C	0.976030	-1.435818	-0.000006
C	-2.549172	-0.724788	-0.000003
C	-2.549174	0.724781	0.000001
N	-1.412168	1.413675	0.000002
C	-0.258363	0.723019	0.000000
C	-0.258361	-0.723022	-0.000004
N	-1.412165	-1.413680	-0.000006
C	-4.971281	0.715975	0.000001
C	-3.801420	1.418040	0.000003
H	-3.778064	2.501994	0.000006
C	-4.971280	-0.715989	-0.000003
C	-3.801416	-1.418051	-0.000005
H	-3.778057	-2.502004	-0.000008
H	-5.920242	1.242279	0.000003
H	-5.920240	-1.242294	-0.000004
C	0.970657	4.061078	0.000012
C	0.957584	2.855312	0.000007
H	0.957963	5.125068	0.000001
C	0.970680	-4.061076	-0.000011
C	0.957595	-2.855310	-0.000011
H	0.958140	-5.125068	0.000257

7.11b' B3LYP/6-311+G* optimized geometry

C	-3.781170	0.723580	0.000000
C	-5.039080	1.403393	0.000001
C	-6.216352	0.711815	0.000001
C	-6.216350	-0.711819	0.000000
C	-5.039077	-1.403394	0.000000
C	-3.781169	-0.723579	0.000000
H	-5.037333	2.486462	0.000001
H	-7.159699	1.247779	0.000001
H	-7.159696	-1.247786	0.000000

H	-5.037328	-2.486464	0.000000
C	-2.564040	1.438477	-0.000001
C	-2.564039	-1.438476	0.000000
C	0.958553	-0.723712	0.000001
C	0.958552	0.723716	0.000001
N	-0.176417	1.403200	0.000001
C	-1.334037	0.721694	0.000000
C	-1.334036	-0.721692	0.000000
N	-0.176416	-1.403196	0.000001
C	3.394359	0.722572	0.000001
C	2.215803	1.424359	0.000001
Cl	2.186165	3.155508	0.000002
C	3.394359	-0.722573	0.000000
C	2.215804	-1.424357	0.000000
Cl	2.186161	-3.155508	-0.000002
Cl	4.912755	1.560704	0.000001
Cl	4.912755	-1.560706	-0.000002
C	-2.546245	4.062512	-0.000007
C	-2.542059	2.857033	-0.000002
H	-2.524080	5.126556	0.000003
C	-2.546250	-4.062511	-0.000001
C	-2.542058	-2.857032	0.000000
H	-2.524049	-5.126554	0.000019

7.11c' B3LYP/6-311+G* optimized geometry

C	-3.525031	0.724698	-0.000001
C	-4.782269	1.404906	0.000001
C	-5.958568	0.712186	-0.000002
C	-5.958567	-0.712193	-0.000008
C	-4.782267	-1.404912	-0.000010
C	-3.525031	-0.724703	-0.000007
H	-4.780517	2.487848	0.000006
H	-6.902180	1.247194	0.000000

H	-6.902178	-1.247203	-0.000010
H	-4.780514	-2.487854	-0.000014
C	-2.310605	1.443268	0.000003
C	-2.310603	-1.443272	-0.000009
C	1.207327	-0.719455	-0.000005
C	1.207326	0.719456	0.000001
N	0.074920	1.407712	0.000004
C	-1.080306	0.726163	0.000000
C	-1.080305	-0.726164	-0.000006
N	0.074922	-1.407712	-0.000008
C	3.653643	0.721442	0.000003
C	2.461417	1.425970	0.000005
C	3.653644	-0.721437	-0.000004
C	2.461419	-1.425966	-0.000007
C	-2.265553	4.065343	0.000015
C	-2.283822	2.860358	0.000008
H	-2.218819	5.129109	0.000148
C	-2.265536	-4.065346	-0.000019
C	-2.283818	-2.860362	-0.000017
H	-2.218679	-5.129106	0.000297
C	2.449801	2.852425	0.000011
N	2.454027	4.006768	0.000016
C	4.901695	1.414035	0.000006
N	5.913186	1.970559	0.000009
C	4.901697	-1.414028	-0.000006
N	5.913189	-1.970551	-0.000008
C	2.449805	-2.852422	-0.000014
N	2.454033	-4.006765	-0.000019

7.15a' B3LYP/6-311+G* optimized geometry

C	-1.184920	-0.726665	0.000000
C	-2.423167	-1.401550	0.000001
C	-3.634545	-0.724069	0.000001
C	-3.634545	0.724069	-0.000001
C	-2.423167	1.401550	-0.000002
C	-1.184920	0.726666	-0.000002
C	0.045306	-1.438276	0.000000
C	0.045306	1.438277	-0.000003
C	3.562969	0.726755	-0.000001
C	3.562969	-0.726756	0.000001
N	2.430075	-1.415059	0.000001
C	1.270658	-0.724860	0.000000
C	1.270659	0.724862	-0.000002
N	2.430076	1.415060	-0.000002
C	5.986103	-0.717106	0.000002
C	4.817891	-1.419290	0.000002
H	4.794888	-2.503248	0.000003
C	5.986103	0.717103	0.000000
C	4.817892	1.419288	-0.000001
H	4.794890	2.503247	-0.000002
H	6.935532	-1.242581	0.000003
H	6.935534	1.242576	0.000001
C	0.045557	-4.062437	0.000004
C	0.063861	-2.856358	0.000002
H	0.056406	-5.126431	-0.000032
C	0.045558	4.062438	-0.000007
C	0.063859	2.856360	-0.000005
H	0.056424	5.126433	0.000086
C	-6.067492	0.715590	0.000000
C	-4.893671	1.409718	-0.000001
H	-4.893060	2.495477	-0.000003
C	-6.067492	-0.715591	0.000002

C	-4.893671	-1.409719	0.000002
H	-4.893059	-2.495478	0.000004
H	-7.014352	1.245746	0.000000
H	-7.014352	-1.245747	0.000003
H	-2.421249	-2.485535	0.000002
H	-2.421251	2.485535	-0.000003

7.15b' B3LYP/6-311+G* optimized geometry

C	2.874220	-0.727062	0.000003
C	5.323087	-0.724118	0.000000
C	5.323089	0.724102	-0.000016
C	2.874222	0.727053	-0.000013
C	1.644549	-1.440915	0.000012
C	1.644554	1.440910	-0.000019
C	-1.870682	0.725700	-0.000008
C	-1.870685	-0.725695	0.000008
N	-0.739648	-1.404420	0.000014
C	0.423463	-0.723552	0.000006
C	0.423465	0.723551	-0.000010
N	-0.739644	1.404423	-0.000016
C	-4.307609	-0.723798	0.000011
C	-3.130615	-1.425564	0.000017
Cl	-3.101285	-3.156687	0.000036
C	-4.307607	0.723810	-0.000004
C	-3.130611	1.425573	-0.000014
Cl	-3.101276	3.156696	-0.000032
Cl	-5.826929	-1.560161	0.000022
Cl	-5.826925	1.560177	-0.000011
C	1.631638	-4.063985	0.000042
C	1.622451	-2.858147	0.000027
H	1.610596	-5.128017	0.000187
C	1.631691	4.063980	-0.000047
C	1.622458	2.858142	-0.000037

H	1.611333	5.128025	0.000229
C	7.755156	0.715492	-0.000019
C	6.581611	1.410138	-0.000025
H	6.581168	2.495769	-0.000036
C	7.755154	-0.715515	-0.000004
C	6.581607	-1.410158	0.000005
H	6.581161	-2.495788	0.000017
H	8.702044	1.245390	-0.000026
H	8.702041	-1.245416	0.000001
C	4.111597	1.401993	-0.000022
H	4.109497	2.485933	-0.000033
C	4.111593	-1.402005	0.000009
H	4.109490	-2.485946	0.000020

7.16a' B3LYP/6-311+G* optimized geometry

C	2.252238	-0.721876	0.000000
C	3.511023	-1.402011	-0.000001
C	4.689219	-0.711848	0.000000
C	4.689219	0.711850	0.000000
C	3.511022	1.402012	0.000001
C	2.252238	0.721877	0.000000
H	3.511513	-2.485313	-0.000001
H	5.632299	-1.248686	-0.000001
H	5.632298	1.248689	0.000001
H	3.511512	2.485315	0.000001
C	1.030189	-1.425665	-0.000001
C	1.030188	1.425666	0.000001
C	-2.661164	0.722487	0.000000
C	-2.661163	-0.722488	0.000000
C	-0.212784	-0.723167	0.000000
C	-0.212784	0.723167	0.000000
C	-5.094152	-0.714516	0.000000
C	-3.918472	-1.408192	-0.000001

C	-5.094153	0.714513	0.000000
C	-3.918473	1.408190	0.000001
C	1.025510	-4.054609	-0.000002
C	1.030273	-2.847724	-0.000002
H	1.023832	-5.118817	0.000002
C	1.025507	4.054609	0.000002
C	1.030272	2.847725	0.000001
H	1.023804	5.118818	0.000005
C	-1.445820	-1.399750	-0.000001
H	-1.445621	-2.483930	-0.000001
C	-1.445820	1.399750	0.000001
H	-1.445622	2.483930	0.000001
H	-3.917851	2.494092	0.000001
H	-6.040498	1.245726	0.000001
H	-6.040497	-1.245729	-0.000001
H	-3.917850	-2.494094	-0.000001

7.16b' B3LYP/6-311+G* optimized geometry

C	3.882826	-0.721989	0.000000
C	5.140737	-1.402618	-0.000001
C	6.318556	-0.711751	0.000000
C	6.318556	0.711751	0.000001
C	5.140738	1.402618	0.000001
C	3.882826	0.721988	0.000000
H	5.140979	-2.485829	-0.000001
H	7.261729	-1.248138	-0.000001
H	7.261729	1.248137	0.000001
H	5.140979	2.485828	0.000002
C	2.661211	-1.427303	-0.000001
C	2.661211	1.427303	0.000001
C	-1.027489	0.723394	0.000000
C	-1.027490	-0.723394	0.000000
C	1.422313	-0.720124	0.000000

C	1.422313	0.720124	0.000000
C	-3.475429	-0.720598	0.000000
C	-2.290882	-1.409409	-0.000001
Cl	-2.297128	-3.154491	-0.000001
C	-3.475429	0.720598	0.000000
C	-2.290882	1.409410	0.000001
Cl	-2.297127	3.154492	0.000001
Cl	-4.995768	-1.561874	-0.000001
Cl	-4.995768	1.561874	0.000001
C	2.645979	-4.055184	-0.000002
C	2.657257	-2.848753	-0.000002
H	2.634817	-5.119550	0.000000
C	2.645980	4.055184	0.000002
C	2.657258	2.848753	0.000002
H	2.634830	5.119550	0.000005
C	0.189214	-1.395365	-0.000001
H	0.195934	-2.475690	-0.000001
C	0.189214	1.395365	0.000001
H	0.195935	2.475690	0.000001

7.16c' B3LYP/6-311+G* optimized geometry

C	3.611986	0.722388	-0.000020
C	4.868617	1.403761	-0.000031
C	6.045814	0.711751	-0.000026
C	6.045814	-0.711751	-0.000009
C	4.868617	-1.403761	0.000002
C	3.611986	-0.722388	-0.000003
H	4.868738	2.486829	-0.000044
H	6.989157	1.247369	-0.000035
H	6.989157	-1.247369	-0.000005
H	4.868737	-2.486829	0.000015
C	2.391568	1.430186	-0.000026
C	2.391568	-1.430186	0.000009

C	-1.289871	-0.722057	0.000009
C	-1.289871	0.722057	-0.000009
C	1.153911	0.722121	-0.000014
C	1.153911	-0.722121	0.000003
C	-3.749897	0.720306	-0.000004
C	-2.551577	1.413622	-0.000015
C	-3.749897	-0.720307	0.000014
C	-2.551576	-1.413622	0.000020
C	2.357779	4.056628	-0.000055
C	2.383446	2.850873	-0.000047
H	2.329101	5.121199	0.000529
C	2.357780	-4.056628	0.000042
C	2.383446	-2.850873	0.000026
H	2.329102	-5.121199	0.000135
C	-0.078022	1.400995	-0.000020
H	-0.073495	2.483945	-0.000033
C	-0.078021	-1.400995	0.000014
H	-0.073495	-2.483945	0.000028
C	-2.556971	2.842012	-0.000034
N	-2.523773	3.996384	-0.000049
C	-4.993452	1.419714	-0.000011
N	-6.001013	1.983877	-0.000016
C	-4.993452	-1.419714	0.000025
N	-6.001013	-1.983877	0.000034
C	-2.556971	-2.842012	0.000038
N	-2.523773	-3.996384	0.000052

Table 7.2. HOMO and LUMO orbital energies, HOMO-LUMO gap, vertical and adiabatic ionization potentials, electron affinities, and excitation energies (all in eV), and ground-state dipole moments (Debye) computed at the B3LYP/6-311+G* level of theory.

	HOMO /LUMO	$\Delta_{HOMO-LUMO}$	IP^{vert} /$IP^{adiabatic}$	EA^{vert} /$EA^{adiabatic}$	S_1^{vert} /$S_1^{adiabatic}$	μ
7.11a'	-5.72	2.37	7.05	2.02	2.07	0.17
	-3.35		6.99	2.10	1.91	
7.11b'	-6.03	2.25	7.29	2.53	1.91	3.69
	-3.78		7.23	2.62	1.75	
7.11c'	-6.66	1.81	7.16	4.39	1.38	11.52
	-4.84		7.08	4.46	0.46	
7.15a'	-5.37	1.87	6.61	2.27	1.58	0.24
	-3.50		6.56	2.34	1.45	
7.15b'	-5.66	1.77	6.85	2.72	1.44	4.44
	-3.89		6.79	2.80	1.31	
7.16a'	-5.28	2.41	6.60	1.57	2.16	0.22
	-2.87		6.55	1.65	2.02	
7.16b'	-5.68	2.39	6.92	2.07	2.13	3.81
	-3.30		6.86	2.15	1.99	
7.16c'	-6.38	2.00	7.62	3.17	1.61	11.74
	-4.38		7.57	3.23	1.48	

7.5 References

[1] Hinsberg, O. *Liebigs Ann. Chem.* **1901**, *319*, 257-286.

[2] Miao, Q.; Nguyen, T.Q.; Someya, T.; Blanchet, G.B.; Nuckolls, C. *J. Am. Chem. Soc.* **2003**, *125*, 10284-10287.

[3] Anthony, J.E. *Angew. Chem. Int. Ed.* **2008**, *47*, 452-483.

[4] Anthony, J.E. *Chem. Rev.* **2006**, *106*, 5028-5048.

[5] Coropceanu, V.; Malagoli, M.; da Silva Filho, D.A.; Gruhn, N. E.; Bill, T.G.; Brédas, J.L. *Phys. Rev. Lett.* **2002**, *89*, 275503.

[6] Yoo, S.; Domercq, B.; Kippelen, B. *Appl. Phys. Lett.* **2004**, *85*, 5427-5429.

[7]. Winkler, M.; Houk, K.N. *J. Am. Chem. Soc.* **2007**, *129*, 1805-1815.

[8] Sakamoto, Y.; Suzuki, T.; Kobayashi, M.; Gao Y.; Fukai, Y.; Inoue, Y.; Sato, F.; Tokito, S. *J. Am. Chem. Soc.* **2004**, *126*, 8138-8140.

[9] Delgado, M.C.R.; Pigg, K.R.; Filho, D.A.D.S.; Gruhn, N.E.; Sakamoto ,Y.; Suzuki ,T.; Osuna, R.M.; Casado, J.; Hernandez, V.; Navarrete, J.T.L.; Martinelli, N.G.; Cornil, J.; Sanchez-Carrera, R.S.; Coropceanu, V.; Bredas, J.L. *J. Am. Chem. Soc.* **2009**, *131*, 1502-1512.

[10] Chen, Z.H.; Muller, P.; Swager, T.M. *Org. Lett.* **2006**, *8*, 273-276.

[11] Salman, S.; Delgado, M.C.R,; Coropceanu, V.; Bredas J.L. *Chem. Mater*. **2009**, *21*, 3593-3601.

[12] Miao, S.; Appleton, A.L.; Berger, N.; Barlow S.; Marder, S.R.; Hardcastle, K.I.; Bunz, U.H.F. *Chem. Eur. J.* **2009**, *15*, 4990-4993.

[13] Bunz, U.H.F. *Chem. Eur. J.* **2009**, *15*, 6780-6789.

[14] Tang, M.L.; Oh, J.H.; Reichardt, A.D.; Bao, Z.N.; *J. Am. Chem. Soc.* **2009**, *131*, 3733-3740.

[15] Anthony, J.E.; Brooks, J.S.; Eaton D.L.; Parkin, S.R. *J. Am. Chem. Soc.* **2001**, *123*, 9482-9483.

[16] Electronegative substitution on π-systems can lead to either blue or red-shifted or almost unchanged absorption spectra, and chlorination for example induces bathochromic shifts in 9,10-dichloroanthracene and some chlorinated nitro-aminodiazobenzene derivatives of disperse red. Such electronegativity effects occur if either the HOMO or the LUMO is particularly stabilized or not; they are especially pronounced in molecules with disjoint orbital structures, where HOMO and LUMO are localized on different parts of the molecule.

[17] Pavlovich, V.S. *J. Appl. Spectroscopy* **2007**, *74*, 180-187.

[18] De Boni, L.; Rodrigues, J.J.; dos Santos, D.S.; Silva, C.H.T.P.; Balogh, D.T.; Oliveira, O.N.; Zilio, S.C.; Misoguti, L.; Mendonca, C.R. *Chem. Phys. Lett.* **2002**, *361*, 209-213.

[19] Zucchero, A.J.; McGrier, P.L.; Bunz, U.H.F. *Acc. Chem. Res.* **2010**, *47*, 397-408.

[20] *Acc Chem. Res.* **2009**, *42*, Thematic Issue 11, Organic Photovoltaics .

[21] Payne, M.M.; Parkin, S.R.; Anthony, J.E. *J. Am. Chem. Soc.* **2005**, *127*, 8028-8029.

[22] Kummer, F.; Zimmermannn, H. *Ber. Bunsenges.* **1967**, *71*, 1119-1125.

[23] Miao, S.; Brombosz, S.M.; Schleyer, P.V.; Wu, J.I.; Barlow, S.; Marder, S.R.; Hardcastle, K.I.; Bunz, U.H.F. *J. Am. Chem. Soc.* **2008**, *130*, 7339-7344.

[24] Appleton, A.L.; Miao, S.; Brombosz, S.M.; Berger, N.J.; Barlow, S.; Marder, S.R.; Lawrence, B.M.; Hardcastle, K.I.; Bunz, U.H.F. *Org. Lett.* **2009**, *11*, 5222-5225.

[25] The stabilization of the formally antiaromatic **7.14a-c** results from the interplay of energetically advantageous enamine groups and the presence of two Clar sextets instead of one for the heteroacenes **7.15a-c**. In the case of the diazatetracenes **7.11**, this delicate energetic balance is such that the overall aromaticity drives the formation of the diazaacenes **7.11**, and the significantly more antiaromatic NH-compounds are not observed as already shown by Hinsberg for the parent diazatetracene in 1901. See refs 1, 26.

[26] Wu, J.I.; Wannere, C.S.; Mo, Y.R.; Schleyer, P.V.; Bunz, U.H.F *J. Org. Chem.* **2009**, *74*, 4343-4349.

[27] These values are obtained from the published absorption data (ref. 9 for **7.6** and ref 10 for **7.9**).

[28] The UV-vis spectra of the NH-compounds **7.14a-c** (see Figure 7.23) are similar to each other, but show a slight hypsochromic, rather than bathochromic, shift when going from the parent to the halogenated species (**7.14a:** λ_{max} = 493 nm; **7.14b:** λ_{max} = 479 nm; **7.14c:** λ_{max} = 482 nm). In **7.15a-c** the absorption shifts from 692 nm (**7.15a**) and 756 nm (**7.15b**) to 759 nm (**7.15c**), a difference of 0.15 eV.

[29] Hansch, C.; Leo, A.; Taft, R.W. *Chem. Rev.* **1991**, *91*, 165.

[30] The very close correspondence between the values of the experimental optical and electrochemical gaps (rather than merely trends in these values) is not necessarily to be expected, and presumably arises from a fortuitous balancing of the exciton binding energy stabilizing the excited state and strong solvation of the relatively small ions formed on oxidation or reduction.

[31] Becke, A.D. *J. Chem. Phys.* **1993**, *98*, 5648.

[32] Lee, C.T.; Yang, W.T.; Parr, R.G. *Phys. Rev. B* **1988**, *37*, 785.

[33] Gaussian 09, Revision **A.1**, Frisch, M. J.; Trucks, G. W.; Schlegel, H. B.; Scuseria, G. E.; Robb, M. A.; Cheeseman, J. R.; Scalmani, G.; Barone, V.; Mennucci, B.; Petersson, G. A.; Nakatsuji, H.; Caricato, M.; Li, X.; Hratchian, H. P.; Izmaylov, A. F.; Bloino, J.; Zheng, G.; Sonnenberg, J. L.; Hada, M.; Ehara, M.; Toyota, K.; Fukuda, R.; Hasegawa, J.; Ishida, M.; Nakajima, T.; Honda, Y.; Kitao, O.; Nakai, H.; Vreven, T.; Montgomery, Jr., J. A.; Peralta, J. E.; Ogliaro, F.; Bearpark, M.; Heyd, J. J.; Brothers, E.; Kudin, K. N.; Staroverov, V. N.; Kobayashi, R.; Normand, J.; Raghavachari, K.; Rendell, A.; Burant, J. C.; Iyengar, S. S.; Tomasi, J.; Cossi, M.; Rega, N.; Millam, N. J.; Klene, M.; Knox, J. E.; Cross, J. B.; Bakken, V.; Adamo, C.; Jaramillo, J.; Gomperts, R.; Stratmann, R. E.; Yazyev, O.; Austin, A. J.; Cammi, R.; Pomelli, C.; Ochterski, J. W.; Martin, R. L.; Morokuma, K.; Zakrzewski, V. G.; Voth, G. A.; Salvador, P.; Dannenberg, J. J.; Dapprich, S.; Daniels, A. D.; Farkas, Ö.; Foresman, J. B.; Ortiz, J. V.; Cioslowski, J.; Fox, D. J. Gaussian, Inc., Wallingford CT, 2009.

Chapter 8: Conclusions

Throughout the body of this work, we have shown the great promise that small, conjugated molecules such as the acenothiadiazoles as well as the N-heteroacenes possess for applications in sensory devices as well as for potential applications as N-type semiconductors. While the breadth of this work has focused on the design, properties and functionalization of acenothiadiazoles an N-heteroacenes, there certainly is a multitude of avenues for which this project to travel down. In these concluding remarks, I would like to summarize the advances made in each chapter of this thesis as well as point to future directions for this very exciting field.

In Chapter 2, the diethynylacenothiadiazoles were introduced. Both the physical and spectroscopic properties, as well as the electrochemical behaviors, were explored. These molecules have potential to be excellent candidates for N-type semiconducting materials. While the focus of this thesis has been on utilizing the acenothiadiazoles as building blocks for a variety of interesting responsive or electronic materials, they should not be overlooked for their own applications. In conjunction with Dr. Henderson at Georgia Tech, we hope to fabricate devices under an inert atmosphere where we can reliably measure charge carrier mobilities in TFT type devices as well as electroluminescence efficiencies in simple LED architectures. This will be the final and true test to show that the crystal packing as well as the photophysical properties that we observe in the benzo-naphtho- and anthraceno-thiadiazloes will lead to efficient N-type semiconductors.

In Chapters 3 and 4, we explored the photophysical properties of bis(arylethynyl)benzenes and bis(arylethynyl)benzothiadiazoles. A Kamlet-Taft analysis of these compounds, along with their protonated/deprotonated congeners, proved invaluable in the interpretation of the influences that the solvent has on their observed solvatochromic behaviors. While the *a*, *b*, and *s* values were generally similar among the two classes of molecules, the benzothiadiazole derivatives were able to exhibit larger emissive spectroscopic responses, show colorimetric responses to metal and protic analytes, and exhibit excellent quantum yields and fluorescence lifetimes. While some rudimentary selectivity was exhibited, these molecules would benefit from being appended with analyte-specific functional groups which contain conjugation to the π-system. This would allow for the detection of any number of analyte and increase the utility of the bis(arylethynyl)benzothiadiazole fluorophore core.

Chapter 5 focused on a different method of functionalizing the alkynyl groups through click chemistry with azides. While the azides had very poor electronic communication between the 1- and 4-positions of the triazole meant that the conjugation could not be extended utilizing aryl azides, the formed triazole did imbue numerous properties on the benzothiadiazole. The R-group of the azide was utilized to confer water-solubility onto the hydrophobic core. The electron-deficient triazole subunits produced molecules that were significantly redshifted from the parent molecules. The thiadiazole-benzothiadiazole moiety served as a metal-recognition site which exhibited high sensitivity and generally good selectivity for nickel and copper. Future work for this project includes many possibilities. A few of the more promising ideas would be to utilize a diazide such as triethylene glycol diazide to produce polymeric materials. These

should display similar binding constants to the small molecules, but have increased sensitivity. A second concept currently underway in our laboratory is to utilize different diethynyl fluorescent cores which possess lone pairs of electrons in suitable positions to allow for the say general binding of metal analytes, but with different selectivity and strength. One example would be the reaction of triethylene glycol monomethyl ether azide with diethynylphenazine.

In Chapter 6, the discussion changed to exploring the properties of the N-heteroacenes. Diethynyldiazatetracenes were produced that were interconvertible with their stable antiaromatic dihydro partners. These compounds were shown to be able to exist due to a balancing of the antiaromatic destabilizing energies with the global aromatic stabilizing forces of the other acene rings in the system.

Chapter 7 continued the work of Chapter 6 by producing both diazatetracenes and diazapentacenes. Here, however, the focus was in designing materials with desirable properties for electronic applications. To this end, tetrahalogenated diaza-tetracene and –pentacene were synthesized. Their anomalous absorption profiles were surprising when compared to the tetrahalogenated pentacenes since no significant redshifts were observed in those molecules. Utilizing FMO calculations we were able to show that the pyrazine subunit plays an important role in disproportionately affecting the orbital coefficients on the HOMO and LUMO of the molecule. Selective substitution with halogens allowed for the dissimilarity of the FMOs to be taken advantage of. If stronger electron withdrawing groups are utilized, even greater redshifts are expected. We currently are pursuing the tetranitrile derivative of diazatetracene and pentacene. With the recent advancements in these materials in our group and in research groups around the world,

acene materials, especially N-heteroacene and acenothiadiazoles, will continue to flourish.

Appendix A: Terpyridine Based Cruciform-Zn^{2+}-Complexes as Anion-Responsive Fluorophores

A.1 Introduction

The detection, identification and quantification of organic and inorganic anions is important in biology, medicine, environmental science and food science.[1,2,3,4,5] While several concepts are successfully employed, our goal was to explore the construction of self-assembled probes capable of differentiating simple inorganic anions. We reasoned that fluorophore-metal cation complexes should be easily accessible and tunable leading to turn-on, dosimeter-type, anion-responsive systems. The operating principle would involve mixing the suitably appended fluorophore with a metal cation (zinc in this specific case) and then expose the fluorophore-metal ion complex to different anions. Depending upon the affinity of the anions for zinc, either

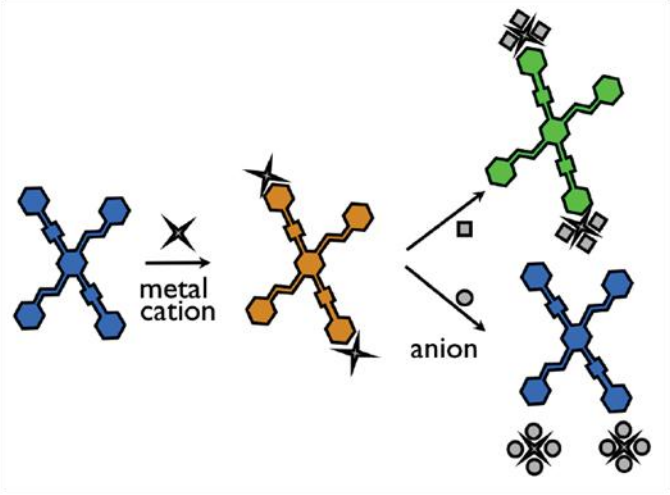

Figure A.1. Working principle of a cruciform-metal-ion-based anion probe.

decomplexation or formation of an "ate"-type complex, incorporating the fluorophore, could result.[6] The only important prerequisite for this type of dosimeter to work is a change in fluorescence upon the addition of the zinc salt and a second change in fluorescence upon uptake of the anions by the zinc-fluorophore complex.

Cruciform chromophores and fluorophores (XF) encompass a family of different molecular architectures.[7,8,9,10,11] The most common cruciform motif is that of a 1,2,4,5-substituted benzene ring, in which the peripheral unsaturated substituents represent the arms of the cross. These 1,2,4,5-substituted benzene-derived XFs display distinct metal cation and acid-induced changes in their fluorescent behavior, including two-stage ratiometric responses. The issue with the hitherto investigated XFs is that their responsive elements, dialkylanilines and pyridines, only allow us to study fluorescence responses towards metal cations in relatively unpolar solvents such as dichloromethane or THF. In more polar and hydrogen bonding solvents, metal coordination of such XFs is weak and the associated spectral responses are invisible unless a highly concentrated solution of metal salt is used. It was therefore of interest to construct XFs that are metal sensitive in more polar solvents. The terpyridine unit is an excellent general metal cation binder, particularly if octahedral or square planar

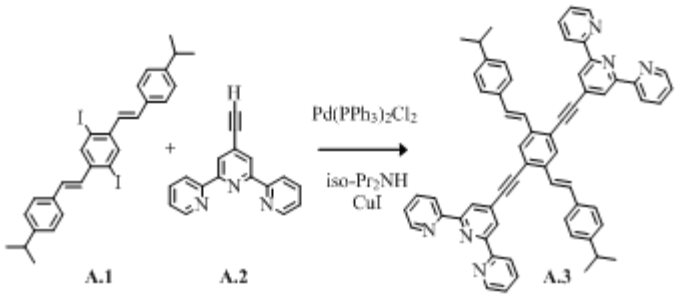

Scheme A.1. Synthesis of the Terpyridine XF **A.3**

coordination geometry can be attained. We therefore envisioned the XF **A.3** as an excellent target compound.

A.2 Results and Discussion

Starting from the literature known distyrylbenzene **A.1**, reaction with ethynylterpyridine[12] **A.2** using 6 mol% $Pd(PPh_3)_2Cl_2$, in diisopropylamine with CuI as cocatalyst,[13] provided XF **A.3** in 52% yield after aqueous workup. Chromatography, resulting in heavy losses, furnished spectroscopically pure **A.3** after subsequent

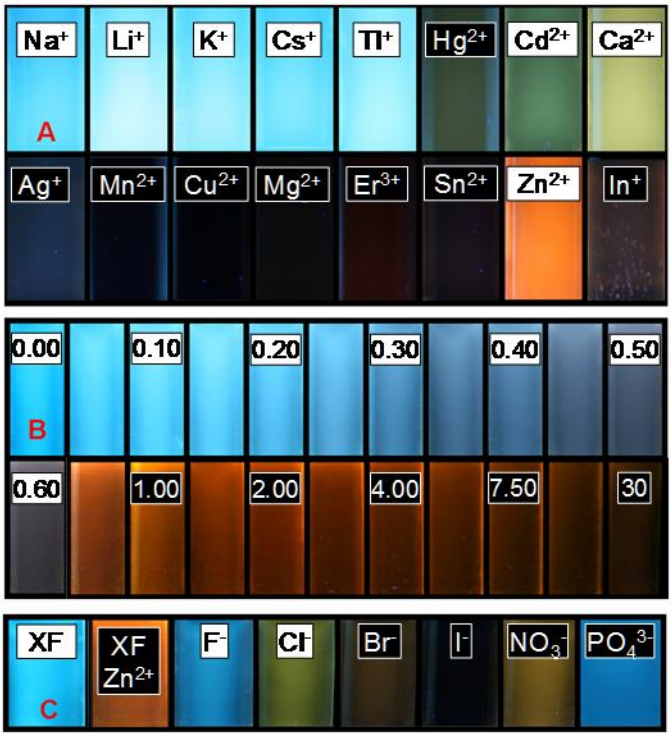

Figure A.2. a) Exposure of **A.3** towards different metal cations as their triflate salts. b) Exposure of **A.3** towards increasing concentrations of zinc triflate. c) Exposure of the **A.3**-zinc complex towards different anions. All experiments were performed in a 9:1 acetone-water mixture under a blacklight at concentrations of 9 x 10^{-3} gL^{-1} (0.010 mM); b) and c) were photographed using a fast shutter speed to prevent overexposure of the solutions containing the highly fluorescent **A.3**. Due to the shutter speed being held constant for b) and c), the solutions of **A.3**-Zn^{2+} appear darker in b) and c) than under actual visual inspection whereas a) is more close to their actual appearance.

crystallization from chloroform/hexanes in 23% yield (silica gel; dichloro-methane:triethylamine gradient, 1:0 to 9:1 vv ratio).

Figure A.2a shows the fluorescence response of the XF **A.3** after the exposure towards a panel of different metal cations as their triflates in a mixture of acetone/water (9:1, vv). We selected an acetone-water mixture because it allows the dissolution of the XF as well as that of the various metal salts and anion-based analytes without problems. We opted for the triflates to exclude anion effects (*vide infra*). Alkali metal cations and Tl^{+} do not change the fluorescence of the XF and do not seem to coordinate at all under these conditions. However, when **A.3** is exposed to Ag^{+}, Mn^{2+}, Cu^{2+}, Mg^{2+}, Er^{3+} or Sn^{2+} we observe that the fluorescence of the XF **A.3** is efficiently quenched.

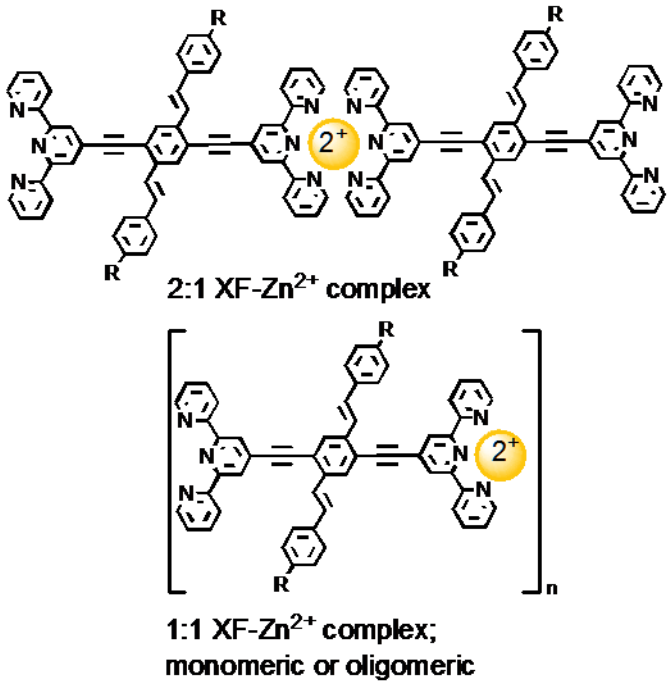

Figure A.3. Possible stoichiometries of zinc-cruciform complexes.

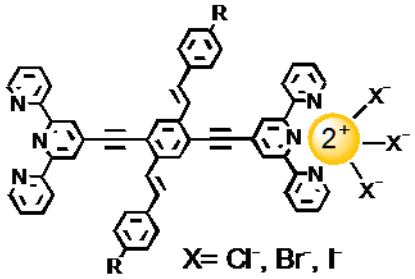

Figure A.4. Proposed structure of the Zn-XF-complex after addition of halide anions.

Upon addition of Ca^{2+}, Cd^{2+}, Hg^{2+}, and In^{3+}, we find that the fluorescence changes to green or brown, while the addition of zinc triflate gives an orange-emissive solution. The fluorescent responses of these latter metals were unexpected as the emission of terpyridine-substituted fluorophores is, according to literature reports, quenched by addition of metal cations such as zinc.[14,15] To investigate this surprising behavior further we explored different ratios of Zn^{2+}/XF **A.3**. Figure 2b shows the results. At a concentration of 1.0 x 10^{-5} $molL^{-1}$ XF **A.3** we observe at a stoichiometric ratio of 1:1 Zn^{2+}/**A.3** an emission change from blue to orange.

Upon addition of more zinc triflate the emission color changes from orange to a dull brown. To obtain the correct binding stoichiometries, we performed ITC (isothermal titration calorimetry). According to the ITC data, a 2:1 complex and a 1:1 (**A.3**/Zn^{2+}) complex are consecutively traversed (Figure A.3). The 1:2 complex apparently is not produced, even upon addition of a large excess of zinc triflate. According to ITC the ΔH of the first complexation step is -6.38 kcal/mol while that of the second step is -10.5 kcal/mol. The analysis of the ITC data using different binding models did not give reasonable results for K_{assoc}. Literature reports of structurally related compounds have shown similar difficulties but estimates for K_{assoc}

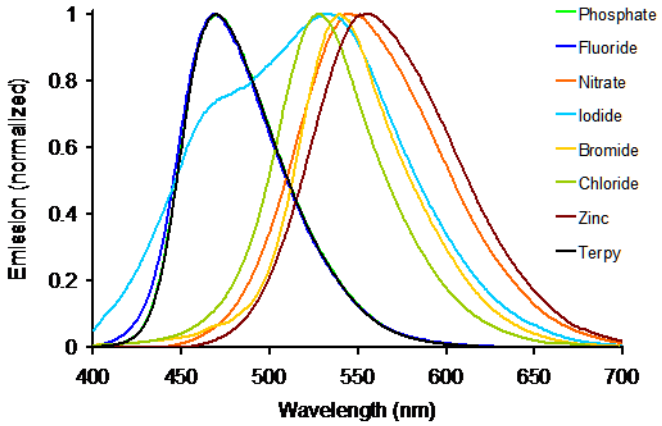

Figure A.5. Normalized emission spectra of the XF **A.3** (Terpy), its zinc complex, and after addition of different anions to the XF **3**-Zn^{2+}-complex. For a non-normalized version of this Figure see Figure A.9.

of 10^6 to $>10^8$ are reported.[14,15] The high binding constant allows access to the stable complex **A.3**-Zn^{2+} without problem. Zinc ions have a high binding affinity for fluoride and phosphate with β-values of 3.04 x 10^{-2} and 5 x 10^{-36}.[16,17] As a consequence, we investigated the reaction of the complex **3**-Zn^{2+} towards different anions. Figure A.2c and Figure A.4 show the results. Addition of fluoride leads to immediate decomplexation and the fluorescence of the starting XF **A.3** is restored. Upon addition of sodium phosphate a similar shift is visible, however, the recovered fluorescence is 20% less than that of the starting XF **A.3**. Iodide and bromide shift and/or quench the fluorescence of the XF-Zn^{2+} complex respectively, while chloride leads to a slight blue shift but not to decomplexation of the XF. Nitrate, a weakly binding anion, has only a minute effect on the fluorescence of the complex. We interpret these findings in the light that phosphate as well as fluoride both removes the zinc stoichiometrically from the XF-Zn^{2+} complex and therefore restore the original fluorescence of the XF **A.3**.

In the case of the exposure of the **A.3**-Zn^{2+} to other halide ions, i.e. Cl^-, Br^- and I^-, we see changes in the emission color which we attribute to the formation of ate-type complexes arising from a 1:1 XF-Zn^{2+} complex. In the case of I^-, significant quenching occurs in addition to the blue shift. Literature values for the complex formation constant between iodide and zinc ions in water suggests partial decomplexation, if we compare the bonding strength of the zinc ions to the terpy ligand with that of the iodide ion.[18] The emission spectrum of **A.3**-Zn^{2+} with I^- does display two local emission maxima, suggesting that both the ate-type complex (λ_{max}= 531 nm) and the decomplexed species (local λ_{max}= 471 nm) are present.

A.3 Conclusions

In conclusion, we have prepared the XF **A.3** containing two terpyridine units. Upon exposure towards metal cations this XF gives emission color changes. In the case of zinc triflate the XF forms 2:1 (**A.3**/Zn^{2+}) and 1:1 (**A.3**/Zn^{2+}) complexes, which could be used to detect halide ions. A clear differentiation of fluoride from the other halides was possible, as only fluoride efficiently decomplexes the XF-Zn^{2+} complex and restores the original fluorescence of the XF **A.3**. This simple system allows for the future construction of libraries of self-assembled[18] anion sensors or dosimeters, by combining suitable cruciform fluorophores containing sensory appendages with different metal ions that display differential anion recognition and/or binding.

This work has been published in *Organic Letters*:

Brombosz, S. M.; Zucchero, A. J; Phillips, R. L.; Vazquez, D.; Wilson, A.; Bunz, U. H. F. *Org. Lett.* **2007**, *22*, 4519-4522.

A.4 Experimental and Supplementary Information

A.4.1 4',4""-((2,5-bis((E)-4-isopropylstyryl)-1,4-phenylene)bis(ethyne-2,1-diyl))di-2,2':6',2"-terpyridine, **A.3**.

Compound **A.1** (0.224 g, 0.362 mmol) was combined with **A.2** (0.233 g, 0.906 mmol), $(PPh_3)_2PdCl_2$ (0.0145 g, 0.0217 μmol), and CuI (8.3 mg, 43 μmol) and was dissolved in THF (10 mL) and diisopropyl amine (5 mL) in a nitrogen purged Schlenk flask. The solution was degassed, capped with a septum and allowed to stir at room temperature for 24 h. The product was poured into water and then extracted with dichloromethane. Removal of the solvent *in vacuo* gave a yellow powder that was purified on a silica column flushing first with dichloromethane then eluting the product with 95:5 dichloromethane : triethylamine. Recrystallization from chloroform and hexanes yielded 67.0 mg of yellow powder. Yield: 21%. MP: 240-241 ^oC. *IR:* 3053, 3012, 2957, 2868, 2213, 1599, 1581, 1565, 1465, 1391, 1262, 1146, 1042, 965, 884, 858, 817, 788, 741, 735 cm^{-1}. *^1H NMR (400 MHz, $CDCl_3$):* δ = 8.76 (d, 4H, $J_{H,H}$ = 3.9 Hz, Ar-H), 8.69 (s, 4H, Ar-H), 8.68 (d, 4H, $J_{H,H}$ = 8.1 Hz, Ar-H), 8.01 (s, 2H, Ar-H), 7.90 (t, 4H, $J_{H,H}$ = 8.0 Hz, Ar-H), 7.69 (d, 4H, $J_{H,H}$ = 16.3 Hz, C=C-H), 7.63 (d, 4H, $J_{H,H}$ = 8.1 Hz, Ar-H), 7.39 (t, 4H, $J_{H,H}$ = 6.5 Hz, Ar-H), 7.35 (d, 2H, $J_{H,H}$ = 16.3 Hz, C=C-H), 7.30 (d, 4H, $J_{H,H}$ = 8.1 Hz, Ar-H), 2.95 (m, 2H, $J_{H,H}$ = 6.9 Hz, $CH_3C\mathbf{H}CH_3$), 1.29 (d, 12H, $J_{H,H}$ =6.9 Hz, $C\mathbf{H_3}CHC\mathbf{H_3}$). *$^{13}C$ NMR (75 MHz, $CDCl_3$):* δ = 155.67, 149.22, 149.10, 137.80, 136.94, 134.73, 133.15, 131.30, 129.30, 127.11, 126.99, 126.91, 124.18, 124.07, 122.83, 121.99, 121.29, 93.67, 92.10, 34.00, 23.95. *MS (FAB, 70-SE) ($C_{62}H_{46}N_6$):* m/z = 877. $\Phi_{Dichloromethane}$ = 0.57. Fluorescence lifetime: τ = 4.7 ns.

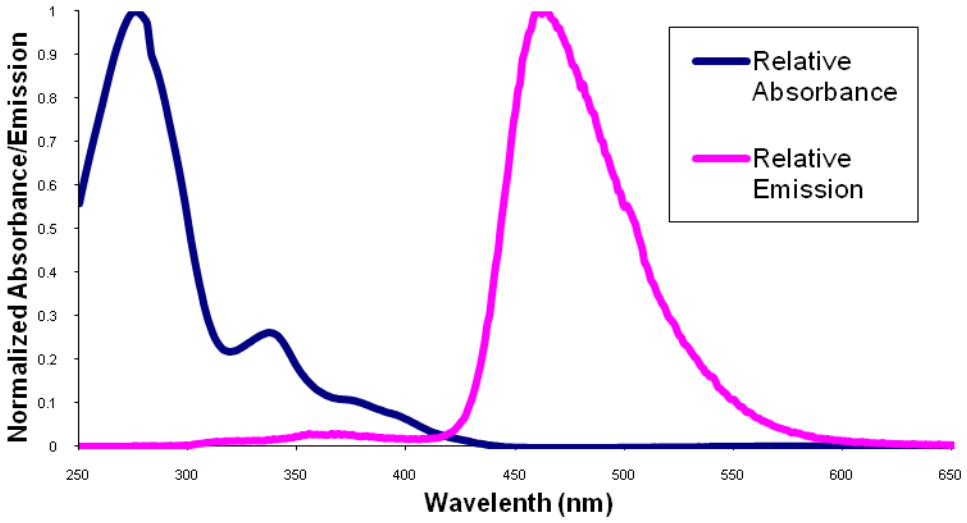

Figure A.6. Normalized Emission and Absorbance Spectrum of XF **A.3** in CH_2Cl_2.

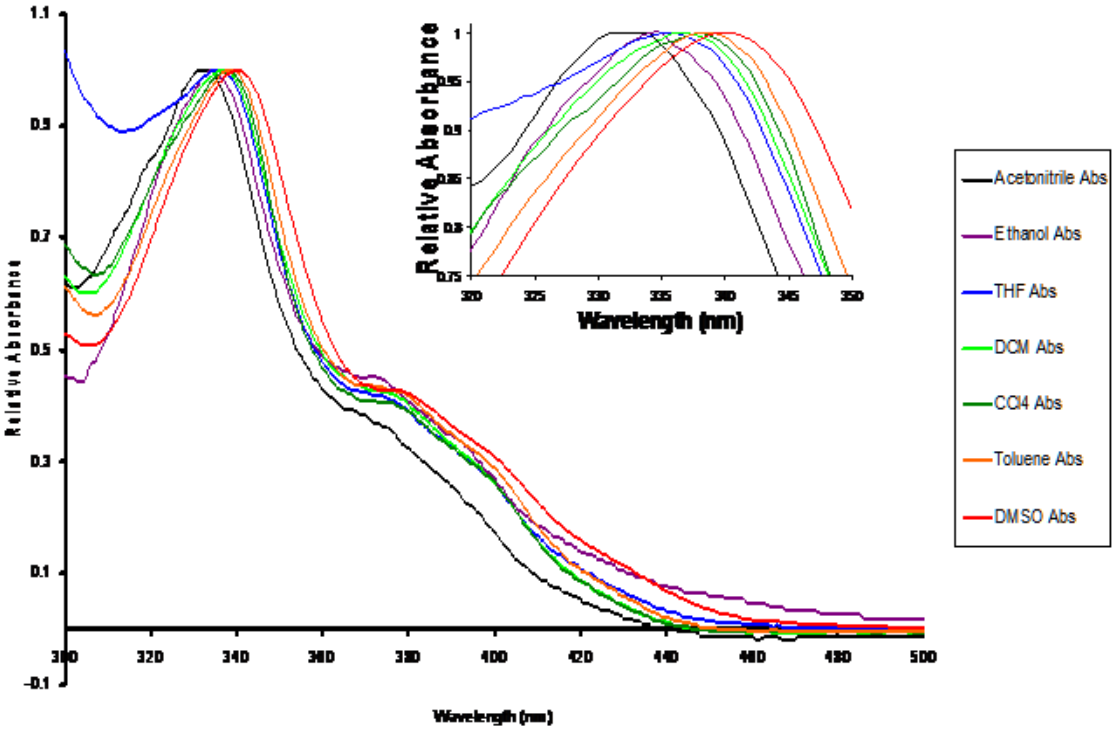

Figure A.7. Absorbance Spectra Showing the Solvatochromatic Effects of the absorbance of XF **A.3** in Various Solvents. Inset Shows More Closely the λ_{max} Region of the Spectra.

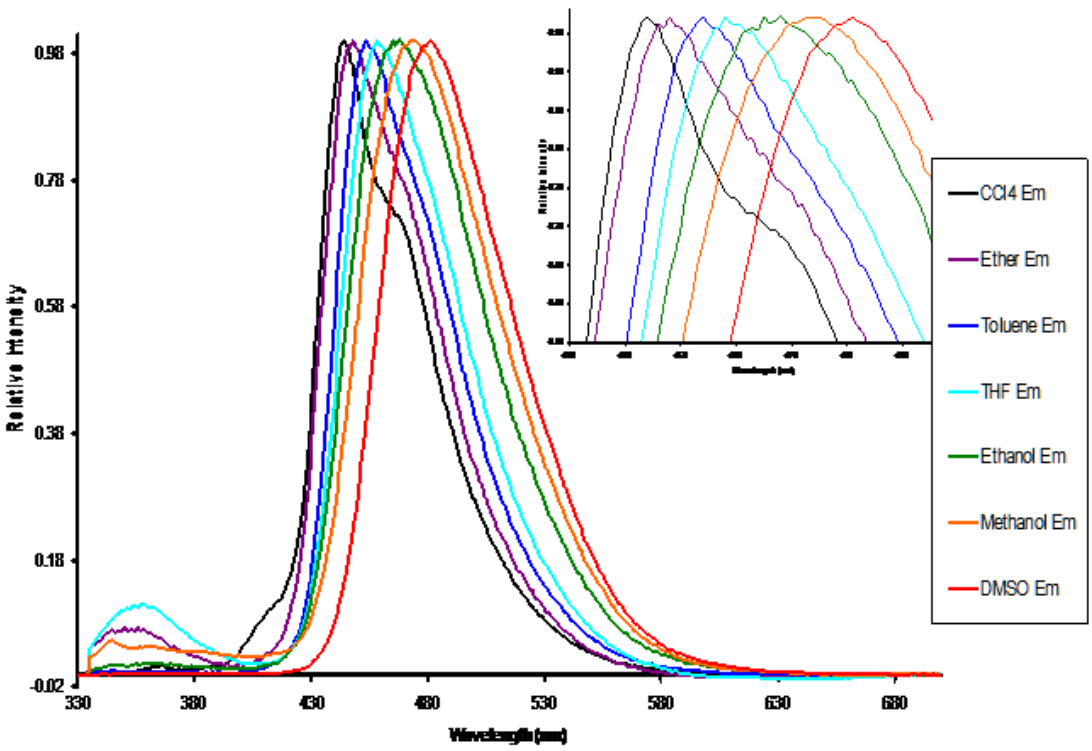

Figure A.8. Emission Spectra Showing the Solvatochromatic Effects of the Fluorescence of XF **A.3** in Various Solvents. Inset Shows More Closely the λ_{max} Region of the Spectra.

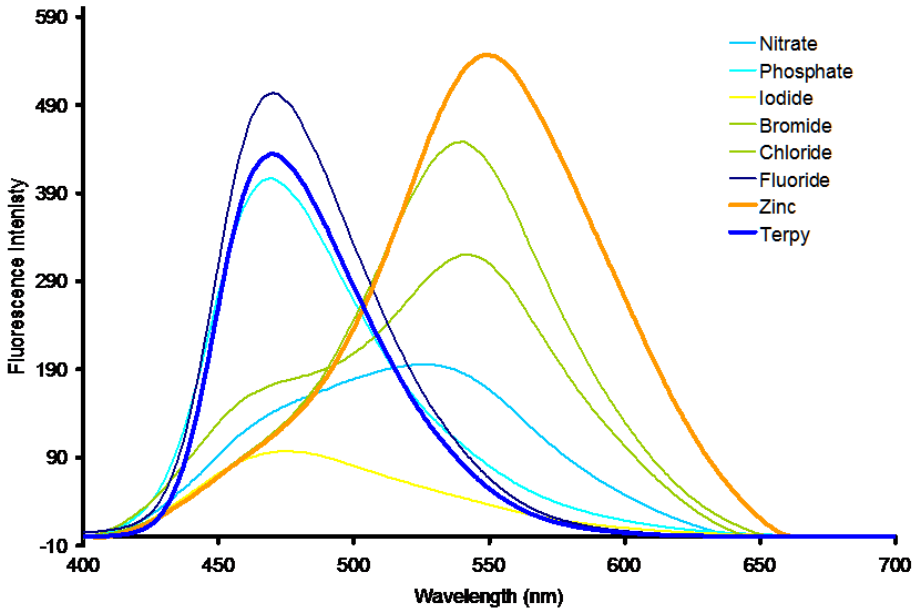

Figure A.9. Non-normalized Emission Spectra of the XF **A.3** (Terpy), its Zinc Complex, and After Addition of Different Anions to the XF **A.3**-Zn^{2+}-Complex.

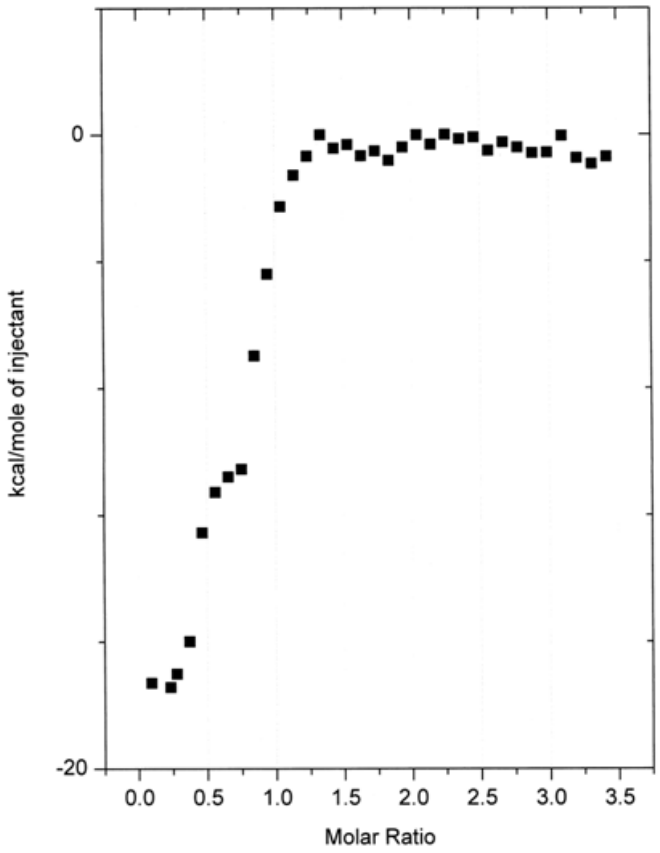

Figure A.10. ITC Curve of XF **A.3** Titrated with ZnOTf. Two Sigmoidal Regions are Visible Indicating Two Bindings Occurring at 0.5 and 1.0 molar ratio of ZnOTf to XF **A.3**.

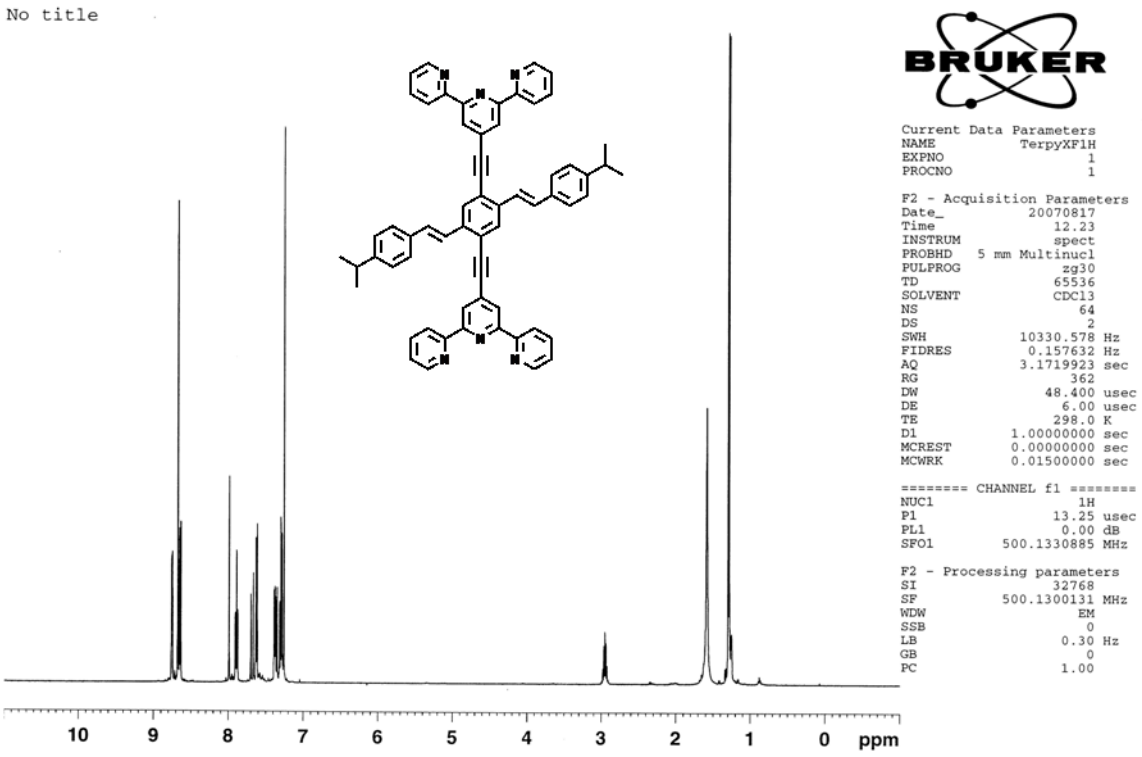

Figure A.11. ^{1}H-NMR of Terpyridine-XF **A.3**

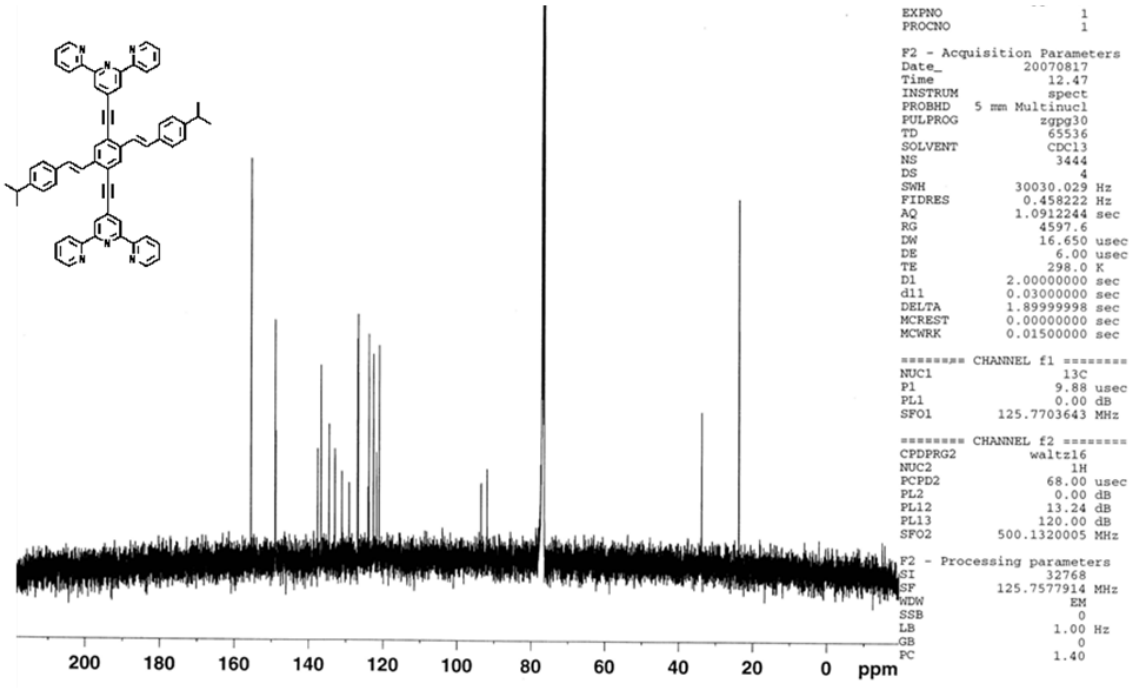

Figure A.12. ^{13}C-NMR of Terpyridine-XF **A.3**

A.5 References

[1] (a) Nguyen, B. T.; Anslyn, E. V. *Coord. Chem. Rev.* **2006**, *250*, 3118-3127. (b) Cabell, L. A.; Best, M. D.; Lavigne, J. J.; Schneider, S. E.; Perreault, D. M.; Monahan, M. K.; Anslyn, E. V. *J. Chem. Soc. Perkin Trans.* **2001**, *2*, 315-323. (c) Snowden, T. S.; Anslyn, E. V. *Curr. Opinion Chem. Biol.* **1999**, *3*, 740-746.

[2] (a) Fabbrizzi, L.; Licchelli, M.; Rabaioli, G.; Taglietti, A. *Coord. Chem. Rev.* **2000**, *205*, 85-108. (b) Keefe, M. H.; Benkstein, K. D.; Hupp, J. T. *Coord. Chem. Rev.* **2000**, *205*, 201-228.

[3] (a) Anzenbacher, P.; Palacios, M. A.; Jursikova, K.; Marquez, M. *Org. Lett.* **2005**, *7*, 5027-5030. (b) Anzenbacher, P.; Jursikova, K.; Aldakov, D.; Marquez, M.; Pohl, R. *Tetrahedron* **2004**, *60*, 11163-11168.

[4] (a) Kim, T. H.; Swager, T. M. *Angew. Chem.* **2003**, *42*, 4803-4806. (b) Takeuchi, M.; Shioya, T.; Swager, T. M. *Angew. Chem.* **2001**, *40*, 3372-3376. (c) Lee, D. H. Im, J. H. Lee, J. H. Hong, J. I. *Tetrahedron Lett.* **2002**, *43*, 9637-9640. (d) Thomas, S. W.; Joly, G. D.; Swager, T. M. *Chem. Rev.* **2007**, *107*, 1339-1386.

[5] (a) Liao, J. H.; Chen, C. T.; Fang, J. M. *Org. Lett.* **2002**, *4*, 561-564. (b) Patterson, S.; Smith, B. D.; Taylor, R. E. *Tetrahedron Lett.* **1997**, *38*, 6323-6326. (a) Mizukami, S.; Nagano, T.; Urano, Y.; Odani, A.; Kikuchi K. *J. Am. Chem. Soc.* **2002**, *124*, 3920-3925.

[6] (a) Fabbrizzi, L.; Marcotte, N.; Stomeo, F.; Taglietti, A. *Angew. Chem. Int. Ed.* **2002**, *41*, 3811. (b) Ojida, A.; Mito-oka, Y.; Sada, K.; Hamachi, I. *J. Am. Chem. Soc.* **2004**, *126*, 2454-2463. (c) Jose, D. A.; Mishra, S.; Ghosh, A.; Shrivastav, A.; Mishra, S. K.; Das A. *Org. Lett.* **2007**, *9*, 1979-1982. (d) O'Neil E. J.; Smith, B. D. *Coord. Chem. Rev.* **2006**, *250*, 3068-3080.

[7] (a) Zucchero, A. J.; Wilson, J. N.; Bunz, U. H. F. *J. Am. Chem. Soc.* **2006**, *128*, 11872-11881. (b) Wilson, J. N.; Bunz, U. H. F. *J. Am. Chem. Soc.* **2005**, *127*, 4124-4125. (c) Wilson, J. N.; Josowicz, M.; Wang, Y. Q.; Bunz, U. H. F. *Chem. Commun.* **2003**, 2962-2963.

[8] (a) Spitler, E. L.; Shirtcliff, L. D.; Haley, M. M. *J. Org. Chem.* **2007**, *72*, 86-96. (b) Marsden, J. A.; Miller, J. J.; Shirtcliff, L. D.; Haley M. M. *J. Am. Chem. Soc.* **2005**, *127*, 2464-2476. (c) Sorensen, J. K.; Vestergaard, M.; Kadziola, A.; Kilsa, K.; Nielsen, M. B. *Org. Lett.* **2006**, *8*, 1173-1176. (d) Tolosa, J.; Diez-Barra, E.; Sanchez-Verdu, P.; Rodriguez-Lopez, J. *Tetrahedron Lett.* **2006**, *47*, 4647-4651.

[9] Zen, A.; Bilge, A.; Galbrecht, F.; Alle, R.; Meerholz, K.; Grenzer, J.; Neher, D.; Scherf, U.; Farrell, T. *J. Am. Chem. Soc.* **2006**, *128*, 3914-3915.

[10] (a) Klare, J. E.; Tulevski, G. S.; Sugo, K.; de Picciotto, A.; White, K. A.; Nuckolls, C. *J. Am. Chem. Soc.* **2003**, *125*, 6030-6031. (b) Miao, Q.; Chi, X. L.; Xiao, S. X.; Zeis, R.; Lefenfeld, M.; Siegrist, T.; Steigerwald, M. L.; Nuckolls C. *J. Am. Chem. Soc.* **2006**, *128*, 1340-1345.

[11] Kang, H.; Evmenenko, G.; Dutta, P.; Clays, K.; Song, K.; Marks, T. J. *J. Am. Chem. Soc.* **2006**, *128*, 6194- 6205.

[12] (a) Pan, Y.; Lu, M.; Peng, Z.; Melinger, J. S. *Org. Biomol. Chem.* **2003**, *1*, 4465-4470. (b) Khatyr, A.; Ziessel, R. *J. Org. Chem.* **2000**, *65*, 3126-3134.

[13] Bunz, U. H. F. *Chem. Rev.* **2000**, *100*, 1605-1645.

[14] (a) Dobrawa, R.; Würthner, F. *Chem. Commun.* **2002**, 1878-1879. (b) Schmittel, M.; Kalsani, B.; Kishore, R. S. K.; Cölfen, H.; Bats, J. W. *J. Am. Chem. Soc.* **2005**, *127*, 11544-11545. (c) Sarkar, A.; Chakravorti, S.; *J. Luminescence* **1995**, *63*, 143-148. (d) Mutai, T.; Cheon, J.-D.; Tsuchiya, G.; Araki, K. *J. Chem. Soc. Perkin Trans.* **2002**, *2*, 862-865. Benniston, A. C. Harriman, A. Lawrie, D. J. Mayeux, A. Rafferty, K. Russell, O. D. *Dalton Trans.* 2003, 4762-4769.

[15] (a) Goodall, W.; Williams, J. A. G. *Chem. Commun.* **2001**, 2514-2515. (b) Ziener, U.; Lehn, J. M.; Mourran, A.; Möller, M. *Chemistry-Eur. J.* **2002**, *8*, 951-957. (c) Goze, C.; Ulrich, G.; Charbonniere, L.; Cesario, M.; Prange, T.; Ziessel R. *Chemistry-Eur. J.* **2003**, *9*, 3748-3755.

[16] (16) Harris, D. C., Quantitative Chemical Analysis, W. H. Freeman, *New York* **2003**. p. AP11.

[17] Wagman, D. D.; Evans, W. H.; Parker, V. B.; Shumm, R.H.; Halow, I.; Bailey, S.M.; Churney, K.L.; Nuttall, R.L.; The NBS Tables of Chemical Thermodynamic Properties, *J. Phys. Chem. Ref. Data, Vol.* 11, Suppl. 2, **1982**.

[18] (a) Knapton, D.; Burnworth, M.; Rowan, S. J.; Weder, C *Angew. Chem.* **2006**, *45*, 5825-5829. (b) Iyer, P. K.; Beck, J. B.; Weder, C.; Rowan, S. J. *Chem. Commun.* **2005**, 319-321.

Appendix B: Hydroxy-Cruciforms

B.1 Introduction

Cruciform fluorophores (tetra-1,2,4,5-vinyl- or -ethynyl-substituted benzenes, XFs) are π -systems with unusual frontier molecular orbitals (FMOs). If one of the axes is donor substituted and the other axis is acceptor substituted, species with *spatially separated* FMOs can result. The HOMO is localized on the donor part of the molecule, while the LUMO is localized on the acceptor part of the molecule. This FMO arrangement leads to a situation in which electronic information can be addressed spatially and for which HOMO and LUMO are manipulated by metal cations or by protons.

We[1] and others[2,3,4,5] have shown that dialkylaniline- and pyridine-containing XFs display unusually large bathochromic or hypsochromic shifts when exposed to zinc, magnesium, calcium and manganese salts or protons.[1,2] The reason for the large shifts in absorption and emission is the independently addressable HOMO and LUMO, enforcing large changes in the HOMO–LUMO gap. Up to now, HOMO–LUMO of XF-types has been addressed by cationic species, binding to the free electron pairs of pyridines and dialkylanilines. In this chapter, we demonstrate that XFs carrying strategically placed phenol functionalities show unusual photophysical effects upon deprotonation and exposure to amines.

B.2 Results and Discussion

The synthesis of hydroxy-XFs starts with the reaction of phosphonate **B.1**[6] with either the protected aldehyde **B.2** or **B.3** to give the distyrylbenzene derivatives **B.4** or **B.5** in 77% and 68% yield, respectively, after chromatography and crystallization. Coupling of **B.4** or **B.5** with 4-tert-butylphenylacetylene in the presence of CuI–$(Ph_3P)_2PdCl_2$ under standard Heck–Cassar–Sonogashira–Hagihara conditions[7] in piperidine furnished the target XFs **B.7** and **B.8**, after aqueous workup, chromatography and subsequent deprotection with trifluoroacetic acid at -78 °C in dichloromethane, as yellow or yellowish–brown solids in 41% and 40% yield respectively (Scheme B.1). The relatively low coupling yield (44 and 48% respectively) is due to losses during the chromatography of the intermediate. Nevertheless, the target XFs are easily available on a 100–200 mg scale. If **B.4** is coupled to **B.9**, we obtain an intermediate in 53% yield, which is

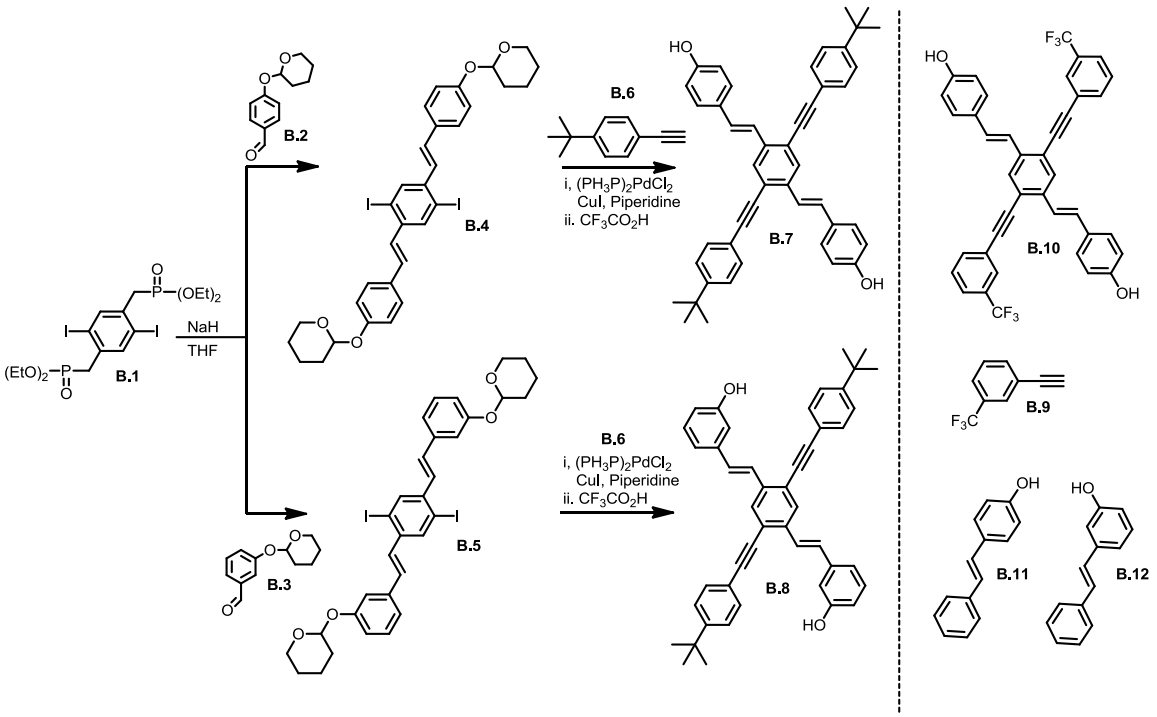

Scheme B.1. Synthesis of hydroxy XFs **B.7**, **B.8**, and **B.10**.

Table B.1. Photophysical data of XFs **B.7**, **B.8**, and **B.10** in dichloromethane

Compound	**B.7**	**B.8**	**B.10**
Absorption (nm)	380	376	404
Emission (nm)	432	423	456
Vibronic Progression (cm^{-1})	876	1219	None
Stokes Shift (cm^{-1})	3167	2955	2822
Φ_{fl} (quantum yields)	0.41	0.72	0.57
τ (ns)	1.42	2.99	NA

deprotected in 85% yield to give **B.10**.

Table B.1 shows the pertinent photophysical data of **B.7**, **B.8** and **B.10**. The XFs **B.7** and **B.8** are similar to each other, as they show blue emission with robust quantum yields. Attachment of $-CF_3$ groups on the aryleneethynylene axis in **B.10** decreases the band gap and leads to significantly red-shifted absorption and emission. The Stokes shifts in these XFs are similar and around 3000 cm^{-1}. The vibronic progression of **B.8** is in the expected range, while that of **B.7** is smaller. The fluorescence spectrum of **B.10** does not show any vibronic bands, suggesting that its excited state is structurally different from its ground state.[8]

We titrated (see Figures B.1 & B.2) **B.7** and **B.8** in a methanol–water mixture with aqueous base (KOH). Figure B.1 shows absorption and emission for **B.8**. Upon addition of hydroxide, *there is no significant change in the absorption spectrum of* **B.8**; the emission of the phenolate of **B.8** is largely quenched. A very weak emission band for the deprotonated form of **B.8** is observed at 515 nm. The invariance of the absorption spectrum is surprising and persists upon addition of a large excess of hydroxide. In the

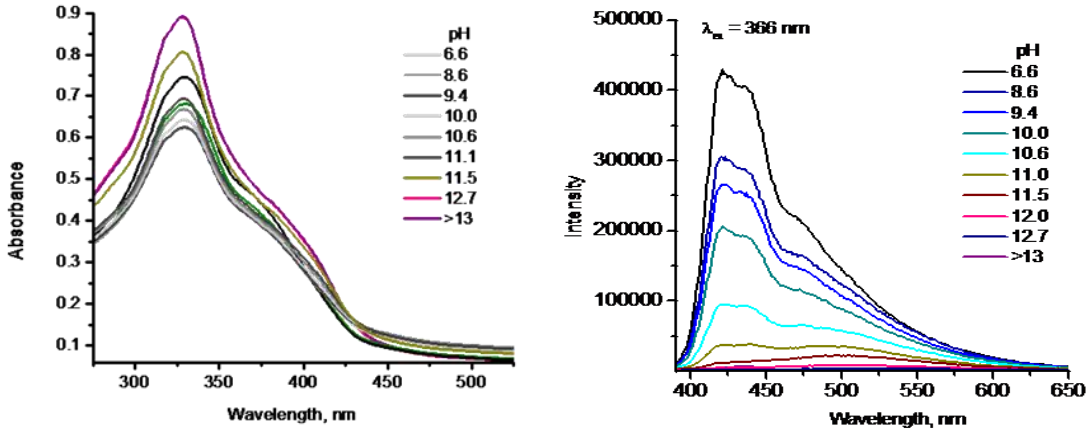

Figure B.1. Uv-vis (left) and emission (right) spectra of XF **B.8** in a 2:1 vol. methanol-water mixture at different pH-values.

case of **B.7**, upon deprotonation (Figure B.2), the absorption spectrum shows an appreciable red shift, as would be expected for a phenolate, with a prominent absorption appearing at 416 nm. At the same time, the emission changes from 476 nm (blue) to 580 nm (yellow). Addition of an excess of KOH solution does not change the emission wavelength further. From the titrations, the pK_a values for **B.7** and **B.8** were determined to be 9.9 and 10.0.

Changes in spectroscopic properties are not only observed upon deprotonation of the XFs **B.7** and **B.8** in methanol–water mixtures, but also when solutions of XFs in dichloromethane are exposed to amines. Figure B.3 shows a photograph of the XFs **B.7**, **B.8** and **B.10** exposed to a panel of different amines, ordered by their increasing pK_a values, while Figure B.4 shows the corresponding emission spectra for **B.7**.

Interestingly, the magnitude in shift and the pK_a-values of the amines do not correlate particularly well, as ethylenediamine (pK_a = 10.7), i.e. not the most basic amine, displays the largest red shift. In the case of the exposure of **B.7** to quinoline or to pyridine,

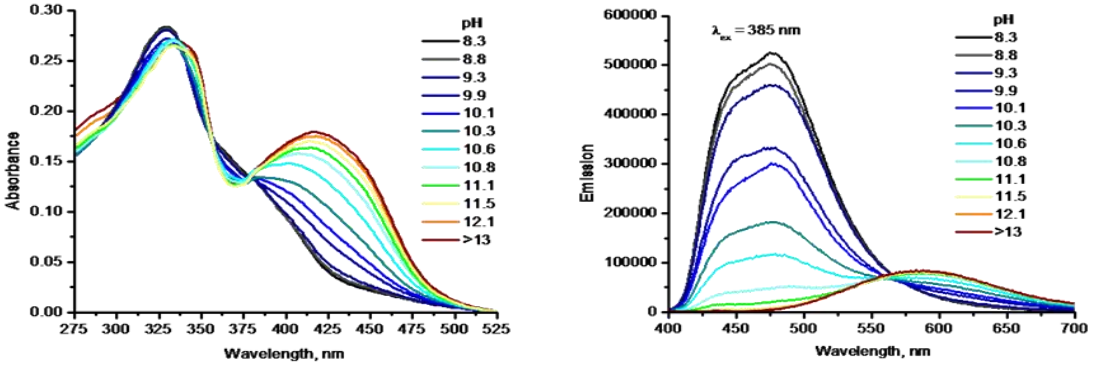

Figure B.2. Uv-vis (left, 417 nm λ_{max} deprotonated form) and emission (right, 474 nm, 596 nm λ_{max}) spectra of XF **B.7** in a 2:1 vol. methanol-water mixture at different pH-values.

fluorescence is quenched, possibly due to a back electron transfer following proton transfer to the basic nitrogen.[9] If the amine under consideration is not very basic, as pyrrole and imidazole, either there is no change of the emission or a mixed color (imidazole) is observed. Similar trends are observed for XF **B.10**, even though the emission intensities are much lower, as expected from the energy gap law.[10]

Exposure of the XF **B.8** to amines in dichloromethane results in quenching (see experimental for spectra) of the emission, similar to that observed on exposure of **B.8** to KOH. The above observations demonstrate that **B.7** and **B.8** are different from hydroxystilbenes **B.11** and **B.12**. The phenolate of stilbene **B.11** is weakly fluorescent, while that of the meta-compound **B.12** is quite fluorescent.[11] In **B.11** and **B.12** the excited state acidity of the phenolic function is significantly enhanced, that of **B.12** more so than that of **B.11**. Neither the XF **B.7** nor **B.8**, on the other hand, shows dramatically enhanced photoacidity in methanol–water mixtures with up to 50% vol. water, [11] which makes them comparable to the weak photoacid 2-naphthol with a pK_a* of 2.8.[12]

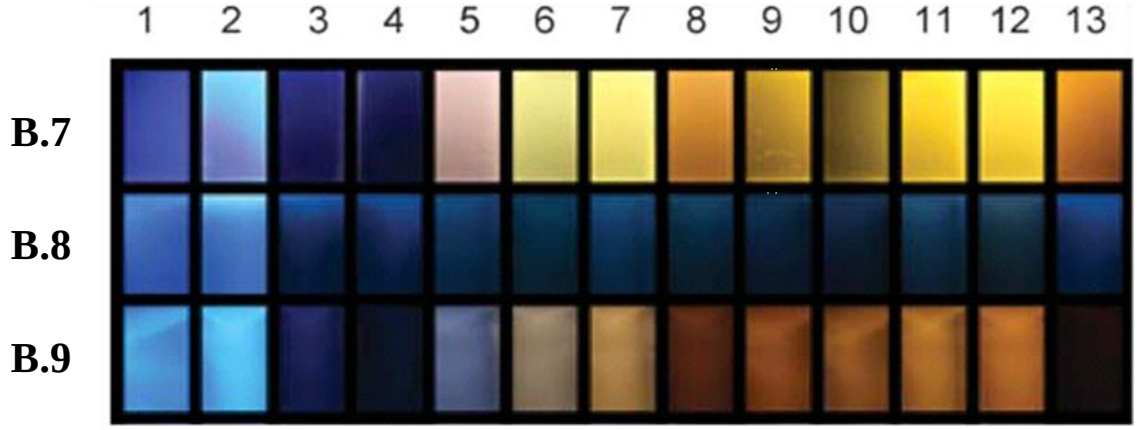

Figure B.3. Photograph of the cruciforms **B.7, B.8,** and **B.10** in DCM: 1) reference; exposure to 2) pyrrole (-), 3) quinoline (4.90), 4) pyridine (5.25), 5) imidazole (6.96; λ_{max}. **B.7** = 551 nm), 6) morpholine (8.33; 555 nm), 7) piperazine (9.83; 556 nm), 8) ethylenediamine (10.7; 579 nm), 9) piperidine (10.8; 564 nm), 10) triethylamine (10.8; 555 nm), 11) diethylamine (11.0; 562 nm), 12) diisopropylamine (11.1; 558 nm), and 13) 1,8-diaza-bicyclo[5.4.0]undec-7-ene (DBU, ~12; 572). The numbers in parenthesis are the pK_a values of the corresponding ammonium ions.

The absorption and emission spectra of **B.7** show a more complex behavior in the presence of amines (Figure B.4). On the one hand, except for 1,8-diaza[5.4.0]bicycloundecene (DBU, pK_a ~ 12), the absorption maxima show a shift of ca. 20 nm and are consistent with a hydrogen-bonded complex.[13] Upon addition of DBU a redshifted feature is observed, which we attribute to the fully bisdeprotonated ground

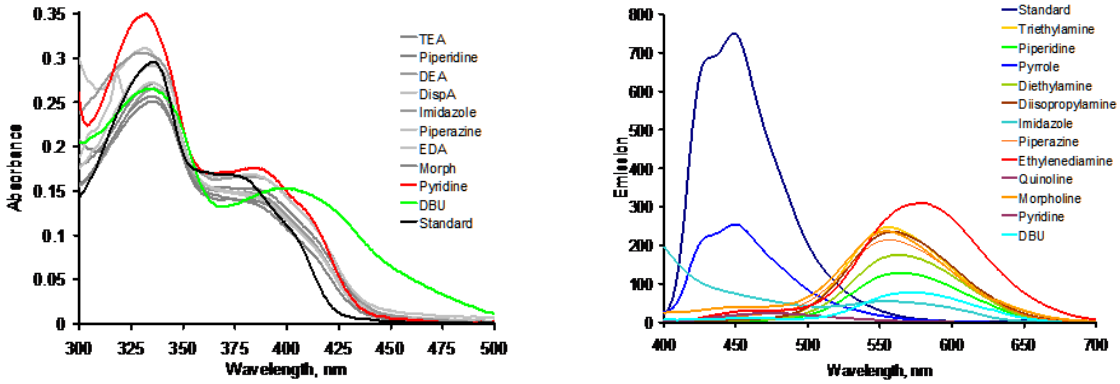

Figure B.4. Absorption spectra (left) of solutions of **B.7** in DCM upon addition of amine (0.1 mL). Emission spectra (right) of solutions of **B.7** in dichloromethane (DCM, 15 mL, vial) upon addition of amine (0.1 mL).

state species, as it is identical to that observed in the KOH-promoted deprotonation of **B.7**. On the other hand, all of the amine complexes exhibit efficient emission from the fully deprotonated (ion pair) state. From these observations, we conclude that in dichloromethane solutions the difference in pK_a (or ΔG of the proton transfer) between **B.7*** and amines is sufficient to produce solvent-separated ion pairs.[14] In the ground state, the observed ΔpK_a results in the formation of hydrogen-bonded complexes.

The observation of different amine-dependent emission characteristics is of potential importance since Lavigne *el al.*[15] have shown that carboxylate-substituted polythiophenes can discern biogenic amines when the absorption spectra of the complexes are compared. Our approach is complementary as we use more sensitive fluorescence spectroscopy.

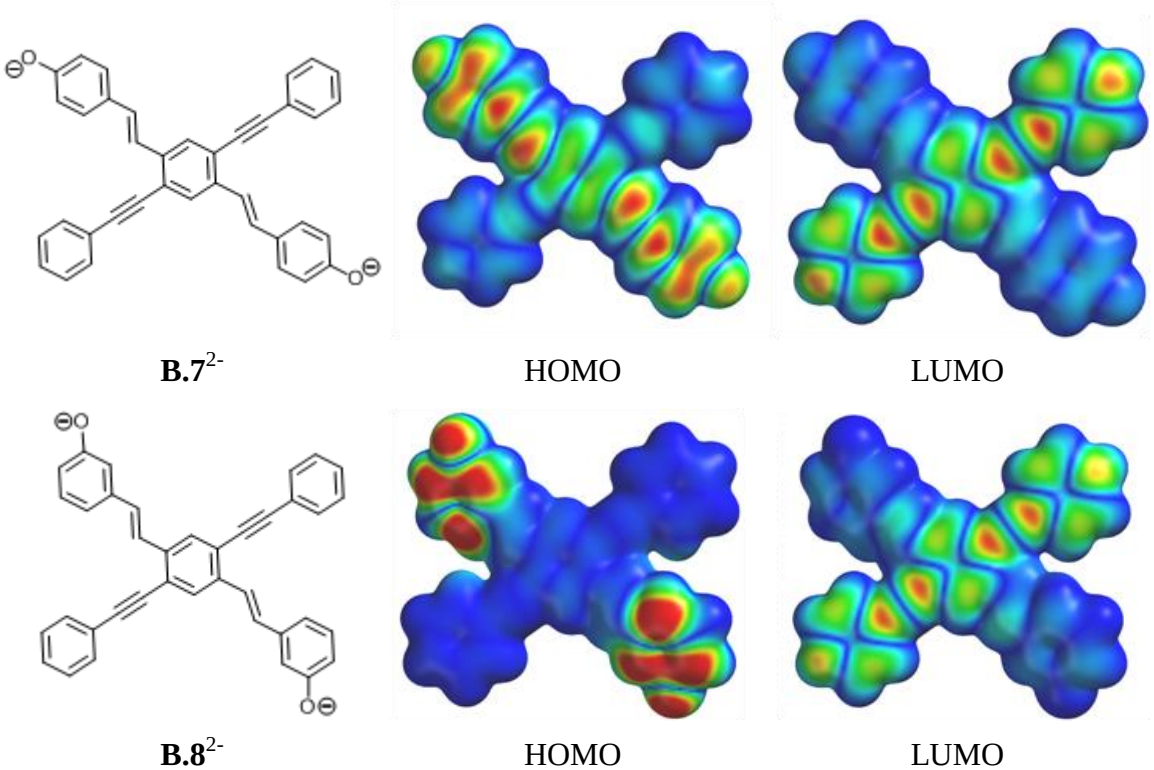

Figure B.5. Density of the frontier molecular orbitals (HOMO and LUMO) of the bisphenolate anions of models of **B.7** and of **B.8** as calculated by B3LYP-6-31G**//B3LYP-6-31G** using SPARTAN.

What is the reason for the dramatic differences in the optical properties of **B.7** and **B.8** upon interaction with bases, i.e. proton dissociation induced red shift vs. quenching? A DFT calculation (Figure B.5) of the FMO-distribution of **B.7** and **B.8** sheds light on this issue. In the dianion of **B.7**, HOMO and LUMO show spatial overlap in the central ring and both absorption and emission is Franck–Condon allowed. In the case of **B.8** the situation is different. Due to the disjoint orbital structure *in which the HOMO is localized only on the two phenolate rings, while the LUMO is strictly localized on the bisarylethynyl axis, there is a vanishingly small spatial overlap between the two frontier molecular orbitals, resulting in a Franck–Condon forbidden transition. Without the quantum chemical calculations, the different spectroscopic properties of* ***B.7***$^{2-}$ *and* ***B.8***$^{2-}$ *would be very hard to rationalize.* Since the 340 nm transition is both invariant with respect to deprotonation and strongly allowed, we conclude that this is a HOMO–LUMO transition in **B.8** but a HOMO–LUMO + n-transition in the deprotonated form of **B.8**, while the weaker HOMO–LUMO transition of the dianion of **B.8** is hidden in the baseline.[3] The allowed transition in the dianion must have a similar gap to the HOMO–LUMO-transition in the neutral compound, explaining the lack of change in the absorption spectra.

B.3 Conclusions

In conclusion, we have prepared the two XFs **B.7** and **B.8** and investigated their photophysical properties upon deprotonation and exposure to amines. We see dramatic differences between the *para* (**B.7**) and the *meta* (**B.8**) XF as a consequence of the different FMO distribution. The dianion **B.8** suffers from a Franck–Condon disallowed

HOMO–LUMO-transition, which is responsible for the observed fluorescence quenching. Potential applications of such materials with separated FMOs include exciton collection and splitting in photovoltaic devices and fluorescence sensors in cases where the XFs are equipped with additional binding elements.

This work has been *Chemical Communications*:

McGrier, P. L.; Solntsev, K. M.; Shönhaber, J.; Brombosz, S. M.; Tolbert, L. M.; Bunz, U. H. F. *Chem. Comm.*, **2007**, 2127.

B.4 Experimental and Supplementary Information

B.4.1 4-((tetrahydro-2H-pyran-2-yl)oxy)benzaldehyde, **B.2**.

4-hydroxybenzaldehyde (5.8, 47.5 mmol) and 3,4-dihydro-2H-pyran (6.4 g, 76.1 mmol) was dissolved in dichloromethane (100 mL) in a 250 mL round bottom flask. Para-toluenesulfonic acid (0.43 g, 2.5 mmol) was added to the reaction mixture along with pyridine (1 mL). The pyridine was added drop wise over a 5 min period. The crude reaction mixture was washed three times with water, dried with magnesium sulfate and reduced until a dark brown oil was obtained. The product was washed with a solution of dilute NaOH and water to remove the starting material. The final product was obtained as a dark brown oil. Yield: 84%. *^{1}H NMR (500 MHz, $CDCl_3$):* δ = 9.90 (s, 1H, Ar-CHO), 7.84 (d, 2H, Ar-H, $J_{H,H}$ = 9 Hz), 7.17 (d, 2H, Ar-H, $J_{H,H}$ = 8.5 Hz), 5.55 (s, 1H, α-C-H), 3.85 (m, 1H, ε-CH), 3.64 (m, 1H, ε-C-H), 2.01 (m, 1H, β-C-H), 1.90 (m, 2H, γ-C-H) 1.71 (m, 2H, δ-C-H), 1.62 (m, 1H, β-C-H). *^{13}C NMR (500 MHz, $CDCl_3$):* δ = 191.19, 162.48, 132.11, 130.77, 116.82, 96.41, 62.34, 30.36, 25.35, 18.77.

B.4.2 3-((tetrahydro-2H-pyran-2-yl)oxy)benzaldehyde, **B.3**.

3-hydroxybenzaldehyde (5.8, 47.5 mmol) and 3,4-dihydro-2H-pyran (6.4 g, 76.1 mmol) was dissolved in dichloromethane (100 mL) in a 250 mL round bottom flask. Para-toluenesulfonic acid (0.43 g, 2.5 mmol) was added to the reaction mixture along with pyridine (1 mL). The pyridine was added drop wise over a 5 min period. The crude reaction mixture was washed three times with water, dried with magnesium sulfate and

reduced until a light brown oil was obtained. The product was washed with a solution of dilute NaOH and water to remove the starting material. The final product was obtained as a light brown oil. Yield: 85%. *^{1}H NMR (500 MHz, $CDCl_3$):* δ = 9.97 (s, 1H, Ar-CHO), 7.56 (s, 1H, Ar-H,), 7.50 (dt, 1H, Ar-H, $J_{H,H}$ = 7.5 Hz, *with long range coupling*), 7.44 (t, 1H, Ar-H, $J_{H,H}$ = 8 Hz), 7.31 (md, 1H, Ar-H, $J_{H,H}$ = 8 Hz, *with long range coupling*), 5.49 (s, 1H, α-C-H), 3.88 (m, 1H, ε-CH), 3.63 (m, 1H, ε-C-H), 2.01 (m, 1H, β-C-H), 1.90 (m, 2H, γ-C-H) 1.71 (m, 2H, δ-C-H), 1.62 (m, 1H, β-C-H). *^{13}C NMR (500 MHz, $CDCl_3$)*: δ = 192.19, 157.90, 138.10, 130.10, 123.63, 123.18, 116.59, 96.59, 62.21, 30.47, 25.40, 18.92.

Note: Compounds **B.4** and **B.5** both contain traces of previously reported halogen exchange material (**B.4a** and **B.5a**) from the precursor **B.1,** which is inseparable but can be used for further reactions.

B.4.3 2,2'-((((1E,1'E)-(2,5-diiodo-1,4-phenylene)bis(ethene-2,1-diyl))bis(4,1-phenylene))bis(oxy))bis(tetrahydro-2H-pyran), **B.4**.

B.1 (0.500 g, 0.681 mmol), NaH (60 mg, 2.50 mmol), and THF (50 mL) were combined. 4-(tetrahydropyran-2-yloxy)-benzaldehyde (0.409 g, 1.98 mmol) was then added. Work up and recrystallization yielded (0.448 g, 77%) of bright yellow crystals. *MP:* 268-270 ºC. *IR:* 2933, 2869, 1600, 1508, 1234, 1170, 1107, 1035, 970, 810. *^{1}H NMR (500 MHz, $CDCl_3$):* δ = 8.07 (s, 2H, Ar-H), 7.58 (d, 4H, Ar-H, $J_{H,H}$ = 8.5 Hz), 7.10 (d, 4H, Ar-H, $J_{H,H}$ = 8.5 Hz), 7.09 (d, 2H, C=C-H, $J_{H,H}$ = 16.5 Hz), 6.95 (d, 2H, CH=CH, $J_{H,H}$ = 16.5

Hz), 5.49 (s, 2H, α-C-H), 3.95 (m, 2H, ε-CH), 3.65 (m, 2H, ε-C-H), 2.04 (m, 2H, β-C-H), 1.91 (m, 4H, γ-C-H) 1.71 (m, 4H, δ-C-H), 1.64 (m, 2H, β-C-H). *^{13}C NMR (500 MHz, $CDCl_3$):* δ = 157.73, 141.10, 136.44, 132.17, 130.63, 129.05, 128.57, 117.14, 100.62, 96.69, 62.47, 30.70, 25.59, 19.13.

B.4.4 2,2'-((((1E,1'E)-(2,5-diiodo-1,4-phenylene)bis(ethene-2,1-diyl))bis(3,1-phenylene))bis(oxy))bis(tetrahydro-2H-pyran), **B.5**.

B.1 (0.500 g, 0.681 mmol), NaH (60 mg, 2.50 mmol), and THF (50 mL) were combined. 3-(tetrahydropyran-2-yloxy)-benzaldehyde (0.409 g, 1.98 mmol) was then added. Work up and recrystallization yielded (0.399 g, 68%) of pale yellow crystals. *MP:* 216-218 ºC. *IR:* 2947, 2873, 1581, 1488, 1251, 1120, 1037, 1014, 970, 904, 869, 777. *^{1}H NMR (500 MHz, $CDCl_3$):* 8.09 (s, 2H, Ar-H), 7.33 (t, 2H, Ar-H, $J_{H,H}$ = 8 Hz), 7.27 (s, 2H, Ar-H), 7.22 (d, 2H, Ar-H, $J_{H,H}$= 5 Hz), 7.20 (d, 2H, C=C-H, $J_{H,H}$ =16 Hz), 7.05 (d, 2H, Ar-H, $J_{H,H}$ = 8.5 Hz), 6.97 (d, 2H, C=C-H, $J_{H,H}$ = 16 Hz), 5.49 (s, 2H, α-C-H), 3.95 (m, 2H, ε-C-H), 3.65 (m, 2H, ε-C-H), 2.04 (m, 2H, β-C-H), 1.91 (m, 4H, γ-C-H) 1.71 (m, 4H, δ-C-H), 1.64 (m, 2H, β-C-H). *^{13}C NMR (500 MHz, $CDCl_3$):* δ = 157.86, 141.18, 138.36, 136.78, 132.70, 131.10, 130.13, 120.87, 116.94, 115.39, 100.69, 96.90, 62.59, 30.81, 25.62, 19.25.

B.4.5 1-ethynyl-3-(trifluoromethyl)benzene, **B.9a**.

^{1}H NMR (300 MHz, $CDCl_3$): δ = 7.72 (s, 1H, Ar-H), 7.62 (d, 1H, Ar-H, $J_{H,H}$ = 7.7 Hz), 7.56 (d, 1H, Ar-H, $J_{H,H}$ = 8.4 Hz), 7.42 (t, 1H, Ar-H, $J_{H,H}$ = 7.3 Hz), 0.26 (s, 9H, -CH_3).

^{13}C NMR (300 MHz, $CDCl_3$): δ = 134.98, 130.90(m), 128.73, 125.52, 124.93(m), 124.14, 121.91, 118.30, 103.28, 96.20. *MS (EI, 70-SE) ($C_{12}H_{13}F_3Si$):* m/z = 242.

B.4.6 2,2'-((((1E,1'E)-(2,5-bis((4-(tert-butyl)phenyl)ethynyl)-1,4-phenylene)bis(ethene-2,1-diyl))bis(4,1-phenylene))bis(oxy))bis(tetrahydro-2H-pyran), **B.7a**.

B.4 (0.297 g, 0.404 mmol) was combined with **B.6** (0.192, g, 1.21 mmol), $(PPh_3)_2PdCl_2$ (5 mg, 7.1 μmol), CuI (5 mg, 33 μmol) and dissolved in THF (50 mL) and piperidine (5 mL) in a nitrogen purged Schlenk flask. The solution was degassed, capped with a septum and allowed to stir at room temperature for 24 h. The product was extracted with dichloromethane, washed three times with water and dried with magnesium sulfate and reduced until a yellow powder was formed, which was purified by chromotagraphy eluting with 70:30 dichloromethane and hexanes yielding 150 mg of yellow crystals. Yield: 47%. *MP:* 186-188 ºC. *IR:* 2939, 2866, 2250, 1602, 1508, 1236, 1170, 1035, 1018, 960, 919, 831, 813. *^1H NMR (500 MHz, $CDCl_3$):* δ = 7.90 (s, 2H, Ar-H), 7.59 (d, 2H, C=C-H, $J_{H,H}$ = 16.5 Hz), 7.57 (d, 4H, Ar-H, $J_{H,H}$ = 8 Hz), 7.54 (d, 4H, Ar-H, $J_{H,H}$ = 8 Hz), 7.45 (d, 4H, Ar-H, $J_{H,H}$ = 8.5 Hz), 7.25 (d, 2H, C=C-H, $J_{H,H}$ = 16.5 Hz), 7.10 (d, 4H, Ar-H, $J_{H,H}$ = 8.5 Hz), 5.49 (s, 2H, α-C-H), 3.95 (m, 2H, ε-C-H), 3.65 (m, 2H, ε-C-H), 2.04 (m, 2H, β-C-H), 1.91 (m, 4H, γ-C-H) 1.71 (m, 4H, δ-C-H), 1.64 (m, 2H, β-C-H), 1.37 (s, 18H, t-butyl). *^{13}C NMR (500 MHz, $CDCl_3$):* δ = 156.97, 151.80, 137.22, 131.29, 130.97, 129.91, 128.43, 127.90, 125.50, 123.89, 122.06, 120.18, 116.67, 96.24, 95.47, 87.38, 62.01, 34.85, 31.18, 30.29, 25.18, 18.70. *MS (FAB, 70-SE) ($C_{56}H_{58}O_4$):* m/z = 794.

B.4.7 2,2'-((((1E,1'E)-(2,5-bis((4-(tert-butyl)phenyl)ethynyl)-1,4-phenylene)bis(ethene-2,1-diyl))bis(3,1-phenylene))bis(oxy))bis(tetrahydro-2H-pyran), **B.8a**.

B.5 (0.399 g, 0.543 mmol) was combined with **B.6** (0.258 g, 1.63 mmol), $(PPh_3)_2PdCl_2$ (5 mg, 7.1 μmol), CuI (5 mg, 33 μmol) and dissolved in THF (50 mL) and piperidine (5 mL) in a nitrogen purged Schlenk flask. The solution was degassed, capped with a septum and allowed to stir at room temperature for 24 h. The product was extracted with dichloromethane, washed three times with water and dried with magnesium sulfate and reduced until a yellow powder was formed, which was purified by chromotagraphy eluting with 70:30 dichloromethane and hexanes yielding 190 mg of yellow crystals. Yield: 44%. *MP:* 266-268 ºC. *IR:* 2947, 2869.8, 2220. 1, 1583.4, 1512.1, 1452.3, 1257.5, 1157.21, 1020.27, 956.6, 831.2, 775.3 *^{1}H NMR (500 MHz, $CDCl_3$):* δ = 7.93 (s, 2H, Ar-H), 7.72 (d, 2H, C=C-H, $J_{H,H}$ = 16.5 Hz), 7.60 (d, 4H, Ar-H, $J_{H,H}$ = 8.5), 7.45 (d, 4H, Ar-H, $J_{H,H}$ = 8.5), 7.36 (s, 2H, Ar-H), 7.32 (t, 2H, Ar-H, $J_{H,H}$ = 8 Hz), 7.27 (d,2H, $J_{H,H}$ = 16.5 Hz, CH=CH), 7.23 (d, 2H, $J_{H,H}$ = 8 Hz Ar-H), 7.02 (d, 2H, $J_{H,H}$ = 8 Hz, Ar-H), 5.49 (s, 2H, α-C-H), 3.95 (m, 2H, ε-C-H), 3.65 (m, 2H, ε-C-H), 2.04 (m, 2H, β-C-H), 1.91 (m, 4H, γ-C-H) 1.71 (m, 4H, δ-C-H), 1.64 (m, 2H, β-C-H), 1.37 (s, 18H, t-butyl). *^{13}C NMR (500 MHz, $CDCl_3$):* δ = 157.92, 152.27, 139.17, 137.68, 131.68, 130.82, 130.08, 129.06, 126.40, 125.93, 122.85, 120.99 120.62, 116.83, 114.74, 96.82, 96.82, 87.73, 62.41, 35.30, 31.65, 30.90, 25.73, 19.26. *MS (FAB, 70-SE) ($C_{56}H_{58}O_4$):* m/z = 794.

B.4.8 2,2'-((((1E,1'E)-(2,5-bis((3-(trifluoromethyl)phenyl)ethynyl)-1,4-phenylene)bis(ethene-2,1-diyl))bis(4,1-phenylene))bis(oxy))bis(tetrahydro-2H-pyran), **B.10a**.

B.4 (0.403 g, 0.549 mmol) was combined with **B.9a** (0.399 g, 1.64 mmol), $(PPh_3)_2PdCl_2$ (5 mg, 7.1 μmol), CuI (5 mg, 33 μmol), KOH (0.500 g, 8.90 mmol) and dissolved in piperidine (5 mL), EtOH (10 mL) and THF (25 mL) in a nitrogen purged Schlenk flask. The solution was degassed, capped with a septum and allowed to stir at room temperature for 24 h. The product was extracted with dichloromethane, washed three times with water and dried with magnesium sulfate and reduced until a yellow powder was formed, which was purified by chromotagraphy eluting with 60:40 dichloromethane and hexanes yielding 280 mg of yellow crystals. Yield: 53%. *MP:* 246-248 ºC. *IR:* 3035, 2943, 2875, 2235, 1600, 1508, 1330, 1240, 1164, 1122, 958, 919, 800. *^{1}H NMR (500 MHz, $CDCl_3$):* δ = 7.92 (s, 2H, Ar-H), 7.90 (s, 2H, Ar-H), 7.79 (d, 2H, Ar-H, $J_{H,H}$ = 8 Hz), 7.66 (d, 2H, Ar-H, $J_{H,H}$ = 8 Hz), 7.56 (t, 2H, Ar-H, $J_{H,H}$ = 8 Hz), 7.54 (d, 2H, C=C-H, $J_{H,H}$ = 16.5 Hz), 7.54 (d, 4H, Ar-H, $J_{H,H}$ = 9 Hz), 7.26 (d, 2H, C=C-H, $J_{H,H}$ = 16.5 Hz), 7.11 (d, 4H, Ar-H, $J_{H,H}$ = 9 Hz), 5.49 (s, 2H, α-C-H), 3.95 (m, 2H, ε-C-H), 3.65 (m, 2H, ε-C-H), 2.04 (m, 2H, β-C-H), 1.91 (m, 4H, γ-C-H) 1.71 (m, 4H, δ-C-H), 1.64 (m, 2H, β-C-H). *^{13}C NMR (500 MHz, $CDCl_3$):* δ = 157.66, 138.01, 134.97, 131.70, 131.42, 131.09, 129.51, 129.14, 128.78 (m), 128.39, 125.49 (m), 125.21, 124.51, 123.76, 123.06, 122.13, 117.18, 96.75, 94.27, 89.88, 30.73, 25.61, 19.15. *MS (FAB, 70-SE) ($C_{50}H_{40}F_6O_4$):* m/z = 818.

B.4.9 4,4'-((1E,1'E)-(2,5-bis((4-(tert-butyl)phenyl)ethynyl)-1,4-phenylene)bis(ethene-2,1-diyl))diphenol, **B.7**.

B.7a (0.080 g, 0.128 mmol) was dissolved in dichloromethane (30 mL) and trifluoroacetic acid (1 mL) was added into a 100-mL round bottom flask kept in a dry ice acetone bath. The solution was allowed to stir at -78 °C for 2 h. The crude reaction

mixture was washed three times with water, dried with magnesium sulfate, filtered and reduced until a brown powder was formed. The resulting brown powder was recrystallized by dissolving in hot chloroform and adding an excess amount of hexanes yielding brown crystals. Yield: 88%. *MP:* 236-238 ºC. *IR:* 3321, 2956, 2852, 2195, 1604, 1512, 1440 1168, 1016, 958, 833, 815. *^{1}H NMR (500 MHz, $CDCl_3$):* δ = 7.89 (s, 2H, Ar-H), 7.57 (d, 4H, Ar-H, $J_{H,H}$ = 8.5 Hz), 7.56 (d, 2H, C=C-H, $J_{H,H}$ = 16.5 Hz), 7.50 (d, 4H, Ar-H, $J_{H,H}$ = 9 Hz), 7.45 (d, 4H, Ar-H, $J_{H,H}$ = 8.5 Hz), 7.24 (d, 2H, C=C-H, $J_{H,H}$ = 16.5 Hz), 6.88 (d, 4H, Ar-H, $J_{H,H}$ = 9 Hz**).** *^{13}C NMR (500 MHz, $CDCl_3$):* δ = 155.97, 152.30, 137.64, 131.72, 130.82, 130.29, 128.93, 128.65, 125.93, 124.14, 122.50, 120.61, 116.15, 95.89, 87.80, 35.30, 31.30. *MS (FAB, 70-SE) ($C_{46}H_{42}O_2$):* m/z = 626.

B.4.10 3,3'-((1E,1'E)-(2,5-bis((4-(tert-butyl)phenyl)ethynyl)-1,4-phenylene)bis(ethene-2,1-diyl))diphenol, **B.8**.

B.8a (0.102 g, 0.163 mmol) was dissolved in dichloromethane (30 mL) and trifluoroacetic acid (1 mL) was added into a 100-mL round bottom flask kept in a dry ice acetone bath. The solution was allowed to stir at -78 °C for 2 h. The crude reaction mixture was washed three times with water, dried with magnesium sulfate and reduced until a green powder was formed. The resulting green powder was recrystallized by dissolving in hot chloroform and adding an excess amount of hexanes yielding green crystals. Yield: 90%. *MP:* 238-240 ºC. *IR:* 3319, 2954, 2862, 1784, 1683, 1591, 1506, 1450, 1265, 1151, 1016, 962, 833, 775. *^{1}H NMR (500 MHz, $CDCl_3$):* δ = 7.89 (s, 2H, Ar-H), 7.65 (d, 4H, C=C-H, $J_{H,H}$ = 16.5 Hz), 7.57 (d, 4H, Ar-H, $J_{H,H}$ = 8.5 Hz), 7.45 (d, 4H,

Ar-H, $J_{H,H}$ = 8.5 Hz), 7.26 (t, 2H, Ar-H, $J_{H,H}$ = 8.5 Hz), 7.22 (d, 2H, C=C-H, $J_{H,H}$ = 16.5 Hz), 7.16 (d, 2H, Ar-H, $J_{H,H}$ = 7 Hz), 7.07 (s, 2H, Ar-H), 6.82 (d, 4H, Ar-H, $J_{H,H}$ = 7 Hz). *^{13}C NMR (500 MHz, $CDCl_3$):* δ = 156.41, 152.40, 139.40, 137.59, 131.78, 130.67, 130.37, 129.30, 126.56, 125.96, 122.81, 120.47, 119.97, 115.57, 113.77, 96.21, 87.57, 35.30, 31.61. *MS (FAB, 70-SE) ($C_{46}H_{42}O_2$):* m/z = 626.

B.4.11 4-((E)-4-((E)-4-((tetrahydro-2H-pyran-2-yl)oxy)styryl)-2,5-bis((3-(trifluoromethyl)phenyl)ethynyl)styryl)phenol, **B.10**.

B.10a (0.120 g, 0.184 mmol) was dissolved in dichloromethane (30 mL) and trifluoroacetic acid (1 mL) was added into a 100-mL round bottom flask kept in a dry ice acetone bath. The solution was allowed to stir at -78 °C for 2 h. The product was extracted with ethyl ether and washed three times with water, dried with magnesium sulfate and reduced until a yellow powder was formed. The resulting yellow powder was recrystallized from methanol yielding yellow crystals. Yield: 85% *MP:* 236-238 ºC. *IR:* 3309, 2923, 2852, 1784, 1697, 1604, 1512, 1328, 1245, 1166, 1122, 962, 806. *^{1}H NMR (500 MHz, THF-d5)* δ = 8.57 (s, 2H, Ar-OH), 7.99 (s, 2H, Ar-H), 7.97 (s, 2H, Ar-H), 7.87 (d, 2H, Ar-H, $J_{H,H}$ = 8 Hz), 7.72 (d, 2H, Ar-H, $J_{H,H}$ = 8 Hz), 7.64 (t, 2H, Ar-H, $J_{H,H}$ = 8 Hz), 7.52 (d, 2H, C=C-H, $J_{H,H}$ = 16.5 Hz), 7.46 (d, 4H, Ar-H, $J_{H,H}$ = 8.5 Hz), 7.34 (d, 2H, C=C-H, $J_{H,H}$ = 16.5 Hz), 6.77 (d, 4H, Ar-H, $J_{H,H}$ = 8.5 Hz). *^{13}C NMR (500 MHz, THF-d5):* δ = 156.86, 136.23, 133.27, 129.77, 129.46, 129.21, 127.99, 127.09, 126.95, 126.61 (m), 123.55 (m), 122.83, 121.46, 120.05, 119.95, 114.05, 91.96, 87.94. *MS (FAB, 70-SE) ($C_{40}H_{24}F_6O_2$)*: m/z = 650.

B.4.12 Absorption and emission spectra of XFs **B.8** and **B.10** with amines.

To investigate the sensory ability of hydroxy cruciforms towards amines, XFs **B.8** and **B.10** were tested. Approximately 0.1 mL of amine was added to each 15 mL vial and its optical properties were measured. The absorption and emission data are shown in Figures B.6-B.9**.**

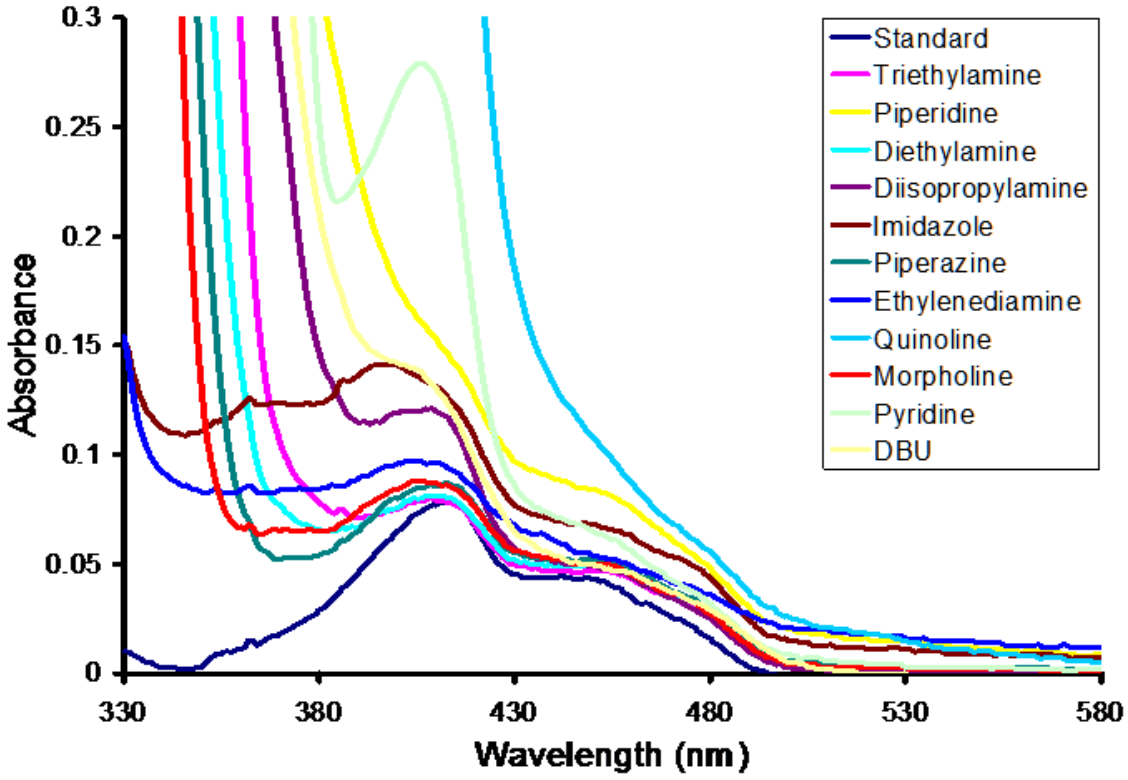

Figure B.6. Absorption spectrum of **B.8** with amines in dichloromethane.

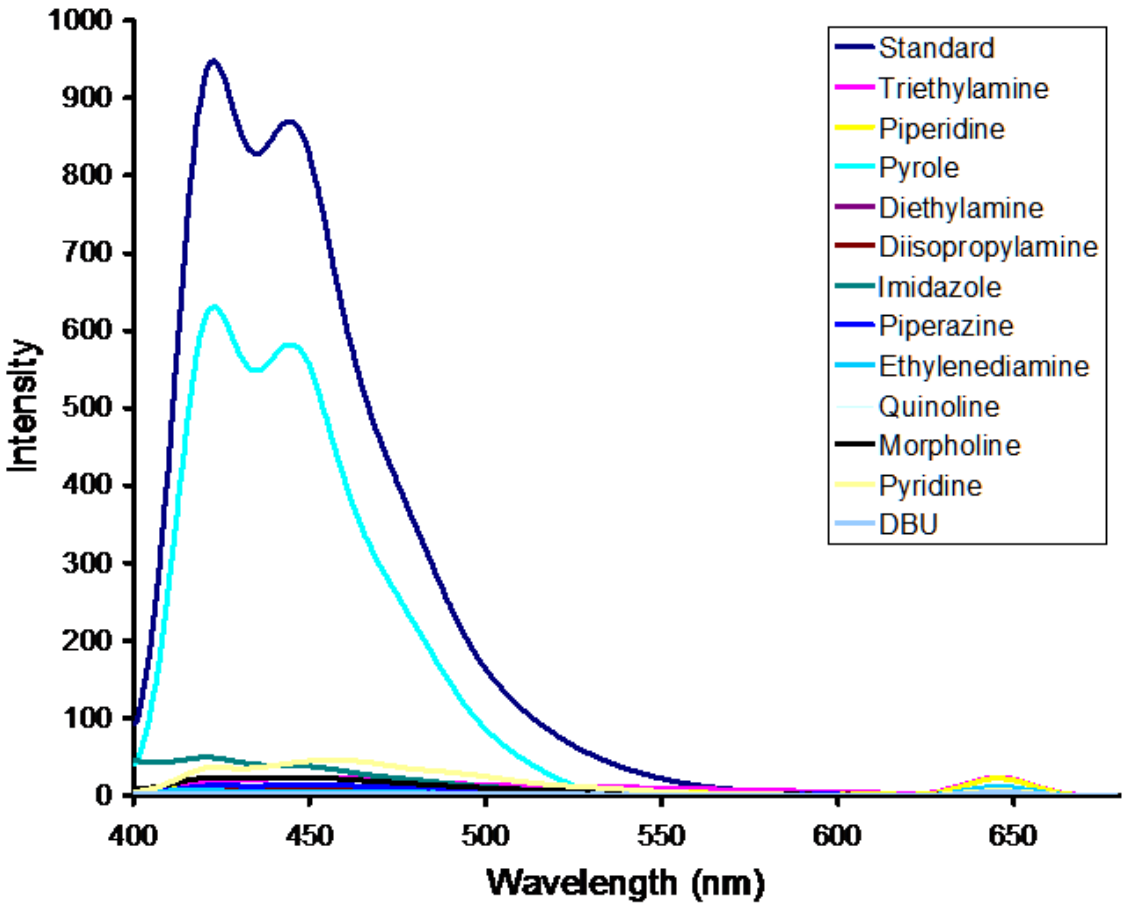

Figure B.7. Emission spectrum of **B.8** with amines in dichloromethane**.**

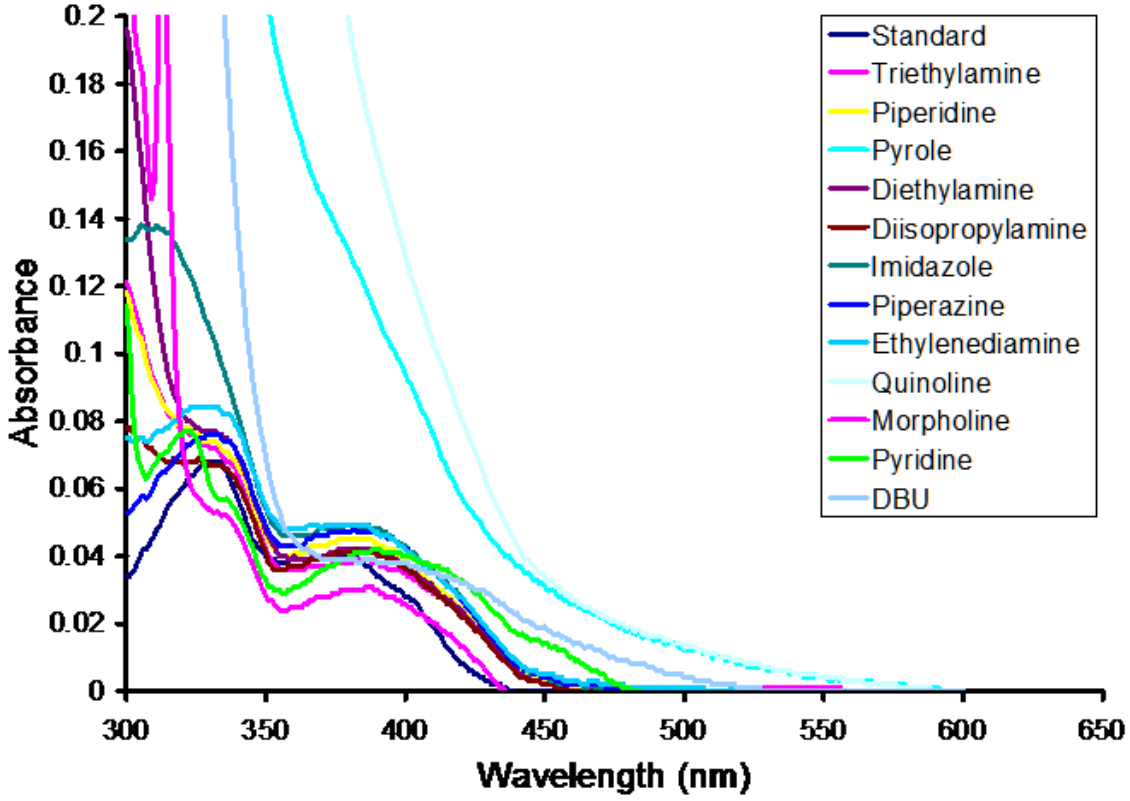

Figure B.8. Absorption spectrum of **B.10** with amines in dichloromethane**.**

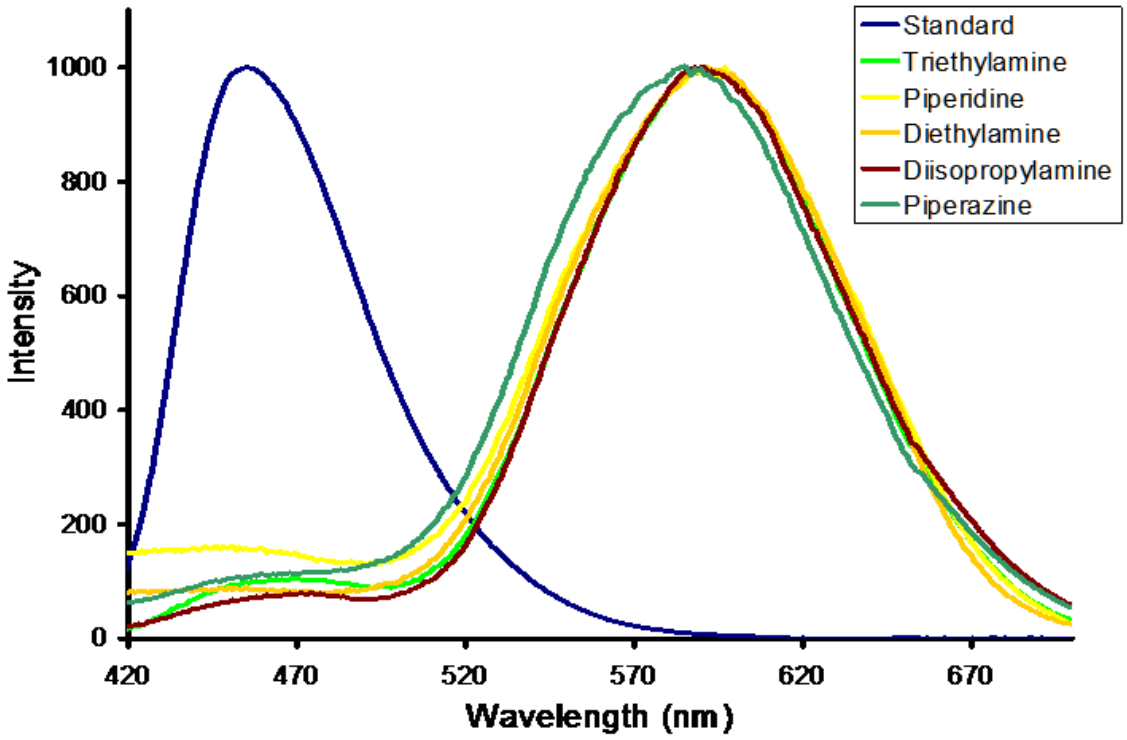

Figure B.9. Normalized emission spectrum of **B.10** with amines in dichloromethane**.**

B.5 Reference

[1] (a) Wilson, J. N. ; Bunz, U. H. F., *J. Am. Chem. Soc.* **2005**, *127*, 4124–4125. (b) Wilson, J. N.; Josowicz, M.; Wang, Y. Q ; Bunz, U. H. F. *Chem. Commun.*, **2003**, 2962– 2963. (c) Zucchero, A. J.; Wilson, J. N. ; Bunz, U. H. F. *J. Am. Chem. Soc.*, **2006**, *128*, 11872-11881. (d) Gerhardt, W. W.; Zucchero, A. J.; Wilson, J. N.; South, C. R.; Bunz, U. H. F.; Weck, M. *Chem. Commun.*, **2006**, 2141–2142.

[2] (a) Spiteler, E. L.; Shirtlcliff, L. D.; Haley, M. M. *J. Org. Chem.* **2007**, *72*, 86–96. (b) Marsden, J. A.; Miller, J. J.; Shirtcliff, L. D.; Haley, M. M. *J. Am. Chem. Soc.* **2005**, *127*, 2464–2476.

[3] (a) Zen, A.; Bilge, A.; Galbrecht, F.; Alle, R.; Meerholz, K.; Grenzer, J.; Neher, D.; Scherf, U.; Farrell, T. *J. Am. Chem. Soc.* **2006**, 128, 3914–3915. (b) Thompson, A. L.; Ahn, T. S.; Thomas, K. R. J. ; Thayumanavan, S.; Martinez, T. J.; Bardeen, C. J. *J. Am. Chem. Soc.* **2005**, *125*, 16348–16349. (c) Meier, H.; Mühling, B.; Kolshorn, H. *Eur. J. Org. Chem.* **2004**, 1033–1042.

[4] (a) Kang, H.; Evmenenko, G.; Dutta, P.; Clays, K.; Song, K.; Marks, T. J. *J. Am.Chem. Soc.* **2006**, *128*, 6194–6205. (b) Hu, K.; Zhu, P. W.; Yu, Y.; Facchetti, A.; Marks, T. J. *J. Am. Chem. Soc.* **2004**, *126*, 15974–15975.

[5] (a) Sorensen, J. K.; Vestergaard, M.; Kadziola, A.; Kilsa, K.; Nielsen, M. B. *Org. Lett.* **2006**, *8*, 1173–1176.

[6] (a) Wilson, J. N.; Windscheif, P. M.; Evans, U.; Myrick, M. L.; Bunz, U. H. F. *Macromolecules*, **2002**, *35*, 8681–8683.

[7] (a) Bunz, U. H. F. *Chem. Rev.* **2000**, *100*, 1605–1644. Sonogashira, K. *J. Organomet. Chem.* **2002**, *653*, 46–49. Negishi, E.; Anastasia, L. *Chem. Rev.* **2003**, *103*, 1979–2017.

[8] Yang, J. S.; Chiou, S. Y.; Liau, K. L. *J. Am. Chem. Soc.* **2002**, *124*, 2518–2527.

[9] (a) Zhou, Q.; Swager, T. M. *J. Am. Chem. Soc.* **1995**, *117*, 12593–12602. (b) Müller, J. G.; Atas, E.; Tan, C.; Schanze, K. S.; Kleiman, V.D. *J. Am. Chem. Soc.* **2006**, *128*, 4007–4016.

[10] (a) Caspar, J. V.; Meyer, T. J.; *J. Phys. Chem.* **1983**, 87, 952–957. (b) Tolbert, L. M.; Nesselroth, S. M.; Netzel, T. L.; Raya, N.; Stapleton, M.; *J. Phys. Chem.* **1992**, *96*, 4492–4496.

[11] (a) Lewis, F. D.; Crompton, E. M. *J. Am. Chem. Soc.* **2003**, 125, 4044–4045, Lewis, F. D.; Sinks, L. E.; Weigel, W.; Sajimon, M. C.; Crompton, E. M. *J. Phys. Chem. A*, *109*, 2443–2451.

[12] Tolbert, L. M.; Solntsev, K. M. *Acc. Chem. Res.* **2002**, *35*, 19–27.

[13] Baba, H.; Suzuki, S. J. *Chem. Phys.* **1961**, *35*, 1118–1127.

[14] Zaitsev, N. K.; Demyashkevich, A. B.; Kuzmin, M. G.; *High Energy Chem.* **1980**, *14*, 116–120.

[15] Nelson, T. L.; O'Sullivan, C.; Greene, N. T.; Maynor, M. S.; Lavigne, J. J. *J. Am.Chem. Soc.* **2006**, *128*, 5640–5641.